

Ludwig-Maximilians-Universität München  
Max-Planck-Institut für Biochemie, Martinsried

**Structural Basis for the Cooperation of Hsp110 and Hsp70  
Molecular Chaperones in Protein Folding**

Dissertation zur Erlangung des Doktorgrades  
der Fakultät für Chemie und Pharmazie  
der Ludwig-Maximilians-Universität München

vorgelegt von  
Sigrun Polier  
aus Höxter

2009

## **Erklärung**

Diese Dissertation wurde im Sinne von §13 Absatz 3 der Promotionsordnung vom 29. Januar 1998 von Herrn Prof. F. Ulrich Hartl betreut.

## **Ehrenwörtliche Versicherung**

Diese Dissertation wurde selbständig, ohne unerlaubte Hilfsmittel erarbeitet.

München, am

Dissertation eingereicht am 20. März 2009

1. Gutachter Prof. Dr. F. Ulrich Hartl

2. Gutachter Prof. Dr. R. Beckmann

Mündliche Prüfung am 18. Mai 2009

## **DANKSAGUNG**

**Die vorliegende Arbeit wurde in der Zeit von September 2006 bis März 2009 in der Abteilung Zelluläre Biochemie des Max-Planck-Instituts für Biochemie in Martinsried angefertigt.**

**Mein besonderer Dank gilt Prof. Dr. F. Ulrich Hartl für die Bereitstellung des überaus interessanten Themas sowie herausragender Arbeitsbedingungen. In zahlreichen Diskussionen habe ich seine bewundernswert geradlinige und logische Herangehensweise an wissenschaftliche Fragestellungen erfahren dürfen.**

**Nicht weniger herzlich möchte ich mich bei Dr. Andreas Bracher bedanken, unter dessen hervorragender Betreuung diese Arbeit erstellt wurde. Sein breiter theoretischer Hintergrund, seine experimentellen Fähigkeiten sowie seine unermüdliche Geduld haben maßgeblich zum Gelingen dieser Arbeit beigetragen. Die vielen spannungsgeladenen Stunden am Synchrotron werden mir genauso wie die mitunter hitzigen Debatten zu mitternächtlicher Stunde unvergesslich bleiben.**

**Darüber hinaus bin ich Dr. Manajit Hayer-Hartl zu großem Dank verpflichtet, die mich mit ihrer Frohnatur und experimentellem Geschick besonders beim Luciferaseassay unterstützt hat. Dr. Zdravko Dragovic danke ich für die Einführung in die Stopped Flow Technik. Bei allen Mitarbeitern der Abteilung Zelluläre Biochemie bedanke ich mich für die äußerst konstruktive Zusammenarbeit und die wirklich angenehme Arbeitsatmosphäre. Besonders hervorheben möchte ich dabei neben den Badminton- und Tennisspielern auch die Teilnehmer am Sprachtandem sowie die Abteilungsmasseurin. Den Mitgliedern des Lunch-Clubs danke ich für die angeregten mittäglichen Unterhaltungen über Wissenschaft und vieles mehr.**

**Christian danke ich von ganzem Herzen. Er hat mir in den letzten Monaten durch sein liebevolles, ausgleichendes Wesen sehr geholfen.**

**Mein herzlichster Dank gilt Mutter, Astrid und Gernot, die mich weit über die Promotion hinaus stets unterstützen, besonders indem sie mir ein sehr geborgenes familiäres Umfeld bereiten. Ihnen möchte ich diese Arbeit widmen.**

**TABLE OF CONTENTS**

|         |   |    |
|---------|---|----|
| 1       | Summary.....  | 1  |
| 2       | Introduction .....  | 3  |
| 2.1     | The protein folding problem.....                            | 3  |
| 2.2     | Protein aggregation <i>in vivo</i> .....                    | 5  |
| 2.3     | Molecular chaperones.....                                   | 9  |
| 2.4     | The chaperonin, Hsp90 and Hsp100 systems.....               | 12 |
| 2.5     | The Hsp70 system .....                                      | 16 |
| 2.5.1   | Structure and reaction cycle of Hsp70.....                  | 16 |
| 2.5.2   | Hsp40 cochaperones induce the ATPase activity of Hsp70..... | 19 |
| 2.5.3   | Hsp70 nucleotide exchange .....                             | 21 |
| 2.5.4   | GrpE .....  | 23 |
| 2.5.5   | BAG domain proteins.....                                    | 24 |
| 2.5.6   | HspBP1 homologs .....                                       | 26 |
| 2.5.7   | Hsp110 homologs.....  | 28 |
| 2.6     | Aim of the study .....                                      | 32 |
| 3       | Materials and Methods .....                                 | 34 |
| 3.1     | Chemicals and biochemicals .....                            | 34 |
| 3.2     | Antibodies.....   | 36 |
| 3.3     | Strains .....   | 37 |
| 3.4     | Media and buffers.....                                      | 38 |
| 3.4.1   | Media.....  | 38 |
| 3.4.2   | Buffers and standard solutions .....                        | 40 |
| 3.5     | Materials and Instruments .....                             | 46 |
| 3.6     | Molecular biological methods .....                          | 48 |
| 3.6.1   | DNA analytical methods .....                                | 48 |
| 3.6.1.1 | DNA quantification .....                                    | 48 |
| 3.6.1.2 | Agarose gel electrophoresis.....                            | 48 |
| 3.6.1.3 | DNA sequencing .....  | 49 |
| 3.6.2   | Purification of DNA fragments and plasmid DNA .....         | 49 |
| 3.6.3   | Cloning strategies .....                                    | 49 |
| 3.6.4   | Polymerase chain reaction.....                              | 50 |
| 3.6.5   | Restriction digest and DNA ligation .....                   | 52 |

---

|         |   |    |
|---------|---|----|
| 3.6.6   | Site-directed mutagenesis .....   | 52 |
| 3.6.7   | Preparation and transformation of competent <i>E. coli</i> cells.....               | 53 |
| 3.6.7.1 | Chemocompetent <i>E. coli</i> cells and chemical transformation .....               | 53 |
| 3.6.7.2 | Electrocompetent <i>E. coli</i> cells and electroporation .....                     | 53 |
| 3.6.8   | Lithiumacetate transformation of <i>S. cerevisiae</i> cells.....                    | 54 |
| 3.6.9   | Construction of <i>sse1</i> mutant <i>S. cerevisiae</i> strains .....               | 55 |
| 3.6.10  | Isolation of chromosomal DNA from <i>S. cerevisiae</i> .....                        | 56 |
| 3.7     | Protein biochemical and biophysical methods .....                                   | 56 |
| 3.7.1   | Protein expression and purification .....   | 56 |
| 3.7.1.1 | Hsp110 homologs .....   | 56 |
| 3.7.1.2 | Hsp70 homologs .....  | 58 |
| 3.7.1.3 | Ydj1p .....   | 60 |
| 3.7.1.4 | Selenomethionine-derivatized proteins .....   | 61 |
| 3.7.2   | Protein analytical methods .....  | 62 |
| 3.7.2.1 | Protein quantification .....  | 62 |
| 3.7.2.2 | SDS-PAGE .....  | 62 |
| 3.7.2.3 | Western blotting .....  | 63 |
| 3.7.2.4 | TCA precipitation .....   | 63 |
| 3.7.2.5 | Edman degradation .....   | 64 |
| 3.7.2.6 | Mass spectrometry .....   | 64 |
| 3.7.2.7 | FFF-MALS .....  | 64 |
| 3.7.2.8 | Circular dichroism spectroscopy .....   | 65 |
| 3.7.3   | Protein crystallization and structure determination.....                            | 66 |
| 3.7.3.1 | Complex formation.....  | 66 |
| 3.7.3.2 | Complex crystallization.....  | 66 |
| 3.7.3.3 | Structure determination .....   | 67 |
| 3.7.3.4 | Structure analysis.....   | 68 |
| 3.7.4   | Functional <i>in vitro</i> assays .....   | 69 |
| 3.7.4.1 | Sse1p/Ssa1N complex formation assay.....  | 69 |
| 3.7.4.2 | Determination of the dissociation constant for the Sse1p/Ssa1N<br>interaction ..... | 69 |
| 3.7.4.3 | Proteinase K resistance assay .....   | 70 |
| 3.7.4.4 | Nucleotide release assay.....   | 71 |
| 3.7.4.5 | Peptide release assay .....   | 71 |

|           |   |     |
|-----------|---|-----|
| 3.7.4.6   | Luciferase refolding assay .....  | 72  |
| 3.7.4.7   | Sse1p/peptide interaction.....  | 72  |
| 3.7.4.7.1 | Peptide scan .....  | 72  |
| 3.7.4.7.2 | Anisotropy measurements .....   | 73  |
| 3.7.4.8   | Luciferase aggregation prevention and refolding assays.....                 | 74  |
| 3.7.4.8.1 | Light scattering assay .....  | 74  |
| 3.7.4.8.2 | Luciferase refolding assay .....  | 74  |
| 3.7.5     | Functional <i>in vivo</i> assays .....                                      | 75  |
| 3.7.5.1   | Yeast growth assay .....  | 75  |
| 3.7.5.2   | Protein expression analysis by Western blotting.....                        | 75  |
| 3.7.5.3   | $\beta$ -galactosidase reporter assay for stress response.....              | 76  |
| 3.7.5.4   | Protein stability analysis.....   | 77  |
| 4         | Results .....   | 78  |
| 4.1       | Complex formation between Hsp110s and Hsp70 NBDs .....                      | 78  |
| 4.2       | Complex crystallization.....  | 82  |
| 4.3       | Structure determination .....   | 84  |
| 4.4       | Structure of the Sse1- $\Delta$ loop/Hsp70N complex.....                    | 89  |
| 4.4.1     | Overview of the complex structure .....                                     | 89  |
| 4.4.2     | Structure of Sse1p-ATP in the complex .....                                 | 90  |
| 4.4.2.1   | The ATP-bound Sse1p NBD .....   | 91  |
| 4.4.2.2   | The Sse1p inter-domain linker .....   | 93  |
| 4.4.2.3   | The Sse1p $\beta$ -sandwich domain.....                                     | 94  |
| 4.4.2.4   | The Sse1p 3HBD.....   | 95  |
| 4.4.3     | Intermolecular interface in the Sse1p/Hsp70 complex.....                    | 97  |
| 4.5       | Biochemical analysis of the cooperation of Hsp110 and Hsp70 chaperones..... | 100 |
| 4.5.1     | Overview of the Sse1p and Ssa1p mutants.....                                | 100 |
| 4.5.2     | Biophysical characterization of the Sse1p variants .....                    | 102 |
| 4.5.3     | Complex formation of Sse1p variants and Ssa1p.....                          | 105 |
| 4.5.4     | Nucleotide exchange activities of the Sse1p variants.....                   | 107 |
| 4.5.5     | Acceleration of Ssa1p peptide release by Sse1p .....                        | 108 |
| 4.5.6     | Mutational analysis of Sse1p function in protein folding.....               | 110 |
| 4.5.7     | Sse1p/peptide interaction.....  | 113 |
| 4.5.8     | Sse1p prevents protein aggregation at elevated temperatures.....            | 114 |
| 4.5.9     | <i>In vivo</i> analysis of the Sse1p mutants.....                           | 116 |

---

|     |   |     |
|-----|---|-----|
| 5   | Discussion.....   | 122 |
| 5.1 | The structure of Sse1p·ATP – a model for the ATP state of Hsp70.....      | 122 |
| 5.2 | Structure and function of the Hsp110/Hsp70 chaperone system.....          | 124 |
| 5.3 | Sse1p interaction with unfolded proteins .....                            | 126 |
| 5.4 | Does Sse1p function require conformational cycling?.....                  | 128 |
| 5.5 | Model for cooperative protein folding by Hsp110 and Hsp70 chaperones..... | 129 |
| 5.6 | Evolution of Hsp70 NEFs .....   | 131 |
| 5.7 | Diversity of NEFs in eukaryotes .....                                     | 132 |
| 6   | References .....  | 137 |
| 7   | Appendices .....  | 148 |
| 7.1 | List of primers .....   | 148 |
| 7.2 | Amino acid sequence alignment of selected Hsp110 and Hsp70 homologs ..... | 151 |
| 7.3 | List of abbreviations .....   | 156 |
| 7.4 | Publication.....  | 161 |
| 7.5 | Lebenslauf .....  | 162 |

## 1 SUMMARY

Protein folding is a crucial process for cell survival. Only natively structured proteins can perform their essential biological functions. Although all structure-relevant information is principally encoded in the amino acid sequence of a protein, the efficient folding of many larger proteins depends on the assistance of molecular chaperones. These proteins bind reversibly to exposed hydrophobic sequences in folding intermediates, thereby preventing aggregation and supporting effective folding.

The Hsp70 family proteins constitute key components of the cellular chaperone network in eukaryotes and bacteria. They are involved in diverse protein processing reactions, reaching from folding and assembly of nascent polypeptides to protein transport across membranes. Regular Hsp70s consist of an N-terminal nucleotide binding domain (NBD) and an allosterically coupled C-terminal substrate binding domain, which is further divided into a  $\beta$ -sandwich domain and a three helix bundle domain (3HBD). Hsp70s perform their cellular functions through ATP-driven cycles of substrate binding and release: In the ATP state, peptide binding is dynamic. ATP hydrolysis results in a dramatic structural rearrangement, leading to a conformation in which hydrophobic peptide segments are locked between 3HBD and  $\beta$ -sandwich domain. Thus, substrate proteins are stably bound in the ADP and apo state. This Hsp70 folding cycle is tightly controlled by a large complement of cochaperones. Whereas J-domain proteins recruit substrates and trigger ATP hydrolysis, nucleotide exchange factors (NEFs) accelerate ADP release. In eukaryotes, four evolutionarily unrelated classes of Hsp70 NEFs have been identified, among which Hsp110 homologs are most abundant. As judged by their conserved domain composition, Hsp110s derive from canonical Hsp70s, but have evolved into NEFs, preserving the ability to stabilize misfolded proteins in solution.

In the present study, the cooperation of Hsp70 and Hsp110 molecular chaperones in protein folding was investigated. First, the crystal structure of a functional complex between the yeast Hsp110 homolog Sse1p and the NBD of human Hsp70 was determined. The structure was solved by selenium multiple wavelength anomalous diffraction and refined at 2.3 Å resolution to a crystallographic R-factor of 19.7%. The structure of Sse1p is characterized by extended domain-domain interactions.  $\beta$ -sandwich domain and 3HBD are arranged along the NBD and point into opposite directions. Importantly, Sse1p has ATP bound, a prerequisite for efficient complex formation with Hsp70. In the complex, the NBD

and 3HBD of Sse1p embrace the Hsp70 NBD, thereby opening the nucleotide binding cleft of Hsp70 and releasing ADP.

In a subsequent mutational analysis, key features of the chaperone complex were targeted. Specifically, amino acid exchanges were introduced (i) in the areas of close surface contacts between Sse1p and Hsp70N, (ii) at the interfaces between individual Sse1p domains, (iii) in the nucleotide binding pocket of Sse1p, and (iv) at the putative substrate binding site in the  $\beta$ -sandwich domain of Sse1p.

Sse1p mutations affecting the interaction between the Hsp70 NBD and the Sse1p 3HBD strongly impaired Hsp70 complex formation and nucleotide exchange. Consistently, these Sse1p variants were less effective than wildtype (wt) Sse1p in supporting substrate release from Hsp70 and Hsp70-mediated refolding of thermally denatured firefly luciferase. *In vivo*, the respective *sse1* mutations caused severe stress and a pronounced growth defect, likely because of reduced substrate flux through the Hsp70 machinery. Taken together, these results define nucleotide exchange on Hsp70 as the main function of Sse1p. Furthermore, they highlight the importance of the interaction between the Hsp70 NBD and the Sse1p 3HBD for the nucleotide exchange activity of Sse1p.

No evidence was found for an ATP-driven, Hsp70-like conformational cycle of Sse1p. Mutations targeting the Sse1p inter-domain communication and the ATPase activity did not impair Sse1p function *in vitro* and *in vivo*.

Mutations at the putative substrate binding cleft of Sse1p aggravated the functional defect of partially NEF-deficient Sse1p mutants *in vitro* and *in vivo*. Thus, direct substrate interactions mediated by the  $\beta$ -sandwich domain may support Hsp70-assisted protein folding in addition to the nucleotide exchange function of Sse1p.

According to our mutational analysis, Hsp110s contribute to Hsp70-assisted protein folding in two ways: Their major function is the acceleration of ADP dissociation from Hsp70 by stabilizing the Hsp70 NBD in an open conformation with low affinity for the nucleotide. Consequently, Hsp110s support the rapid conformational cycling of Hsp70 and thus efficient substrate binding and release. In addition, Hsp110s may directly interact with the unfolded substrate upon binding to Hsp70. By holding the misfolded protein chain, Hsp110s might cooperatively aid Hsp70 in remodeling the substrate *via* large-scale thermal motions of the Hsp70 PBD.

## 2 INTRODUCTION

Proteins (derived from *proteios* (Greek), meaning "of the first rank") are the most abundant molecules in biology other than water. Forming the most versatile group of macromolecules in living cells, they play essential roles in virtually all biological processes: For example, they work as enzymes, assume structural and transport functions, allow motion and are key components in immune defense, signal transduction and regulation.

### 2.1 The protein folding problem

Proteins are built up from 20  $\alpha$ -L-amino acids, which vary in size, shape, charge, hydrogen-bonding capacity, and chemical reactivity and thus allow these molecules to mediate a wide range of functions. As encoded in the genomic sequence, the amino acid residues are connected to a linear polymer (primary structure) *via* planar, rigid, and kinetically stable amide bonds. The spatial arrangement of amino acid residues which are adjacent in the linear sequence is referred to as secondary structure. The most commonly observed elements of secondary structure are  $\alpha$ -helix,  $\beta$ -sheet, and  $\beta$ -turn. The tertiary structure of a protein designates the spatial arrangement of amino acid residues that are distant from each other in the primary structure. Large proteins often consist of several distinct polypeptide chains, so-called subunits. The three-dimensional arrangement of these subunits is termed quaternary structure.

In the early 1960s, Anfinsen and coworkers proved in refolding experiments with RNase A the reversibility of protein unfolding. This implies that the native state of a protein is thermodynamically the most stable one under physiological conditions. Moreover, all information needed to specify the three-dimensional structure of a protein is contained in its amino acid sequence (Anfinsen *et al.*, 1961; Haber and Anfinsen, 1961, 1962; Anfinsen, 1973), which is why the latter is also referred to as the second half of the genetic code (Goldberg, 1985): The primary structure forms the link between the one-dimensional sequences of DNA and RNA and the three-dimensional protein structure necessary for the protein's biological function. The biological activity of a protein further requires structural flexibility. Consequently, the native state of proteins is only marginally more stable than the unfolded state with a free enthalpy of unfolding between 30 and 70 kJ/mol (Jaenicke, 1996). The small stabilization is mainly due to non-covalent interactions such as hydrophobic core development, hydrogen bonding, and salt-bridge formation. The latter can counterbalance the

decrease in entropy of the protein chain that accompanies the increasing level of order during the folding process.

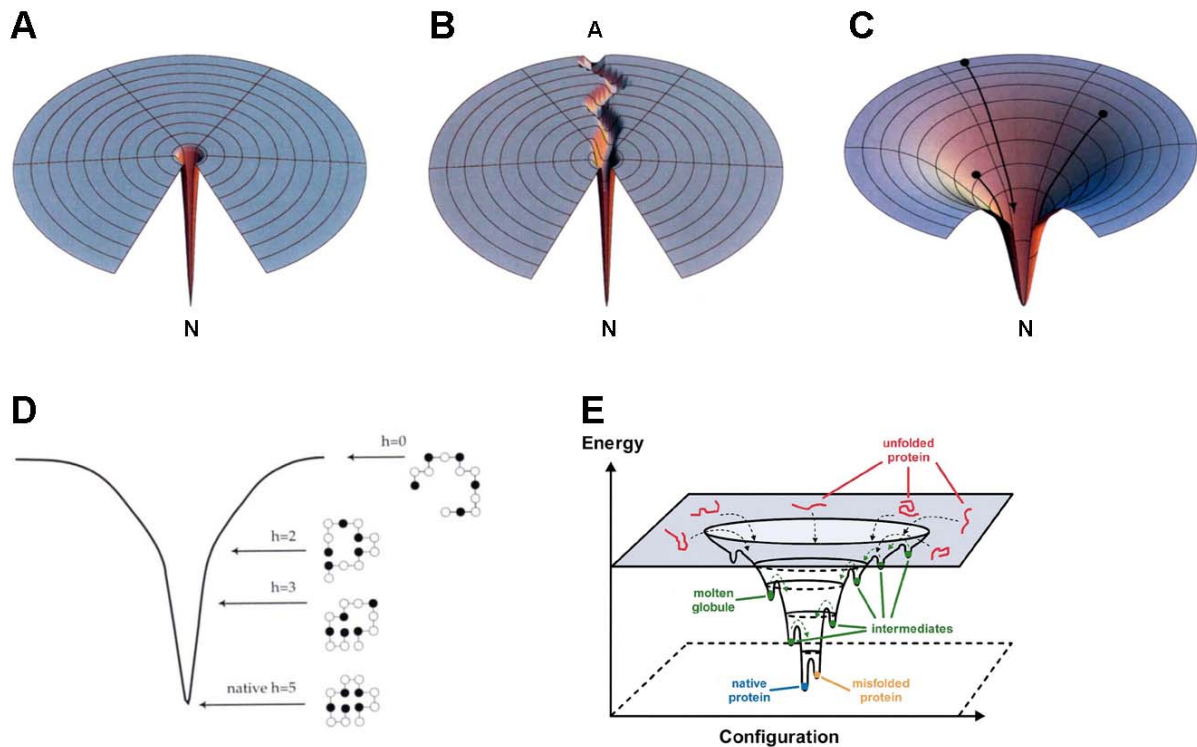


**Figure 2-1: Folding energy landscapes.**

Energy landscapes describe the internal free energy of a polypeptide chain as a function of its conformational properties.

(A) In a landscape with equal energy levels for all denatured states, the protein chain searches for its native state N randomly (Dill and Chan, 1996).

(B) Specific folding pathways narrow down the accessible conformational space, so that an unfolded chain A can reach its native state N faster than in panel (A) (Dill and Chan, 1996).

(C) According to the folding funnel concept, folding of the polypeptide chain leads to a progressive reduction of both internal free energy and conformational freedom (Dill and Chan, 1996).

(D) A slice through (C) is shown. In the lattice model, black beads represent hydrophobic and white beads polar amino acids,  $h$  stands for the number of hydrophobic contacts. The polypeptide chain can occupy many denatured, open conformations ( $h = 0$ ) and few compact conformations ( $h = 2$  or  $3$ ). The native state ( $h = 5$ ) is characterized by a nearly complete lack of conformational entropy (Dill and Chan, 1996).

(E) The multiple conformations of unfolded protein (top) fall into a folding funnel consisting of an almost infinite number of local minima, each of which represents a possible folding state of the polypeptide chain. Most of these states are transient folding intermediates. Some of them (e.g. molten globules) are characterized by a more stable structure, others act as folding traps that irreversibly capture the protein in a misfolded state (Schultz, 2000).

How does an unfolded protein find its way to its native conformation? In the following, this question shall be addressed using the energy landscape model (Figure 2-1). An energy landscape describes the internal free energy of each protein conformation as a function of its degrees of freedom, such as the dihedral bond angles along the peptide backbone for example (Figure 2-1E). The possibility that proteins fold by a purely random search of all accessible conformations was excluded by Levinthal as the time required for folding would be unrealistically long:  $10^{50}$  years for a protein with 100 amino acids (Levinthal, 1968; Kim and

Baldwin, 1982). Such a scenario would correspond to an energy landscape, in which all denatured states of the protein have the same energy level and only the native state is more stable (Figure 2-1A). To solve this so-called "Levinthal paradox", Levinthal postulated the existence of specific folding pathways (Figure 2-1B). Beginning from a denatured conformation A, the protein reaches the native state N by passing the energy landscape through a well-defined sequence of folding events. Intermediates and transition states confine the accessible conformational space, thereby allowing folding to proceed in a physiologically relevant time frame. Later, the one-dimensional pathway concept of sequential events was replaced by the multi-dimensional folding funnel concept of parallel events (Figure 2-1C,D,E). In this model, the folding states of a protein are not defined species, but rather ensembles of individual chain conformations, and multiple folding routes are possible to reach the native state. Brownian motion leads to individual conformational fluctuations in the folding chains bringing into contact even distant amino acid residues. Because native-like interactions tend to be more stable than non-native ones, the low-energy native state can be found. As a folding chain progresses towards lower internal free energies, the chain's conformational entropy narrows down to that of the final native structure (Dill and Chan, 1996; Schultz, 2000). Two-state folding kinetics can be symbolized by a smooth funnel-shaped landscape without significant kinetic traps (Figure 2-1C). Especially small proteins fold highly cooperatively within microseconds to seconds without significantly populating any intermediate state (Jackson, 1998). Their folding pathway can be best described by the nucleation-condensation model, in which a non-stable folding nucleus of a small number of key residues forms, about which the remainder of the structure can then condense (Kim and Baldwin, 1982; Ptitsyn, 1998; Dobson, 2004; Jahn and Radford, 2008). In contrast, multi-exponential folding is represented by an energy landscape with intermediates (valleys) and transition states (hills, Figure 2-1E). Intermediates can emerge from a hydrophobic collapse for example, which results within a few milliseconds in so-called molten globules. From these marginally stabilized, compact intermediates with native-like secondary structure, the native structure then develops (Ptitsyn *et al.*, 1990; Matthews, 1993; Ptitsyn, 1995).

## 2.2 Protein aggregation *in vivo*

Although it is generally accepted that the three-dimensional structure of a protein is determined by its primary sequence, a complete reversibility of unfolding is often only observed for small proteins. During the refolding of larger proteins, intermediates exposing

hydrophobic surfaces accumulate at slow folding steps and promote aggregation. Rate-limiting steps are for example the formation and reorganization of disulphide bonds or the *cis-trans* isomerization of peptidylprolyl bonds.

*In vivo*, aggregation poses a serious and universal problem not only because it reduces the efficiency of protein folding but also because it may lead to the formation of cytotoxic aggregates. Aggregation-prone species may arise both during protein synthesis at the ribosome and as a consequence of protein unfolding under stress conditions. During *de novo* synthesis, non-native features are exposed for a time range of seconds to minutes as protein domains are thought to complete folding only when their entire sequence has emerged from the ribosome (Hartl and Hayer-Hartl, 2002). Compared to *in vitro*-experiments – which are usually performed in polymer-free buffer solutions – aggregation is aggravated *in vivo* by the high intracellular concentrations of macromolecules, namely proteins, nucleic acids, and polysaccharides (300-400 g/l). Typically, 20-30 % of the interior of a cell are occupied by macromolecules and therefore unavailable for other molecules, a phenomenon referred to as macromolecular crowding or the excluded volume effect. How does the excluded volume effect stimulate protein aggregation? First, it leads to an increase in the effective concentration of the non-native protein chains. Second, if two unfolded protein chains bind to each other, the total volume which they occupy will be reduced. As a consequence, the remainder of the present macromolecules can disperse better, thus increasing their entropy and reducing the total free energy of the whole solution (Ellis, 2001; Hartl and Hayer-Hartl, 2002; Ellis and Minton, 2006; Zhou *et al.*, 2008).

Protein aggregation accompanies numerous late-onset diseases in humans, including Alzheimer's disease ( $\beta$ -amyloid peptide and tau protein), Parkinson's disease ( $\alpha$ -synuclein), Huntington's disease (huntingtin with expanded polyglutamine stretch), and spongiform encephalopathies (prion protein). Each of these diseases appears to result from a specific misfolded protein that can neither be refolded nor effectively degraded by the cell, but instead accumulates in intra- or extracellular aggregates in a variety of organs including liver, spleen and brain (Figure 2-2B panel E) (Dobson, 1999, 2003; Soto, 2003; Dobson, 2004; Hinault *et al.*, 2006; Jahn and Radford, 2008). Although the properties of the involved proteins vary significantly when soluble – e.g.  $\alpha$ -synuclein is a natively unfolded protein, in contrast to the other proteins – they share many characteristics in the aggregated state. Thus, all of them aggregate into amyloid fibrils in which  $\beta$ -strands of polypeptide chains are orientated perpendicular to the fibril axis (Figure 2-2A). Strikingly, such fibrils can also be formed by proteins that are not associated with disease, such as myoglobin for example (Fändrich *et al.*,

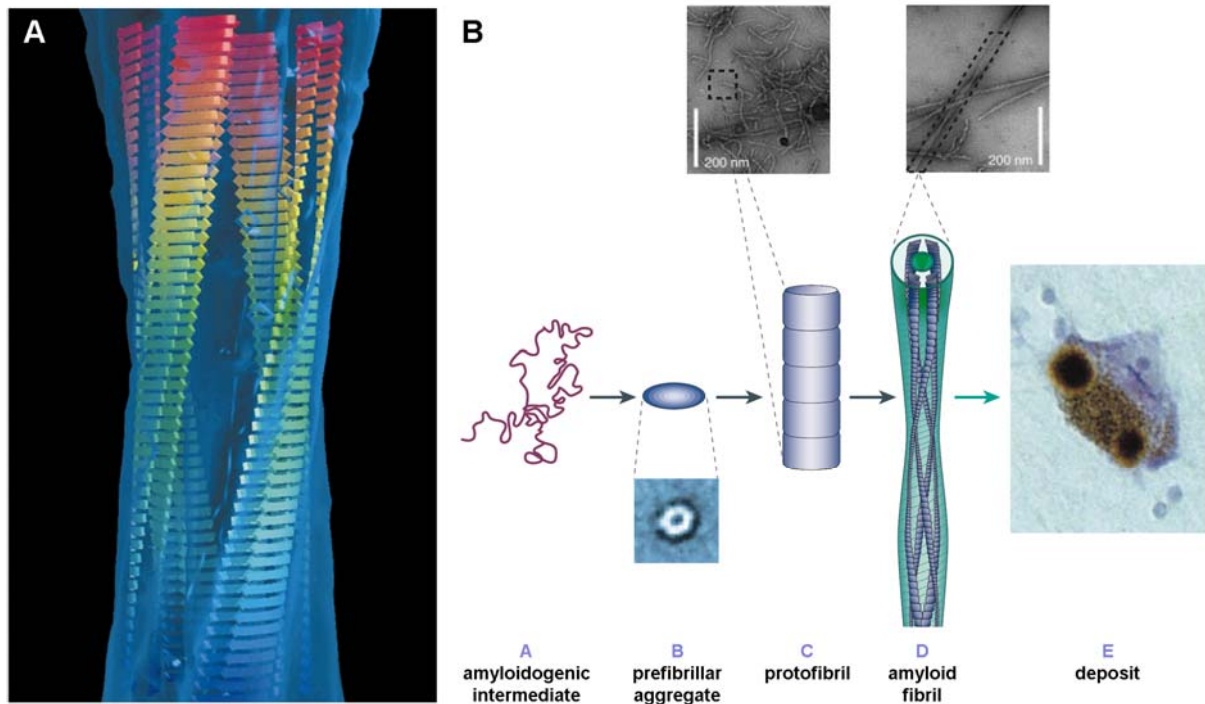


**Figure 2-2: Amyloid formation.**

(A) A molecular model of an amyloid fibril grown from the SH3 domain of the p85 $\alpha$  subunit of bovine phosphatidylinositol-3'-kinase has been fitted into its cryo-electron microscopy electron density. The fibril consists of four twisted protofilaments that form a hollow tube with a diameter of 60 Å. The depicted model presents one possibility how the  $\beta$ -strands of the aggregating protein species could be arranged in the protofibrils (Dobson, 1999; Jiménez *et al.*, 1999).

(B) A schematic overview over the mechanism of amyloid fibril formation is depicted. Partially folded or unfolded proteins (A) associate and form soluble aggregates (B) that assemble further to protofibrils (C) and mature fibrils (D). The amyloid fibrils often accumulate in plaques or other structures such as the Lewy bodies occurring in the course of Parkinson's disease (E). For each aggregated species, an electron microscopy picture is shown (adapted from Dobson, 2003).

2001). Thus – although critically depending on the physicochemical properties of the individual protein – the amyloid conformation seems to be a generic feature of polypeptide chains that, however, is normally not apparent in living cells. Only if the extensive side-chain interactions stabilizing the native state of a protein are sufficiently weakened (for example due to high temperature, low pH, mutations, faulty proteolytic processing or age-associated aberrant functions in the chaperone system), proteins unfold and may form amyloid fibrils. The  $\beta$ -sheet core structure of these fibrils is mainly defined by hydrogen bonds involving the polypeptide main chain. With the latter being an integral element of all proteins, it becomes evident why fibrils arising from different polypeptides are similar in appearance. Not only the final aggregate structure but also the aggregation pathways of different polypeptides exhibit pronounced similarities (Figure 2-2B). In a thermodynamically unfavorable slow step, unfolded or partially folded proteins (panel A) first associate non-specifically to form soluble oligomers, so-called aggregation nuclei, from which larger molecule assemblies can grow rapidly. The earliest aggregates that are detectable by electron microscopy have bead-like

structures (panel B). They are often amorphous or micellar in nature and expose polypeptide stretches buried in the native state, others form defined ring-shaped species. In the next step, these prefibrillar aggregates assemble to short, thin, sometimes curly protofilaments or protofibrils (panel C). By lateral association as well as limited structural reorganization, the latter finally transform into stable mature, insoluble fibrils with a diameter of 70 to 120 Å (panel D), which are deposited into cellular aggregates (panel E). Interestingly, increasing evidence suggests that the major pathogenic protein species in aggregation-associated neuronal diseases are not the final amyloid fibrils, but the prefibrillar aggregates exposing hydrophobic surfaces that can interfere deleteriously with other proteins or membranes (gain-of-function hypothesis). Thus, fibril and deposit formation may represent a cellular protection mechanism. Besides the gain-of-function hypothesis, two further hypotheses have been proposed to explain how protein misfolding and aggregation might be associated with neuronal apoptosis (Soto, 2003; Luheshi *et al.*, 2008): From the perspective of the loss-of-function hypothesis, activity loss of the protein, which is depleted during aggregation, results in the failure of crucial cellular processes. In contrast, the brain inflammation hypothesis suggests that the protein aggregates lead to a chronic inflammatory reaction in the brain which causes neuronal death. It appears probable that a combination of these mechanisms occurs in many diseases.

*In vivo*, aggregation is minimized by different means. First, polypeptide sequences that favor efficient cooperative folding over aggregation have evolutionarily been favored. This has been possible as the key residues that nucleate protein folding seem to differ from those that nucleate protein aggregation. In general, the aggregation propensity of sequences of functional proteins is reduced significantly compared to random polypeptide sequences, for example by avoiding long stretches of alternating polar and non-polar amino acids that lead to amyloidogenic amphiphilic  $\beta$ -sheets, by introducing stabilizing *cis*-peptidylprolyl bonds, or by protecting the edge-strands of native  $\beta$ -sheets from forming intermolecular hydrogen bonds (Dobson, 2004; DePristo *et al.*, 2005; Jahn and Radford, 2008). Second, the cellular environment has been evolved to support folding. Thus, pH and in mammals also the temperature are carefully controlled. Furthermore, proteolytic systems such as the ubiquitin-proteasome machinery or autophagy have been developed for the degradation and removal of misfolded proteins (Glickman and Ciechanover, 2002; Pickart and Cohen, 2004; Ciechanover, 2006; Rajawat and Bossis, 2008). Of particular importance are molecular chaperones that are not only able to prevent aggregation but can also disentangle already aggregated proteins and

support their refolding. In the following sections, these folding mediators will be described in detail.

### 2.3 Molecular chaperones

Molecular chaperones are a large and diverse class of proteins that assist the non-covalent assembly and disassembly of other macromolecular structures without being part of the final native structures (Ellis and Hemmingsen, 1989; Ellis and Minton, 2006). They bind reversibly to exposed hydrophobic sequences and increase the efficiency of the overall folding process rather indirectly by reducing the probability of competing reactions such as aggregation. Importantly, they do not actively contribute conformational information to the folding process or increase the rate of individual folding steps. Acceleration of rate-limiting steps is performed by so-called folding catalysts such as peptidylprolyl or protein disulfide isomerases (Dobson, 2003, 2004).

Many chaperones belong to one of the following five protein families of heat shock proteins (Hsps): the small Hsps (sHsps), which lack ATPase activity, and the ATPases Hsp100, Hsp90, Hsp70, and Hsp60. In eukaryotes, their expression is induced by heat shock transcription factors (HSFs) that – under cellular stress conditions such as heat shock or oxidative injury – bind to heat shock elements (HSEs) upstream of genes encoding Hsps (Shamovsky and Nudler, 2008). Hsps assist in prevention of misfolding and aggregation as well as in resolubilization and degradation of partially denatured or aggregated proteins. Interestingly, the ability to express Hsps under stress diminishes with increasing age – probably one reason why the aggregation-associated neurodegenerative diseases described above tend to occur late in life (Hinault *et al.*, 2006). In eukaryotes, Hsps are predominantly found in the cytoplasm, nucleus, and mitochondria. The chaperones of the endoplasmic reticulum (ER) are named glucose-regulated proteins (Grps) because they are induced by glucose starvation rather than by heat shock. Glucose starvation disrupts the glycosylation function of the ER and causes misfolded proteins to accumulate in the ER lumen. However, Grps are structurally and functionally related to Hsps (Easton *et al.*, 2000). Besides being critical in stress-challenged systems, molecular chaperones also perform essential constitutive functions under normal physiological conditions. Often dependent on ATP hydrolysis, they assist the folding of nascent polypeptide chains both co- and post-translationally, are involved in un- and refolding of polypeptides that are transferred across cellular membranes, and guide

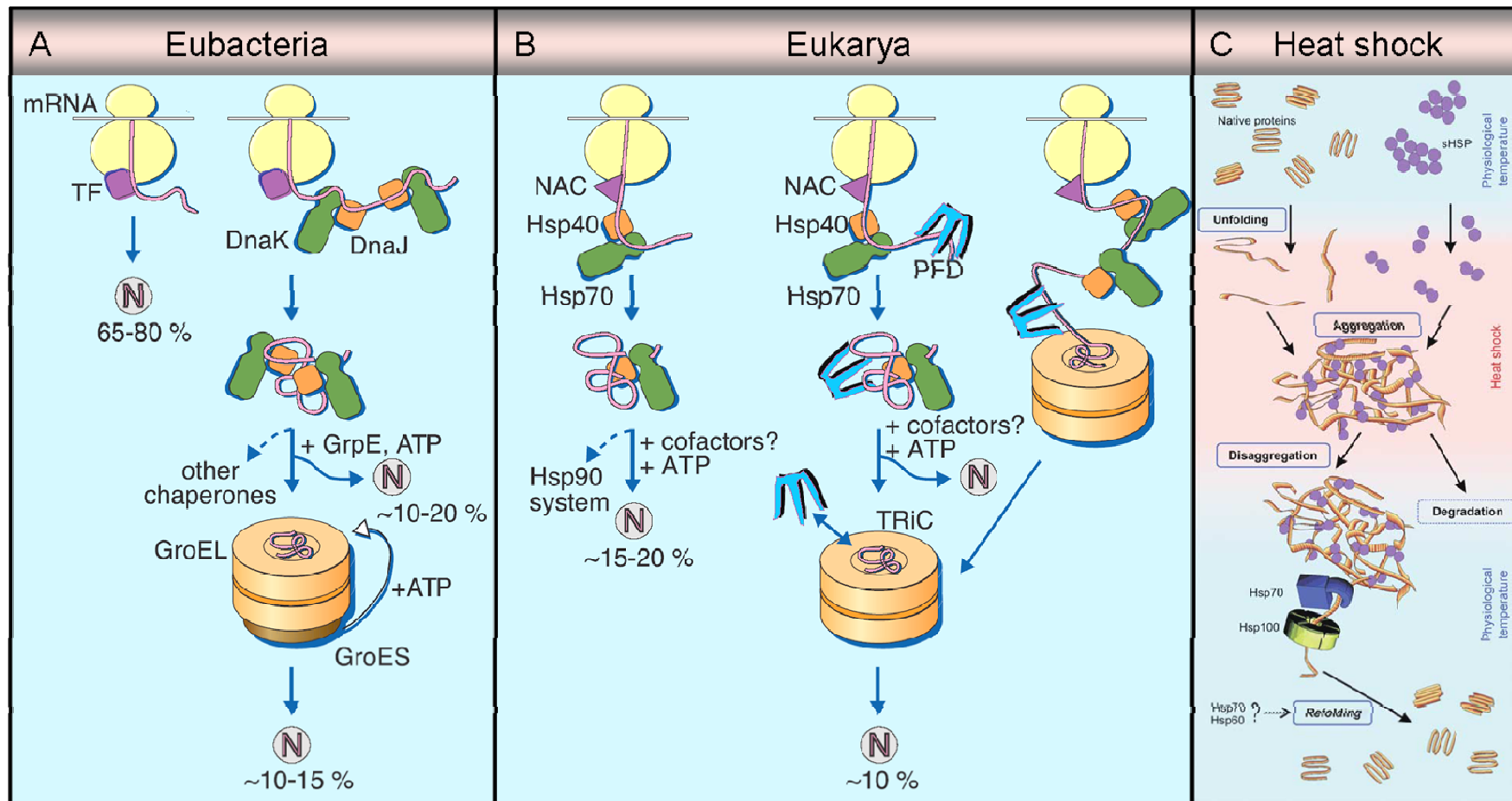


**Figure 2-3: Cytosolic chaperone networks in bacteria and eukaryotes.**

(A) In bacteria, most small proteins fold rapidly without any further chaperone assistance after interaction with TF. Larger proteins are subsequently bound by the DnaK machinery (DnaK/DnaJ/GrpE) and optionally transferred to the post-translational chaperonin system GroEL-GroES (adapted from Hartl and Hayer-Hartl, 2002).

(B) In eukaryotes, NAC is associated to ribosomes similar to TF in bacteria. Most proteins fold upon ribosome release without further assistance or after interaction with the Hsp70 system. The proper folding of kinases and transcription factors requires additional binding to Hsp90. Approximately 10 % of the proteins are further transferred to the chaperonin TRiC working co- as well as post-translationally. In case of actin and tubulin, this transfer is mediated by PFD (adapted from Hartl and Hayer-Hartl, 2002).

(C) An increase of temperature leads to the activation of oligomeric sHsps that bind to partially unfolded protein intermediates. Destabilized proteins that co-aggregate with sHsps can be efficiently resolubilized and refolded by Hsp100 chaperones cooperating with Hsp70 (adapted from Liberek *et al.*, 2008).

N: native protein; NAC: nascent chain-associated complex; PFD: prefoldin; sHsp: small heat shock protein; TF: trigger factor; TRiC: TCPI ring complex.

the assembly of oligomeric complexes (Ellis and Minton, 2006). Remarkably, while prokaryotes rely on a universal set of chaperones executing both stress response and housekeeping duties, eukaryotes have evolved distinct chaperone networks to carry out these functions: Stress-inducible Hsps protect the proteome under stress conditions, whereas CLIPS (chaperones linked in protein synthesis) are stress-repressed and involved in protein biogenesis (Albanese *et al.*, 2006). Figure 2-3 illustrates the sophisticated cellular chaperone network, the general principles of which are conserved from prokaryotes to eukaryotes: Nascent polypeptides with exposed hydrophobic residues and unstructured backbone regions are bound by chaperones during synthesis and transferred between the cooperating folding helpers until their native state is reached (Hartl and Hayer-Hartl, 2002; Young *et al.*, 2004; Liberek *et al.*, 2008). Generally, the first chaperones that contact the nascent chains are ribosome-bound. In bacteria, the emerging polypeptide chain is met by trigger factor, an ATP-independent chaperone shielding hydrophobic stretches to keep the nascent protein soluble (Figure 2-3A). In eukaryotes, the ribosome-associated complex (RAC) and possibly also the nascent chain-associated complex (NAC) are supposed to have similar functions (Figure 2-3B). RAC is a stable heterodimer, which in *S. cerevisiae* consists of the Hsp70-related Ssz1p and the J-domain protein zuotin. Zuotin contains an Hsp70 as well as a ribosome binding domain. It has been suggested that RAC recruits Hsp70 proteins to the ribosome where the latter are likely to assist the folding of nascent chains. NAC is also a ribosome-bound heterodimer that contacts emerging polypeptide chains and seems to influence the fidelity of the co-translational targeting of nascent chains to the ER. Most small proteins (65-80 % of all prokaryotic proteins) probably fold rapidly upon synthesis without further assistance. The remaining chains bind to the Hsp70 system consisting of an Hsp70 protein, such as bacterial DnaK or eukaryotic Hsp70, and a cooperating J-domain (Hsp40) protein as well as a nucleotide exchange factor (NEF). Approximately 10 to 20 % of the nascent chains are able to fold properly with the help of Hsp70 alone. A subset of slow folding proteins (10-15 % of the total protein) is subsequently passed on to the cylindrical chaperonins, namely GroEL-GroES in bacteria and tailless complex peptide 1 (TCP1) ring complex (TRiC) in eukaryotes. GroEL-GroES encapsulates the substrate in a protecting cavity for final folding. Eukaryotes have evolved further chaperones with their protein repertoire being more complex than the bacterial one: Actin and tubulin nascent chains are for example bound by prefoldin, which cooperates with TRiC. Other proteins, especially kinases and transcription factors, require Hsp90 to reach their final native structures. Above all under destabilizing, aggregation-promoting stress conditions, two further classes of chaperones perform important

tasks in pro- as well as in eukaryotes (Figure 2-3C and Figure 2-4E,F): Small Hsps bind to aggregates thereby modulating the physicochemical properties of the latter in a way that Hsp100 chaperones together with Hsp70 can effectively resolubilize the aggregated proteins to pass them back into the chaperone network. Whereas the remaining paragraphs of this introduction are dedicated to a detailed description of the Hsp70 chaperone system, the chaperonins, the Hsp90 system and the Hsp100 chaperones shall be introduced shortly in the next section (Figure 2-4).

## 2.4 The chaperonin, Hsp90 and Hsp100 systems

The chaperonins are a conserved class of large double-ring complexes of approximately 800 kDa with a central cavity (Figure 2-4A) (Leroux and Hartl, 2000; Hartl and Hayer-Hartl, 2002; Spiess *et al.*, 2004; Young *et al.*, 2004; Saibil, 2008). They can be divided into two subgroups: The group I chaperonins, also known as Hsp60s, are found in bacteria as well as in organelles of endosymbiotic origin, while the group II chaperonins are of archaeal and eukaryotic origin. The *E. coli* group I chaperonin GroEL is composed of seven identical subunits per ring and acts in cooperation with the homoheptameric 'capping' cofactor GroES. The latter serves as a detachable lid for the cavity and creates a folding chamber that encloses polypeptide substrates. In contrast, the group II chaperonin TRiC from the eukaryotic cytosol contains eight different subunits per ring and works independently of a GroES-like cochaperone. Instead, it is characterized by a built-in lid. While GroEL was only observed to promote post-translational folding, TRiC is also able to work co-translationally. Key features of the interaction between the chaperonins and their non-native substrates are (i) internalization and isolation to prevent aggregation, (ii) confinement, i.e. restriction of conformational space and thus smoothening of the energy landscape, to avoid the formation of certain trapped intermediates, and (iii) passive or possibly active unfolding of kinetically trapped intermediates. GroEL is functionally asymmetric with a positive intra- and a negative inter-ring allostery. After capturing the non-native substrate *via* hydrophobic interactions with the so-called *trans* ring<sup>1</sup>, simultaneous ATP and GroES binding results in large scale conformational rearrangements. First, the cavity of the *trans* ring is significantly enlarged so that the substrate protein can be encapsulated. Second, the *trans* ring's surface properties shift from hydrophobic to hydrophilic during the transition (Figure 2-4B). In addition, GroES

---

<sup>1</sup> The *trans* ring is defined as the free end of the GroEL-GroES complex, whereas the *cis* ring is the GroES-bound ring.

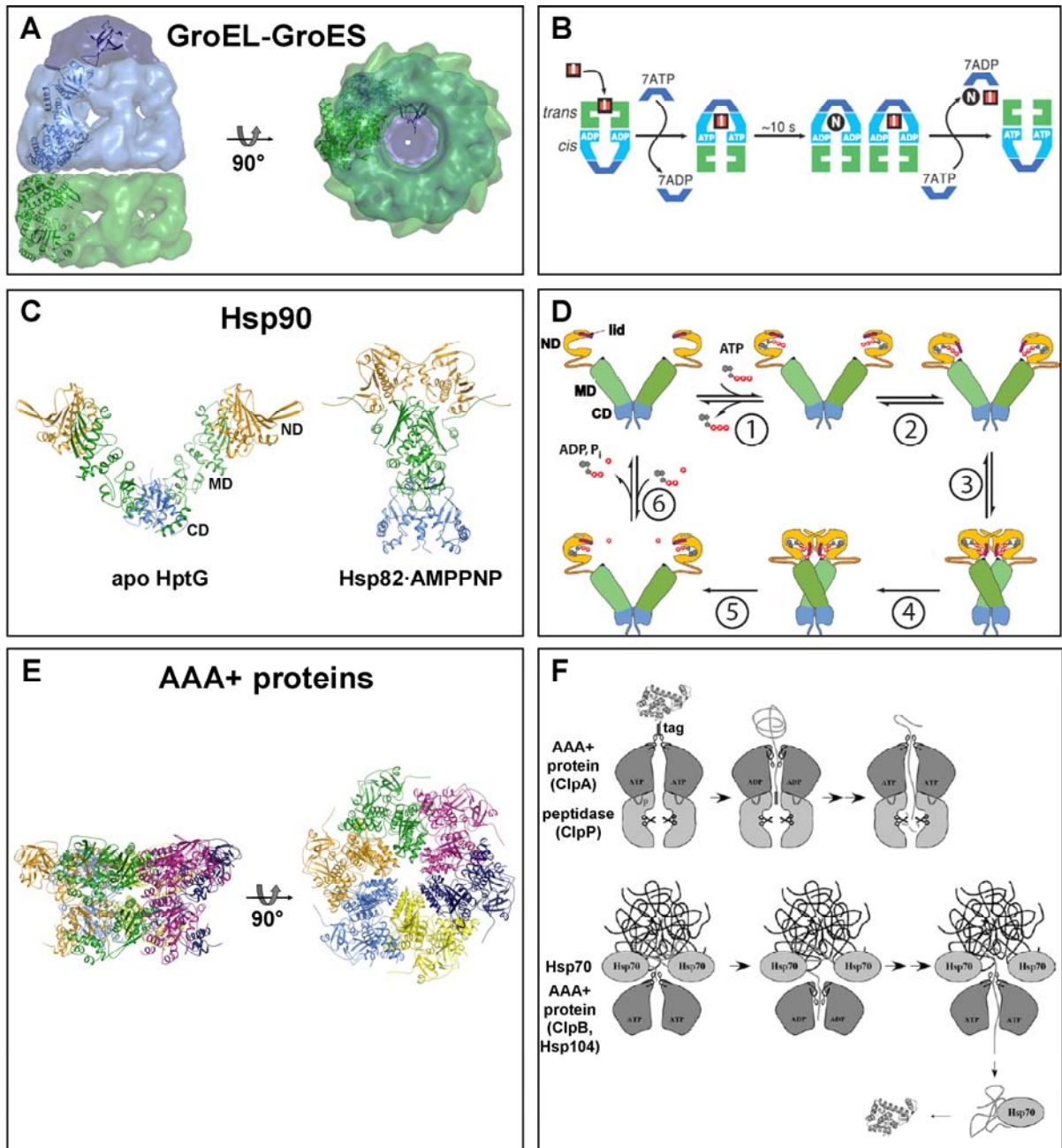


**Figure 2-4: Important cellular chaperone systems.**

(A) Frontal and top views of the GroEL-GroES-(ADP)<sub>7</sub> complex are shown in surface representation. The *trans* ring is colored in green, the *cis* ring in blue, and GroES in dark blue. One monomer of each GroEL ring as well as one GroES monomer are highlighted in ribbon representation (PDB entry code 1GRL (Braig *et al.*, 1994)).

(B) The mechanism of GroEL-GroES mediated protein folding is illustrated. GroEL and GroES are colored as in (A). I: folding intermediate; N: native protein. See text for details (Hartl and Hayer-Hartl, 2002).

(C) The crystal structure of the nucleotide-free *E. coli* Hsp90 HptG is shown in ribbon representation on the left. The N-terminal domain (ND) is colored in orange, the middle domain (MD) in green, and the C-terminal domain (CD) in blue. The apo HptG dimer is characterized by an open V-shape (PDB entry code 2IOQ (Shiau *et al.*, 2006)). On the right, the structure of the AMPPNP bound yeast Hsp90, Hsp82, is depicted. Nucleotide binding leads to conformational changes resulting in a compact and twisted dimer (PDB entry code 2CG9 (Ali *et al.*, 2006)).

(D) The ATPase cycle of Hsp90 is shown schematically. Hsp90 domains are colored as in (C). See text for details (adapted from Wandinger *et al.*, 2008).

(E) Frontal and top views of the murine protein p97 are shown in ribbon representation. The six monomers are colored in green, violet, dark blue, yellow, blue, and orange, respectively. p97 is involved in both membrane fusion and ubiquitin dependent protein degradation. p97 was the first class I AAA+ protein crystallized as an intact oligomer and its structure serves as a useful model for the structure of Hsp100 chaperones (PDB entry code 1R7R (Huyton *et al.*, 2003)).

**Figure 2-4 continued: Important cellular chaperone systems.**

(F) The functions of AAA+ proteins in protein degradation (upper panel) and disaggregation (lower panel). Whereas specifically tagged proteins (tag) are degraded by an AAA+ protein/ClpP complex, aggregates are dissolved by an AAA+ protein/Hsp70 complex. The P-element as well as the mobile loops harboring aromatic amino acids necessary for the threading activity for AAA+ proteins are highlighted. See text for details (adapted from Mogk *et al.*, 2008).

binding causes the dissociation of both ADP and GroES from the former *cis* ring. Folding is allowed to proceed for approximately 10 s, then the ATP is hydrolyzed. Subsequent binding of ATP/GroES to the *trans* ring induces the opening of the cage and substrate release. Non-native substrate can be recaptured until it has reached its native structure. Bioinformatic analysis suggests that a large fraction of GroEL substrates have an  $\alpha/\beta$  fold and a molecular weight of up to 60 kDa. However, GroEL can also assist the folding of proteins which are too large to be encapsulated.

Hsp90 is an abundant chaperone found in the cytoplasm, ER and mitochondria of eukaryotes as well as in eubacteria (Young *et al.*, 2004; Saibil, 2008; Wandinger *et al.*, 2008). It stabilizes client proteins such as transcription factors, regulatory kinases, or steroid hormone receptors until they are activated by downstream effectors. The known Hsp90 substrates lack common structural features, but have been suggested to be characterized by protein instability. Hsp90 is a flexible dimer with each monomer consisting of an N-terminal nucleotide binding domain (ND) followed by a middle domain (MD) and a C-terminal dimerization domain (CD; Figure 2-4C). The basal ATPase activity of Hsp90 is rather low: Human Hsp90 hydrolyzes one molecule of ATP every 20 minutes. A model for the Hsp90 ATPase cycle is illustrated in Figure 2-4D. Upon ATP binding (step 1), the ND undergoes a conformational change causing the so-called ATP lid to close over the nucleotide binding pocket (step 2). Subsequently, a short N-terminal segment is released from its original position and aligns with the respective part of the other monomer (step 3) leading to the formation of a compact dimer, in which the monomers are twisted around each other and in which the ND and MD are tightly associated. This conformation is ATPase active (step 4). After ATP hydrolysis, the NDs dissociate, the ATP lids open (step 5) and ADP and P<sub>i</sub> are released (step 6) so that Hsp90 is ready for another cycle. Strikingly, more than a dozen of distinct Hsp90 cofactors have been found to modulate Hsp90 activity. Some of them regulate the Hsp90 ATPase activity by binding preferentially to a specific Hsp90 conformation. The main class of cofactors are the tetratricopeptide repeat (TPR) domain proteins, which interact with the ultimate C-terminal EEVD motif of Hsp90. One TPR domain protein is the Hsp organizing protein (HOP), known as Sti1p in *S. cerevisiae*. It is thought to physically link Hsp90 and Hsp70 by binding to the EEVD motifs of both chaperones, thereby possibly

coordinating substrate transfer from Hsp70 to Hsp90. Currently, the mechanism by which Hsp90 binds its substrates is not clear. Recent electron microscopy studies suggest that substrates might bind asymmetrically to one side of the dimer.

The Hsp100 chaperones are members of the AAA+ superfamily (ATPases associated with various cellular activities). They play crucial roles in both degradation and refolding of misfolded proteins, depending on whether they associate with a peptidase or a chaperone system, respectively (Figure 2-3C and Figure 2-4F) (Liberek *et al.*, 2008; Mogk *et al.*, 2008; Saibil, 2008). Their activity strictly relies on the AAA domain, which not only binds and hydrolyzes ATP but also mediates oligomerization to hexameric rings. Depending on the composition of a monomer, AAA+ proteins are divided into two subgroups: The monomers of class I proteins contain two AAA domains (Figure 2-4E), monomers of class II proteins only one. The functional diversity of the AAA+ proteins arises from additional specific domains. Thus, the prokaryotic class I protein ClpA for example possesses a conserved P-element, through which it interacts with the barrel-shaped heptameric peptidase ClpP (Figure 2-4F, upper panel). In the complex, the AAA+ protein unfolds substrate proteins specifically tagged for degradation by threading them through its central channel to prepare them for degradation in the proteolytic chamber of the peptidase. The mechanical force required for the threading activity is mainly generated by conserved aromatic residues that are located on mobile loops at the central pore and bind and release the substrate in a nucleotide-controlled manner. In contrast to ClpA, the class I proteins ClpB (*E. coli*) or Hsp104 (*S. cerevisiae*) do not interact with peptidases but with Hsp70 and promote protein disaggregation rather than degradation. Other than ClpA, ClpB/Hsp104 does not contain a P-element but is characterized by a so-called M-domain that is strictly required for the cooperation with Hsp70. The disaggregation activity of the Hsp70-ClpB/Hsp104 complex confers thermotolerance to the cells. Interestingly, ClpB homologs are only found in lower eukaryotes and plants which both have restricted motility and therefore cannot evade environmental stress like higher animals. The following model has been suggested for the Hsp70-ClpB/Hsp104 disaggregation process (Figure 2-4F, lower panel): Hsp70 is thought to loosen single polypeptides at the surface of the aggregate and to mediate their transfer to the central pore of ClpB/Hsp104. ClpB/Hsp104 then exerts a ClpA-like threading activity. After translocation, the polypeptide is likely to be refolded by the Hsp70 chaperone system.

## 2.5 The Hsp70 system

Hsp70s are key components of the cellular chaperone network in eukaryotes, bacteria, and some archaea. They perform a central role at the interface of protein folding, degradation and transport (Figure 2-3). Hsp70s coordinate between upstream chaperones such as the ribosome-bound folding helpers and downstream components such as the chaperonins, Hsp90, Hsp100, the proteasome, or the mitochondrial import receptor TOM70 (70 kDa translocase of the outer mitochondrial membrane), a key component for protein import into this organelle (Young *et al.*, 2004). In addition to the cooperation with the listed systems, a vast ensemble of specialized cochaperones as well as a diversification into distinct *hsp70* genes allow Hsp70s to execute a broad spectrum of cellular functions (Mayer and Bukau, 2005). The diversification distinguishes Hsp70s from most other chaperone families, which do not usually have multiple representatives in the same organism. *E. coli* for example harbors three Hsp70s. In the budding yeast *S. cerevisiae*, the Hsp70 superfamily contains 14 homologs, 10 of which are classic Hsp70s. The latter can be functionally divided into two groups, the "generalists" (for example Ssa1-4p in *S. cerevisiae* with Ss standing for Stress seventy) and the "specialists" (for example the ribosome-associated Ssb1p and 2p in *S. cerevisiae*) (Morano, 2007). Another distinctive criterion for Hsp70s is their expression pattern: Their expression is either constitutive (e.g. mammalian Hsc70) or inducible by various environmental stimuli (e.g. mammalian Hsp70) and may depend on the stage of development (e.g. mammalian Hsc70t).

Considering the central role of Hsp70s in cellular protein biology, it is not surprising that these chaperones are involved in human disease. As an anti-apoptotic protein, Hsp70 is complicit in cancer progression. Moreover, Hsp70 has a protective effect in neurodegenerative diseases.

### 2.5.1 Structure and reaction cycle of Hsp70

All Hsp70 homologs share a common architecture comprising an N-terminal nucleotide binding domain (NBD, 45 kDa) with similarity to actin and a C-terminal peptide binding domain (PBD, 25 kDa) (Mayer and Bukau, 2005; Genevoux *et al.*, 2007). The NBD consists of two lobes, termed I and II, which are separated by a deep cleft, at the bottom of which the nucleotide is bound (Figure 2-5A). Each lobe is further divided into two small subdomains, a and b. The PBD is composed of a  $\beta$ -sandwich domain (15 kDa) comprising two four-stranded  $\beta$ -sheets with four upwards protruding loops (inner loops L<sub>1,2</sub> and L<sub>4,5</sub>, outer loops L<sub>3,4</sub> and

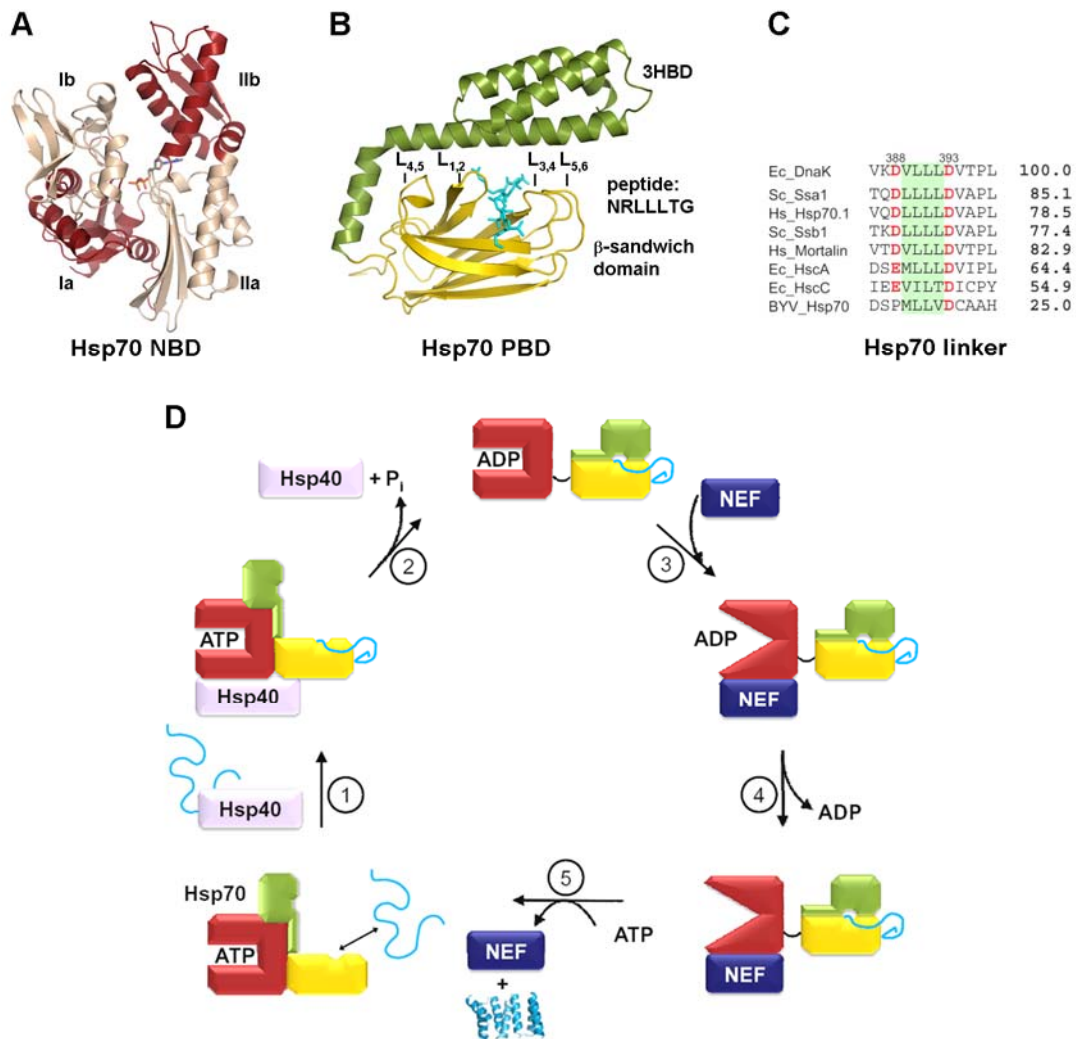


**Figure 2-5: Hsp70 structure and reaction cycle.**

A: The structure of the ADP-bound NBD of Hsp70 is shown. The NBD is depicted in ribbon and ADP in stick representation. The NBD subdomains are indicated, Ia and IIb are colored in red, Ib and IIa in light pink.

B: The structure of the PBD of DnaK in complex with a substrate peptide is shown. The PBD is depicted in ribbon and the bound peptide in stick representation. The  $\beta$ -sandwich subdomain of the PBD is colored in yellow, the 3HBD in green. The peptide NRLLLTG is shown in cyan. Loops are labeled (PDB entry code 1DKZ (Zhu *et al.*, 1996)).

C: Amino acid sequence alignment of the linker regions of evolutionarily distant Hsp70s. The numbers indicate the percentage of pairwise sequence identity of the entire protein sequences relative to *E. coli* DnaK. Ec, *E. coli*; Hs, *H. sapiens*; Sc, *S. cerevisiae*; BYV, *Beet yellow virus* (Vogel *et al.*, 2006b).

D: Hsp70-mediated folding relies on two different conformational states of Hsp70. In the ATP state, peptide binding is dynamic, while in the ADP and apo state, hydrophobic sequences exposed by unfolded proteins (represented as a blue line) are stably bound. Interconversion between the two states is catalyzed by J-proteins (Hsp40s) and NEFs. Hsp40s recognize unfolded substrates and recruit them to Hsp70 (step 1). Substrate as well as transient J-protein binding trigger ATP hydrolysis by Hsp70 (step 2). NEFs catalyze the dissociation of ADP from Hsp70 by stabilizing an open conformation of its NBD (steps 3 and 4). Upon rebinding of ATP, the interdomain linker is sequestered between the NBD and the PBD, the PBD opens and the substrate is released for folding (step 5).

$L_{5,6}$ ) and a lid-like three helix bundle domain (3HBD; Figure 2-5B) (Zhu *et al.*, 1996). The peptide binding cleft is formed by  $\beta$ -strands 1 and 2 as well as the loops  $L_{1,2}$  and  $L_{3,4}$ , with the latter taking part in backbone-backbone hydrogen bonds with the extended substrate peptide. NBD and PBD are connected by a conserved linker containing a stretch of four hydrophobic

amino acids flanked by two aspartic acid residues (Figure 2-5C). This linker has been suggested to be important for the NBD/PBD inter-domain communication: Whereas it is flexible and exposed in the nucleotide-free as well as in the ADP state of the NBD, it is buried at the NBD/PBD interface in the ATP state (Figure 2-5D) (Laufen *et al.*, 1999; Rist *et al.*, 2006; Vogel *et al.*, 2006a; Vogel *et al.*, 2006b; Swain *et al.*, 2007; Chang *et al.*, 2008).

Hsp70s are likely to perform all their cellular functions by a similar fundamental mechanism of substrate binding and release (Mayer *et al.*, 2000; Mayer and Bukau, 2005). The substrate binding characteristics of the PBD are governed allosterically by the nucleotide status of the NBD (Figure 2-5D). In both the ATP and the ADP states, the PBD is thought to exist in equilibria of open and closed conformations. However, the rates for opening ( $k_o$ ) and closing ( $k_c$ ) are suggested to vary significantly between the two states – in the ATP state ( $k_o > k_c$ ), substrate binding is dynamic, whereas in the ADP and apo state ( $k_o < k_c$ ), unfolded proteins are stably bound.

Three structural features of the PBD are of particular importance for substrate binding (Mayer *et al.*, 2000; Mayer and Bukau, 2005). The most important element is a hydrophobic pocket that accommodates a single hydrophobic side chain of the substrate and is the main contributor to the substrate binding energy. The hydrophobic nature of the central cavity and the negative surface potential in the surroundings of the cavity explain the substrate specificity of Hsp70s for extended peptides exposing hydrophobic as well as positively charged amino acid residues. The second important element is the so-called arch which is formed by two residues of loop L<sub>1,2</sub> and L<sub>3,4</sub> and encloses the backbone of the bound peptide. Interestingly, the arch-forming residues are the only substrate-contacting residues of the hydrophobic cavity that are highly variable in sequence and thus may contribute to the substrate specificity and functional specialization of Hsp70s. As third element, the  $\alpha$ -helical lid (3HBD) ensures tight binding of the substrate protein in the ADP state. Arch and lid form a two-gated closing device. Extensive rearrangements in lid, arch and hydrophobic cavity are necessary for both substrate binding and release (Figure 2-5D steps 2 and 5).

The transition from the ATP to the ADP state of Hsp70 is triggered by J-proteins (Hsp40s) (see chapter 2.5.2). They recognize unfolded substrate proteins, recruit them to Hsp70 (Figure 2-5D step 1) and induce ATP hydrolysis, thus enabling tight substrate binding (Figure 2-5D step 2). The reverse transition from the ADP to the ATP state and, consequently, substrate release is accelerated by NEFs (discussed in detail in chapters 2.5.3, 2.5.4, 2.5.5, 2.5.6, and 2.5.7). NEF binding stabilizes an open conformation of the Hsp70 NBD (Figure 2-5D step 3) and thereby triggers the release of bound ADP (Figure 2-5D step 4). Subsequent

rebinding of ATP, which is present in higher concentrations than ADP under physiological conditions, induces opening of the lid and the substrate is released for folding (Figure 2-5D step 5) (Mayer and Bukau, 2005).

The mechanism by which Hsp70s facilitate substrate folding is not yet clear (Mayer and Bukau, 2005). According to the kinetic partitioning model, repeated cycles of substrate binding and release by Hsp70 keep the concentration of the unfolded substrate sufficiently low to prevent aggregation and to give free molecules the opportunity to reach their native fold. The local unfolding model suggests that binding and release cycles induce local unfolding of misfolded parts in the substrate polypeptide thereby allowing kinetically trapped proteins to fold properly. However, both models are unable to explain the disaggregation and membrane translocation activities of Hsp70 molecules. For these Hsp70 functions, the so-called entropic pulling model has been suggested (Sousa and Lafer, 2006; Goloubinoff and De Los Rios, 2007): Hsp70 may bind to a hydrophobic peptide segment of either the aggregated protein or the protein emerging from the translocation pore in the mitochondrial matrix or ER. If only a few amino acid residues span the space between the chaperone binding site and the aggregate or pore, the thermal movements of Hsp70 will be sterically restricted. To increase its freedom of movement, the substrate-locked Hsp70 is thought to tumble away from the aggregate or pore. The resulting gain in entropy could balance the enthalpic costs for aggregate disentangling in case of protein disaggregation. In case of protein translocation, the entropic pulling force might be used to accelerate the unfolding of the cytosolic part of the substrate protein as well as substrate import.

### **2.5.2 Hsp40 cochaperones induce the ATPase activity of Hsp70**

In absence of cochaperones, ATP hydrolysis is the rate-limiting step in the reaction cycle of most Hsp70s. Since the stimulation of ATP hydrolysis by substrate binding itself reaches only two- to ten-fold and thus is too low to drive the functional Hsp70 cycle, inefficient Hsp70 cycling induced by unspecific peptide interactions is avoided. However, synergistically with J-domain cochaperones, protein substrates increase ATP hydrolysis significantly – more than 1000-fold in the case of *E. coli* DnaJ (Mayer and Bukau, 2005; Genevaux *et al.*, 2007). It has been suggested that repositioning of the Hsp70 linker region by J-protein binding plays a crucial role in the transmission of the "J signal" to the Hsp70 active site (Vogel *et al.*, 2006b; Jiang *et al.*, 2007; Swain *et al.*, 2007).

J-proteins are a heterogeneous group of multi-domain proteins (Figure 2-6C), the number of which typically exceeds the number of Hsp70s in an organism (Qiu *et al.*, 2006). Six J-protein-encoding genes were identified in the *E. coli*, 22 in the *S. cerevisiae*, and at least 41 in the human genome. Specific J-proteins have been found in the cytosol, the nucleus, endosomes, mitochondria, the ER, and at ribosomes. Their expression can be ubiquitous as well as tissue-specific. Whereas some J-proteins functionally interact only with distinct Hsp70s, others cooperate with several different ones.

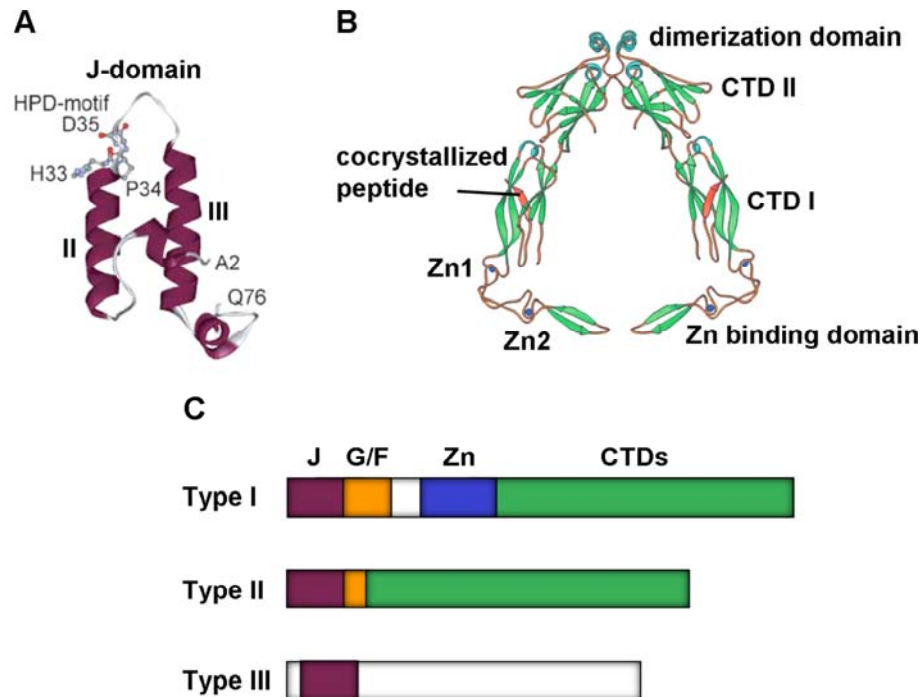


**Figure 2-6: J-domain proteins.**

(A) An NMR structure of the J-domain of *E. coli* DnaJ is shown in ribbon representation (PDB entry code 1XBL (Pellecchia *et al.*, 1996)). The conserved HPD motif is highlighted by ball-and-stick representation, helices II and III are labeled (adapted from Mayer and Bukau, 2005).

(B) A model for the C-terminal part of the Ydj1p dimer is shown in ribbon representation.  $\alpha$ -helices are colored blue,  $\beta$ -strands green. The two zinc atoms, which are coordinated by the cysteine-rich region, are shown as blue spheres. Whereas the second zinc centre (Zn2) might be involved in Hsp70 chaperone cycle activation, the first zinc centre (Zn1) is likely to contribute to substrate binding by Ydj1p. The C-terminal domain (CTD) is composed of two homologous  $\beta$ -barrel subdomains, CTDs I and II. CTD I is essential for substrate binding: The peptide substrate GWLYEIS (red) binds by extending a  $\beta$ -sheet of CTD I. Specifically, the central leucine inserts into a hydrophobic pocket on the surface of Ydj1p. Homodimerization of Ydj1p occurs *via* the ultimate C-terminal tail. The dimer is characterized by a large cleft between the monomers, which might accommodate the substrate (PDB entry code for the monomeric Ydj1p peptide binding fragment in complex with the substrate peptide 1NLT (Li *et al.*, 2003) and for the dimeric Ydj1p C-terminal fragment 1XOA (Wu *et al.*, 2005)).

(C) The subdomain organization of the three classes of J-proteins is illustrated schematically. J: J-domain, purple; G/F: glycine and phenylalanine rich region, orange; Zn: Zn<sup>2+</sup> binding domain, blue; CTDs: C-terminal domains, green.

All J-proteins are characterized by the presence of a conserved, usually N-terminal J-domain, which is necessary for Hsp70 binding (Qiu *et al.*, 2006). The J-domain has approximately 70 amino acids and consists of four  $\alpha$ -helices (Figure 2-6A). Helices II and III form a compact antiparallel coiled-coil fold and are connected by an exposed loop that

comprises the highly conserved HPD (His Pro Asp)-motif critical for the interaction with Hsp70. Moreover, strictly conserved positive residues in helix II contribute to the J-protein/Hsp70 interaction (Genevaux *et al.*, 2002). The Hsp70 NBD is contacted at the cleft between subdomain Ia and IIa as well as at the inter-domain linker (Suh *et al.*, 1998; Suh *et al.*, 1999; Jiang *et al.*, 2007). Although the Hsp70 NBD is thought to be the major binding site for J-proteins, the Hsp70 PBD also seems to contribute vitally to the J-protein interaction (Suh *et al.*, 1998; Suh *et al.*, 1999).

Based on the presence of further conserved domains in addition to the J-domain, three groups of J-proteins are distinguished (Figure 2-6C) (Walsh *et al.*, 2004; Qiu *et al.*, 2006; Genevaux *et al.*, 2007). Type I proteins such as *E. coli* DnaJ, yeast Ydj1p, and human Hdj2, consist of (i) a J-domain, (ii) a flexible glycine and phenylalanine (G/F)-rich region, (iii) a central Zn coordinating cysteine-rich domain and (iv) a less conserved C-terminal region involved in substrate binding and homodimerization (Figure 2-6B). The G/F-rich region is known to be critical for the specific function of some J-proteins, but its precise role is still not understood. It may play a role in the inter-domain coordination between the J-domain and the substrate binding regions (Tzankov *et al.*, 2008). Compared to type I proteins, type II proteins (e.g. yeast Sis1p and human Hdj1) have a less conserved G/F-rich region and lack the cysteine-rich domain. Type I and II J-proteins seem to have similar functions and to work as general purpose catalysts of the Hsp70 ATPase activity. Both can interact with non-native substrate proteins, which they recruit to their Hsp70 partners. In contrast, type III proteins seem to be much more specialized: Apart from the shared J-domain, different type III J-proteins possess a variety of distinct domains, which allows them to perform specific functions. Importantly, several type III proteins are thought to assist the recruitment of a select isoform of Hsp70 to discrete cellular sites. The *S. cerevisiae* type III J-protein zuotin or the human homolog MPP11, both components of the cognate RAC complexes, recruit distinct Hsp70s to the ribosome for example (see also chapter 2.3).

### 2.5.3 Hsp70 nucleotide exchange

NMR studies suggest that the NBD of Hsp70s is highly flexible (Zhang and Zuiderweg, 2004; Mayer and Bukau, 2005). A shearing and tilting motion of the lobes towards each other leads to an opening and closing of the nucleotide binding cleft with the opening frequency depending on the bound nucleotide (nucleotide-free > ADP > ADP + P<sub>i</sub> > ATP) and the Hsp70 isoform. Based on the nucleotide dissociation rates, three classes of Hsp70 molecules

can be distinguished with *E. coli* DnaK, *E. coli* HscA, and human Hsc70 serving as prototypes: Compared to DnaK, the spontaneous nucleotide dissociation rates of bovine Hsc70 and HscA are approximately 20- and 700-fold higher, respectively. These differences between the Hsp70s are thought to result from subtle structural variations in their NBDs with the most important ones being located close to the nucleotide binding site at the interface between the two Hsp70 lobes (Brehmer *et al.*, 2001). In DnaK, three conserved elements seem to stabilize this interface and therefore ADP binding (Figure 2-7A,B): a hydrophobic patch at the top of the inter-lobe cleft (Ile58-Leu228 in *Geobacillus kaustophilus* DnaK) and two salt bridges (Arg55-Asp233, upper; Lys54-Glu236, lower). In agreement with looser nucleotide binding, Hsc70 homologs lack the hydrophobic contact as well as the upper salt bridge, and HscA homologs do not possess any of the three elements (Figure 2-7B).

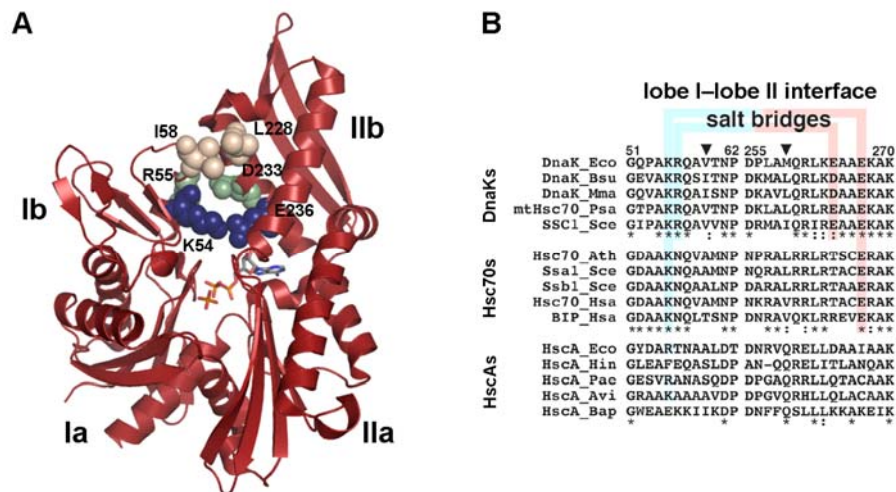


**Figure 2-7: Structural differences in the NBDs of Hsp70s.**

(A) The NBD of *Geobacillus kaustophilus* DnaK is shown in ribbon representation and colored in red. ADP and P<sub>i</sub> are depicted in stick representation. The hydrophobic interaction of Ile58-Leu228 and the salt bridges R55-D233 and K54-E236 at the interface of the nucleotide binding cleft are visualized in purple, green and blue, respectively (PDB entry code 2V7Y (Chang *et al.*, 2008)).

(B) Amino acid sequences of the lobe I-lobe II interface of Hsp70 homologs are aligned according to the structures of *B. taurus* Hsc70 (ADP-bound, PDB entry code 1HSC) and *E. coli* DnaK (nucleotide-free and GrpE-bound, PDB entry code 1DKG). The presence or absence of the *E. coli* DnaK salt bridges Arg56-Glu264 and Lys55-Glu267 as well as of the hydrophobic interaction Val59-Met259 (black arrowheads) in various homologs is presented. The asterisk indicates sequence identity, the colon sequence similarity within the three Hsp70 subgroups. Eco: *E. coli*, Bsu: *Bacillus subtilis*, Mma: *Methanosarcina mazei*, Psa: *Pisum sativum*, Sce: *S. cerevisiae*, Ath: *Arabidopsis thaliana*, Hsa: *Homo sapiens*, Hin: *Haemophilus influenzae*, Pac: *Pseudomonas aeruginosa*, Avi: *Acetobacter vinelandii*, Bap: *Buchneria aphidicola* (adapted from Brehmer *et al.*, 2001).

Correlating with their ADP dissociation rates, the three Hsp70 subfamilies vary in their dependence on NEFs (Mayer and Bukau, 2005). While bacterial DnaK strictly requires the NEF GrpE to perform its chaperone activities, HscA homologs – which are characterized by high spontaneous dissociation rates – seem to work independently of a NEF. Eukaryotic Hsc70 homologs have intermediate ADP dissociation rates and depend on NEFs only when ATP hydrolysis is strongly stimulated. Under these conditions nucleotide dissociation

becomes rate-limiting for substrate release from Hsp70. In the eukaryotic cytosol and ER, three classes of NEFs have been identified so far, the BAG (Bcl2-associated athanogene) domain proteins, homologs of Fes1p/HspBP1 (Hsp70 binding protein 1) and homologs of Hsp110/Grp170. Their significance becomes evident when considering that dysfunction of the human ER homolog of HspBP1 leads to the rare inherited neurodegenerative disease Marinesco-Sjögren syndrome (Anttonen *et al.*, 2005; Senderek *et al.*, 2005). Furthermore, Hsp110/Grp170 homologs were shown to be essential for cell viability: Removal of cytosolic Hsp110 from yeast and deletion of *grp170* in mice is lethal for both species (Kitao *et al.*, 2001; Shaner *et al.*, 2004).

#### 2.5.4 GrpE

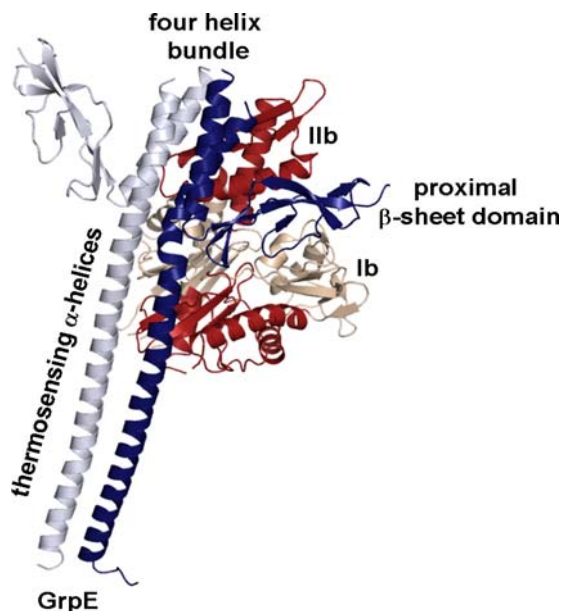


**Figure 2-8: DnaK in complex with its NEF GrpE.** A ribbon representation of the dimeric GrpE in complex with the NBD of DnaK is shown. The NBD of DnaK is colored in red tones as in Figure 2-5A. Subdomains Ib and IIb are indicated. Whereas the GrpE monomer proximal to DnaK is colored in dark blue, the distal monomer is represented in light blue. Important structural features are labeled (PDB entry code 1DKG (Harrison *et al.*, 1997)).

*GrpE* (growth P-like gene E) is an essential, stress-inducible gene, which codes for the NEF of *E. coli* DnaK, GrpE (Harrison, 2003). GrpE forms homodimers. Each monomer consists of an unordered segment at the N-terminus, a helix hairpin composed of a long and a short  $\alpha$ -helix, and a C-terminal  $\beta$ -sheet domain (Figure 2-8) (Harrison *et al.*, 1997). Homodimerization is mediated by the  $\alpha$ -helical domain.

In the cocrystal structure with the NBD of DnaK, essentially all DnaK contacts involve only one – the so-called proximal – GrpE monomer, which is bent towards the DnaK NBD and thus leads to asymmetry in the GrpE dimer (Figure 2-8). The bulk of the GrpE/DnaK interactions are mediated by the protruding proximal  $\beta$ -sheet domain. The latter binds mainly through hydrophobic contacts to the mouth of the nucleotide binding cleft of DnaK and forces subdomain IIb to rotate outward by  $14^\circ$ . This open conformation of the NBD is incompatible with tight nucleotide binding. Interestingly, GrpE almost indiscriminately stimulates the dissociation of ADP and ATP from DnaK (Brehmer *et al.*, 2001). In addition to the mouth of the DnaK NBD, two loops – the so-

called GrpE signature loop in subdomain IIb and a loop in subdomain Ia – were shown to be essential for GrpE binding (Buchberger *et al.*, 1994; Brehmer *et al.*, 2001).

The long helices of GrpE not only contribute to DnaK binding but are also thought to serve as a thermosensor. At elevated temperature, they undergo a reversible helix-to-coil transition ( $T_M \approx 50\text{ }^\circ\text{C}$ ), which reduces the nucleotide exchange activity of GrpE towards DnaK (Grimshaw *et al.*, 2001; Gelinas *et al.*, 2002, 2003; Siegenthaler and Christen, 2005, 2006). Consequently, the fraction of ADP-bound DnaK/substrate complexes is suggested to rise transiently, which is likely to contribute to the prevention of protein aggregation under non-permissive conditions.

Independently of its NEF activity, GrpE is also thought to promote substrate release from the DnaK PBD with the help of its unordered N-terminal region, which seems to serve as a pseudo-substrate for DnaK (Chesnokova *et al.*, 2003; Harrison, 2003; Brehmer *et al.*, 2004; Moro *et al.*, 2007).

### 2.5.5 BAG domain proteins

In eukaryotes, GrpE homologs have only been found in bacteria-derived compartments, namely in mitochondria (e.g. MgeI in *S. cerevisiae*) and chloroplasts. The NEFs that perform nucleotide exchange on eukaryotic Hsp70s in the cytosol and ER are evolutionarily independent of GrpE. One group of these NEFs are BAG domain proteins (BDPs).

BDPs form a heterogeneous family of multi-domain proteins (Takayama and Reed, 2001; Alberti *et al.*, 2003; Mayer and Bukau, 2005; Kabbage and Dickman, 2008). As illustrated for the eight human BDPs in Figure 2-9A, their common feature is the so-called BAG domain, which is located at the C-termini and mediates the interaction with the Hsp70 partners. The further domain composition is specific for each BDP, allowing individual BDPs to interact with distinct target proteins as well as to assume different localizations in the cell. As a consequence, similar to type III J-proteins, BDPs have been suggested to serve as molecular adaptors, which are able to recruit Hsp70 chaperones to specific substrates or cellular compartments. BDPs have been reported to regulate a variety of cellular processes, often in cooperation with Hsp70. For example, human BAG-1 and Hsp70 are involved (i) in the regulation of Raf-1 protein kinase (Song *et al.*, 2001), (ii) in the regulation of the transcriptional activity of androgen receptors (Froesch *et al.*, 1998), or (iii) in protein degradation (Lüders *et al.*, 2000; Alberti *et al.*, 2002). Human BAG-4 – also known as silencer of death domains (SODD) – has been suggested to recruit Hsp70 to tumor necrosis

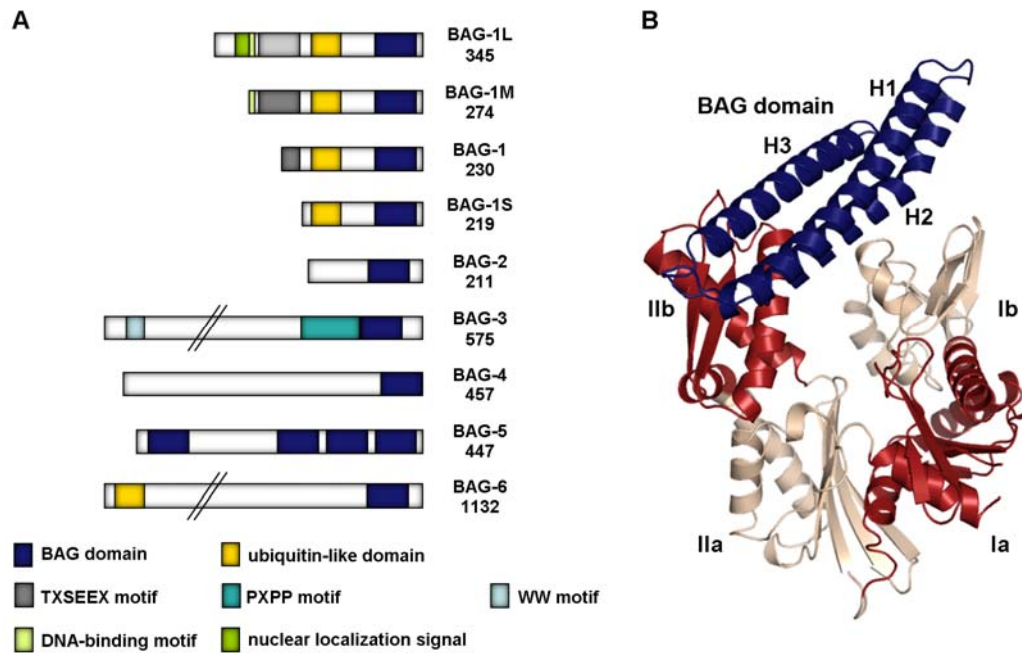


**Figure 2-9: BAG domain proteins.**

(A) The subdomain organization of the eight human BDPs is illustrated schematically. BAG-1L, BAG-1M, and BAG-1S are splicing variants of BAG-1. BAG domain, dark blue; ubiquitin-like domain, yellow; TXSEEX motif, gray; PXXP motif, cyan; WW motif, light blue; DNA-binding motif, light green; nuclear localization signal, green. The number of amino acids of the individual BDPs is indicated.

(B) A ribbon representation of the BAG domain of BAG-1 in complex with the NBD of Hsc70 is shown. The NBD of Hsc70 is colored in red tones as in Figure 2-5A, its subdomains are indicated. The BAG domain is colored in dark blue and the three helices of the three helix bundle are labeled (PDB entry code 1HX1 (Sondermann *et al.*, 2001)).

factor receptor 1 (TNFR1) to prevent ligand-independent oligomerization of the latter (Jiang *et al.*, 1999).

Homologs of the BAG domain were found in diverse organisms ranging from yeast to mammals. The BAG domain is essential and sufficient for the nucleotide exchange function of BDPs. It contains 110 to 124 amino acids arranged in three anti-parallel helices of 30 to 40 amino acids each (Figure 2-9B) (Sondermann *et al.*, 2001). Helices two and three contact Hsc70 subdomains Ib and Iib mainly *via* highly conserved electrostatic interactions. Helix one might fix the orientation of the two other  $\alpha$ -helices to facilitate efficient Hsc70 binding. Hsc70 complex formation with the BAG domain leads to an outward rotation of Hsc70 subdomain Iib by  $14^\circ$  relative to the structure of ADP-bound Hsc70. Since this open conformation of the NBD is characterized by a distorted nucleotide binding site, the BAG domain accelerates ADP dissociation and consequently substrate release from Hsp70. Remarkably, the conformational states of the Hsc70 and DnaK NBDs stabilized by the BAG domain and GrpE, respectively, are very similar. The fact that the two NEFs are structurally unrelated, but employ the same molecular switch in Hsp70 suggests a convergent evolution of

the two proteins. Interestingly, the human Hsp70 interacting protein (HIP) was reported to antagonize the NEF activity of BAG-1 (Höhfeld *et al.*, 1995).

### 2.5.6 HspBP1 homologs

HspBP1 homologs represent another distinct class of conserved NEFs for eukaryotic Hsp70s (Kabani *et al.*, 2002b). In contrast to BDPs, HspBP1 homologs are single domain proteins and consequently might act as general, non-specialized NEFs for Hsp70 chaperones.

HspBP1 is a relatively abundant protein in the human cytosol that has a higher expression level than Hsp70-1 in both normal and tumor cells (Tanimura *et al.*, 2007). Initially, HspBP1 was identified as an Hsp70-interacting protein that inhibited Hsp70-mediated protein refolding (Raynes and Guerriero, 1998; Tzankov *et al.*, 2008). Later studies revealed its NEF activity on Hsc70 (Kabani *et al.*, 2002b).

The *S. cerevisiae* HspBP1 ortholog is named Fes1p and was found to be four times more abundant than the membrane-anchored yeast BDP Snl1p *in vivo* (Fes1p: Snl1p: Ssa1/2p = 4: 1: 189) (Kabani *et al.*, 2002a; Ghaemmaghani *et al.*, 2003). Deletion of *FES1* causes a temperature-sensitive phenotype. Fes1p exchanges nucleotide on the yeast Hsp70 homologs Ssa1p and Ssb1p and supports efficient *de novo* protein folding *in vivo* (Kabani *et al.*, 2002a; Shomura *et al.*, 2005; Dragovic *et al.*, 2006a). Interestingly, Fes1p seems to act during protein translation (Kabani *et al.*, 2002a; Dragovic *et al.*, 2006b). It competes with RAC for Ssb1p binding. As the two proteins have opposed functions – whereas RAC promotes ATP hydrolysis on Ssb1p and thus tight substrate binding, Fes1p accelerates ADP-ATP exchange – this finding could be of importance for the regulation of Ssb1p in co-translational protein folding.

Sls1p/Sil1p (also termed BAP (BiP-associated protein) in mammalian cells) was identified as ER-luminal HspBP1 homolog in mammals and yeast. It exchanges nucleotide on BiP, the Hsp70 homolog of the ER. In yeast, Sls1p/Sil1p is involved in the translocation of proteins into the ER as well as in ER-associated degradation (ERAD), probably by increasing the efficiency of the ER-resident Hsp70 Kar2p, the yeast homolog of BiP (Boisramé *et al.*, 1996; Boisramé *et al.*, 1998; Kabani *et al.*, 2000; Babour *et al.*, 2008). As mentioned in chapter 2.5.3 already, mutations in *SIL1* cause the Marinesco-Sjögren syndrome, a rare autosomal recessive cerebellar ataxia complicated by cataracts, developmental delay and myopathy (Anttonen *et al.*, 2005; Senderek *et al.*, 2005). In mice, loss of Sil1 function causes

an abnormal accumulation of ubiquitinated proteins in the ER and nucleus of cerebellar Purkinje cells leading to the neurodegeneration of the latter.

Figure 2-10A shows the crystal structure of the core domain of human HspBP1 (BP1c) bound to lobe II of Hsp70 (Shomura *et al.*, 2005). BP1c is an all  $\alpha$ -helical protein containing four central Armadillo repeats (ARM1-4) flanked by capping helices at the chain termini. In the complex, BP1c wraps around subdomain IIb of the NBD of Hsp70. A high degree of surface and charge complementarity leads to an extended and tight interface between the two proteins. As most residues involved in the intermolecular contacts are highly conserved, it is likely that all HspBP1 homologs bind to their Hsp70 partners in a similar manner (Shomura *et al.*, 2005; Dragovic *et al.*, 2006b).

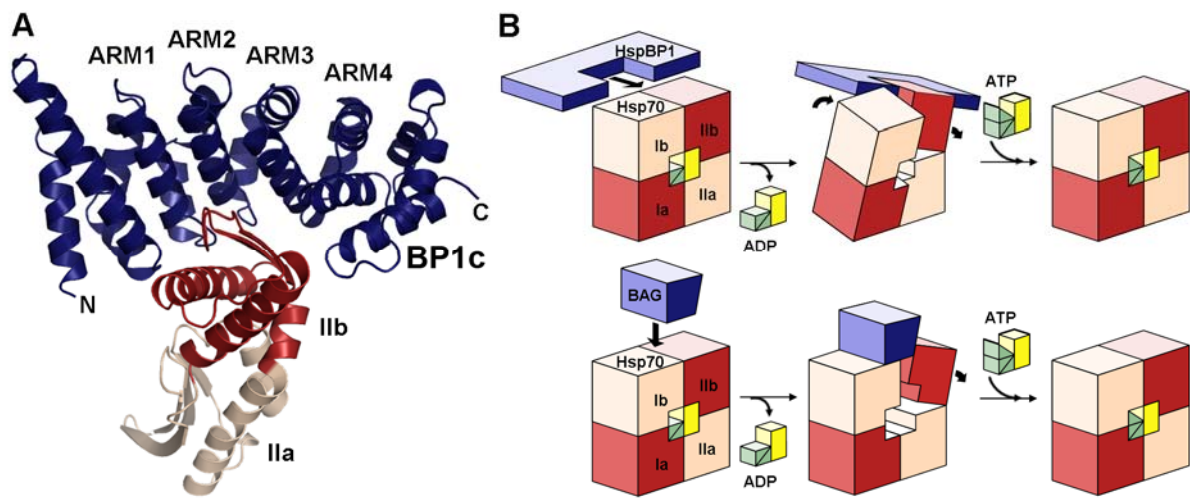


**Figure 2-10: HspBP1.**

(A) The complex of BP1c and Hsp70 lobe II is shown in ribbon representation. BP1c is colored in dark blue and the four Armadillo repeats as well as N- and C-termini are labeled. Lobe II of DnaK is colored in red tones as in Figure 2-5A, its subdomains are indicated (PDB entry code 1XQS (Shomura *et al.*, 2005)).

(B) Schematic models for the nucleotide exchange mechanisms of HspBP1 and BAG-1/GrpE. HspBP1 binding is suggested to result in a distortion of Hsp70 lobe I as well as in an opening of lobe II (upper panel). BAG-1 and GrpE lock subdomain IIb in an open conformation (lower panel). In both cases, the twisted Hsp70 NBD conformations are incompatible with ADP binding. ATP rebinding leads to the dissociation of the NEF/Hsp70 complexes (adapted from Shomura *et al.*, 2005).

The suggested mechanism for HspBP1-driven nucleotide exchange on Hsp70 differs from the one proposed for GrpE and the BAG domain (Figure 2-10B) (Shomura *et al.*, 2005). Whereas the BAG domain binds to the central nucleotide binding cleft from the top by making contacts with both subdomains Ib and IIb, HspBP1 contacts subdomain IIb from the side. A NBD conformation as found in the BAG/GrpE complex would lead to sterical interference between NBD subdomain Ib and the N-terminus of HspBP1. Consequently, HspBP1 is thought to distort lobe I and to separate it from lobe II in addition to stabilizing an outward rotation of subdomain IIb. This notion is in agreement with experimental data

showing that NBD lobe I is protease-sensitive in the HspBP1, but protease-resistant in the BAG domain complex. The separation of the two lobes in the HspBP1/NBD<sub>Hsc70</sub> complex is likely to trigger ADP release.

It has been suggested that the different conformations imposed on the Hsp70 NBD by HspBP1 and the BAG domain might regulate the crosstalk between the PBD and downstream effectors such as the cochaperone CHIP (C-terminus of heat shock cognate 70 stress protein-interacting protein) (Demand *et al.*, 2001; Alberti *et al.*, 2004). CHIP was reported to form ternary complexes with both HspBP1/Hsc70 and BAG-1/Hsc70. It negatively regulates Hsp70 ATPase and chaperone activities and – as an E3 ubiquitin ligase – supports the ubiquitination of unfolded Hsp70 substrates. Whereas the degradation function of CHIP is inhibited by HspBP1, it is stimulated by BAG-1.

### 2.5.7 Hsp110 homologs

Hsp110/Grp170 homologs form the third and probably principal class of eukaryotic NEFs. While Hsp110s are predominantly located in the cytosol, Grp170s are ER-luminal proteins. In humans and mice, three Hsp110 family members have been identified: Hsp110 – more precisely the constitutively expressed Hsp105 $\alpha$  and its heat-inducible splicing variant Hsp105 $\beta$  –, Apg-1, and Apg-2 (A: ATP binding domain, p: peptide binding domain, g: germ cell derived) (Easton *et al.*, 2000). After Hsp70 and Hsp90, Hsp110 is the third most abundant Hsp in most mammalian cell lines and tissues studied so far. In heat-shocked chinese hamster ovary (CHO) cells, Hsp110 accounts for 0.7 % of total cell protein compared to 3.2 % for Hsc70 and Hsp70 combined and 1.2 % for Hsp90 (Subjectek *et al.*, 1982). Hsp110 is broadly expressed in diverse mammalian tissues. However, expression levels are tissue-specific: While the constitutive expression of Hsp110 is low in heart and skeletal muscle for example, it is highly expressed in liver and brain (Lee-Yoon *et al.*, 1995; Yasuda *et al.*, 1995; Oh *et al.*, 1997). Apg-1 and Apg-2 are primarily expressed in the gonads; their expression levels in all other mouse tissues are low (Kaneko *et al.*, 1997a; Kaneko *et al.*, 1997b).

*S. cerevisiae* possesses two Hsp110 homologs, Sse1p and Sse2p, which are both upregulated upon stress. Under normal growth conditions, only *SSE1* is abundantly expressed (Mukai *et al.*, 1993). For log-phase cells, a ratio of Sse1/2p to Ssa1/2p of 1 to 8 was determined (Ghaemmaghami *et al.*, 2003).

Interestingly, Hsp110/Grp170 homologs are distant relatives of canonical Hsp70s and as such belong to the Hsp70 superfamily (Morano, 2007). Like regular Hsp70s, they are

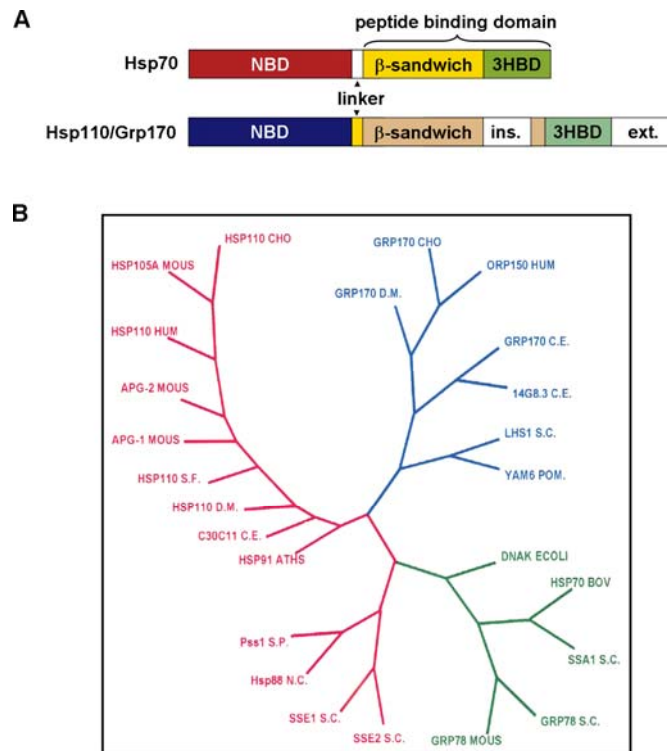


**Figure 2-11: Hsp110 homologs.**

(A) Hsp110s/Grp170s share the general domain composition with Hsp70s. Hsp70 domains are colored as introduced in Figure 2-5. Compared to Hsp70s, Hsp110s/Grp170s are characterized by an insertion (ins.) into the  $\beta$ -sandwich domain and a C-terminal extension (ext.).

(B) The unrooted phylogenetic tree for canonical Hsp70 and Hsp110/Grp170 homologs illustrates the degree of relationship between regular Hsp70s (green), Hsp110s (red), and Grp170s (blue) based on a sequence alignment. While regular bacterial and eukaryotic Hsp70s share high sequence identity, Hsp110/Grp170 homologs are much more variable. Grp170s are almost as diverged from Hsp110s as from Hsp70s. The Hsp110s from yeast and *Neurospora crassa* are slightly more similar to the Hsp70/DnaK family than the Hsp110s and Grp170s from higher eukaryotes. ATHS: *Arabidopsis thaliana*; BOV: bovine; C.E.: *Caenorhabditis elegans*; CHO: Chinese Hamster Ovary; D.M.: *Drosophila melanogaster*; ECOLI: *Escherichia coli*; HUM: human; MOUS: mouse; N.C.: *Neurospora crassa*; POM.: *Saccharomyces pombe*; S.C.: *Saccharomyces cerevisiae*; S.F.: *Strongylocentrotus franciscanus*; S.P.: *Saccharomyces pombe* (adapted from Easton *et al.*, 2000).

composed of an N-terminal NBD followed by a linker, a  $\beta$ -sandwich domain and a C-terminal 3HBD (Figure 2-11A). However, most Hsp110s and Grp170s differ from Hsp70s by an additional C-terminal extension and a large acidic insertion into the  $\beta$ -sandwich domain. The latter is considerably longer in Grp170s. Furthermore, the Hsp110/Grp170 domains are much more divergent than the highly conserved domains of canonical Hsp70s (Shaner and Morano, 2007). While yeast Ssa1p and human Hsp70 share 74 % overall sequence identity, yeast Sse1p and human Hsp110 are only 32 % identical. The sequence identity between the yeast and human Grp170 homologs, Lhs1p and Orp150 (oxygen-regulated protein), drops to 21 %. Strikingly, Grp170s are essentially as diverged from Hsp110s as from regular Hsp70s regarding the overall sequence similarity (Figure 2-11B) (Easton *et al.*, 2000).

Deletion of *hsp110* or *grp170* genes can have severe consequences for the cell, highlighting their importance. Whereas yeast cells lacking the *SSE1* gene are characterized by

a growth defect, deletion of *SSE2* alone does not lead to any phenotype. Deletion of both *SSE1* and *SSE2*, however, is lethal for yeast (Mukai *et al.*, 1993; Shaner *et al.*, 2004; Raviol *et al.*, 2006b). Surprisingly, mammalian Hsp110 does not complement the deletion of *SSE1* suggesting a significant functional divergence between the Hsp110 homologs in different organisms (Shaner *et al.*, 2004). Strikingly, the deletion of Grp170 leads to embryonic lethality in mice (Kitao *et al.*, 2001). The yeast Grp170 gene *LHS1* is not essential for cell viability, however (Baxter *et al.*, 1996; Craven *et al.*, 1996; Hamilton and Flynn, 1996).

Initially, Hsp110 homologs were shown to confer thermotolerance to cells *in vivo* and, comparable to canonical Hsp70s, to prevent aggregation of denatured proteins *in vitro* as well as to sustain them in a folding-competent state (Oh *et al.*, 1997; Brodsky *et al.*, 1999; Oh *et al.*, 1999). However, Hsp110s were found unable to fold proteins independently of regular Hsp70s (Oh *et al.*, 1997; Raviol *et al.*, 2006a). In contrast to canonical Hsp70s, the ATPase activity appears not essential for Hsp110s: Although Sse1p shows a basal ATPase activity that is comparable to the ATPase rates of canonical Hsp70s, its biological function only depends on ATP binding but not on ATP hydrolysis (Shaner *et al.*, 2004; Raviol *et al.*, 2006a). In contrast to a mutation abolishing Sse1p ATPase activity (K69M), a point mutation impairing ATP binding (G205D) cannot completely complement the deletion mutant  $\Delta SSE1\Delta SSE2$ . It was shown that nucleotide binding, and especially ATP binding, stabilizes Sse1p, indicating nucleotide-dependent conformational changes (Raviol *et al.*, 2006a; Shaner *et al.*, 2006).

In addition to its function in aggregation prevention, early studies revealed a cooperation between Sse1p and Hsp90 (Liu *et al.*, 1999; Goeckeler *et al.*, 2002). For example, Sse1p is required for the effective *in vitro* expression of functional glucocorticoid receptor, a model substrate of the Hsp90 chaperone machinery. Furthermore, the Hsp90-dependent degradation of the mammalian von Hippel-Lindau tumor suppressor is abrogated in yeast lacking *SSE1*, indicating that Sse1p contributes to the turnover of this protein (McClellan *et al.*, 2005).

Subsequent studies then suggested that Hsp110 functionally cooperates with the Hsp70 system. Coimmunoprecipitation studies showed that mammalian Hsp110 forms high molecular weight complexes with Hsp70 and the sHsp Hsp25 *in vivo* as well as *in vitro* (Hatayama *et al.*, 1998; Wang *et al.*, 2000). Similarly, Sse1p was found to stably heterodimerize with Ssa1/2p and Ssb1/2p, while Sse2p only seems to bind to Ssa1p (Shaner *et al.*, 2005; Yam *et al.*, 2005; Shaner *et al.*, 2006). Taking into account the relative concentrations of Sse1p, Ssa1-4p, and Ssb1/2p in the cell, virtually the entire pool of cellular

Sse1p would conceivably be captured in these chaperone complexes. Whereas the Ssb1/2p·Sse1p complex was proposed to play a role in co-translational nascent chain stabilization, Ssa1-4p·Sse1p seems to act mostly at a post-translational stage to facilitate the folding of a more restricted protein subset. Since loss of Sse1p enhances polypeptide binding to both Ssa1p and Ssb2p, Sse1p has been suggested to work as an important regulator of the Hsp70/substrate interaction (Yam *et al.*, 2005). Consistent with this notion were the observations that (i) Lhs1p, the yeast Grp170 homolog, acts as a NEF on Kar2p, the yeast ER-resident Hsp70 (Steel *et al.*, 2004) and that (ii) Sse1p stimulates the steady state ATPase activity of Ssa1p synergistically with the type I J-protein Ydj1p (Shaner *et al.*, 2005).

Assumptions that Hsp110s might work as NEF for Hsp70s were affirmed by the Hartl and Bukau laboratories (Dragovic *et al.*, 2006a; Raviol *et al.*, 2006b). *In vitro*, yeast Sse1p exchanges nucleotide on Ssa1p as well as on Ssb1p, Sse2p catalyzes nucleotide exchange on Ssa1p and human Hsp110 on human Hsp70. This suggests a conserved interaction between Hsp110 and Hsp70 chaperones in all eukaryotes. In further support of this hypothesis, Sse1p is even able to exchange nucleotide on mammalian Hsc70. Protein truncation studies revealed the Hsp70 and Hsp110 regions that are necessary to form a functional heterodimeric complex: Whereas almost the entire Sse1p molecule is required for nucleotide exchange activity, the NBD of Hsc70 was shown to be sufficient for functional complex formation with Sse1p (Dragovic *et al.*, 2006a; Shaner *et al.*, 2006).

Along with nucleotide exchange, mammalian Hsp110 accelerates substrate release from the Hsp70 chaperone *in vitro*. Moreover, in concert with the respective Hsp70 and Hsp40 chaperones, Sse1p and Hsp110 promote the *in vitro* as well as the *in vivo* refolding of firefly luciferase with regard to both rate and yield (Dragovic *et al.*, 2006a; Raviol *et al.*, 2006b). Reports on an inhibitory effect of Hsp110 homologs on *in vitro* substrate refolding can be explained by differences in the experimental conditions (Yamagishi *et al.*, 2000; Shaner *et al.*, 2006). For example, the stoichiometry of Hsp110s and Hsp70s seems to be important for proper function because deletion as well as overexpression of *SSE1* is toxic for yeast (Shaner *et al.*, 2004; Dragovic *et al.*, 2006a). Two further observations support an *in vivo* role of Sse1p in a functional chaperoning complex with Ssa1p and Ydj1p: First, the budding yeast mating pheromone alpha factor precursor (pp $\alpha$ F), whose translocation into the ER is Ssa1p-dependent, accumulates in a  $\Delta$ *SSE1* strain and second, a  $\Delta$ *SSE1* $\Delta$ *YDJ1* strain is inviable (Shaner *et al.*, 2004; Shaner *et al.*, 2006).

Interestingly, the NEF function of Sse1p was recently also found to be required for efficient *de novo* formation as well as stable propagation of [*PSI*<sup>+</sup>], the prion form of the *S.*

*cerevisiae* translation release factor Sup35 (Fan *et al.*, 2007; Kryndushkin and Wickner, 2007; Sadlish *et al.*, 2008). Possibly, Sse1p exerts its function by increasing the cytosolic level of substrate-free Ssa1p, whose overexpression was shown to stimulate prion formation. In addition, Sse1p might promote the transition to the prion form in a NEF-independent manner by directly stabilizing early intermediates in the Sup35 prion conversion and thereby facilitating seed formation. Alternatively, Sse1p may also bind to existing prion fibers and thus inhibit the disaggregating curing function of Hsp104 (Sadlish *et al.*, 2008). Interestingly, in contrast to  $[PSI^+]$  propagation,  $[URE3]$  (the prion form of *S. cerevisiae* Ure2p) propagation is disrupted not only by depletion but also by overproduction of Sse1p. This indicates a highly prion-specific effect of Sse1p (Kryndushkin and Wickner, 2007).

Notably, the cytosolic NEFs Sse1p and Fes1p catalyze nucleotide exchange on the same Hsp70 partners. However, their functions seem to be only partially redundant. Overexpression of *FES1* rescues a  $\Delta SSE1\Delta SSE2$  strain, but not as effectively as expression of *SSE1*. Possibly, complexes of Hsp70 with Sse1p and Fes1p, respectively, are adapted to different substrate spectra. For example, being an Hsp70 family member, Sse1p might specifically recognize substrates (Dragovic *et al.*, 2006a; Dragovic *et al.*, 2006b).

## 2.6 Aim of the study

Recent studies have revealed that Hsp110 homologs trigger nucleotide exchange on canonical Hsp70s and support efficient folding of Hsp70 substrates *in vitro* as well as *in vivo* (Dragovic *et al.*, 2006a; Raviol *et al.*, 2006b). However, the mechanism by which Hsp70 and Hsp110 cooperate in protein folding is largely unclear. Specifically, it remains to be clarified how Hsp110s exchange nucleotide on their Hsp70 partners. Strikingly, almost the entire length of Sse1p (77 kDa) is required for functional interaction with Hsp70 (Dragovic *et al.*, 2006a). This is particularly surprising when considering that the much smaller BAG domain (13 kDa) is also sufficient for nucleotide exchange on Hsp70. Furthermore, the role of direct Hsp110/substrate interactions in Hsp70-mediated protein folding is still elusive. Possibly, additional Hsp110 functions beyond nucleotide exchange could explain why the NEF Fes1p cannot completely complement the loss of Hsp110 in yeast (Raviol *et al.*, 2006b). Finally, it is not clear yet whether Hsp70-like allosteric coupling between the Hsp110 NBD and PDB is required for Hsp110 function.

The goal of the present study was to solve the crystal structure of a complex between an Hsp110 and an Hsp70 protein, preferably using one of the best-studied systems, i.e. human

Hsp110 and Hsp70/Hsc70 or yeast Sse1p and Ssa1p/Ssb1p. The structure would open a rational strategy to investigate the cooperation between the two chaperones by mutational analysis. Specific amino acid exchanges at the interface between the two complex partners should reveal the structural requirements for nucleotide exchange by Hsp110 homologs. Mutations at the putative peptide binding site in the  $\beta$ -sandwich domain of the Hsp110 protein should clarify the role of direct Hsp110/substrate interactions. Amino acid exchanges at Hsp110 domain-domain interfaces should reveal whether inter-domain signaling is similarly important for Hsp110 as for Hsp70 chaperones. The combination of both structural and functional data should lead to a model for the cooperation of Hsp110 and Hsp70 in protein folding.

## 3 MATERIALS AND METHODS

### 3.1 Chemicals and biochemicals

Unless otherwise stated, chemicals were of *pro analysi* quality and purchased from **Sigma-Aldrich** (Steinheim, Germany) or **Merck** (Darmstadt, Germany).

**BioMol** (Hamburg, Germany): HEPES

**Bio-Rad** (München, Germany):

- Bradford protein assay reagent
- Ethidium bromide

**Biozym Scientific GmbH** (Hessisch Oldendorf, Germany): Agarose

**Clontech** (Heidelberg, Germany): Herring testis carrier DNA

**Difco** (Heidelberg, Germany):

- Bacto Agar
- Bacto Tryptone
- Bacto peptone
- Bacto Yeast Extract
- Bacto Yeast Nitrogen Base

**Dr. D.J. Thiele, Ph.D., Duke University Medical Center** (Durham, USA): pYEP-SSA3-*lacZ*

**Fermentas** (St. Leon-Rot, Germany):

- GeneRuler 1 kb DNA Ladder
- PageRuler Prestained Protein Ladder
- PageRuler Protein Ladder
- Restriction enzyme *EheI*

**Fluka** (Deisenhofen, Germany):

- ADA
- Bis-Tris
- H<sub>2</sub>O<sub>2</sub>
- Luminol
- polyethylene glycols of different molecular weights
- Sodium cacodylate

**GE Healthcare** (München, Germany):

- Chelating Sepharose

- Chloramphenicol
- DEAE-Sepharose
- MES

**Hampton Research** (Aliso Viejo, USA):

- Crystal Screen
- Crystal Screen 2
- Crystal Screen Lite
- Index Screen

**Invitrogen** (Karlsruhe, Germany): pPROEX HTb

**Dr. J.L. Brodsky** (University of Pittsburgh, Pittsburgh, USA):

- 6-carboxyfluorescein labeled peptide LICGFRVFLMYRF
- Unlabeled LICGFRVFLMYRF

**J.M. Gabler Saliter GmbH & Co. KG** (Obergünzburg, Germany): Skim milk powder

**JPT Peptide Technologies GmbH** (Berlin, Germany): Luciferase peptide membrane

**Metabion** (Martinsried, Germany):

- dNTPs
- *mi*-Plasmid Miniprep Kit
- oligonucleotides (primers)
- oligopeptide dansyl-NRLLLTGC

**Mo Bi Tec** (Göttingen, Germany): MABA-ATP

**MPI for Biochemistry, Department of Cellular Biochemistry** (Martinsried, Germany):

Protein complex screen (Radaev and Sun, 2002; Radaev *et al.*, 2006)

**MPI for Biochemistry, Core Facility** (Martinsried, Germany): Oligopeptides

**New England Biolabs** (Frankfurt am Main, Germany):

- BSA
- Restriction endonucleases
- T4 DNA ligase
- Vent DNA polymerase

**Promega** (Mannheim, Germany):

- Luciferase Assay System (#E1501)
- *Pfu* polymerase
- PureYield Plasmid Midiprep System
- *Taq* polymerase
- Wizard *Plus* SV Minipreps DNA Purification System

- Wizard SV Gel and PCR Clean-Up System

**Qiagen** (Hilden, Germany):

- Crystallization Screen NeXtal ProComplex Suite
- Qiagen Plasmid Midi Kit
- QIAprep Spin Miniprep Kit

**Roche** (Basel, Switzerland):

- AMP-PNP
- Benzonase
- DTT
- EDTA-free Complete protease inhibitor cocktail
- Expand Long Template PCR System
- Hexokinase
- Proteinase K
- Shrimp alkaline phosphatase

**Roth** (Karlsruhe, Germany):

- Ampicilin
- IPTG

**Serva** (Heidelberg, Germany):

- Acrylamide-Bis
- BSA (fraction V)
- Coomassie Blue R250
- PMSF
- SDS

**Stratagene** (Heidelberg, Germany): Herculase Enhanced DNA Polymerase

### 3.2 Antibodies

Rabbit polyclonal Hsp12 antibody:

generous gift from **Dr. M. Haslbeck** (TU München, Germany), dilution 1:2000

Rabbit polyclonal Hsp42 antibody:

generous gift from **Dr. M. Haslbeck** (TU München, Germany), dilution 1:2000

Mouse monoclonal Hsp70 (MA3-007) antibody:

**Thermo Fisher Scientific** (Waltham, USA), dilution 1:1000

|  |   |
|--|---|
| Rabbit polyclonal Hsp104 (PA3-016) antibody: | <b>Thermo Fisher Scientific</b> (Waltham, USA), dilution 1:2430   |
| Rabbit polyclonal Ssa1 antibody:             | <b>Dr. K. Siegers, MPI for Biochemistry</b> (Martinsried, Germany), dilution 1:5000                     |
| Rabbit polyclonal Ssa3/Ssa4 antibody:        | generous gift from <b>Dr. E. Craig</b> (University of Wisconsin, Madison, USA), dilution 1:2000         |
| Rabbit polyclonal Sse1 antibody:             | <b>Dr. Z. Dragovic, MPI for Biochemistry</b> (Martinsried, Germany), dilution 1:5000                    |
| Goat polyclonal Ydj1 (yN-18) antibody:       | <b>Santa Cruz Biotechnology, inc.</b> (Heidelberg, Germany), dilution 1:133                             |
| Rabbit polyclonal luciferase antibody:       | <b>Department of Cellular Biochemistry, MPI for Biochemistry</b> (Martinsried, Germany), dilution 1:500 |
| Mouse polyclonal PGK antibody:               | <b>Invitrogen</b> (Karlsruhe, Germany), dilution 1:3333   |
| HRP-conjugated secondary antibodies:         | <b>Sigma-Aldrich</b> (Steinheim, Germany), dilution 1:3333  |

### 3.3 Strains

| Strain                             | Genotype  | Origin                              |
|------------------------------------|---|-------------------------------------|
| <b><i>E. coli</i></b>              |   |                                     |
| DH5 $\alpha$                       | <i>supE44</i> $\Delta$ <i>lacU169</i> ( $\phi$ 80 <i>lacZ</i> $\Delta$ <i>M15</i> ) <i>hsdR17</i><br><i>recA1</i> <i>endA1</i> <i>gyrA96</i> <i>thi-1</i> <i>relA1</i>  | Invitrogen<br>(Karlsruhe, Germany)  |
| BL21<br>(DE3)                      | B F <sup>-</sup> <i>ompT</i> <i>hsdS</i> (r <sub>B</sub> <sup>-</sup> m <sub>B</sub> <sup>-</sup> ) <i>dcm</i> <sup>+</sup> <i>gal</i> $\lambda$ (DE3)  | Stratagene<br>(Heidelberg, Germany) |
| BL21<br>(DE3)<br>codon plus<br>RIL | B F <sup>-</sup> <i>ompT</i> <i>hsdS</i> (r <sub>B</sub> <sup>-</sup> m <sub>B</sub> <sup>-</sup> ) <i>dcm</i> <sup>+</sup> Tet <sup>r</sup><br><i>gal</i> $\lambda$ (DE3) <i>endA</i> Hte [ <i>argU</i> <i>ileY</i> <i>leuW</i> Cam <sup>r</sup> ] | Stratagene<br>(Heidelberg, Germany) |
| <b>Yeast</b>                       |   |                                     |
| YPH499                             | <i>MAT</i> $\alpha$ <i>ade2-101</i> <sup>ochre</sup> <i>his3</i> $\Delta$ 200 <i>leu2</i> $\Delta$ 1<br><i>lys2-801</i> <sup>amber</sup> <i>trp1</i> $\Delta$ 63 <i>ura3-52</i>   | Sikorski and Hieter,<br>1989        |

| Strain | Genotype   | Origin  |
|--------|--|---|
| SB472  | <i>MAT<math>\alpha</math> ade2-101<sup>ochre</sup> his3<math>\Delta</math>200 leu2<math>\Delta</math>1 lys2-801<sup>amber</sup> trp1<math>\Delta</math>63 ura3-52 sse1::His3 sse2::KanMX4 pCM189-SSE1-URA3</i> | Dr. S. A. Schäuffelhut, MPI for Biochemistry (Martinsried, Germany) |
| SB537  | <i>MAT<math>\alpha</math> ade2-101<sup>ochre</sup> his3<math>\Delta</math>200 leu2<math>\Delta</math>1 lys2-801<sup>amber</sup> trp1<math>\Delta</math>63 ura3-52 sse1::His3</i>                               | Dr. S. A. Schäuffelhut, MPI for Biochemistry (Martinsried, Germany) |
| MW141  | <i>MAT<math>\alpha</math> his3-11,15 leu2-3,112 trp1 ura3-52 ssa1::HIS3 ssa2::LEU2 ssa4::URA3 pGal1-SSAI</i>   | Deshaies <i>et al.</i> , 1988                                       |

### 3.4 Media and buffers

#### 3.4.1 Media

Unless otherwise stated, media were prepared with deionized water and autoclaved after preparation.

**LB medium:** 10 g/l Bacto Tryptone  
5 g/l Bacto Yeast Extract  
10 g/l NaCl  
(15 g/l agar for solid medium)  
adjust pH 7.0 with 5 M NaOH

**M9 minimal medium:** 775 ml H<sub>2</sub>O (autoclaved)  
20 ml 20 % (w/v) glucose (sterile-filtered)  
2 ml 1 M MgSO<sub>4</sub> (autoclaved)  
0,1 ml 1 M CaCl<sub>2</sub> (autoclaved)  
200 ml 5x M9 salts (autoclaved)

**5x M9 salts:** 64 g/l Na<sub>2</sub>HPO<sub>4</sub>·7H<sub>2</sub>O  
15 g/l KH<sub>2</sub>PO<sub>4</sub>  
2,5 g/l NaCl  
5 g/l NH<sub>4</sub>Cl

- Psi broth:** 5 g/l Bacto Yeast Extract  
20 g/l Bacto Tryptone  
5 g/l MgSO<sub>4</sub>  
adjust pH 7.6 with 5 M KOH
- SC medium (1 l):** 6,7 g/l Bacto Yeast Nitrogen Base  
2 g/l drop-out mix (see below)  
adjust pH 5.6, autoclave  
  
50 ml 40 % (w/v) glucose (sterile-filtered)  
  
if required:  
55.3 mg/l adenine (autoclaved)  
22.4 mg/l uracil (autoclaved)  
219.0 mg/l L-leucine (autoclaved)  
62.9 mg/l L-histidine (autoclaved)  
182.6 mg/l L-lysine (autoclaved)  
81.7 mg/l L-tryptophane (sterile-filtered)
- SC plates:** as SC medium, but add 20 g/l agar  
Agar solution and Bacto Yeast Nitrogen Base/drop-out mix solution need to be autoclaved separately to prevent acidic hydrolysis of the agar, which would occur due to the low pH of the Bacto Yeast Nitrogen Base/drop-out mix solution.
- 5-FOA medium/plates:** as SC medium/plates, but add 1 g/l 5-FOA after autoclaving
- Drop-out mix:** 5 g of each to the following L-amino acids: alanine, arginine, asparagine, aspartic acid, cysteine, glutamine, glutamic acid, glycine, isoleucine, methionine, phenylalanine, proline, serine, threonine, tryptophane, tyrosine  
5 g myo-inositol  
0.5 g p-aminobenzoic acid  
triturate to homogeneity, store as powder  
  
The following compounds are prepared separately:

| compound | final conc.<br>in SC medium<br>(mg/l) | stock<br>solution<br>(g/l) | volume<br>to pipette<br>in SC<br>medium<br>(ml/l) | comment   |
|----------|---------------------------------------|----------------------------|---|---|
| adenine  | 55.3                                  | 5.53                       | 10.0  | heat up for<br>dissolving                             |
| uracil   | 22.4                                  | 2.24                       | 10.0  | heat up in<br>NaHCO <sub>3</sub><br>for<br>dissolving |
| L-Leu    | 219.0                                 | 13.20                      | 16.6  | heat up for<br>dissolving                             |
| L-His    | 62.9                                  | 12.57                      | 5.0   | -   |
| L-Lys    | 182.6                                 | 18.26                      | 10.0  | -   |
| L-Trp    | 81.7                                  | 8.17                       | 10.0  | sterile filter  |

**YPD medium (1 l):** 10 g/l Bacto Yeast Extract  
20 g/l Bacto Peptone  
50 ml 40 % (w/v) glucose (sterile-filtered)  
(10 g/l agar for solid medium)

**YP-gal medium (1 l):** 10 g/l Bacto Yeast Extract  
20 g/l Bacto Peptone  
50 ml 40 % (w/v) galactose (sterile-filtered)  
(10 g/l agar for solid medium)

### 3.4.2 Buffers and standard solutions

Buffers were prepared with deionized water (electrical resistance 18.2 MΩ·cm).

**Alkaline lysis buffer:** 1.85 M NaOH  
1 M β-mercaptoethanol

---

|                                      |   |
|--------------------------------------|---|
| <b>Antibiotic solutions (1000x):</b> | 100 mg/ml ampicillin<br>28 mg/ml chloramphenicol<br>25 mg/ml kanamycin                  |
| <b>ATP buffer:</b>                   | 50 mM HEPES-NaOH pH 7.4<br>20 mM NaCl<br>2 mM MgCl <sub>2</sub><br>2 mM DTT<br>3 mM ATP |
| <b>Buffer A:</b>                     | 10 mM HEPES-KOH pH 7.5<br>10 mM KCl<br>1 mM MgCl <sub>2</sub>                           |
| <b>Buffer A1:</b>                    | 25 mM HEPES-NaOH pH 7.5<br>10 mM NaCl<br>4 mM MgCl <sub>2</sub>                         |
| <b>Buffer C:</b>                     | 10 mM K-phosphate pH 7.5<br>0.5 mM MgCl <sub>2</sub><br>0.5 mM ATP                      |
| <b>Buffer D:</b>                     | 10 mM HEPES-NaOH pH 7.5<br>150 mM NaCl<br>5 mM EDTA<br>5 mM β-mercaptoethanol           |
| <b>Buffer E:</b>                     | 10 mM HEPES-NaOH pH 7.5<br>150 mM NaCl<br>4 mM MgCl <sub>2</sub>                        |
| <b>Buffer L:</b>                     | 25 mM HEPES-KOH pH 7.5<br>300 mM KCl<br>4 mM MgCl <sub>2</sub>                          |

---

|                                      |  |
|--------------------------------------|--|
| <b>Buffer L1:</b>                    | 25 mM HEPES-NaOH pH 7.5<br>300 mM NaCl<br>4 mM MgCl <sub>2</sub>                             |
| <b>Buffer R:</b>                     | 25 mM HEPES-KOH pH 7.8<br>50 mM KCl<br>5 mM MgOAc<br>1 mM DTT                                |
| <b>Buffer S:</b>                     | 50 mM HEPES-NaOH pH 7.4<br>500 mM NaCl<br>2 mM MgCl <sub>2</sub><br>2 mM DTT                 |
| <b>Buffer Z:</b>                     | 100 mM Na-phosphate pH 7.0<br>10 mM KCl<br>1 mM MgSO <sub>4</sub><br>50 mM β-mercaptoethanol |
| <b>Coomassie destainig solution:</b> | 10 % (v/v) ethanol<br>10 % (v/v) acetic acid   |
| <b>Coomassie stainig solution:</b>   | 0.1 % (w/v) Serva Coomassie Blue R250<br>40 % (v/v) ethanol<br>10 % (v/v) acetic acid        |
| <b>DEAE buffer:</b>                  | 25 mM HEPES-KOH pH 7.4<br>20 mM KCl<br>4 mM MgCl <sub>2</sub><br>2 mM DTT<br>1 mM ATP        |

---

|                                 |  |
|---------------------------------|--|
| <b>DNA-loading buffer (6x):</b> | 0.25 % (w/v) bromophenol blue<br>0.25 % (w/v) xylene cyanol FF<br>40 % (w/v) sucrose in H <sub>2</sub> O   |
| <b>ECL solution I:</b>          | 100 mM Tris-HCl pH 8.8<br>2.5 mM luminol (3-aminophthalhydrazid; stock: 250 mM in DMSO, dark, 4 °C)<br>0.4 mM p-coumaric acid (stock: 90 mM in DMSO, dark, 4 °C) |
| <b>ECL solution II:</b>         | 100 mM Tris-HCl pH 8.5<br>5.4 mM H <sub>2</sub> O <sub>2</sub>   |
| <b>Glycerol buffer:</b>         | 50 % (v/v) glycerol in buffer R  |
| <b>GTP buffer:</b>              | 50 mM HEPES-NaOH pH 7.4<br>20 mM NaCl<br>2 mM MgCl <sub>2</sub><br>2 mM DTT<br>1 mM GTP  |
| <b>HKM2 buffer:</b>             | 10 mM HEPES-KOH pH 7.4<br>150 mM KCl<br>1 mM MgCl <sub>2</sub>   |
| <b>HKM3 buffer:</b>             | 10 mM HEPES-KOH pH 7.4<br>150 mM KCl<br>4 mM MgCl <sub>2</sub>   |
| <b>PBS (10x):</b>               | 92 mM Na <sub>2</sub> HPO <sub>4</sub> ·2H <sub>2</sub> O<br>16 mM NaH <sub>2</sub> PO <sub>4</sub> ·H <sub>2</sub> O<br>1.5 M NaCl<br>adjust pH 7.2 with NaOH   |

---

|                                  |  |
|----------------------------------|--|
| <b>PBST:</b>                     | 1x PBS<br>0.1 % (v/v) Tween 20   |
| <b>Ponceau S stain:</b>          | 0.2 % (w/v) Ponceau S<br>3 % (v/v) trichloro acetic acid   |
| <b>Protoplast buffer:</b>        | 100 mM Tris-HCl pH 7.5<br>10 mM EDTA<br>143 mM $\beta$ -mercaptoethanol<br>0.2 mg/ml Zymolyase 20T<br>0.1 mg/ml RNaseA |
| <b>Regeneration buffer A:</b>    | 8 M urea<br>1 % (w/v) SDS<br>0.1 % (v/v) $\beta$ -mercaptoethanol  |
| <b>Regeneration buffer B:</b>    | 400 ml H <sub>2</sub> O<br>500 ml ethanol<br>100 ml acetic acid  |
| <b>SDS-loading buffer (2x):</b>  | 100 mM Tris-HCl pH 6.8<br>4 % (w/v) SDS<br>200 mM DTT<br>20 % (v/v) glycerol<br>0.2 % (w/v) bromphenolblue             |
| <b>SDS-running buffer (10x):</b> | 250 mM Tris<br>2.5 M glycine<br>1 % (w/v) SDS  |
| <b>Stripping buffer:</b>         | 62.5 mM Tris-HCl pH 6.7<br>100 mM $\beta$ -mercaptoethanol<br>2 % (w/v) SDS  |

---

|                                 |   |
|---------------------------------|---|
| <b>TAE buffer (50x):</b>        | 2 M Tris-acetate<br>50 mM EDTA pH 8.0   |
| <b>TBS (10x):</b>               | 500 mM Tris-HCl pH 8.0<br>1.37 M NaCl<br>27 mM KCl  |
| <b>TBST (10x):</b>              | 200 mM Tris-HCl pH 7.5<br>1.37 M NaCl<br>1 % (v/v) Tween 20   |
| <b>TfbI buffer (200 ml):</b>    | 30 mM K-acetate<br>100 mM RbCl<br>10 mM CaCl <sub>2</sub><br>15 % (v/v) glycerol<br>adjust pH 5.8 with 0.1 M acetic acid<br>adjust final volume of 180 ml with deionized H <sub>2</sub> O<br>autoclave<br>add 20 ml of sterile-filtered 500 mM MnCl <sub>2</sub> ·2H <sub>2</sub> O |
| <b>TfbII buffer:</b>            | 10 mM MOPS<br>75 mM CaCl <sub>2</sub><br>10 mM RbCl <sub>2</sub><br>15 % glycerol<br>adjust pH 6.5 with 0.1 M NaOH<br>sterile filter  |
| <b>Urea-SDS-loading buffer:</b> | 200 mM Tris-HCl pH 6.8<br>8 M urea<br>5 % (w/v) SDS<br>0.1 mM EDTA<br>143 mM β-mercaptoethanol<br>0.03 % (w/v) bromphenolblue   |

|                              |                     |
|------------------------------|---------------------|
| <b>Western Blot buffer:</b>  | 50 mM Tris          |
|                              | 20 % (v/v) methanol |
|                              | 192 mM glycine      |
| <b>Yeast lysis solution:</b> | 0.2 M NaOH          |
|                              | 1 % (w/v) SDS       |

### 3.5 Materials and Instruments

**Agilent Technologies** (Santa Clara, USA): variable wavelength detector Agilent 1100 series

**Applied Photophysics** (Surrey, UK): SX.18V stopped-flow instrument

**Bachofer** (Reutlingen, Germany): Hybridization oven

**B. Braun Melsungen AG** (Melsungen, Germany): Orbital shaker Certomat R

**Beckman Coulter GmbH** (Krefeld, Germany):

- Centrifuges (GS-6R, Allegra-6R, Avanti J-25 with rotors JLA 10.500 and JA 25.50, J6-MI with rotor JS 4.2)
- DU 640 UV/VIS Spectrophotometer
- DU 800 UV/VIS Spectrophotometer
- Optima LE 80K ultracentrifuge with rotor 45 Ti

**Berthold** (Huntsville, USA): Luminometer LB9507

**Biometra** (Göttingen, Germany): PCR thermocycler

**Bio-Rad** (München, Germany):

- Gene Pulser Xcell electroporation system with electroporation cuvettes (0.1 cm)
- Horizontal agarose gel electrophoresis system (Wide) Mini-SUB CELL GT
- Mini Protean II electrophoresis cell
- Power Pac 300

**BioScience, Inc.** (Salt Lake City, USA): Pre-lubricated Sorenson safe seal microcentrifuge tubes, RNase/DNase-free

**Biospec** (Bartlesville, USA): Bead Beater

**Eppendorf** (Hamburg, Germany):

- Centrifuges (5415D and 5417R)
- Pipettes (2.5, 10, 20, 100, 200, 1000 µl)
- Thermomixer comfort

**Fisher Scientific** (Schwerte, Germany): Accumet Basic pH meter

**Fuji/Raytest** (Straubenhardt, Germany):

- Fuji-LAS3000 luminescence and densitometry system with Image Reader LAS-3000
- Gel imaging software: AIDA v.3.5.0

**GE Healthcare** (München, Germany):

- Äkta FPLC
- Äkta Purifier
- Electrophoresis Power Supply – EPS 600
- Ettan LC
- Prepacked chromatography columns (HiLoad 16/60 Superdex 200 prep grade, HiLoad 26/60 Superdex 200 prep grade, HiPrep 26/10 Desalting, HiTrap Chelating HP, MonoQ HR 10/10, MonoQ HR 10/16, NAP-5 Sephadex G25 desalting column, NAP-10 Sephadex G25 desalting column, NAP-25 Sephadex G25 desalting column, Superose 12 PC 3.2/30, Superose 12 HR 10/30)

**Hampton Research** (Aliso Viejo, USA):

- Cryo tong
- Magnetic wand
- Mounted cryo loops
- Siliconized glass square cover slides (22 mm)
- VDX Plate with sealant

**Heidolph** (Schwabach, Germany): Heatable magnetic stirrer**Hellma** (Mühlheim, Germany): Quartz cells**Heraeus** (Hanau, Germany): Function line incubator**Horiba Jobin Yvon GmbH** (München, Germany): Spex Fluorolog 3 (with software FluorEssence)**Jasco** (Groß-Umstadt, Germany):

- J-715 spectrometer with peltier-thermostat
- UV/VIS spectrophotometer V-560

**Mettler Toledo** (Gießen, Germany): Balances (AG285 and PB602)**Millipore** (Schwalbach, Germany):

- Centriprep concentrators (10.000 and 30.000 Da MWCO)
- Steritop Filtration System (pore size 0.22 µm)

**Misonix** (Farmingdale, USA): Sonicator 3000**Molecular Dimensions Limited** (Cambridgeshire, Great Britain):

- Magnetic cryo vials and cryo caps with data matrix

- ESRF sample changer kit

**MPI for Biochemistry** (Martinsried, Germany): Western Blot system (semi-dry)

**MWG AG Biotech** (Ebersberg, Germany): Gel documentation system

**New Brunswick Scientific** (Nürtingen, Germany): Innova 44 incubator shaker

**Olympus Corporation** (Tokyo, Japan): Stereo-zoom microscopes SZXZ-ILLK and SZH-ILLK200

**Sartorius** (Göttingen, Germany):

- Laboratory water purification system Arium
- Sterile filters Minisart (pore size 0.22 and 0.45  $\mu\text{m}$ )
- Vivaspin 500 concentrators (10.000 and 30.000 Da MWCO)
- Vivaspin 20 concentrators (10.000 and 30.000 Da MWCO)

**Scientific Industries, Inc.** (Bohemia, USA): Vortex-Genie 2

**Taylor-Wharton** (Theodore, USA): Dry shippers

**Whatman GmbH** (Dassel, Germany): Whatman Protran nitrocellulose transfer membrane

**Wyatt Technology** (Santa Barbara, USA):

- FFF-MALS with DAWN EOS MALS detector and Optilab DSP refractive index detector
- software ASTRA

## 3.6 Molecular biological methods

### 3.6.1 DNA analytical methods

#### 3.6.1.1 DNA quantification

DNA concentrations were determined by UV spectroscopy. DNA solutions were appropriately diluted with water, and DNA-free water served as a reference. At a wavelength of 260 nm, one absorption unit corresponds to 50 ng/ $\mu\text{l}$  double stranded DNA in water. The absorbance ratio 260/280 nm for pure DNA should be approximately 1.85. Deviations from this value indicate quality deficiencies caused by impurities such as RNA or protein (Sambrook *et al.*, 1989).

#### 3.6.1.2 Agarose gel electrophoresis

Agarose gels contained 0.8 % (w/v) agarose in 1x TAE buffer. Agarose was melted by heating. For the visualization of double stranded DNA, 1  $\mu\text{g/ml}$  ethidium bromide was added.

Prior to being loaded on the gel, DNA samples were mixed with 6x DNA-loading buffer. Agarose gel electrophoresis was performed in 1x TAE buffer at a constant voltage of 80 V.

### 3.6.1.3 DNA sequencing

The integrity of all plasmid inserts was verified by DNA sequencing performed by the sequencing service of the Core Facility of the MPI for Biochemistry in Martinsried. For one sequencing reaction, approximately 5 µl of 100 ng/µl plasmid are needed. Sequencing chromatograms were checked with the help of the program Chromas (C. McCarthy, Griffith University, Australia), and comparative sequence analysis was performed using the MultAlin analysis program (Corpet, 1988; <http://bioinfo.genopole-toulouse.prd.fr/multalin/multalin.html>).

### 3.6.2 Purification of DNA fragments and plasmid DNA

For purification of DNA fragments after agarose gel electrophoresis (e.g. after PCR, see chapter 3.6.4) or after enzymatic reactions (e.g. after restriction digest, see chapters 3.6.5 and 3.6.6), anion exchange chromatography was conducted using the Wizard SV Gel and PCR Clean-Up System. Differing from the producer's recommendations, only one washing step with 500 µl of Membrane Wash Solution was performed.

For isolation and purification of plasmid DNA from overnight *E. coli* DH5a cultures, the QIAprep Spin Miniprep Kit, the Wizard *Plus* SV Miniprep DNA Purification System, the *mi*-Plasmid Miniprep Kit, or the Qiagen Plasmid Midi Kit was used according to the manufacturer's instructions.

### 3.6.3 Cloning strategies

To construct *sse1-Δloop*, in which *SSE1* codons 503-524 are replaced by four codons (GCCGGATCCGAG, GGATCC: *Bam*HI restriction site) coding for AGSD, pProEX-*SSE1* (Dragovic *et al.*, 2006a) was used as a template. The C-terminal *SSE1* fragment (residues 525-693) was cloned into the expression plasmid pProEX HTb (Invitrogen) using the restriction sites for *Bam*HI and *Xho*I. This construct was digested with *Bam*HI, and the N-terminal *SSE1* fragment (residues 1-502), which was amplified with primers providing restriction sites for *Ehe*I and *Bam*HI, was ligated to its C-terminal counterpart. Then, the whole *sse1-Δloop*

construct was amplified *via* PCR and cloned into pPROEX HTb using the *EheI* and *XhoI* restriction sites. A list of the utilized primers can be found in chapter 7.1.

*SsaIN* (codons 1-378 from *SSAI*) was amplified from pPROEX-*SSAI* (Shomura *et al.*, 2005) and cloned into pPROEX HTb between the restriction sites for *BamHI* and *XhoI*.

*SSE2* was amplified from yeast genomic DNA (YPH499) and cloned into pPROEX HTb between the restriction sites for *EheI* and *XhoI*.

Point mutants of *SSE1*, *SSAI*, and *ssaIN* were produced *via* a polymerase chain reaction (PCR)-based mutagenesis strategy, which relies on the amplification of the respective full-length plasmid (pPROEX-*SSE1*, pPROEX-*SSAI*, pPROEX-*ssaIN*) using blunt end primers containing the required nucleotide alterations (Weiner *et al.*, 1994). Nucleotides that diverge from the wt DNA sequences were always introduced in the forward primer.

Yeast expression plasmids for the Sse1p variants were constructed as follows: The coding regions for wildtype (wt) and mutant variants of Sse1p were excised from the pPROEX expression plasmids by digestion with *EheI* and *XhoI* and inserted into the yeast expression plasmid pRS415ADH (Sikorski and Hieter, 1989; Mumberg *et al.*, 1995) complementarily cleaved with *SmaI* and *XhoI*. Amplification of the constructed yeast expression plasmids was performed in *E. coli* DH5 $\alpha$  cells.

The pPROEX expression plasmids for His<sub>6</sub>-Sse1p, His<sub>6</sub>-Sse1C, His<sub>6</sub>-Hsp110 (Dragovic *et al.*, 2006a), His<sub>6</sub>-Ssa1p, His<sub>6</sub>-Fes1p (Shomura *et al.*, 2005), and His<sub>6</sub>-Hsp70N (Becker *et al.*, 2002) have been described previously. The yeast expression plasmids pGal1-*SSAI* (Deshaies *et al.*, 1988) and pCM189-*SSE1* (Dragovic *et al.*, 2006a) have been described as well. The pPROEX-expression plasmids for His<sub>6</sub>-Ssb1N and His<sub>6</sub>-Ydj1p were cloned by Dr. A. Bracher and N. Tzvetkov, respectively (both MPI for Biochemistry, Martinsried, München).

The sequences of all plasmids generated in this study were confirmed by DNA sequencing.

### 3.6.4 Polymerase chain reaction

Amplification of DNA fragments was achieved by PCR. To amplify *sse1- $\Delta$ loop* (Sse1 $\Delta$ (503-524)) and *ssaIN* (NBD of Ssa1p) from plasmid DNA, the *Pfu* polymerase was utilized. In contrast, the Expand Long Template PCR System (Roche) was used for the amplification of *SSE2* from genomic DNA as well as for the PCR-based site-directed mutagenesis on *SSE1* and *SSAI*. The Expand Long Template PCR System is a mix of *Taq* DNA polymerase and the proofreading *Tgo* DNA polymerase, which is optimized to efficiently amplify large and

genomic DNA fragments. The compositions of the different PCR solutions and the conditions for the thermal cycling are summarized in Table 3-1 and Table 3-2, respectively. Primers are listed in chapter 7.1. PCR products were analyzed by agarose gel electrophoresis, excised from the gel, and purified.

**Table 3-1: PCR mixtures.**

| Solution components | Amplification of <i>sse1-<math>\Delta</math>loop</i> and <i>ssa1N</i> | Amplification of <i>SSE2</i> and site-directed mutagenesis  |
|---------------------|---|---|
| template DNA        | 100 ng plasmid DNA  | 100 ng genomic ( <i>SSE2</i> ) or plasmid DNA (mutagenesis) |
| primers             | 0.5 $\mu$ M each  | 0.8 $\mu$ M each  |
| dNTPs               | 200 $\mu$ M each  | 250 $\mu$ M each  |
| polymerase          | 3 U <i>Pfu</i> DNA polymerase   | 4.38 U Expand Long Template polymerase                      |
| polymerase buffer   | 1x <i>Pfu</i> buffer  | 1x Expand Long Template buffer 1                            |
| total volume        | 50 $\mu$ l  | 50 $\mu$ l  |

**Table 3-2: Thermal cycling conditions for PCR amplification.**

|           | Step | Purpose              | Amplification of <i>sse1-<math>\Delta</math>loop</i> and <i>ssa1N</i> |           | Amplification of <i>SSE2</i> and site-directed mutagenesis |             |
|-----------|------|----------------------|---|-----------|--|-------------|
|           |      |                      | temperature   | duration  | temperature  | duration    |
|           | 1    | initial denaturation | 95 °C   | 2 min     | 95 °C  | 5 min       |
| 30 cycles | 2    | cycle denaturation   | 95 °C   | 1 min     | 95 °C  | 30 s        |
|           | 3    | primer annealing     | 50 °C   | 30 s      | 52 °C  | 45 s        |
|           | 4    | primer extension     | 72 °C   | ~1 min/kb | 72 °C  | ~1.5 min/kb |
|           | 5    | final extension      | 72 °C   | 4 min     | 72 °C  | 10 min      |
|           | 6    | cooling              | 4 °C  | $\infty$  | 4 °C   | $\infty$    |

### 3.6.5 Restriction digest and DNA ligation

For the cloning of *sse1-Δloop*, *ssa1N*, and *SSE2*, purified PCR products (45 μl, see chapter 3.6.4) or plasmid DNA (1-1.5 μg) were digested with 1 μl of the respective restriction enzyme/s (see chapter 7.1) in a total volume of 60 μl. Digests were performed in the recommended reaction buffers and in presence of 6 μg BSA at 37 °C for 1 h. While digested PCR products were directly purified by anion exchange chromatography, linearized plasmids were separated from the excised segment by agarose gel electrophoresis prior to purification.

Purified insert and plasmid DNA – both dissolved in water – were used for ligation. Approximately 100 ng of digested plasmid DNA (pProEX HTb) and an approximately five-fold excess of complementarily digested DNA insert were incubated with 200 U of T4 DNA ligase in a total volume of 10 μl. The reaction was performed in T4 DNA ligase reaction buffer for 2-5 h at room temperature (RT). Afterwards the reaction mix was transformed in *E. coli* DH5α cells (see chapters 3.6.7.1 and 3.6.7.2). The integrity of the inserts was checked by restriction analysis and subsequent DNA sequencing. In the restriction analysis, 5 μl of the constructed plasmids were incubated with 0.25 μl of the respective restriction enzymes and 5 μg BSA in a total volume of 20 μl at 37 °C for 1 h.

### 3.6.6 Site-directed mutagenesis

For the generation of pProEX expression plasmids of Sse1p and Ssa1p mutants, the purified PCR products generated by whole plasmid PCR (see Table 3-1 and Table 3-2 in chapter 3.6.4) were incubated with *DpnI*. *DpnI* digests methylated DNA and thus degrades the template DNA. In contrast, the non-methylated linear PCR products bearing the intended point mutations were left intact. For digestion, 44 μl of purified PCR product were incubated with 20 U of *DpnI* in NEB buffer 4 for 1 h at 37 °C. The total reaction volume was 50 μl. After enzyme inactivation for 20 min at 80 °C and DNA purification, the mutated linear sequences were circularized by ligation: In 10 μl reactions, 8 μl of DNA were incubated with 400 U of T4 DNA ligase in T4 DNA ligase reaction buffer. Ligation was performed for at least 3 h at RT. For amplification, the ligation product was transformed into electrocompetent *E. coli* DH5α cells (see chapter 3.6.7.2). The integrity of the insert was checked by restriction analysis (see chapter 3.6.5) and subsequent DNA sequencing.

### 3.6.7 Preparation and transformation of competent *E. coli* cells

#### 3.6.7.1 Chemocompetent *E. coli* cells and chemical transformation

Chemically competent *E. coli* cells were prepared by the RbCl-method (Hanahan, 1983). 100 ml of Psi broth were inoculated with 1 ml of an overnight culture of the respective strain and incubated at 37 °C to an OD<sub>550</sub> of 0.48. While being chilled on ice for 15 min, the culture was mixed frequently to speed up the cooling process. Then, the culture was transferred into two 50 ml-Falcon tubes and spun in a Beckman GS-6R centrifuge for 20 min at 3400 rpm and 0 °C. The supernatant was discarded, and the pellet was resuspended in 40 ml of sterile, pre-chilled TfbI buffer. After incubation on ice for 15 min, cells were centrifuged again (10 min, 3400 rpm, 0 °C), gently resuspended in 4 ml of sterile, pre-chilled TfbII buffer, and incubated on ice for 15 min. 50 µl aliquots were pipetted into Eppendorf tubes pre-chilled at -20 °C, immediately frozen in liquid nitrogen and stored at -80 °C.

For transformation, 50 µl of chemically competent *E. coli* cells were thawed on ice and mixed with 50-100 ng plasmid DNA or 5 µl ligation reaction. After incubation on ice for 30 min, cells were heat-shocked at 42 °C for 45 s or at 37 °C for 5 min and subsequently cooled on ice for 2 min. Next, cells were diluted with 950 µl of LB medium and incubated in a shaker for 1 h at 37 °C. For plasmid amplification in DH5α, cells were centrifuged in a table centrifuge (Eppendorf 5415D) at 5000 rpm for 2 min, resuspended in approximately 100 µl of medium, plated on selective LB agar plates, and incubated overnight at 37 °C. Plasmid isolation from liquid overnight cultures was performed as described in chapter 3.6.2. For protein overexpression in a BL21 strain (see chapter 3.7.1), 1 l of LB medium supplemented with the required antibiotics was directly inoculated with 300-1000 µl of the transformation mixture followed by overnight incubation at 30, 34, or 37 °C to an OD<sub>600</sub> of 0.6.

#### 3.6.7.2 Electrocompetent *E. coli* cells and electroporation

For the preparation of electrocompetent *E. coli* DH5α cells, 500 ml of LB medium were inoculated with 5 ml of an overnight culture of the strain and grown at 37 °C to an OD<sub>600</sub> of 0.7. Cells were chilled on ice for 15 min and pelleted by centrifugation for 20 min at 4200 rpm and 4 °C (Beckmann centrifuge Avanti J-25 with rotor JS 4.2). Cells were washed with (i) 500 ml of ice-cold autoclaved water and with (ii) 250 ml of 10 % (v/v) ice-cold sterile glycerol. Then, cells were resuspended in 10 ml of 10 % (v/v) ice-cold sterile glycerol and centrifuged for 20 min at 6400 rpm and 4 °C (Beckmann centrifuge Avanti J-25 with rotor JA 25.50). Finally, cells were resuspended in 1.5 ml of 10 % (v/v) ice-cold sterile glycerol. 40 µl

aliquots were pipetted into Eppendorf tubes pre-chilled at  $-20\text{ }^{\circ}\text{C}$ , immediately frozen in liquid nitrogen and stored at  $-80\text{ }^{\circ}\text{C}$ .

To transform electrocompetent *E. coli* DH5 $\alpha$  cells, 40  $\mu\text{l}$  cells were thawed on ice, mixed with  $\leq 5\text{ }\mu\text{l}$  of ligation reaction, and transferred to an electroporation cuvette (0.1 cm) pre-chilled on ice. Electroporation was performed by applying a pulse of 1250 V (25  $\mu\text{F}$ , 200  $\Omega$ ; Gene Pulser Xcell). Immediately after the pulse, cells were taken up in 800  $\mu\text{l}$  of LB medium, incubated in a shaker at  $37\text{ }^{\circ}\text{C}$  for 1 h, centrifuged at 5000 rpm for 2 min in a table centrifuge (Eppendorf 5415D), resuspended in approximately 100  $\mu\text{l}$  of medium, spread on selective LB plates, and incubated overnight at  $37\text{ }^{\circ}\text{C}$ . Plasmid isolation from liquid overnight cultures was performed as described in chapter 3.6.2.

### 3.6.8 Lithiumacetate transformation of *S. cerevisiae* cells

In the present study, all yeast transformations were performed according to the lithiumacetate (LiAc) method (see chapter 3.7.5) (Schiestl and Gietz, 1989; Gietz *et al.*, 1995). An YPD overnight culture of the respective yeast strain grown at  $30\text{ }^{\circ}\text{C}$  was diluted with YPD medium to an  $\text{OD}_{600}$  of  $\sim 0.15$  in a total volume of 50 ml. When the culture had reached an  $\text{OD}_{600}$  of  $\sim 0.5$  ( $30\text{ }^{\circ}\text{C}$ , 200 rpm), cells were harvested by centrifugation at 3000 g for 5 min. The pellet was resuspended in 25 ml of autoclaved water and centrifuged again. Next, cells were washed with 1 ml of 100 mM LiAc and transferred into an Eppendorf tube. After 15 s of centrifugation at top speed, the pellet was resuspended in 100 mM LiAc to a final volume of 500  $\mu\text{l}$ . For each transformation, cells from 50  $\mu\text{l}$  were pelleted by centrifugation at 3000 g for 5 min. The following components were added sequentially: 240  $\mu\text{l}$  of sterile-filtered 50 % (v/v) PEG-3350, 36  $\mu\text{l}$  of 1 M LiAc, 5  $\mu\text{l}$  of 10 mg/ml herring testes carrier DNA, 60  $\mu\text{l}$  of autoclaved  $\text{H}_2\text{O}$ , and 5  $\mu\text{l}$  of plasmid DNA (100 ng to 10  $\mu\text{g}$ ). After vigorous mixing for 1 min, the mixture was incubated in a shaker at  $30\text{ }^{\circ}\text{C}$  for 30 min. Then, cells were heat-shocked at  $42\text{ }^{\circ}\text{C}$  for 20 min and harvested by a 15 s centrifugation at 7000 rpm (Eppendorf 5415D). Cells were resuspended in 1 ml of YPD medium, incubated in a shaker at  $30\text{ }^{\circ}\text{C}$  for 3 h, pelleted by centrifugation, and resuspended in 100  $\mu\text{l}$  of appropriate selective medium. Cells were grown on selective plates at  $30\text{ }^{\circ}\text{C}$  for 2 d.

### 3.6.9 Construction of *sse1* mutant *S. cerevisiae* strains

To test the functionality of the Sse1p variants *in vivo*, the ability of the mutants to complement the lethal phenotype of the combined deletion of *SSE1* and *SSE2* in yeast cells was tested. For the construction of  $\Delta SSE1\Delta SSE2$  yeast strains, which express the different Sse1p variants, a method called plasmid shuffling was applied. In this approach, a rescue plasmid coding for wt *SSE1* in the double deletion strain is replaced by the various *sse1*-mutant encoding plasmids.

Specifically, the *S. cerevisiae* strain SB472 (genotype, *MAT $\alpha$  ade2-101<sup>ochre</sup> his3 $\Delta$ 200 leu2 $\Delta$ 1 lys2-801<sup>amber</sup> trp1 $\Delta$ 63 ura3-52 sse1::His3 sse2::KanMX4 pCM189-SSE1-URA3*) was utilized, in which the lethal phenotype of  $\Delta SSE1\Delta SSE2$  is rescued by the *SSE1* expression plasmid pCM189-SSE1-URA3. SB472 was transformed with the different pRS415ADH yeast expression plasmids, which code for the *sse1* variants (see chapter 3.6.3) as well as for a leucine selection marker, and cells were grown on SC-His-Ura-Leu plates at 30 °C for 2 d. In the next step, 10-50 colonies were picked, resuspended in 200  $\mu$ l of autoclaved water, and streaked on SC-His-Ura-Leu plates to get single colonies. After 2 d at 30 °C single colonies were picked and incubated at 30 °C for 2 d on non-selective YPD plates, a medium, on which the rescue plasmid pCM189-SSE1-URA3 is not stringently required. In order to actively select against pCM189-SSE1-URA3, single colonies of each strain were picked and streaked on SC-Leu medium containing 5-FOA and uracil (30 °C, 2 d). The non-toxic 5-FOA compound is converted to toxic 5-fluorouracil in yeast strains expressing the functional *URA3* gene (orotidine-5'-monophosphate decarboxylase). Consequently, only yeast cells that have lost pCM189-SSE1-URA3 and express a functional *sse1* mutant can multiply. Loss of pCM189-SSE1-URA3 was confirmed by the fact that cells grew on SC-Leu but not on SC-Leu-Ura plates (30 °C, 2 d). For generation of cryo stocks, the Sse1p variant-expressing strains were finally grown on YPD medium (30 °C, 2 d).

Since mutants *sse1*-(2+3) and *sse1*-(2+4) could not complement the  $\Delta SSE1\Delta SSE2$  double deletion, these two mutants were transformed into the  $\Delta SSE1$  *S. cerevisiae* strain SB537 (genotype, *MAT $\alpha$  ade2-101<sup>ochre</sup> his3 $\Delta$ 200 leu2 $\Delta$ 1 lys2-801<sup>amber</sup> trp1 $\Delta$ 63 ura3-52 sse1::His3*). Furthermore, SB537 was transformed with pRS415ADH-SSE1 and the original plasmid pRS415ADH. Cells were plated on SC-Leu and grown at 30 °C for 2 d.

### 3.6.10 Isolation of chromosomal DNA from *S. cerevisiae*

Genomic yeast DNA served as template for the amplification of yeast genes (see chapter 3.6.4). It was isolated from 2 ml of an YPH499 overnight culture grown to early stationary phase at 30 °C. After harvesting by centrifugation at 3000 g for 3 min and washing with 1 ml of autoclaved water, cells were resuspended in 200 µl of protoplast buffer and incubated at 37 °C for 1 h. To prevent sedimentation, cells were gently mixed from time to time. After addition of 200 µl of yeast lysis solution and gentle mixing, the cell suspension was incubated at 65 °C for 20 min and rapidly chilled on ice. Addition of 200 µl of 5 M KAc and gentle mixing of the cell suspension were followed by 15 min of incubation on ice. Precipitated potassium dodecylsulfate and denatured proteins were removed by centrifugation for 3 min at 20000 g and RT, and the supernatant was transferred to a new tube. For precipitating the DNA, 600 µl of isopropanol were added. After gentle mixing, the solution was incubated at RT for 5 min. Centrifugation for 30 s at 20000 g and RT lead to the sedimentation of the chromosomal DNA. The pellet was washed with 70 % ethanol for 10 min at RT. After renewed centrifugation, the DNA was dried for 1-2 min in vacuum and subsequently dissolved in 35 µl of autoclaved water.

## 3.7 Protein biochemical and biophysical methods

### 3.7.1 Protein expression and purification

All protein purification steps were performed at 4 °C unless otherwise stated.

#### 3.7.1.1 Hsp110 homologs

Sse1-Δloop was expressed as an N-terminally His-tagged fusion protein using *E. coli* BL21(DE3) cod<sup>+</sup> RIL as host and LB supplemented with ampicillin (Amp) and chloramphenicol (Cm) as culture medium. At an OD<sub>600</sub> of 0.6, protein expression was induced with 0.2 mM IPTG, and cells were subsequently grown at 18 °C for 16 h. Cells were harvested by centrifugation at 5000 g and 4 °C for 45 min. The cell mass from a 6 l culture was resuspended in 180 ml of buffer L1 supplemented with 10 mM imidazole, 5 mM β-mercaptoethanol, 1 mM PMSF, and 1x Complete protease inhibitor cocktail. Cell lysis *via* ultrasonication was performed on ice by applying ten 25 s pulses of maximum output level interrupted by breaks of 1 min 35 s. After removal of cell debris by centrifugation at 50000 g and 4 °C for 30 min, the supernatant was sterile-filtered and loaded on a 5 ml Ni<sup>2+</sup>-HiTrap

Chelating Sepharose column equilibrated in buffer L1 containing 10 mM imidazole. The column was washed with 10 CV of the same buffer, and His<sub>6</sub>-Sse1-Δloop was eluted by applying a linear gradient of 10 to 1000 mM imidazole in buffer L1 over 50 ml. The protein content of the 5 ml fractions was analyzed by SDS-PAGE (see chapter 3.7.2.2). For cleavage of the His<sub>6</sub>-tag, the protein-containing fractions were incubated with His<sub>6</sub>-TEV protease at a molar ratio of 20:1 in the presence of 1 mM DTT and 4.25 mM EDTA at 4 °C overnight. To remove bound nucleotide, the protein solution was dialyzed three times for 24 h against buffer D. After exchanging buffer D against buffer E, the dialysate was passed through 5 ml Ni<sup>2+</sup>-HiTrap Chelating Sepharose equilibrated in the same buffer to remove residual His<sub>6</sub>-Sse1-Δloop and His<sub>6</sub>-TEV protease. Aliquots of the concentrated flow-through fraction (11.8 mg/ml) were frozen in liquid nitrogen and stored at -80 °C.

Wt Sse1p and Sse2p as well as the Sse1p mutants were expressed and purified similarly to Sse1-Δloop. The modifications are described in the following. Protein expression was induced with 0.25 mM IPTG at 18 °C for at least 16 h. Instead of NaCl, KCl was used in all buffers employed during the purification process. After Ni-affinity chromatography in buffer L (10-1000 mM imidazole) and TEV protease cleavage, the protein solutions were (i) diluted to a final concentration of 40-60 mM imidazole with buffer L or (ii) buffer-exchanged against HKM2 and subsequently supplemented with 20 mM imidazole. Next, the protein solutions were passed over a second 5 ml Ni<sup>2+</sup>-HiTrap Chelating column equilibrated (i) in buffer L with 20 mM imidazole or (ii) in HKM2 buffer with 20 mM imidazole, respectively. The flow-through fractions were concentrated ( $\geq 4$  mg/ml) and dialysed against HKM2 overnight. Alternatively, the concentrated flow-through fractions were directly flash-frozen in liquid nitrogen. Immediately prior to use, soluble aggregates were removed by Superose 12 size exclusion chromatography using HKM2 buffer as running buffer.

To obtain nucleotide-free Sse1p, purified His<sub>6</sub>-Sse1p (in buffer E) was incubated with shrimp alkaline phosphatase (3.3 U/mg protein, 1 h, 25 °C). For the phosphatase incubation, the buffer was augmented with 50 mM Tris pH 8.5 and 5 mM MgCl<sub>2</sub>. To remove the phosphatase, the protein sample was supplemented with 10 mM imidazole, and Ni-affinity chromatography in buffer L (10-1000 mM imidazole) was performed. TEV protease cleavage, sample dilution to a final concentration of ~40 mM imidazole, renewed Ni-affinity chromatography in buffer L supplemented with 20 mM imidazole, and dialysis against HKM2 were conducted as described above.

Hsp110 was also purified similarly to Sse1-Δloop. Protein expression was induced with 0.8 mM IPTG at 18 °C for 16 h. Ni-affinity chromatography in buffer L1 (10-1000 mM

imidazole) and TEV protease cleavage were followed by anion exchange chromatography. Specifically, after dilution with buffer A1 to a final concentration of ~180 mM NaCl, the protein solution was loaded on MonoQ, which had been equilibrated in buffer A1. The column was washed with 5 CV of the same buffer and developed with a NaCl gradient from 10 to 1000 mM over 10 CV. Hsp110-containing fractions were supplemented with 20 mM imidazole and passed over a second Ni-affinity chromatography column equilibrated in buffer E containing 20 mM imidazole. The flow-through fractions were pooled and buffer-exchanged against buffer E. After concentration to 11.3 mg/ml, Hsp110 aliquots were snap-frozen in liquid nitrogen and stored at -80 °C.

### 3.7.1.2 Hsp70 homologs

Ssa1p, Ssa1N and the corresponding mutants were expressed as N-terminally His-tagged fusion proteins using *E. coli* BL21(DE3) cod+ RIL as host and LB supplemented with Amp and Cm as culture medium. At an OD<sub>600</sub> of 0.6, protein expression was induced with 0.25 mM IPTG, and cells were subsequently grown at 18 °C overnight. Cell harvesting, cell lysis *via* ultrasonication (in buffer L supplemented with 10 mM imidazole, 5 mM β-mercaptoethanol, 1 mM PMSF, and 1x Complete protease inhibitor cocktail), Ni-affinity chromatography (in buffer L with an imidazole gradient from 10 to 1000 mM), and TEV protease cleavage were performed as described for Sse1-Δloop in chapter 3.7.1.1. After dilution with buffer A to a final concentration of ~100 mM KCl, the protein solutions were loaded on MonoQ. The column was washed with 12.5 CV buffer A and developed with a KCl gradient from 10 to 1000 mM in 25 CV buffer A. The Ssa1 variant-containing fractions were augmented with 20 mM imidazole and passed through 5 ml Ni<sup>2+</sup>-HiTrap Chelating Sepharose equilibrated in HKM2 supplemented with 20 mM imidazole. The flow-through fractions were dialyzed against HKM2 at 4 °C overnight, concentrated to ≥ 1.25 mg/ml, snap-frozen in liquid nitrogen and stored at -80 °C. Prior to use, soluble aggregates were removed by Superose 12 size exclusion chromatography using HKM2 buffer as running buffer. If necessary, nucleotide bound to Ssa1p was either removed by incubation of the protein solution with 50 mM EDTA (1 h, 4 °C) and subsequent Superose 12 size exclusion chromatography with 150 mM KCl, 10 mM HEPES-KOH pH 7.5 serving as running buffer or by incubation with shrimp alkaline phosphatase after the initial Ni-affinity chromatography (3.3 U/mg protein, 1 h, 25 °C). For the phosphatase incubation, the buffer was augmented with 50 mM Tris pH 8.5 and 5 mM MgCl<sub>2</sub>. Next, the buffer of the protein sample was exchanged against buffer L supplemented with 10 mM imidazole, and the phosphatase was removed by Ni-affinity chromatography (in

buffer L with an imidazole gradient from 10 to 1000 mM). TEV protease cleavage and the further purification were conducted as described above.

Alternatively, Ssa1p was purified from the *S. cerevisiae* strain MW141 (genotype, *MAT $\alpha$  his3-11,15 leu2-3,112 trp1 ura3-52 ssal::HIS3 ssa2::LEU2 ssa4::URA3 pGal1-SSA1*) (Deshaies *et al.*, 1988). MW141 was streaked on YP-Gal plates and incubated at 30 °C for 2 d. Next, a 50 ml YP-Gal culture, which was inoculated with 4 colonies and grown at 30 °C overnight, was used to inoculate 6 l of YP-Gal medium. Cells were grown to an OD<sub>600</sub> of ~8 at 30 °C and harvested by centrifugation at 5000 g and 4 °C for 45 min yielding ~80 g of yeast cell mass. The pellet was resuspended in 10 % sterile glycerol and dripped into liquid nitrogen. The resulting granulate was stored at -80 °C. For lysis, cells were thawed at RT for ~1 h and resuspended in 150 ml of buffer S containing 0.5 mM EDTA, 1 mM PMSF, and 1x Complete protease inhibitor cocktail. Lysis was performed in an iced bead beater with 400 g of glass beads ( $\varnothing$  425-600  $\mu$ m) by applying 20 cycles of 30s pulses interrupted by breaks of 90 s. Then the glass beads were separated by vacuum filtration and thoroughly washed with 100 ml of buffer S containing 0.5 mM EDTA, 1 mM PMSF, and 1x Complete protease inhibitor cocktail. The combined filtrates were subjected to centrifugation using a Beckmann centrifuge with JLA 10.500 rotor at 4000 rpm and 4 °C for 10 min. After centrifugation of the resulting supernatant in a JLA 10.500 rotor at 10000 rpm and 4 °C for 30 min, the new supernatant was centrifuged in a Beckmann ultracentrifuge with a 45 Ti rotor at 36000 rpm and 4 °C for 1 h. The lipid drops on the surface of the supernatant were removed, and the clarified lysate was passed over ~20 ml ATP-agarose resin, which had been prepared by swelling 1.5 g of lyophilized powder in H<sub>2</sub>O and which had subsequently been equilibrated in buffer S. After washing the resin with (i) 5 CV of buffer S and (ii) 5 CV of GTP buffer, the sample was eluted with 5 CV of ATP buffer. The Ssa1p-containing fractions were identified by SDS-PAGE as well as by Western blotting (see chapters 3.7.2.2 and 3.7.2.3) and applied to a 10 ml DEAE-Sepharose column. After washing with 10 CV of DEAE buffer, the column was developed by applying a linear gradient of 20-1000 mM KCl in 20 CV of DEAE buffer. The protein-containing fractions were identified with the Bio-Rad protein assay and were analyzed by SDS-PAGE as well as by Western blotting. A slight contamination with Sse1p/Sse2p was apparent. 15  $\mu$ l aliquots containing 10-15 mg/ml Ssa1p were frozen in liquid nitrogen and stored at -80 °C.

His<sub>6</sub>-Ssb1N (amino acids 1-384) was expressed in *E. coli* BL21(DE3) cod+ RIL at 18 °C overnight after induction with 0.25 mM IPTG. Cell harvesting, cell lysis *via* ultrasonication, and Ni-affinity chromatography were performed as described for Sse1- $\Delta$ loop

in chapter 3.7.1.1. TEV protease cleavage was executed at RT, but otherwise as for Sse1- $\Delta$ loop. After dilution with buffer A1 to a final concentration of  $\sim$ 100 mM NaCl, the protein sample was loaded on MonoQ, which was subsequently developed with a linear gradient of 10-1000 mM NaCl in 20 CV buffer A1. Augmented with 20 mM imidazole, the Ssb1N-containing fractions were passed through Ni<sup>2+</sup>-HiTrap Chelating Sepharose equilibrated in buffer L1 supplemented with 20 mM imidazole. The flow-through fraction was dialyzed against HKM3 buffer at 4 °C overnight, concentrated to  $\sim$ 7 mg/ml, snap-frozen in liquid nitrogen and stored at -80 °C.

His<sub>6</sub>-Hsp70N (amino acids 1-382) was expressed in *E. coli* BL21(DE3) cod<sup>+</sup> RIL at 18 °C overnight after induction with 0.8 mM IPTG. Cell harvesting, cell lysis *via* ultrasonication (in buffer L supplemented with 10 mM imidazole, 5 mM  $\beta$ -mercaptoethanol, 1 mM PMSF, and 1x Complete protease inhibitor cocktail), Ni-affinity chromatography (in buffer L with a linear gradient from 10 to 1000 mM imidazole), and TEV protease cleavage were performed as described for Sse1- $\Delta$ loop in chapter 3.7.1.1. After buffer exchange against HKM2, the protein solution was passed through Ni<sup>2+</sup>-HiTrap Chelating Sepharose equilibrated in the same buffer. Next, the buffer of the concentrated flow-through fraction was exchanged against buffer A, and the protein sample was loaded on MonoQ, which was developed by applying a linear gradient of 10 to 1000 mM KCl in 5 CV of buffer A. The Hsp70N-containing fraction (6.7 mg/ml) was snap-frozen in liquid nitrogen and stored at -80 °C.

### 3.7.1.3 Ydj1p

After induction with 1 mM IPTG, His<sub>6</sub>-Ydj1p was expressed in *E. coli* BL21(DE3) cod<sup>+</sup> RIL at 18 °C overnight. Cell harvesting, ultrasonication (in buffer L supplemented with 10 mM imidazole, 5 mM  $\beta$ -mercaptoethanol, 1 mM PMSF, and 1x Complete protease inhibitor cocktail), Ni-affinity chromatography (in buffer L with a linear gradient from 10 to 1000 mM imidazole) and TEV protease cleavage were performed as described for Sse1- $\Delta$ loop in chapter 3.7.1.1. After dilution with buffer A to a final concentration of  $\sim$ 70 mM KCl, the protein solution was loaded on MonoQ, which was equilibrated in buffer A and developed with a KCl-gradient from 10 to 1000 mM over 25 CV. The Ydj1p-containing fraction was diluted with buffer L, supplemented with 20 mM imidazole and passed through 5 ml Ni<sup>2+</sup>-HiTrap Chelating Sepharose equilibrated in buffer L augmented with 20 mM imidazole. The concentrated flow-through fraction was dialyzed against HKM2 at 4 °C overnight. 50 and

100  $\mu$ l aliquots containing 16.8 mg/ml Ydj1p were snap-frozen in liquid nitrogen and stored at -80 °C.

#### 3.7.1.4 Selenomethionine-derivatized proteins

For the preparation of selenomethionine (SeMet)-labeled Sse1- $\Delta$ loop and Hsp70N, *E. coli* BL21(DE3) cod<sup>+</sup> RIL cells were transformed with pProEX-*sse1- $\Delta$ loop* or pProEX-*hsp70N*, respectively, and grown on LB plates containing Amp and Cm at 37 °C overnight. For both pProEX-*hsp70N*-transformed as well as pProEX-*sse1- $\Delta$ loop*-transformed cultures, four 4 ml LB-Amp-Cm cultures were then inoculated with one single colony each and incubated at 37 °C for 1 h. In the next step, 20  $\mu$ l of each culture were used to inoculate four 4 ml LB-Amp-Cm cultures. After overnight incubation at 37 °C, the cultures were harvested by centrifugation at 3000 g and 4 °C for 10 min. The sedimented cells were resuspended in 4 ml of M9 medium, centrifuged again, and resuspended as before in 4 ml of M9 medium. For both pProEX-*hsp70N*-transformed and pProEX-*sse1- $\Delta$ loop*-transformed cells, the four respective pre-cultures were used to inoculate three 1 l M9-Amp-Cm cultures, which were pre-warmed to 37 °C and subsequently grown at 37 °C. At an OD<sub>600</sub> of 0.6, the following amino acids were added under vigorous shaking: 125 mg/l L-lysine (in H<sub>2</sub>O), 100 mg/l L-phenylalanine (in 0.5 M HCl), 100 mg/l L-threonine (in 0.1 M HCl), 50 mg/l L-isoleucine (in 0.1 M HCl), 50 mg/l L-leucine (in 0.5 M HCl), 50 mg/l L-valine (in 0.5 M HCl), and 60 mg/l L-selenomethionine (in 0.1 M HCl) (modified from Van Duyne *et al.*, 1993). An equivalent amount of 2 M NaOH was added to neutralize the added HCl. After 15 min of further growth at 37 °C, Sse1- $\Delta$ loop and Hsp70N protein expression was induced with 0.2 and 0.8 mM IPTG, respectively. The cultures were grown at 18 °C for ~16 h. Cell harvesting, ultrasonication (in buffer L supplemented with 10 mM imidazole, 10 mM  $\beta$ -mercaptoethanol, 1 mM PMSF, and 1x Complete protease inhibitor cocktail), and Ni-affinity chromatography (in buffer L with a linear gradient from 10 to 1000 mM imidazole) were performed as described for Sse1- $\Delta$ loop in chapter 3.7.1.1. After TEV protease cleavage – which was conducted in additional presence of 10 mM  $\beta$ -mercaptoethanol, but otherwise as for Sse1- $\Delta$ loop – the sample buffers were exchanged against HKM2 buffer, and the protein solutions were passed through Ni<sup>2+</sup>-HiTrap Chelating Sepharose equilibrated in the same buffer. The SeMet-Sse1- $\Delta$ loop- and SeMet-Hsp70N-containing flow-through fractions were concentrated to 5 and 6.7 mg/ml, augmented with 10 mM  $\beta$ -mercaptoethanol, flash-frozen in liquid nitrogen, and stored at -80 °C.

### 3.7.2 Protein analytical methods

#### 3.7.2.1 Protein quantification

Protein concentrations were determined spectrophotometrically by measuring the absorption of the protein solution at 280 nm. Protein solutions were appropriately diluted with buffer, and protein-free buffer solution served as a reference. The theoretical molar extinction coefficients  $\epsilon_{280\text{nm}}$ , which were calculated from the respective protein sequences using the ProtParam tool at the ExPASy proteomics server (<http://us.expasy.org/tools/protparam.html>, (Pace *et al.*, 1995)), were used to convert the measured absorption into concentration according to the Lambert-Beer-law.

For nucleotide-containing protein solutions as well as for solutions containing a mixture of proteins, protein concentrations were measured colorimetrically at a wavelength of 595 nm, using the Bio-Rad protein assay reagent according to the manufacturer's recommendations (Bradford, 1976). Unless otherwise stated, a calibration curve with BSA was prepared as a reference. Irrespectively of the applied method, the readings of three independent measurements were averaged for each protein concentration determination.

#### 3.7.2.2 SDS-PAGE

Table 3-3: Composition of resolving and stacking gels for SDS-PAGE.

| solution component<br>(for 10 ml)      | resolving gel |             |             |             | stacking gel |
|--|---------------|-------------|-------------|-------------|--------------|
|  | 8 % AA        | 10 % AA     | 12 % AA     | 15 % AA     | 5 % AA       |
| H <sub>2</sub> O                       | 4.6 ml        | 4.0 ml      | 3.3 ml      | 2.3 ml      | 6.8 ml       |
| 30 % acrylamide (AA) /<br>0.8 % bis-AA | 2.7 ml        | 3.3 ml      | 4.0 ml      | 5.0 ml      | 1.7 ml       |
| 1.5 M Tris (pH 8.8)                    | 2.5 ml        | 2.5 ml      | 2.5 ml      | 2.5 ml      | -            |
| 1.0 M Tris (pH 6.8)                    | -             | -           | -           |             | 1.25 ml      |
| 10 % SDS                               | 100 $\mu$ l   | 100 $\mu$ l | 100 $\mu$ l | 100 $\mu$ l | 100 $\mu$ l  |
| 10 % ammonium persulfate               | 100 $\mu$ l   | 100 $\mu$ l | 100 $\mu$ l | 100 $\mu$ l | 100 $\mu$ l  |
| TEMED                                  | 6 $\mu$ l     | 4 $\mu$ l   | 4 $\mu$ l   | 4 $\mu$ l   | 10 $\mu$ l   |

The content of protein solutions was analyzed by discontinuous Tris-glycine sodium dodecylsulfate polyacrylamide gel electrophoresis (SDS-PAGE). This method allows the separation of proteins primarily according to their molecular weight (Laemmli, 1970). Gels were prepared according to Table 3-3 (Maniatis *et al.*, 1989). To improve gel quality, the resolving gels were covered with a layer of isopropanol immediately after casting. Before being loaded onto the gels, protein samples were mixed with 2x SDS-loading dye, boiled at

94 °C for 5 min, and spun briefly at maximum speed in a table centrifuge (Eppendorf 5415D). Electrophoresis was performed in SDS-electrophoresis buffer at a constant voltage of 200 V. After electrophoresis, gels were stained with Coomassie staining and destained with Coomassie destaining solution. Unless otherwise stated, photos of the gels were taken with the gel documentation system of MWG AG Biotech (Ebersberg, Germany).

### 3.7.2.3 Western blotting

For immunoblotting, a slightly modified published protocol was applied (Towbin *et al.*, 1979). After separation by SDS-PAGE, proteins were transferred from the gel to a nitrocellulose membrane with the help of a semi-dry Western blotting unit. The transfer was performed in Western blot buffer at a constant current of 80 mA/gel for 60-90 min and checked by Ponceau staining. Blots were subsequently blocked for 1 h with 3-5 % (w/v) milk powder in TBST or PBST. After incubation with the primary antibody (dilution see chapter 3.2) in TBST/PBST + 3 % (w/v) milkpowder for 1-3 h at RT or overnight at 4 °C, the blots were washed twice with TBST/PBST + 3 % (w/v) milkpowder for 5 min. Incubation with a horseradish peroxidase (HRP)-conjugated secondary antibody (dilution 1:3333) in TBST/PBST + 3 % (w/v) milkpowder for 1-3 h at RT followed. Finally, the blots were washed three times with TBST/PBST for 5 min. For immunodetection, ECL (enhanced chemiluminescence) solution was freshly prepared by mixing equal amounts of ECL solutions I and II. ECL solution II was always supplemented with 0.05 % (v/v) of 8.8 M H<sub>2</sub>O<sub>2</sub> prior to use. Membranes were covered with the detection mixture, and protein bands were detected and documented with the Fuji-LAS3000 luminescence and densitometry system. If necessary, blots were stripped by incubation with stripping buffer at 70 °C for 45 min.

### 3.7.2.4 TCA precipitation

For TCA (trichloro acetic acid) precipitation of purified proteins, a two-fold volume of 20 % (w/v) TCA was added to the protein sample, resulting in a final TCA concentration of 13 % (w/v). After incubation on ice for 15 min and centrifugation at 20000 g and 4 °C for 15 min, the protein pellet was washed with 1 ml of ice-cold acetone and pelleted again by centrifugation at 20000 g and 4 °C for 10 min. The washing step was repeated three times. Next, the pelleted sample was incubated at RT until all residual acetone was evaporated and dissolved in 15 µl of 1x SDS-loading buffer. In case of incomplete removal of TCA, the color of the bromphenolblue of the SDS-loading buffer became yellow, and 1 M Tris-HCl pH 8.5

was added until the color turned back to blue. The sample was boiled at 94 °C for 5 min and subjected to SDS-PAGE analysis.

### **3.7.2.5 Edman degradation**

To find out, whether Sse1- $\Delta$ loop (and also Sse1p) was degraded by Proteinase K at the N-terminus (see chapter 3.7.4.3), N-terminal sequencing was conducted. 20  $\mu$ M of Sse1 $\Delta$ loop were incubated with 10 mM ATP in HKM2 buffer at RT for 30 min. Then 0.5  $\mu$ g/ml Proteinase K were added and the reaction solution was incubated at RT for 30 min. After stopping the degradation reaction with 2 mM PMSF, the sample was chilled on ice for 2 min and centrifuged at RT for 2 min. The supernatant was concentrated to 7.1 mg/ml, and N-terminal sequencing of the degradation product was performed by the Core Facility of the MPI for Biochemistry in Martinsried.

### **3.7.2.6 Mass spectrometry**

The molecular weight of Sse1- $\Delta$ loop- $\Delta$ C was determined by mass spectrometry. 20  $\mu$ M Sse1- $\Delta$ loop were incubated with 10 mM ATP in HKM3 buffer at RT for 30 min. Then 0.5  $\mu$ g/ml Proteinase K were added and the reaction solution was incubated at RT for 50 min. After stopping the degradation reaction with 10 mM PMSF, the sample was chilled on ice for 2 min and centrifuged at RT for 2 min. The molecular weight of the degradation product in the supernatant was determined by electrospray ionization (ESI) mass spectrometry by Dr. Sonya Schermann (MPI for Biochemistry, Martinsried, Germany).

### **3.7.2.7 FFF-MALS**

The stoichiometries of the Sse1- $\Delta$ loop/Ssa1N, the Sse1- $\Delta$ loop/Ssb1N, and the Sse1- $\Delta$ loop/Hsp70N complexes were analyzed by field flow fractionation (FFF) followed by multiangle light scattering (MALS). Complexes were prepared as described in chapter 3.7.3.1 for the Sse1- $\Delta$ loop/Hsp70N complex. For FFF, 80  $\mu$ g of the distinct protein complexes were injected. HKM2 was used as running buffer with the injection flow set to 0.2 ml/min and the elution, detector and cross flows to 1 ml/min. The spacer foil separating the two plates that form the sample channel was 490 nm thick. The ultrafiltration membrane covering the permeable bottom plate had a MWCO of 10 kDa. The fractionation device was connected to three successive detectors: a DAWN EOS MALS detector (690 nm laser), a variable wavelength detector (absorbance at 280 nm, Agilent 1100 series), and an Optilab DSP

refractive index detector (690 nm). Masses were calculated using the ASTRA software with the  $dn/dc$  value set to 0.185 ml/g. The FFF-MALS experiments were performed by Dr. Manajit Hayer-Hartl (MPI for Biochemistry, Martinsried, Germany).

### 3.7.2.8 Circular dichroism spectroscopy

The secondary structure and melting behavior of the Sse1p variants and Sse2p were analyzed by circular dichroism (CD) spectroscopy. Far-UV CD spectra as well as thermal and GdnHCl-induced transitions were measured with a Jasco J-715 spectrometer equipped with a Peltier-thermostat using 0.1 cm cuvettes. The proteins were analyzed at a concentration of 2.5  $\mu$ M (Sse1C 5.7  $\mu$ M) in buffer C.

Wavelength scans were recorded at 4 °C (before and after heating of the protein sample) and 42 °C in a wavelength range of 195 to 250 nm. The band width was set to 1 nm, the response to 2 s, the data pitch to 0.1 nm, and the scanning speed to 50 nm/min. For each protein spectrum, two scans were averaged and corrected by the corresponding buffer spectrum. The measured mean ellipticity  $\theta$  (in mdeg) was converted into the mean molar ellipticity per amino acid residue  $[\theta]_{MRW}$  (in  $\text{deg cm}^2 \text{dmol}^{-1}$ ) using the equation  $[\theta]_{MRW} = \theta / (c \cdot d \cdot N_{AS} \cdot 10)$ . Therein,  $c$  stands for the protein concentration in M,  $d$  for the cell path length in cm, and  $N_{AS}$  for the number of amino acid residues of the investigated protein. Sse1p, Sse1- $\Delta$ loop, the Sse1p point mutation variants, Sse1C, and Sse2p have 695, 677, 695, 302, and 695 amino acid residues, respectively. Finally, the CD spectra were smoothed by applying a fast fourier transformation (FFT) filter. For Sse1p, additionally a CD spectrum in HKM2 buffer supplemented with 6 M GdnHCl was measured.

Temperature scans were measured at 222 nm in a temperature range of 4 to 70 °C. The band width was set to 1 nm, the response to 16 s, the data pitch to 0.1 °C, and the scanning speed to 60 °C h<sup>-1</sup>. The measured mean ellipticity  $\theta$  was converted into the mean molar ellipticity per amino acid residue  $[\theta]_{MRW}$  as described above. The thermal transitions were smoothed by applying a FFT filter. To determine the melting temperature of the Sse1p variants, the thermal transitions were fitted to a two state model with fixed baselines for the native and denatured protein using the program Grafit 3.0 (Erithacus Software, Staines, Great Britain). To check the reversibility of partial unfolding of the Sse1p variants, thermal unfolding and subsequent refolding transitions were measured in a temperature range from 4 to 42 °C.

For Sse1p, a GdnHCl-induced equilibrium transition was measured in HKM2 buffer at 20 °C. The protein concentration was 2.5  $\mu$ M and the GdnHCl concentrations reached from 0

to 6 M. To ensure establishment of the equilibrium, the protein samples were incubated at 20 °C for 2 h prior to measurement. For each sample, the molar ellipticity at 222 nm was recorded for 30 s in intervals of 0.5 s. The final molar ellipticities represent the average values of these data points corrected by a buffer baseline. The band width was set to 1 nm and the response to 8 s.

### **3.7.3 Protein crystallization and structure determination**

#### **3.7.3.1 Complex formation**

The native as well as the SeMet-substituted complexes of Sse1- $\Delta$ loop and Hsp70N were formed by mixing equimolar amounts of the purified proteins in the presence of a four-fold excess ATP. Free ATP and unbound Hsp70N were removed by gel filtration on Superose 12 using HKM2 buffer. Fractions containing the complex were pooled and concentrated to 6.3 mg/ml and 8.5 mg/ml, respectively, and Complete protease inhibitor cocktail was added.

#### **3.7.3.2 Complex crystallization**

Native as well as the SeMet-substituted complexes of Sse1- $\Delta$ loop and Hsp70N were crystallized by the hanging drop vapor diffusion method. Mixtures of 1  $\mu$ l of the protein solution and 1  $\mu$ l of the precipitant solution were equilibrated against 500  $\mu$ l of the precipitant solution. Siliconized cover slides and 24-well plates with silicon grease as sealant were used. Initial screening of crystallization conditions was carried out at both 20 and 4 °C using the precipitant solution kits Crystal Screen, Crystal Screen 2, Crystal Screen Lite, Index Screen, NeXtal ProComplex Suite, and Protein complex screen (Radaev and Sun, 2002; Radaev *et al.*, 2006). In selected conditions of the two latter screens, crystals of the Sse1- $\Delta$ loop/Hsp70N complex were observed after days to weeks at 4 °C. The protein content of the crystals was checked by 10 % SDS-PAGE. For sample preparation, the crystals were washed in 1  $\mu$ l of cryo solution (35 % of PEG plus glycerol) and subsequently dissolved in 8  $\mu$ l of HKM2 buffer. After addition of 8  $\mu$ l of 2x SDS-loading buffer and heat denaturation, the complete protein sample was analyzed as described in chapter 3.7.2.2.

For the native complex, the final optimized precipitant solution contained 17 % (w/v) polyethylene glycol (PEG)-6000, 50 mM KCl, 100 mM HEPES-KOH pH 7.5. For the SeMet-substituted complex, the optimized precipitant solution was 15 % (w/v) PEG-6000, 100 mM Tris-HCl pH 8.0, 10 mM DTT. For cryo-protection, the crystals were transferred stepwise into cryo solution: First, the crystals were incubated in a 1:1 mixture of precipitant and cryo

solution for ~10 min, then they were transferred to 100 % cryo solution for ~10 min. The cryo solutions were 20 % (w/v) PEG-6000, 15 % (v/v) glycerol, 200 mM KCl, 100 mM HEPES-KOH pH 7.5 for the native complex and 22 % (w/v) PEG-6000, 13 % (v/v) glycerol, 100 mM Tris-HCl pH 8.0 for the SeMet-substituted complex. Finally, the crystals were fished with nylon loops fitted onto magnetic bases and immediately flash-frozen in liquid nitrogen.

### 3.7.3.3 Structure determination

Diffraction data were collected by the oscillation method at beamline X10SA of the Swiss Synchrotron Light Source (SLS; Villigen, Switzerland) at a temperature of 100 K. Prior to the MAD experiment, SeMet incorporation into the crystallized protein complex was verified by collecting an X-ray fluorescence excitation spectrum in the energy range of the  $K_I$  absorption edge of selenium (12614-12693 eV). From the excitation spectrum, the anomalous scattering factors  $f'$  and  $f''$  were calculated using the program Chooch (Evans and Pettifer, 2001). As collection wavelengths for the MAD datasets, the maximum of  $f''$  (12.662 keV, peak), the minimum of  $f'$  (12.657 keV, inflection point), and a remote wavelength clearly above the absorption edge (12.757 keV) were chosen. After initial autoindexing of the reflections from diffraction images, which were collected at perpendicular orientations of the crystal, and automated estimation of the mosaicity, a data collection strategy was devised with the STRATEGY option of the program IPMosflm using the ANOMALOUS flag and data collection simulation with TESTGEN (Leslie, 1992). To acquire almost complete and sufficiently redundant datasets, 150 images were recorded in a range of  $90^\circ$  with an increment of  $0.6^\circ$  and an exposure of 1 s per image. The distance between the mounted crystal and the CCD detector was set to 290 mm corresponding to a resolution of 2.6 Å for the given wavelength at the detector edge. In order to minimize radiation damage during data collection, the primary X-ray beam was attenuated to 17 % intensity with metal filters. For obtaining maximum resolution in the reference dataset, a second remote dataset was measured at higher intensity (30 %) after shifting the crystal laterally to an unexposed region and setting the crystal- detector distance to 250 mm (2.3 Å).

The images were integrated with IPMosflm, and Scala (Evans, 1997) was used for internal scaling of the individual datasets. Then the different datasets were compared and normalized with XPrep (Bruker, Madison, USA). In the XPrep-processed data, 25 selenium sites were determined from the anomalous differences by direct methods using ShelX-D (Uson and Sheldrick, 1999). Sharp was used to refine the heavy atom sites and to calculate the phases (de la Fortelle and Bricogne, 1997). Density modification was carried out with

Resolve (Terwilliger, 2000) using the default options and assuming a 58 % solvent content. Identifying and applying the correct non-crystallographic symmetry by Resolve was essential for calculation of phases sufficiently good for interpretable electron density maps. Building of a partial model and sequence docking were carried out with ArpWarp6.1 (Perrakis *et al.*, 1999). Thereby, a backbone coverage of 71 % was achieved, and 51 % of the side chains were automatically built. Subsequent iterative manual model building and refinement were performed with Coot (Emsley and Cowtan, 2004) and Refmac5 (Murshudov *et al.*, 1997). Residues without detectable side chain density were modeled as alanines. The TLS (translation libration screw) refinement option of Refmac5 improved the refinement statistics significantly towards the end of the refinement: Upon TLS refinement, the R-factors were reduced by ~6 %. Using the TLS option, the anisotropic thermal motions of sections in the model ("TLS groups") that behave like rigid bodies can be modeled expending only few parameters. For modeling anisotropic motions of individual atoms, large amounts of data, i.e. high resolution data (typically ~1.3 Å), would be required. TLS groups were assigned according to the domain structure of the proteins: (i) NBD of Sse1- $\Delta$ loop (residues 2-396) including ATP, Mg<sup>2+</sup>, and K<sup>+</sup>, (ii)  $\beta$ -sandwich domain of Sse1- $\Delta$ loop (residues 397-540), (iii) 3HBD of Sse1- $\Delta$ loop (residues 541-655), (iv) subdomains Ia, Ib, IIa of Hsp70N (residues 4-229, 308-382), and (v) subdomain IIb of Hsp70N (residues 230-307). Solvent molecules were assigned to the respective TLS groups.

A 2.3 Å native dataset isomorphous to the MAD data was solved using the SeMet structure as an initial model. In order to reduce model bias, ArpWarp6.1 was used to autobuild a partial model (83 % backbone and 75 % side chain coverage), which was complemented by manual model building. The refined native model exhibited superior quality compared to the SeMet model and hence was used for further structural analysis.

#### 3.7.3.4 Structure analysis

The stereochemistry of the model was evaluated by the program Procheck (Laskowski *et al.*, 1993). Coordinates were aligned with Lsqman (Kleywegt and Jones, 1994) and Lsqkab (Kabsch, 1976). The sequence alignment was prepared with MultAlin (Corpet, 1988) and ESPript (Gouet *et al.*, 1999). The interaction surface in the Sse1p/Hsp70 complex was analyzed with Areaimol (Lee and Richards, 1971), Contact (Skarzynski, 1988), and Naccess (Hubbard and Thornton, 1993). Surface shape complementarity between the complex partners was estimated using SC (Lawrence and Colman, 1993). Rotation axes were determined with

the DynDom server (Hayward and Berendsen, 1998). Figures were generated with the program Pymol (DeLano, 2002).

### 3.7.4 Functional *in vitro* assays

#### 3.7.4.1 Sse1p/Ssa1N complex formation assay

To investigate the nucleotide dependence of Sse1p/Ssa1N complex formation, the proteins (17.2  $\mu$ M each) were mixed in absence of nucleotide or in presence of 40  $\mu$ M ADP or ATP. HKM2 buffer was added to a final volume of 30  $\mu$ l. The mixture was applied to an analytical Superose 12 column operated at RT in HKM2 buffer. 50  $\mu$ l fractions were collected, 5  $\mu$ l of which were analyzed by SDS-PAGE (see chapter 3.7.2.2). In addition, 0.5  $\mu$ l of the mixture applied to size exclusion chromatography were loaded on the 10 % gel. Photos of the gels were taken with the Fuji-LAS3000 luminescence and densitometry system. The protein bands in the complex-containing fractions were analyzed by densitometry (AIDA). For quantification, the quotient of  $(Ssa1N_{\text{complex}}/Sse1p_{\text{complex}})/(Ssa1N_{\text{load}}/Sse1p_{\text{load}})$  was calculated. The quotients determined from three independent experiments were averaged. For comparison, the quotient from the experiment performed in presence of ATP was set to 1.

To estimate the relative binding affinities of the Sse1p variants for Ssa1N, the same experimental setup was used. The proteins were always mixed in presence of 40  $\mu$ M ATP.

#### 3.7.4.2 Determination of the dissociation constant for the Sse1p/Ssa1N interaction

A stoichiometric complex of His<sub>6</sub>-Sse1p and ATP was prepared by incubation of the protein with 0.5 mM ATP at 25 °C for 10 min in HKM2 buffer. After removal of unbound ATP *via* a NAP 25 desalting column, the complex was kept on ice. The concentration was determined by a Bio-Rad protein assay calibrated with nucleotide-free His<sub>6</sub>-Sse1p as reference protein. Aliquots were snap-frozen in liquid nitrogen and stored at -80 °C. In a total volume of 1 ml, His<sub>6</sub>-Sse1p·ATP (0.2  $\mu$ M) was incubated for 30 min at 25 °C under vigorous shaking with increasing concentrations of Ssa1N (0.1-2.0  $\mu$ M) and 150  $\mu$ l of Ni<sup>2+</sup>-charged chelating Sepharose. The reaction buffer was HKM2 supplemented with 20 mM imidazole. The gel beads were sedimented by centrifugation, and 800  $\mu$ l of the supernatant were removed. 800  $\mu$ l of HKM2 buffer containing 347 mM imidazole were added to the slurry, and the mixture was incubated as above for 5 min, followed by centrifugation. Samples of the supernatants at low and high imidazole concentrations were subjected to SDS-PAGE. Photos of the gels were taken with the Fuji-LAS3000 luminescence and densitometry system. The Ssa1N content was

analyzed by densitometry (AIDA) using an Ssa1N concentration series as standard. As a control for background binding to the beads, another set of experiments without His<sub>6</sub>-Sse1p was performed. The amount of His<sub>6</sub>-Sse1p-bound Ssa1N was calculated with the following formula:  $[\text{bound Ssa1N}] = [\text{Ssa1N}_{\text{high imidazole}}] - [\text{Ssa1N}_{\text{low imidazole}}]/5$  and plotted against  $[\text{Ssa1N}_{\text{low imidazole}}]$ . The resulting points were fitted with the program Grafit 3.0 (Erithacus Software, Staines, Great Britain) using the following equation:  $[\text{bound Ssa1N}] = [\text{His}_6\text{-Sse1p}] \cdot [\text{Ssa1N}_{\text{low imidazole}}]/(K_D + [\text{Ssa1N}_{\text{low imidazole}}])$  assuming a 1:1 complex and no background binding. The dissociation constant determination was conducted by Dr. Andreas Bracher.

#### 3.7.4.3 Proteinase K resistance assay

To test the protease resistance of Sse1p, Sse1- $\Delta$ loop, and Hsp110, 3  $\mu\text{M}$  of the respective Hsp110 homolog were incubated with 0, 0.5, 1, 2, 4, 8, 16, 32, 64, and 128  $\mu\text{g/ml}$  Proteinase K in HKM3 buffer for 30 min at RT ( $V_{\text{total}} = 50 \mu\text{l}$ ). After terminating the degradation reaction by adding 100 mM PMSF to a final concentration of 9 mM, the samples were chilled on ice for 5 min and centrifuged at RT for 2 min. 10  $\mu\text{l}$  of the supernatants were mixed with 10  $\mu\text{l}$  2x SDS-loading buffer and denatured at 94  $^{\circ}\text{C}$  for 5 min. 10  $\mu\text{l}$  of each sample were loaded onto an 8 % SDS gel and subjected to SDS-PAGE (see chapter 3.7.2.2). In a second series of experiments the influence of ATP on protein stability was tested: Prior to Proteinase K exposure, the Hsp110 homologs were incubated with 1 mM ATP for 30 min at RT.

The Proteinase K resistance of the NBDs of Ssb1p and Hsp70 were analogously investigated. However, 7  $\mu\text{M}$  instead of 3  $\mu\text{M}$  protein were used.

Furthermore, the Proteinase K resistance of the following complexes was analyzed: Sse1p/Ssb1N (51.8  $\mu\text{M}$ ), Sse1- $\Delta$ loop/Ssa1N (31.3  $\mu\text{M}$ ), Sse1 $\Delta$ -loop/Ssb1N (53.2  $\mu\text{M}$ ), Sse1- $\Delta$ loop/Hsp70N (53.0  $\mu\text{M}$ ), and Hsp110/Hsp70N (41.0  $\mu\text{M}$ ). The individual purified proteins were mixed at the indicated concentrations and in presence of 100  $\mu\text{M}$  ATP (1 mM for Sse1- $\Delta$ loop/Ssa1N). Free ATP and unbound Hsp70N were removed by gel filtration on Superose 12 using HKM3 or HKM2 (for Sse1- $\Delta$ loop/Ssa1N and Sse1- $\Delta$ loop/Hsp70N) as running buffer. The complexes were principally eluted in two 500  $\mu\text{l}$  fractions, which were pooled. In a total volume of 60  $\mu\text{l}$ , 50  $\mu\text{l}$  of the complex fractions were incubated with Proteinase K (concentrations see above) at RT for 30 min. The protease reaction was stopped with 3.3 mM PMSF. The further procedure was the same as described for the Proteinase K degradation of the Hsp110 homologs. Instead of 10  $\mu\text{l}$ , 15  $\mu\text{l}$  of the SDS samples were loaded onto 8 % SDS gels.

#### 3.7.4.4 Nucleotide release assay

To determine whether (i) the NBD of Hsp70 homologs is sufficient for a functional interaction with Sse1p and whether (ii) the different Sse1p variants can still trigger nucleotide release from Hsp70, nucleotide release assays were performed. Nucleotide release kinetics of the fluorescent nucleotide analog MABA-ADP (N8-(4N'-methylantraniloylaminobutyl)-8 aminoadenosine 5'-diphosphate) from the Hsp70 NBD were followed in a stopped-flow setup as previously described (Gässler *et al.*, 2001). All components were in HKM2 buffer containing 1 mM DTT. Hsp70·MABA-ADP complexes were formed by incubating 2.5  $\mu$ M Hsp70N, Ssa1N or Ssa1p with an equimolar amount of MABA-ADP at 30 °C for 30 min. The nucleotide exchange factor solutions contained 250  $\mu$ M ATP (2.5 mM ATP) and either 2.5  $\mu$ M NEF (25  $\mu$ M NEF) or no protein (values in parentheses are for experiments with 25  $\mu$ M Sse1p variant). For the determination of the nucleotide release rates, equal volumes of the solutions were rapidly mixed at 30 °C in the stopped-flow apparatus. Release of labeled nucleotide was monitored by the decrease in fluorescence of the unbound MABA-ADP. The excitation wavelength was adjusted to 360 nm, and a cut-off filter at 420 nm was used for detection. The two slits of the monochromator were set to 5 nm and 2.5 nm, respectively. During the first second, 200 datapoints were collected; during the following 20 s further 200 datapoints were recorded. Each experiment was repeated four times. Rates were determined from the average of the individual fluorescence traces using the program Grafit 3.0 (Erithacus Software, Staines, Great Britain).

#### 3.7.4.5 Peptide release assay

To test whether amino acid substitutions in Sse1p influence substrate release from the Hsp70 partner, a peptide release assay was conducted. Peptide release rates were determined with a stopped-flow instrument using dansyl-labeled NR peptide (dansyl-NRLLLTGC, D-NR) (Gässler *et al.*, 2001). All components were in HKM2 buffer containing 1 mM DTT. For preparation of an Ssa1p·ADP·D-NR complex, 2.5  $\mu$ M ADP-bound Ssa1p were pre-incubated with an equimolar amount of D-NR for 30 min at 30 °C. For preparation of a nucleotide-free Ssa1p·D-NR complex, an Ssa1p·ADP·D-NR mixture was treated with 2 U of shrimp alkaline phosphatase in 50 mM Tris-HCl pH 8.5 for 3 h at 25 °C. Next, the solution was diluted with HKM2 and DTT to a final Ssa1p/D-NR concentration of 2.5  $\mu$ M. The Ssa1p·D-NR or Ssa1p·ADP·D-NR complexes were then mixed (volume ratio 1:1) at 30 °C with 250  $\mu$ M unlabeled NR and 250  $\mu$ M ATP in the presence or absence of 2.5  $\mu$ M of the distinct Sse1p variant. For control, the substrate-chaperone complex was mixed with unlabeled NR or with

unlabeled NR and Sse1p in absence of ATP. Release of D-NR was monitored by the decrease in fluorescence of the unbound D-NR. The excitation wavelength was adjusted to 334 nm, and a cut-off filter at 385 nm was used for detection. The two slits of the monochromator were set to 5 nm and 2.5 nm, respectively. During the first second, 500 datapoints were collected; during the following 20 s further 500 datapoints were recorded. Each experiment was repeated four times. Rates were determined from the average of the individual fluorescence traces using the program Grafit 3.0 (Erithacus Software, Staines, Great Britain).

#### **3.7.4.6 Luciferase refolding assay**

To test the influence of amino acid substitutions in Sse1p on luciferase refolding, firefly luciferase (100 nM) was incubated in buffer R at 42 °C in the presence of 3 μM Ssa1p for 10 min. Refolding was initiated by addition of 3 μM Ydj1p, 0.5 μM Sse1p variant, and 3 mM ATP and allowed to proceed at 30 °C. The utilized Ssa1p was purified from yeast (see chapter 3.7.1.2, stock concentration 148.9 μM). The Ydj1p and Sse1p variant stocks were diluted with glycerol buffer to 37.6 and 8.9 μM, respectively, prior to use. For control, luciferase was (i) denatured and refolded in absence of any chaperone, (ii) denatured and refolded in presence of Ssa1p, and (iii) denatured in presence of Ssa1p and refolded in presence of Ydj1p, but absence of Sse1p. At the indicated time points, 1 μl aliquots were mixed with 20 μl of buffer R supplemented with 3 mM ATP and 1 mg/ml BSA. After addition of 50 μl of luciferase assay reagent (diluted 1:5 with buffer R supplemented with 3 mM ATP and 1 mg/ml BSA), activity was determined in a luminometer (1 s delay, 1 s measurement) with the 100 % value corresponding to the enzyme activity of native luciferase in buffer R containing 3 mM ATP prior to heating. Each experiment was repeated independently for at least three times.

#### **3.7.4.7 Sse1p/peptide interaction**

##### **3.7.4.7.1 Peptide scan**

The Sse1p peptide binding specificity was assessed in a peptide scan. 13 amino acid long peptides, which covered the sequence of firefly luciferase and partially overlapped by ten amino acids, were covalently linked to a cellulose-PEG-membrane by their C-termini (JPT Peptide Technologies GmbH). An additional β-alanine was added between the peptide and the membrane, and all cysteines were replaced by serines. Acetylation of the N-termini of the peptides ensured higher stability against degradation. Furthermore, the uncharged N-acetyl

group mimicked the luciferase region as found in the native protein better than the charged  $\text{NH}_3^+$ -group. Each of the 180 peptide spots carried approximately 5 nmol of peptide.

After rinsing the dry peptide membrane for 5 min in methanol, it was washed three times for 10 min in TBS and blocked in TBS + 1 % (w/v) milkpowder for 3 h at RT. Subsequently, it was incubated with 10  $\mu\text{g}/\text{ml}$  Sse1p in TBS + 1 % (w/v) milkpowder at RT overnight. Afterwards, the membrane was washed three times for 5 min in TBST buffer. For detection of peptide-bound Sse1p, the membrane was incubated with Sse1p antiserum in TBST + 1 % (w/v) milkpowder (dilution 1:5000) at RT for 45 min and washed twice with TBST buffer for 5 min. Then, the membrane was incubated with a HRP-conjugated secondary antibody in TBST + 1 % (w/v) milkpowder for 45 min. After three-fold washing in TBST, peptide binding was visualized using ECL solutions I and II as described in chapter 3.7.2.3. In order to detect direct hybridization of the antibodies with the peptide spots, a control experiment was performed, in which the incubation step with Sse1p was omitted.

For regeneration, the membrane was washed three times for 10 min in water, followed by four 30 min incubation steps at 50 °C in stripping buffer. Afterwards, the membrane was sequentially incubated in 10x PBS and in TBST. Both steps were performed at RT for 20 min and repeated three times. If re-used within a few days, the membrane was stored in TBST at 4 °C. For long-term storage, the membrane was dried and kept at -20 °C. Specifically, it was washed three times with TBS for 10 min. After two-fold washing with methanol for 1 min, the membrane was air dried. If this regeneration procedure was not successful in reducing residual staining, the membrane was regenerated as follows: The membrane was sequentially washed twice with water, three times with regeneration buffer A, three times with regeneration buffer B, once with water, and three times with TBST. Each washing step was conducted at RT for 10 min. If this regeneration protocol failed as well, the membrane was incubated with 0.1 M HCl for 1 h, followed by three 10 min washing steps in TBS.

#### 3.7.4.7.2 Anisotropy measurements

To test Sse1p peptide binding in solution, anisotropy measurements with a fluorescently labeled substrate peptide were performed. Specifically, 6-carboxyfluorescein conjugated LICGFRVVL MYRF (LIC-peptide) was used. The peptide was dissolved in DMF (609  $\mu\text{M}$ ), and the stock solution was stored at -80 °C. For the experiment, a 1  $\mu\text{M}$  aqueous stock solution of the peptide was freshly prepared in siliconized tubes. 11 different Sse1p dilutions (0, 0.5, 1, 2, 5, 10, 20, 50, 100, 200, 500 nM) in HKM2 buffer containing 10 nM of the labeled LIC-peptide were incubated at RT for 20 min (total volume 350  $\mu\text{l}$ ) in siliconized

tubes. Anisotropy measurements were performed at 20 °C using a Fluorolog 3 spectrofluorimeter and a cylindric fluorescence cuvette. Excitation and emission wavelengths were set to 494 and 521 nm, respectively. Both excitation and emission slit widths were adjusted to 5 nm, the integration time was set to 0.3 s.

### **3.7.4.8 Luciferase aggregation prevention and refolding assays**

#### **3.7.4.8.1 Light scattering assay**

The aggregation prevention activity of Sse1p was tested in light scattering experiments using a Fluorolog 3 spectrofluorimeter. The light scattering by 100 nM firefly luciferase was monitored in a cylindric fluorescence cuvette during incubation at 42 °C in presence or absence of 0.5 μM Sse1p (total volume 300 μl). Sterile-filtered and degassed buffer R supplemented with 3 mM ATP served as reaction buffer. Excitation as well as emission wavelengths were set to 350 nm. The excitation slit width was adjusted to 2 nm, the emission slit width to 1 nm. One datapoint per second was collected. To correct for fluctuations in the excitation light source, the reference signal (R) was recorded in addition to the actual signal (S). For evaluation, the ratio of S/R was used.

#### **3.7.4.8.2 Luciferase refolding assay**

The capacity of the Sse1p variants to keep firefly luciferase in a folding competent state at elevated temperatures was tested as follows: 100 nM firefly luciferase were thermally denatured at 42 °C for 25 min in buffer R containing 3 mM ATP and 0.5 μM Sse1p variant. Refolding was initiated by addition of 3 μM Ssa1p and 3 μM Ydj1p and allowed to proceed at 30 °C (for further details see chapter 3.7.4.6). For control, luciferase was (i) denatured and refolded in absence of any chaperone, (ii) denatured in absence of any chaperone and refolded in presence of Ssa1p and Ydj1, (iii) denatured in presence of BSA and refolded in presence of Ssa1p and Ydj1, (iv) denatured in absence of any chaperone and refolded in presence of Ssa1p, Ydj1, and Sse1p, and (v) denatured in presence of BSA and refolded in presence of Ssa1p, Ydj1, and Sse1p. At the indicated time points, 1 μl aliquots were mixed with 20 μl of buffer R supplemented with 3 mM ATP and 1 mg/ml BSA. After addition of 50 μl of luciferase assay reagent (diluted 1:5 with buffer R supplemented with 3 mM ATP and 1 mg/ml BSA), activity was determined in a luminometer (1 s delay, 1 s measurement) with the 100 % value corresponding to the enzyme activity of native luciferase in buffer R

containing 3 mM ATP prior to heating. Each experiment was repeated independently for at least three times.

### 3.7.5 Functional *in vivo* assays

#### 3.7.5.1 Yeast growth assay

It was tested whether the ectopically expressed Sse1p mutants can support the growth of the  $\Delta SSE1\Delta SSE2$  *S. cerevisiae* strain SB472 to the same extent as ectopically expressed wt Sse1p. Therefore, glycerol stocks of modified SB472 cells expressing the various variants (see chapter 3.6.9) were streaked on YPD plates and incubated at 30 °C for 2 d. Next, cells from 3-6 colonies were inoculated onto 20 ml of YPD medium and grown at 30 °C overnight. After dilution to an OD<sub>600</sub> of 0.15 in a total volume of 20 ml, cultures were grown for 5 h at 30 °C until they reached mid-log phase (OD<sub>600</sub>  $\approx$  0.5). For each strain, an OD<sub>600</sub> corresponding to 0.5 in 1 ml was harvested by centrifugation at 5000 rpm for 5 min (Eppendorf 5415D), and the cell pellets were resuspended in 1 ml of autoclaved water. From each suspension, four ten-fold serial dilutions in water were prepared. 4  $\mu$ l of each dilution were spotted onto YPD agar plates, which were subsequently incubated at 30 or 37 °C for 2 d. The viability of  $\Delta SSE1$  SB537 strains transformed with either pRS415ADH, pRS415ADH-*SSE1*, pRS415ADH-*sse1*-(2+3) or pRS415ADH-*sse1*-(2+4) was tested in an analogous experimental setup.

#### 3.7.5.2 Protein expression analysis by Western blotting

Western blotting of whole cell lysates was performed to analyze the expressions levels of the Sse1p variants as well as of various chaperones (Hsp12p, Hsp42p, Hsp104p, Ssa1p, Ydj1p) in modified  $\Delta SSE1\Delta SSE2$  SB472 strains harboring *sse1* mutant expression plasmids (see chapter 3.6.9). As a control, the expression levels of Sse1p and the listed chaperones in YPH499 cells was determined. Cell lysates were prepared from cultures that were grown in YPD medium to mid-log phase at 30 °C and again 4 h after shifting the growth temperature to 37 °C. Cell lysis was performed as follows: The equivalent to an OD<sub>600</sub> of 10 in 1 ml was harvested (Beckmann GS-6R, 3400 rpm, 5 min, 4 °C), and the pellet was resuspended in 2 ml fresh medium. 450  $\mu$ l of the cell suspension were then supplemented with 450  $\mu$ l of ice-cold 30 mM NaN<sub>3</sub>, the mixture was centrifuged at 14000 rpm and 4 °C for 2 min (Eppendorf 5417R), and the cell pellet was immediately frozen in liquid nitrogen. The sedimented cells were resuspended in 1 ml of ice-cold, autoclaved H<sub>2</sub>O and 150  $\mu$ l of alkaline lysis buffer were added. During the incubation time of 10 min, the cell suspension was vigorously mixed for five times at least. To precipitate the proteins, 150  $\mu$ l of 50 % (w/v) TCA were added. After

incubation on ice for 20 min, the mixture was centrifuged at 14000 rpm and 4 °C for 10 min (Eppendorf 5417R), and the pellet was resuspended in 500 µl of chilled acetone. Short centrifugation of the suspension at 14000 rpm and 4 °C was followed by dissolving the pellet in 100 µl of urea-SDS-loading buffer. The sample was incubated at 65 °C for 15 min and briefly centrifuged. 15 µl of the sample were loaded on a 10 % SDS gels (15 % for Hsp12 detection). Western blotting was performed as described in chapter 3.7.2.3, the utilized dilutions for the different primary antibodies are indicated in chapter 3.2. The protein band of endogenous phosphoglycerate kinase (PGK) was used as a loading control.

The expression level of Ssa3p in modified SB472 and SB537 strains, which harbor an expression plasmid for a distinct *sse1* variant as well as a β-galactosidase reporter plasmid (see chapter 3.7.5.3), was estimated using a slightly modified protocol compared to the one described above. For each strain, an OD<sub>600</sub> corresponding to 2.5 in 1 ml was harvested from a mid-log phase culture grown in SC-Leu-Ura medium at 30 °C. The cell pellets were washed with 1 ml of ice-cold, autoclaved H<sub>2</sub>O and immediately snap-frozen in liquid nitrogen. After further incubation of the cultures at 37 °C for 3.5 h, another sample was drawn. Alkaline lysis of the cells was conducted as described above. 10 µl of the final samples were separated by 10 % SDS-PAGE and further analyzed by Western blotting.

The expression levels of Sse1p, Sse1-(2+9) and Sse1-(2+10) in modified SB537 were analyzed as described above, but 10 µl of the final samples were loaded on a 10 % SDS gel. SB537 cells transformed with the original plasmid pRS415ADH served as a control.

### 3.7.5.3 β-galactosidase reporter assay for stress response

To investigate whether modified SB472 and SB537 strains, which ectopically express *sse1* variants, are more stressed than wt YPH499 cells, the mutant strains as well as YPH499 were transformed with pYEP-*SSA3-lacZ*, a yeast plasmid coding for β-galactosidase under control of the stress-inducible *SSA3* promoter (see chapter 3.6.8). Since pYEP-*SSA3-lacZ* also codes for an uracil selection marker, mutant strains were incubated on SC-Leu-Ura plates after transformation at 30 °C for 2 d. Transformed YPH499 was grown on SC-Ura plates. For the β-galactosidase assay, a suspension culture of each strain was grown in SC-Leu-Ura (SC-Ura for YPH499) at 30 °C to mid-log phase. Three times an OD<sub>600</sub> corresponding to 2.5 in 1 ml was harvested from each culture. The pellets were washed with 1 ml of ice-cold, autoclaved H<sub>2</sub>O and were immediately snap-frozen in liquid nitrogen. After the remainder of the cultures was incubated at 37 °C for 3.5 h, three further samples were drawn for each strain. Next, the sedimented cells were resuspended in 700 µl of buffer Z. For membrane permeabilization,

50  $\mu$ l of chloroform and 50  $\mu$ l of 0.1 % (w/v) SDS were added to the cell suspensions. Furthermore, chloroform and 0.1 % (w/v) SDS were added to three aliquots of 700  $\mu$ l buffer Z, which served as a control. The samples were vigorously mixed for 10 s and incubated at 30 °C for 5 min. Then 200  $\mu$ l of ONPG-solution (4 mg/ml in buffer Z) were added to each sample, and the mixtures were incubated at 30 °C for 5-6 min. Following termination of the  $\beta$ -galactosidase reactions by addition of 350  $\mu$ l of 1 M Na<sub>2</sub>CO<sub>3</sub>, the samples were clarified by centrifugation. The absorbance of the supernatants of the cell suspensions was measured at 420 nm against the supernatant of one of the control samples. If necessary, appropriate dilutions were prepared. The specific  $\beta$ -galactosidase activity was expressed in Miller units and calculated as follows:  $(\text{dilution factor} \cdot A_{420} \cdot 1000) / (\text{OD}_{600} \cdot \text{time of incubation with ONPG in min})$ .  $A_{420}$  was the average value from triplicate samples. For cells grown at 30 °C, three independent experiments were conducted; for cells additionally grown at 37 °C, the  $\beta$ -galactosidase reporter assay was repeated twice (four times for the YPH499 strain). In addition to the reporter gene expression, the endogenous *SSA3* expression levels of the cultures were checked by Western blotting as described in chapter 3.7.5.2.

#### 3.7.5.4 Protein stability analysis

In order to assess the stability of the mutant forms of *sse1* expressed by modified SB472 at 30 °C, cycloheximide chase experiments were performed (Hiller *et al.*, 1996; Park *et al.*, 2007). For each strain, the equivalent to an OD<sub>600</sub> of 10 in 1 ml was harvested from a mid-log phase YPD culture (Beckmann GS-6R, 3400 rpm, 5 min, 4 °C). After washing with 2 ml of fresh medium, the pellets were resuspended in 2 ml of fresh medium, and protein biosynthesis was terminated by addition of the translation elongation inhibitor cycloheximide to a final concentration of 0.48 mg/ml. 450  $\mu$ l of the cell suspensions were then supplemented with 450  $\mu$ l of ice-cold 30 mM NaN<sub>3</sub>, the mixtures were centrifuged at 14000 rpm and 4 °C for 2 min (Eppendorf 5417R), and the cell pellets were immediately snap-frozen in liquid nitrogen (time point 0 h). The remainder of the cell cultures was further incubated at 30 °C, and samples were taken as described above after 1, 2, and 3 h. Alkaline lysis was performed as described in chapter 3.7.5.2, and 15  $\mu$ l of the final samples were analyzed by 10 % SDS-PAGE and Western blotting (chapters 3.2 and 3.7.2.3).

## 4 RESULTS

### 4.1 Complex formation between Hsp110s and Hsp70 NBDs

To investigate how Hsp70s and Hsp110s cooperate in protein folding as well as to elucidate the mechanistic basis for nucleotide exchange by Hsp110s on Hsp70s, we set out to solve the crystal structure of an Hsp110/Hsp70 complex. The first objective was to find protein constructs of Hsp70 and Hsp110 suitable for crystallization. In addition, we characterized these Hsp70/Hsp110 complexes by biochemical and biophysical methods: We investigated the nucleotide dependence of complex formation and determined the stoichiometry, the dissociation constant as well as the stability of the complex.

First, we optimized the Hsp70 partner for crystallization purposes. Earlier studies had revealed that the Hsp70 NBD is sufficient to form functional complexes with the NEFs GrpE, BAG-1, and HspBP1 (Harrison *et al.*, 1997; Sondermann *et al.*, 2001; Shomura *et al.*, 2005). We found that this is also the case for complex formation with Hsp110 family members. In size exclusion chromatography experiments, the NBDs of the yeast Hsp70 homologs Ssa1p (Ssa1N) and Ssb1p (Ssb1N) as well as of human Hsp70 (Hsp70N) coeluted with the ATP-bound yeast Hsp110 homolog Sse1p (Figure 4-1A and data not shown; for nucleotide dependence of complex formation see below). In absence of Sse1p, the NBDs eluted later, at the expected molecular weight. Complex formation was also observed for Hsp70N and its cognate NEF Hsp110 (data not shown). Furthermore, we could show that Sse1p is able to exchange nucleotide on Hsp70 NBDs. Sse1p·ATP accelerated the dissociation of the fluorescent probe MABA-ADP from Ssa1N and full-length Ssa1p as well as from heterologous Hsp70N to a similar degree when compared to the spontaneous dissociation (63-, 93-, and 103-fold, respectively; Figure 4-1B). For DnaK, the dissociation constant of MABA-ADP is comparable to that of unlabeled ADP, confirming that the presence of the fluorophore does not affect the binding mode of the nucleotide (Theyssen *et al.*, 1996). Two main conclusions can be drawn from these results: First, the interaction of cytosolic Hsp110s with the NBDs of Hsp70 homologs is sufficient for binding and nucleotide exchange. Second, the interaction between Hsp70s and Hsp110s seems to be highly conserved, since it not only occurs between endogenous pairs (Sse1p/Ssa1N, Sse1p/Ssb1N; Hsp110/Hsp70N) but also between heterologous partner proteins (Sse1p/Hsp70N). The latter finding might be a consequence of the remarkably high degree of sequence identity between the NBDs of canonical Hsp70 homologs (approximately 75 % sequence identity between yeast and human cytosolic orthologs).

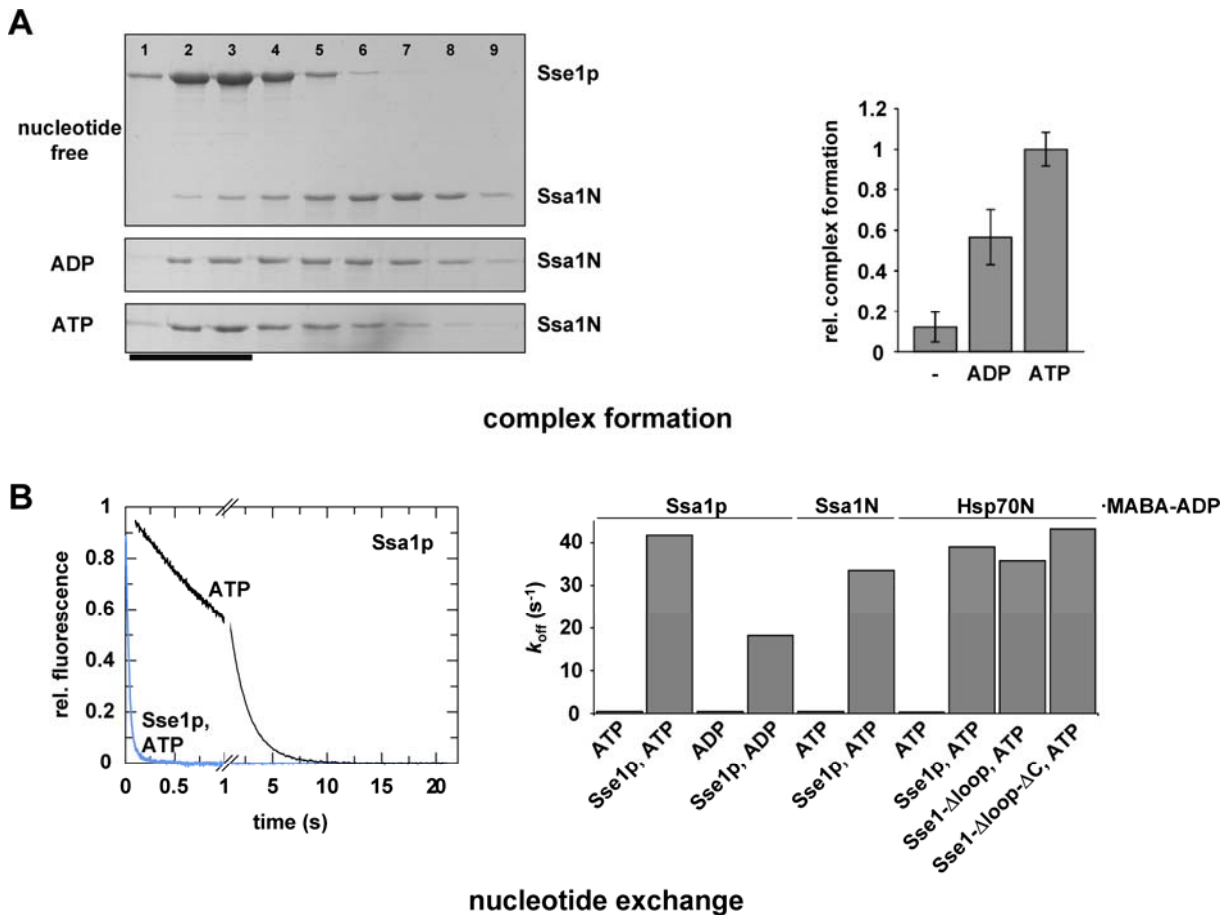


**Figure 4-1: Biochemical characterization of the Sse1p/Hsp70 interaction.**

(A) Sse1p/Ssa1N complex formation is most efficient in presence of ATP. A mixture of Sse1p, Ssa1N (17.2  $\mu$ M each) and either no nucleotide, ADP or ATP (40  $\mu$ M) was applied to a Superose 12 size exclusion chromatography column. Fractions were analyzed by SDS-PAGE (left panel), and the intensities of the Ssa1N bands in complex-containing fractions (lanes 1-3) were quantified by densitometry (right panel). Each gel filtration run was repeated three times, standard deviations (SDs) are indicated.

(B) Sse1p exchanges nucleotide on all tested Hsp70 proteins. The fluorescent probe MABA-ADP was bound to 2.5  $\mu$ M of an Hsp70 protein (Ssa1p, Ssa1N or Hsp70N, as indicated) and mixed in a stopped-flow apparatus with a solution containing 250  $\mu$ M ATP or ADP and either 2.5  $\mu$ M NEF or no protein. The fluorescence traces of four mixing experiments were averaged (left panel), and the decline in fluorescence was fitted with a mono- or bi-exponential model. The bars in the right panel indicate the rate constants for the dominant dissociation process in a representative experiment.

Not only the Hsp70 but also the Hsp110 partner protein was optimized for crystallization purposes. Compared to Hsp70 chaperones, the sequences of Hsp110/Grp170 homologs contain a poorly conserved and presumably flexible insertion in the  $\beta$ -sandwich domain and an extension at the ultimate C-terminus. Since these additional segments are comparatively short in yeast Sse1p and since Sse1p was found to be more stable than human Hsp110 (see below), Sse1p was chosen as Hsp110 partner in the complex. Several examples exist for dramatic improvements in crystallizability by removal of presumably disordered, charged loop insertions, for example in the cases of the Hsp90/Sba1 (Ali *et al.*, 2006) and the cap binding complex (Mazza *et al.*, 2001) structures. Therefore, we replaced the acidic insertion within the  $\beta$ -sandwich domain of Sse1p (amino acid residues 503-524) by the

peptide linker sequence AGSD. This substitution did neither affect protein stability nor nucleotide exchange activity compared to full-length Sse1p (Figure 4-1B, Figure 4-2C, and data not shown). The modified Sse1p variant was termed Sse1- $\Delta$ loop. Furthermore, the C-terminus (amino acid residues 658-693) of Sse1- $\Delta$ loop could be removed without perturbing the nucleotide exchange factor activity (Sse1- $\Delta$ loop- $\Delta$ C, Figure 4-1B). Thus, both variable segments in the Sse1p sequence are expendable for Hsp70N binding and nucleotide exchange activity.

Morano and coworkers reported that heterologous complex formation between Sse1p and C-terminally truncated bovine Hsp70 occurred most efficiently in presence of ATP (Shaner *et al.*, 2006). This is contrary to expectations since a NEF should compete with the nucleotide for Hsp70. In order to test whether nucleotide addition was indeed required for complex formation, we investigated the nucleotide dependence of complex formation for the Sse1p/Ssa1N complex (Figure 4-1A). While almost no complex formation was detectable by size exclusion chromatography in the absence of nucleotide, Ssa1N coeluted with Sse1p upon incubation with ATP or, to a lesser extent, after incubation with ADP. Analysis by size exclusion chromatography ensured that excessive nucleotide was removed. When ATP was included in the running buffer – as expected – no complex formation was observed (data not shown). Consistent with weaker complex formation in presence of ADP, Sse1p·ADP triggered nucleotide dissociation on Ssa1p less efficiently than Sse1p·ATP (Figure 4-1B).

Size distribution analysis of the complex-containing gel filtration fractions by field flow fractionation (FFF) followed by multiangle light scattering (MALS) analysis indicated 1:1 stoichiometry for all examined Sse1- $\Delta$ loop/NBD<sub>Hsp70</sub> complexes (Figure 4-2A). For the Sse1p/Ssa1N complex, we determined a  $K_D$  value of  $\sim 0.4 \mu\text{M}$  (Figure 4-2B), which is close to the  $K_D$  of  $\sim 0.1 \mu\text{M}$  reported for the interaction of the full-length proteins (Raviol *et al.*, 2006b), suggesting that the Hsp70 PBD does not contribute much to Hsp110 binding.

Limited proteolysis experiments with Proteinase K revealed that Sse1p and Sse1- $\Delta$ loop were significantly stabilized in presence of ATP and by complex formation with an Hsp70 NBD; Figure 4-2C shows the experiment for the Sse1p/Ssa1N complex (see also Shaner *et al.*, 2006). As demonstrated by mass spectrometry and Edman degradation, only the 36 C-terminal residues of the ATP-bound Sse1- $\Delta$ loop were removed, indicating that this region is accessible and presumably unstructured (data not shown). As mentioned above, these amino acid residues (658-693) are dispensable for function (Figure 4-1B and see also Shaner *et al.*, 2004). By contrast, human Hsp110 was found to be highly sensitive to Proteinase K also in presence of ATP and Hsp70N (data not shown). These data are consistent with the

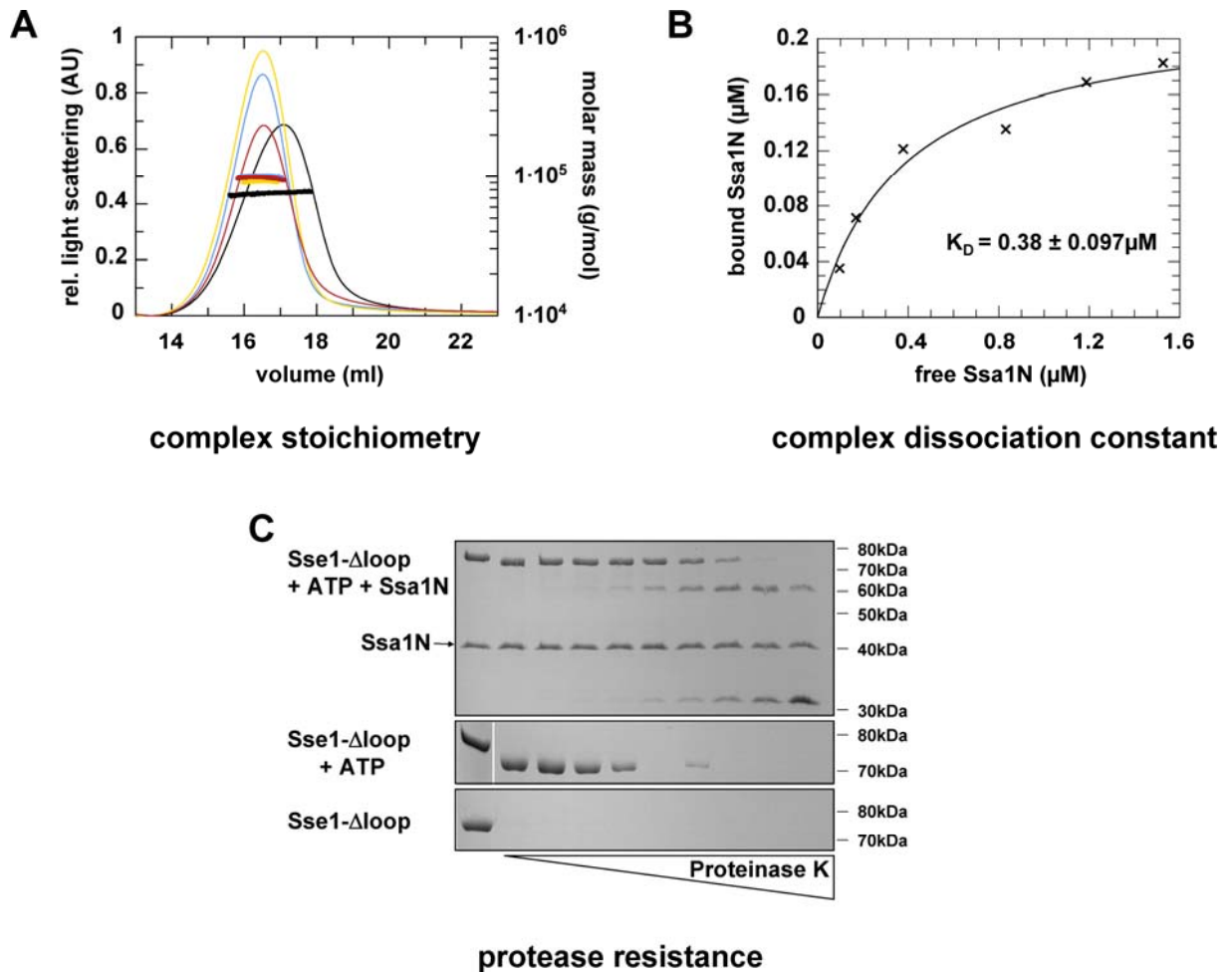


**Figure 4-2: Biochemical characterization of the Sse1p/Hsp70 interaction.**

(A) Sse1- $\Delta$ loop forms binary complexes with Hsp70 NBDs. The molar masses of the Sse1- $\Delta$ loop complexes as well as for uncomplexed Sse1- $\Delta$ loop were analyzed by FFF followed by MALS. The molecular masses of Sse1- $\Delta$ loop (black), Sse1- $\Delta$ loop/Ssa1N (blue), Sse1- $\Delta$ loop/Ssb1N (yellow), and Sse1- $\Delta$ loop/Hsp70N (red) were determined to 75.6 kDa (75.3 kDa), 101.1 kDa (117.0 kDa), 91.5 kDa (117.2 kDa), and 97.5 kDa (118.1 kDa), respectively. The numbers in brackets indicate the theoretical molecular masses calculated with the ExPASy ProtParam tool. In the graph, the horizontal lines across the peaks indicate the molar masses and homogeneities of the respective protein bands.

(B) The Sse1p/Ssa1N interaction is characterized by a similar  $K_D$  value as the Sse1p/Ssa1p interaction. The  $K_D$  value for complex formation between Sse1p and Ssa1N was estimated from the distribution of Ssa1N between supernatant and  $\text{Ni}^{2+}$  resin-bound His-tagged Sse1p at different Ssa1N concentrations. His-tagged Sse1p was pretreated with ATP and used at a concentration of 0.2  $\mu\text{M}$ .

(C) Sse1- $\Delta$ loop-ATP and Ssa1N form a protease-resistant complex. The indicated purified proteins were incubated with a series of increasing concentrations of Proteinase K (0, 0.5, 1, 2, 4, 8, 16, 32, 64, and 128  $\mu\text{g/ml}$ ) for 30 min at RT. The samples were analyzed by 8% SDS-PAGE. While nucleotide-free Sse1- $\Delta$ loop was degraded already at a Proteinase K concentration of 0.5  $\mu\text{g/ml}$ , Sse1- $\Delta$ loop was significantly stabilized in the presence of ATP. Further stabilization was observed in the additional presence of Ssa1N.

observation that Hsp110 was fragmented – likely by residual *E. coli* proteases – after incubation of an Hsp110/Hsp70N complex at 20 °C for 24 h, whereas the Sse1- $\Delta$ loop/Ssb1N complex remained unchanged under the same conditions. The Sse1- $\Delta$ loop/Ssa1N complex was shown to be stable for at least six days, when stored at 4 °C and in presence of protease inhibitor (data not shown).

## 4.2 Complex crystallization

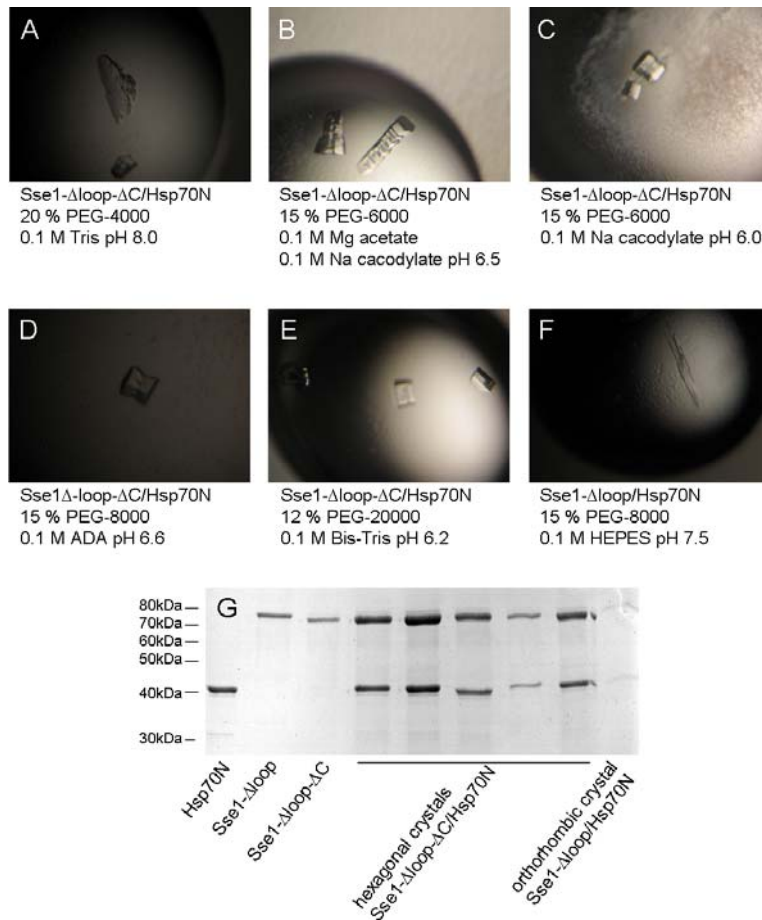


**Figure 4-3: Initial crystals for the Hsp110/Hsp70 complex.**

(A)-(E) The Sse1- $\Delta$ loop- $\Delta$ C/Hsp70N complex crystallized as hexagonal rods in many conditions (200-500  $\mu$ m). In all pictures, sideviews of the rods are shown; the crosssections had hexagonal shape. All precipitant solutions contained PEG and low salt concentrations or no salt at all. The protein concentration was 6.3 mg/ml, the sample buffer was HKM2. Crystallization was performed by the hanging drop vapor diffusion method in presence of Complete protease inhibitor at 4  $^{\circ}$ C.

(F) Sse1- $\Delta$ loop/Hsp70N initially crystallized as splayed rods in the indicated precipitant solution (~300  $\mu$ m). The protein concentration was 7.2 mg/ml. Apart from that, the experimental setup was identical to (A)-(E).

(G) Both crystal forms contained the two complex partners. To check the protein content, crystals washed with cryo buffer were dissolved in HKM2 buffer and applied to 10 % SDS-PAGE analysis. Since the dissolved orthorhombic Sse1- $\Delta$ loop/Hsp70N crystal was small, the corresponding protein bands were very pale after Coomassie staining. For comparison, purified Hsp70N, Sse1- $\Delta$ loop, and Sse1- $\Delta$ loop- $\Delta$ C were loaded on the gel as well.

The complexes were formed by mixing the respective Sse1p construct (Sse1- $\Delta$ loop or Sse1- $\Delta$ loop- $\Delta$ C) with an equimolar amount of one of the Hsp70 NBDs in presence of an excess of ATP. Unbound ATP and NBD were removed by size exclusion chromatography. Since the Sse1- $\Delta$ loop/Ssa1N complex was stable at 4  $^{\circ}$ C and in presence of protease inhibitor for at least six days (see chapter 4.1), all crystallization trials were performed under these conditions. Protein crystals were obtained from screens, which are specifically designed for the crystallization of protein-protein complexes and are characterized by mild pH conditions (Radaev and Sun, 2002; Radaev *et al.*, 2006). While we were unable to obtain regular crystals from complexes containing Ssa1N or Ssb1N, large (up to ~500  $\mu$ m) crystals of Hsp70N-containing complexes were found. From Sse1- $\Delta$ loop- $\Delta$ C/Hsp70N, hexagonal columns grew in many conditions that all contained PEGs of different molecular weights as a precipitant (Figure 4-3A-E). Crystallographic analysis showed that all these crystals had virtually the

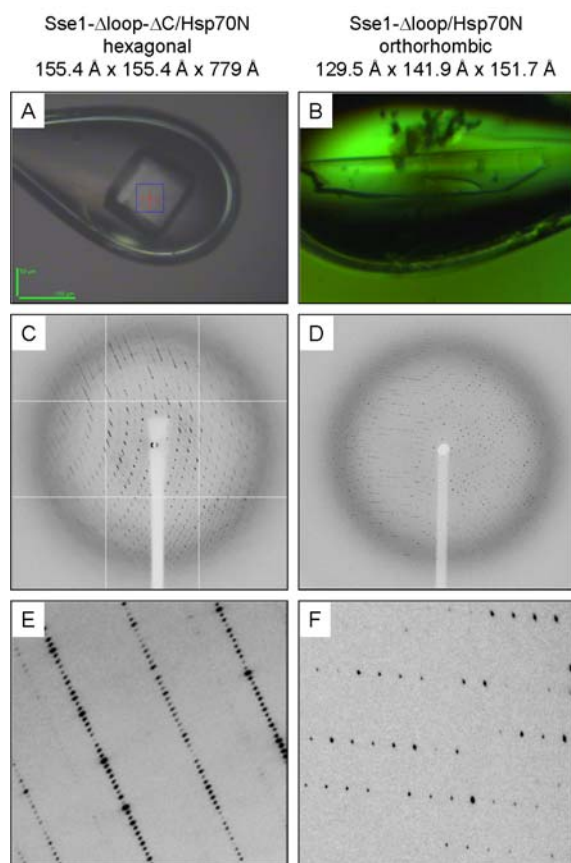


**Figure 4-4: Optimized crystals for the Hsp110/Hsp70 complex.**

(A) A hexagonal crystal (150  $\mu\text{m}$ ) of Sse1- $\Delta\text{loop-}\Delta\text{C}$ /Hsp70N mounted in a cryo loop is shown. The six-fold axis runs diagonally from the upper left to the lower right. During mounting, we aimed at orienting the long six-fold axis of the crystals along the rotation spindle of the goniometer to avoid spot overlap in the diffraction pattern. The blue box indicates the size and position of the X-ray beam during data collection.

(B) An orthorhombic crystal (300  $\mu\text{m}$ ) of Sse1- $\Delta\text{loop}$ /Hsp70N mounted in a cryo loop is shown.

(C) A diffraction image of a hexagonal crystal is depicted. As a consequence of the long  $c$  axis of the crystal (779  $\text{\AA}$ ), the reflections along the  $c$  direction (from upper left to lower right) were very close to each other in the reciprocal space. Furthermore, the anisotropy of the diffraction pattern becomes apparent: In  $c$  direction, the resolution was much better than in the other directions. The white vertical bar is the shadow of the beam stop, which prevents the primary beam to hit the detector in the center of the image. The diffuse halo at around 3.5  $\text{\AA}$  resolution is caused by X-ray scattering of unordered water molecules in the sample.

(D) A diffraction image of an orthorhombic crystal is depicted. The shadow of the beam stop and the diffuse halo resulting from X-ray scattering of water molecules are explained in (C).

(E) Magnification of a region of the diffraction image depicted in (C), highlighting the closeness of the reflections in  $c$  direction. Please note, that the rows of reflections have alternating intensities.

(F) Magnification of a region of the diffraction image depicted in (D). Since the unit cell of the orthorhombic crystals is much smaller than the one of the hexagonal crystals, the reflections are well separated in all three directions.

same unit cell dimensions. Remarkably, these crystals were only obtained when Sse1- $\Delta\text{loop-}\Delta\text{C}$  was produced *via* limited proteolysis of Sse1- $\Delta\text{loop}$ -ATP. Complexes formed with cloned and purified Sse1- $\Delta\text{loop-}\Delta\text{C}$  did not crystallize. Sse1- $\Delta\text{loop}$ /Hsp70N initially crystallized as splayed rods in 15 % PEG-8000, 0.1 M HEPES pH 7.5 (Figure 4-3F). Diffraction experiments at a microfocus beamline indicated that these rods were clusters of small crystals, whose diffraction power was however superior to the one of the hexagonal crystals. Optimization resulted in large, monocrystalline rods.

SDS-PAGE analysis confirmed that both crystal forms contained the two complex partners at apparent 1:1 stoichiometry (Figure 4-3G). The band patterns of the dissolved crystals were comparable to the one of the initial protein samples, indicating that further proteolysis did not occur.

Analysis of the diffraction datasets collected from the hexagonal crystals showed that the latter belonged to spacegroup  $P6_5$  or  $P6_1$  with unit cell dimensions of  $a \cdot b \cdot c = 155.4 \text{ \AA} \cdot 155.4 \text{ \AA} \cdot 779 \text{ \AA}$  (Figure 4-4A). The large  $c$  axis corresponded to a very small reciprocal lattice length and thus caused problems of spot overlap and misindexing (Figure 4-4E). Interestingly, every second diffraction order in  $a$  and  $b$  directions was very weak, indicating a superlattice structure in these directions (Figure 4-4E). The diffraction patterns were remarkably anisotropic, with resolution limits of  $3.2 \text{ \AA}$  along  $c$  and below  $4 \text{ \AA}$  in the other directions for the largest crystals (data obtained at ESRF beamline ID23-1, Figure 4-4C). With a Matthews coefficient of  $2.15 \text{ \AA}^3/\text{Da}$  (Matthews, 1968), the asymmetric unit was expected to contain 11 copies of the complex. The second crystal form was likely to harbor only two complexes per asymmetric unit and belonged to spacegroup  $P2_12_12_1$  with lattice parameters of  $a \cdot b \cdot c = 129.5 \text{ \AA} \cdot 141.9 \text{ \AA} \cdot 151.7 \text{ \AA}$  (Figure 4-4B,D,F and Table 4-1). Large crystals diffracted to  $2.3 \text{ \AA}$  resolution at SLS beamline X10SA. This crystal form was hence clearly superior for structure solution compared to the hexagonal lattice, and structure solution with the latter crystals was not followed up.

### 4.3 Structure determination

Structure solution by X-ray crystallography is achieved by summation of so-called structure factors, complex numbers which are characterized by an amplitude and a phase. While the amplitudes of the structure factors can be derived from the intensities of the reflections in the diffraction pattern (Figure 4-4C-F), the phase information is lost during the data collection process and can only be obtained indirectly. To solve the phase problem, a technique called multiple wavelength anomalous diffraction (MAD) can be applied. In MAD, the anomalous diffraction of heavy atoms is utilized for phase calculation. Anomalous diffraction occurs in the region of the absorption edge of heavy atoms and results in small differences in the intensities of symmetry-related reflections, which have the same intensity in normal elastic Thomson scattering. From the differences, the heavy atom substructure can be calculated, and the phases of the structure factors for the complete protein can be derived in a second step.

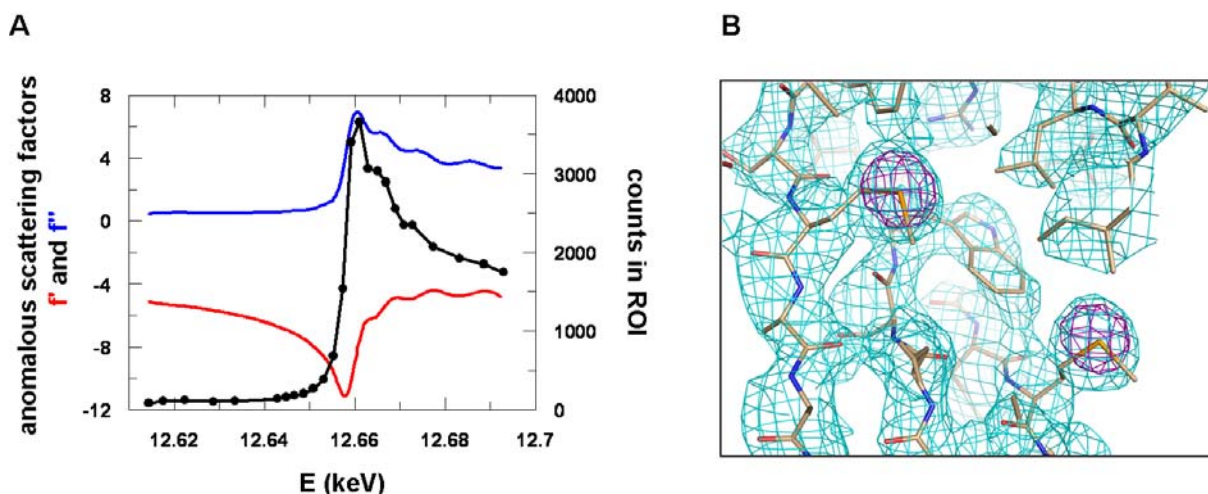


**Figure 4-5: Complex structure determination using MAD with selenium as anomalous scatterer.**

(A) An X-ray fluorescence excitation scan of a crystal containing the SeMet-derivatized complex is shown. The fluorescence excitation spectrum (black) was measured in the energy range of the  $K_I$  absorption edge of selenium. From the excitation spectrum, the anomalous scattering factors  $f'$  (red) and  $f''$  (blue) were calculated using the program Chooch (Evans and Pettifer, 2001). As collection wavelengths for the MAD datasets, the maximum of  $f''$  (12.662 keV, peak), the minimum of  $f'$  (12.657 keV, inflection point), and a remote wavelength clearly above the absorption edge (12.757 keV) were chosen.

(B) The experimental electron density map of a section of the  $\beta$ -sandwich domain of Sse1- $\Delta$ loop (chain A) is depicted. The electron density map (cyan) was calculated with 2.35 Å resolution data and was contoured at a  $\sigma$ -level of 1.2. The anomalous difference map is colored in violet ( $\sigma$ -level: 15), indicating the two selenium atoms in this section. The final model for the structure is shown in stick representation with carbon atoms colored in brown, nitrogen atoms in blue, oxygen atoms in red, and selenium atoms in orange.

In the present study, selenium was used as anomalous scatterer. Selenium was introduced by incorporation of the unnatural amino acid SeMet at methionine positions. Since selenium and sulphur have comparable covalence radii, SeMet is almost isosteric to methionine and virtually does not disrupt the protein structure. For incorporation, SeMet was added to the growth medium of the *E. coli* Sse1- $\Delta$ loop and Hsp70N expression strains, whose methionine biosynthesis was suppressed using catabolite repression. Crystals of the SeMet-labeled complex grew under similar conditions as crystals of the native complex and also belonged to space group  $P2_12_12_1$  with lattice parameters of  $a \cdot b \cdot c = 129.9 \text{ \AA} \cdot 141.5 \text{ \AA} \cdot 150.4 \text{ \AA}$  and a resolution limit of 2.35 Å (Table 4-1). The X-ray fluorescence excitation scan of the crystal shown in Figure 4-5A confirmed the incorporation of selenium into the complex proteins. In addition, the energy-dependent values of the anomalous scattering factors  $f'$  and  $f''$  of selenium were calculated from the fluorescence spectrum. For the MAD data collection, the two X-ray energies were selected, at which the contribution of  $f'$  and  $f''$  to the overall scattering factor of selenium  $f_{\text{anom}}$  was maximal ( $f_{\text{anom}} = f + \Delta f + if'' = f' + if''$ ). For the third reference dataset, an energy above the absorption edge was chosen (see chapter 3.7.3.3). From the anomalous differences within and between the datasets, the positions of 25 out of 34 selenium atoms in the asymmetric unit were determined by direct methods using ShelX-D

(Uson and Sheldrick, 1999) (Figure 4-5B). The heavy atom positions were refined and initial phases were calculated with Sharp (de la Fortelle and Bricogne, 1997). After density modification with Resolve (Terwilliger, 2000), readily interpretable electron density maps were obtained, starting from which a partial model could be automatically built using ArpWarp6.1 (Perrakis *et al.*, 1999) (Figure 4-5B). Subsequently, five cycles of iterative manual model building and refinement ( $R_{\text{free}}$  26.2 %, Table 4-1) were performed with Coot (Emsley and Cowtan, 2004) and Refmac5 (Murshudov *et al.*, 1997), respectively. In order to exclude any artifacts that could result from the substitution of methione by SeMet in the crystallized proteins, the final SeMet model was then used to solve a native dataset (see chapter 4.1), which was almost isomorphous to the MAD data and had a slightly higher resolution limit (2.3 Å). Automatic as well as subsequent manual model building were performed as described for the SeMet derivative. The structure was refined to a crystallographic R-factor of 19.7 % ( $R_{\text{free}}$  24.4 %, Table 4-1). Interestingly, application of the TLS refinement option of Refmac5, which implements anisotropic thermal motions of defined protein subdomains into the crystallographic refinement, improved the refinement statistics for both the SeMet-substituted and the native structure significantly (see chapter 3.7.3.3). Thus, it is likely that the protein domains in the Sse1- $\Delta$ loop/Hsp70N complex undergo rigid-body movements with respect to each other.

For both the SeMet-derivatized and the native crystal, the asymmetric unit contained two virtually identical copies of the Sse1- $\Delta$ loop/Hsp70N complex (r.m.s.d. of C $\alpha$  atom positions 0.714 Å, Figure 4-6A,C). The final model of the native protein complex comprised Sse1- $\Delta$ loop residues 2-500 and 525-654 in chain A as well as residues 2-498 and 526-655 in chain C. Interpretable electron density was not present for the non-natural linker sequence replacing Sse1p residues 503-524 and for the C-terminal segment of Sse1- $\Delta$ loop (residues 656-693). Both elements seem to be unstructured, which was corroborated for the C-terminus by the results of limited proteolysis with Proteinase K (see chapter 4.1). Furthermore, the model contained Hsp70 residues 4-382 for both chains B and D. Electron density in the ATP binding pocket of both Sse1- $\Delta$ loop molecules could be unambiguously assigned to ATP in complex with Mg<sup>2+</sup> and K<sup>+</sup> ions (Figure 4-6D). In addition, four further Mg<sup>2+</sup> ions, one glycerol molecule and 661 ordered water molecules were included into the final model. 207 of the water molecules were found at equivalent positions in the two copies of the complex. As judged by the program Procheck (Laskowski *et al.*, 1993), the model obeyed reasonable stereochemistry with 91.8 % of the  $\psi$ - $\phi$  torsion angles lying in the most favored regions of the Ramachandran plot, namely the regions of the secondary structure elements  $\alpha$ -helix,  $\beta$ -sheet,

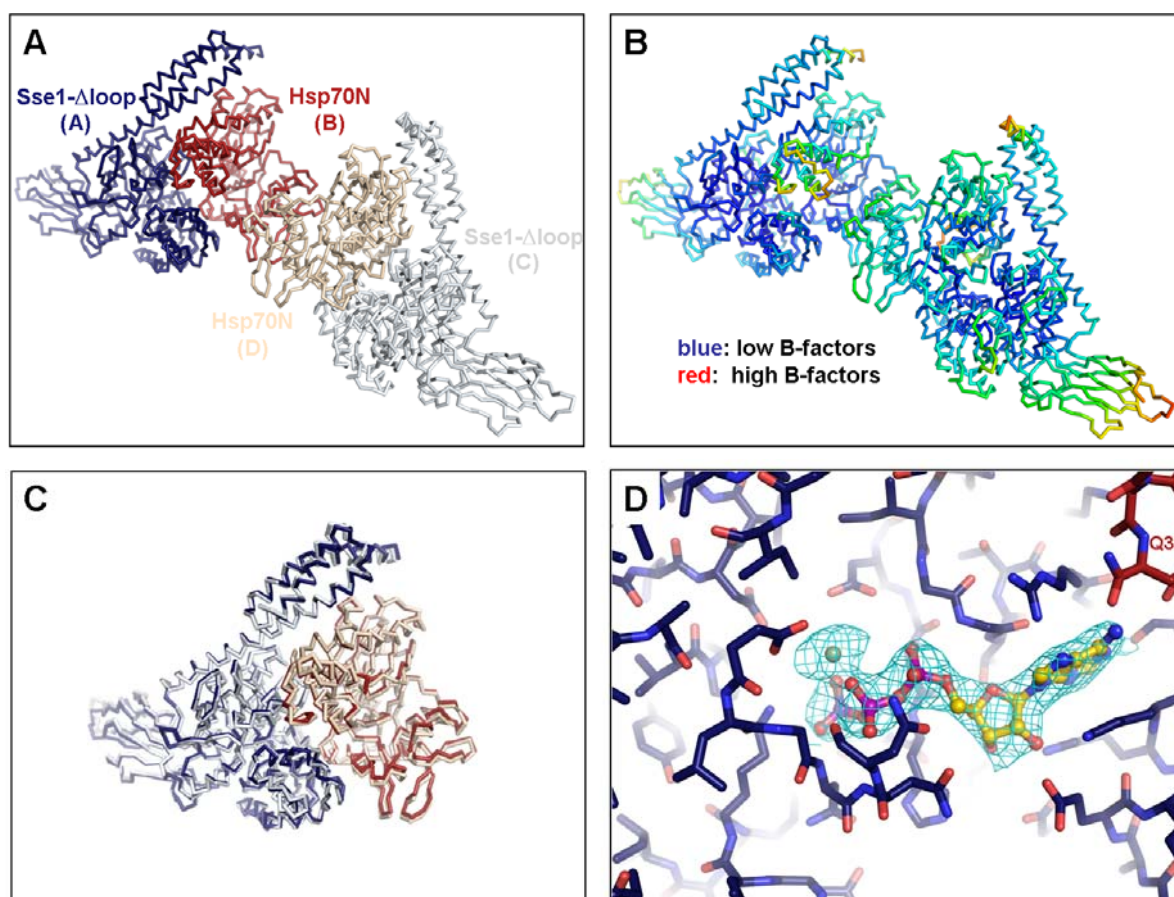


**Figure 4-6: Evaluation of the complex structure.**

(A) The asymmetric unit of both the SeMet-derivatized and the native crystal contained two copies of the Sse1- $\Delta$ loop/Hsp70N complex. Complex 1 consists of chains A and B, complex 2 of chains C and D.

(B) A B-factor plot for both complexes is shown. B-factors are represented in rainbow colors: Regions with low B-factors are colored in blue, regions with high B-factors are shown in red. In both complexes, the C-terminus and  $\beta$ -sandwich domain of Sse1- $\Delta$ loop as well as subdomain IIb of Hsp70N are the most flexible regions. Overall, complex AB is slightly better ordered than complex CD.

(C) A superposition of complexes AB and CD is shown. The two complexes are virtually identical. The r.m.s.d. of C $\alpha$  atom positions was determined to 0.714 Å.

(D) The nucleotide binding pocket of Sse1- $\Delta$ loop (chain A) is depicted. ATP is shown in ball-and-stick representation, and its experimental electron density is colored in cyan. The complexed Mg<sup>2+</sup> is represented as a green sphere. K<sup>+</sup> was only found in the electron density of the native complex. Carbon atoms of Sse1- $\Delta$ loop are colored in dark blue, carbon atoms of ATP in yellow. Note the hydrogen bond contact between the amino group of the adenine base and Q33 of Hsp70N (dark red, chain B) in the right upper corner. Heteroatoms are indicated as follows: nitrogen in blue, oxygen in red, and phosphorus in magenta. Atoms in the foreground are omitted for clarity.

and left-handed  $\alpha$ -helix (Ramachandran *et al.*, 1963) (Table 4-1). 7.6 % of the  $\psi$ - $\phi$  torsion angles were found in the additionally allowed, and 0.6 % in the generously allowed region. Only one residue, Gln409 of chain A, was declared as Ramachandran outlier. Overall, the complex of chains A and B was characterized by slightly lower B-factors than the complex of chains C and D, meaning that its electron density map was somewhat better defined (Figure 4-6B). For this reason, the structure of complex AB is discussed in the following. The data collection and refinement statistics for the SeMet-derivatized as well as the native crystals are summarized in Table 4-1.

**Table 4-1: Data collection and refinement statistics.**

(\*: values in parenthesis for outer resolution shell; \*\*: as defined in Scala (Evans, 1997); \*\*\*: as defined in Procheck (Laskowski *et al.*, 1993))

| <b>dataset</b>                    | <b>peak</b>                 | <b>infl</b>                 | <b>rm</b>                     | <b>native</b>               |
|-----------------------------------|-----------------------------|-----------------------------|-------------------------------|-----------------------------|
| beamline                          | SLS, X10SA                  | SLS, X10SA                  | SLS, X10SA                    | SLS, X10SA                  |
| wavelength (Å)                    | 0.9792                      | 0.9795                      | 0.9719                        | 0.9780                      |
| space group                       | $P2_12_12_1$                |                             |                               | $P2_12_12_1$                |
| cell dimensions,<br>a, b, c (Å);  | 129.88, 141.47,<br>150.44;  |                             |                               | 129.50, 141.90,<br>151.68;  |
| $\alpha, \beta, \gamma$ (°)       | 90, 90, 90                  |                             |                               | 90, 90, 90                  |
| resolution limits (Å)*            | 80.85 - 2.6<br>(2.74 - 2.6) | 80.85 - 2.6<br>(2.74 - 2.6) | 80.85 - 2.35<br>(2.48 - 2.35) | 75.81 - 2.3<br>(2.42 - 2.3) |
| $R_{\text{merge}}$ ***            | 0.064 (0.353)               | 0.064 (0.366)               | 0.058 (0.472)                 | 0.073 (0.506)               |
| I/sigma ***                       | 12.1 (2.5)                  | 12.0 (2.5)                  | 12.0 (2.3)                    | 11.8 (2.5)                  |
| multiplicity *                    | 3.6 (3.1)                   | 3.6 (3.1)                   | 3.7 (3.4)                     | 3.7 (3.5)                   |
| completeness (%) *                | 99.8 (99.0)                 | 99.8 (99.0)                 | 99.9 (99.7)                   | 100 (100)                   |
| complexes /a.u.                   | 2                           | 2                           | 2                             | 2                           |
| solvent content (%)               | 56.2                        |                             |                               |                             |
| Wilson B-factor (Å <sup>2</sup> ) | 59.91                       | 60.06                       | 50.11                         | 45.99                       |
| <b>Phasing</b>                    |                             |                             |                               |                             |
| sites                             | 25 (Se)                     | -                           |                               | -                           |
| phasing power ano                 | 0.948                       | 0.493                       | 0.565                         |                             |
| phasing power iso                 | 0.546                       | 0.906                       | -                             |                             |
| mean FoM                          |                             |                             | 0.378                         | -                           |
| <b>Refinement</b>                 |                             |                             |                               |                             |
| resolution range                  | -                           | -                           | 20 - 2.35                     | 20 - 2.3                    |
| reflections (test set)            | -                           | -                           | 109627 (5797)                 | 117858 (6248)               |
| $R_{\text{work}}$                 | -                           | -                           | 0.210                         | 0.197                       |
| $R_{\text{free}}$                 | -                           | -                           | 0.262                         | 0.244                       |
| number of atoms                   | -                           | -                           | 15835                         | 16199                       |
| r.m.s.d. bonds (Å)                | -                           | -                           | 0.012                         | 0.014                       |
| r.m.s.d. angles (°)               | -                           | -                           | 1.430                         | 1.430                       |
| Ramachandran plot ***             |                             |                             |                               |                             |
| % most favored region             | -                           | -                           | 90.8                          | 91.8                        |
| % additionally allowed            | -                           | -                           | 8.5                           | 7.6                         |

## 4.4 Structure of the Sse1- $\Delta$ loop/Hsp70N complex

### 4.4.1 Overview of the complex structure

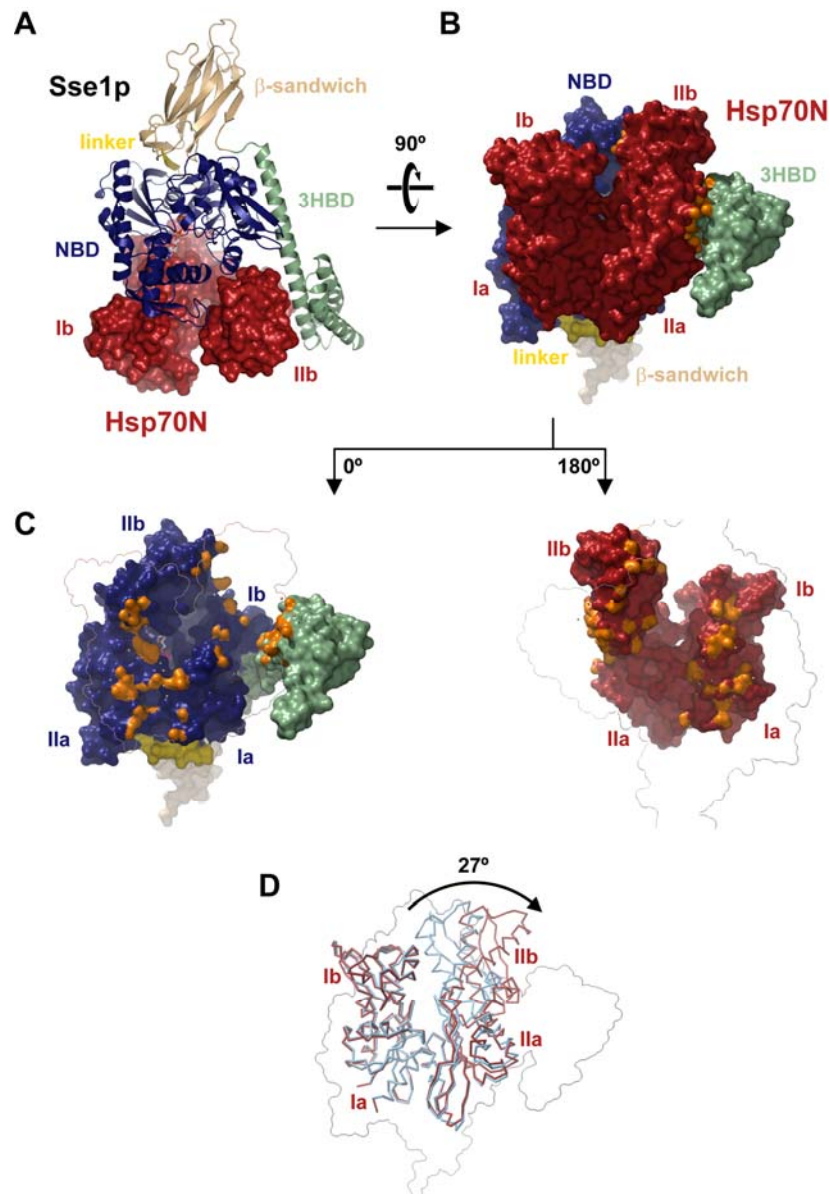


**Figure 4-7: Crystal structure of the Sse1p·ATP/Hsp70N complex.**

(A) The frontal view of the complex illustrates the domain organization of the yeast Hsp110 homolog Sse1p. Sse1p is shown in ribbon representation with the NBD colored in dark blue, the linker segment in yellow (in the background), the  $\beta$ -sandwich domain in brown, and the 3HBD in green. The NBD of human Hsp70, Hsp70N, is shown in surface representation in dark red. The subdomain structure of Hsp70N is indicated.

(B) A bottom view of the complex in surface representation is shown using the same coloring scheme as in panel (A).

(C) Cut-away views on the Sse1p/Hsp70N interface are shown. The position of the interaction partner is indicated by its outline. Atoms mediating the Sse1p/Hsp70N interaction are colored in orange. Water molecules connecting the binding partners *via* hydrogen bonds are indicated as beige spheres. Sse1p-bound ATP is shown in ball-and-stick representation. The subdomain structures of the NBDs are indicated, and the color code for the protein domains corresponds to the one introduced in (A).

(D) Superposition of an Hsp70N·ADP complex (light blue, structure solved by Dr. A. Bracher) with nucleotide-free Hsp70N (red) crystallized in this study illustrates the 27° rotation of Hsp70N subdomain IIb upon binding of Sse1p. The position of Sse1p is indicated by an outline. The orientation of the structure is the same as in panel (C). Please note that subdomain IIb of the Hsp70N·ADP complex would clash with Sse1p subdomain IIb.

As a member of the Hsp70 superfamily, Sse1p shares the general domain organization of canonical Hsp70 proteins, consisting of an N-terminal Hsp70/actin-type NBD, a  $\beta$ -sandwich domain and a C-terminal 3HBD (Figure 4-7A). In the crystallized complex, the latter two Sse1p domains are arranged along the NBD and point into opposite directions. This domain arrangement differs from the one observed for the isolated PBD of DnaK, in which the 3HBD forms a lid over the peptide binding cleft of the  $\beta$ -sandwich domain (Figure 2-5; Zhu *et al.*, 1996).

All interactions with the NBD of Hsp70 are mediated by the NBD and the 3HBD of Sse1p. (In the following description of the crystal structure, Sse1p will be used instead of Sse1- $\Delta$ loop, assuming that all observations made for Sse1- $\Delta$ loop are also valid for wt Sse1p.) Specifically, the NBDs of Sse1p and Hsp70 are oriented towards each other with contacts between subdomains Iib and Ib, Iia and Ia, and Ib and Iib of Sse1p and Hsp70, respectively (Figure 4-7C). Furthermore, the 3HBD of Sse1p tightly contacts the flank of Hsp70 subdomain Iib. As a consequence, subdomain Iib of Hsp70 is clamped between the 3HBD and the flank of subdomain Iib of Sse1p, and rotated 27 ° sideways with respect to the rest of the NBD (Figure 4-7A,C,E). In this open conformation, the binding sites for the adenosine moiety on subdomain Iib and the catalytic and triphosphate binding residues on lobe I of the Hsp70 NBD are moved apart, diminishing the affinity for adenine nucleotides and thus facilitating nucleotide exchange. This mechanism of nucleotide exchange resembles the conformational switch induced by GrpE in DnaK and by the BAG domain of BAG-1 in Hsc70, although the conformational change in the Hsp70 binding partner is less pronounced in these complexes ( $\sim$ 14 ° rotation of subdomain Iib) (Harrison *et al.*, 1997; Sondermann *et al.*, 2001). In line with these findings, the Hsp70 NBD is stable against proteolysis in complex with Sse1p or BAG, while HspBP1, which operates by a different mechanism, induces a partially protease sensitive conformation of the NBD (Figure 4-1E, data not shown and Shomura *et al.*, 2005).

#### 4.4.2 Structure of Sse1p·ATP in the complex

Overall, the structure of the Hsp70N-complexed Sse1p·ATP is stabilized by extended and intimate domain-domain interactions, which are predominantly hydrophobic in character (Figure 4-7A,B). In addition, as indicated by the results of limited proteolysis, ATP binding contributes to the stability of the multi-domain protein, which is highly protease-sensitive in the absence of nucleotide (Figure 4-2C and Shaner *et al.*, 2004). Notably, the NBD/linker,

NBD/ $\beta$ -sandwich domain, and NBD/3HBD interfaces are also highly conserved within canonical Hsp70s, despite limited overall sequence similarity between canonical Hsp70s and Hsp110s. Thus, it appears plausible that the conformation found for Sse1p·ATP in complex with Hsp70N might serve as a good model for the transient ATP state of canonical Hsp70s, which is characterized by low-affinity peptide binding (see also chapter 5.1 and Liu and Hendrickson, 2007).

#### 4.4.2.1 The ATP-bound Sse1p NBD

Very similar to the known structures of canonical Hsp70 NBDs, the NBD of Sse1p consists of two lobes (lobes I and II), which enclose a central nucleotide binding pocket. The individual lobes of Sse1p superimpose well with the respective lobes of an ADP-bound Hsc70 NBD (Jiang *et al.*, 2007). For lobe I, 197 of 209 Sse1p C $\alpha$  atoms could be aligned with an r.m.s.d. of 0.933 Å. For lobe II, 170 of 176 C $\alpha$  atoms were aligned with an r.m.s.d. of 1.19 Å. However, the orientations of the lobes with respect to each other differ between the structures. Compared to the Hsc70 NBD, the two lobes of the Sse1p NBD are twisted against each other by  $\sim 23^\circ$  around a rotation axis diagonally traversing the NBD (Figure 4-8A). As a consequence, the tip of subdomain IIb shifts approximately 8 Å in comparison to the Hsc70 structure. Since the bound nucleotide is close to the rotation axis, the shifts are not as drastic in its vicinity. Only this twisted subdomain topology of the Sse1p NBD appears to enable the intricate interactions with Hsp70N (see chapter 4.4.1). The Sse1p lobe arrangement seems to be stabilized by extensive inter-domain interactions with the linker segment (residues 385-399) (chapter 4.4.2.2), the  $\beta$ -sandwich domain (chapter 4.4.2.3), and the N-terminal segment of the 3HBD (chapter 4.4.2.4). Additionally, backbone contacts from both lobes to the  $\gamma$ -phosphate of ATP might contribute to the stabilization of the Sse1p NBD (Figure 4-8B).

The ATP binding mode observed in the Hsp70N-complexed Sse1p resembles the interactions found in previous structures of canonical Hsp70s in complex with nucleotides (Figure 4-8B) (Wilbanks and McKay, 1995; O'Brien *et al.*, 1996). Whereas lobe I interacts with the triphosphate moiety of ATP, the adenosine moiety is bound by subdomain IIb. Furthermore, also Mg<sup>2+</sup> and K<sup>+</sup> are coordinated in an Hsp70-like manner. The conformations of the AMP moieties of Sse1p-bound ATP and Hsc70N-bound ADP are very similar (Figure 4-8C) (Jiang *et al.*, 2007). However, the catalytic residues Lys69 and Asp174, counterparts to Hsc70 residues Lys71 and Glu175, are displaced in Sse1p, explaining how ATP remained intact during several weeks at 4 °C which passed between crystallization set-up and crystal mounting. A number of highly conserved Hsp70 residues, which directly interact with the

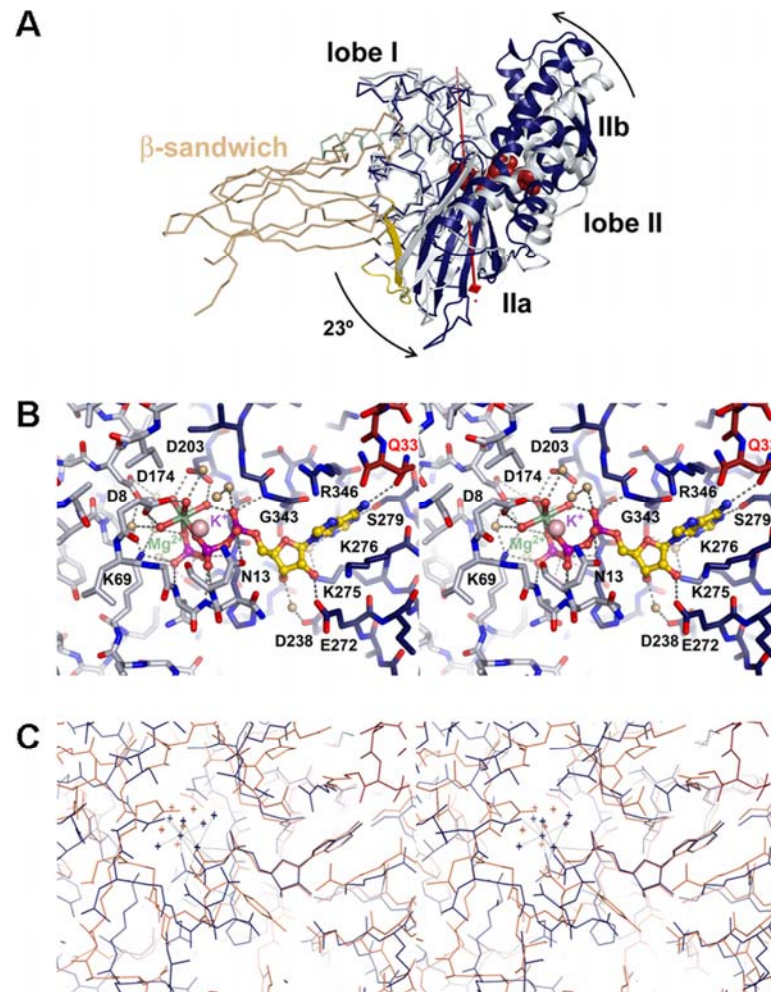


**Figure 4-8: The NBD of Sse1p.**

(A) The superposition of the NBDs of Sse1p-ATP and bovine Hsc70-ADP (PDB entry code 1HPM (Wilbanks and McKay, 1995)) illustrates the twisted lobe arrangement in Sse1p. Sse1p domains are colored as in Figure 4-7, and Hsc70N is represented in white. The rotation axis for reorientation of the lobes in Sse1p is indicated in red. ATP is shown as red space-filling model. To highlight lobe II and the linker, these two elements are represented as ribbons; the remaining backbone is shown as  $\alpha$  trace.

(B) A stereo representation of ATP bound to Sse1p as observed in the complex with Hsp70N is shown. The orientation of the structure is the same as in Figure 4-6D. ATP-Mg<sup>2+</sup> is shown in ball-and-stick representation. A potassium ion in contact with the triphosphate moiety is shown as a pink sphere. Hydrogen bond contacts are indicated by dashed lines. Bridging water molecules are shown as beige spheres. Carbon atoms in lobes I and II are colored in grey and dark blue, respectively. Carbon atoms of Hsp70N (right upper corner) are shown in red, carbon atoms of ATP in yellow. Heteroatoms are indicated as follows: magnesium in green, nitrogen in blue, oxygen in red, and phosphorus in magenta. ATP-Mg<sup>2+</sup> contacting residues in the foreground are labeled. The  $\gamma$ -phosphate is in direct hydrogen-bond contact to the amide groups of residues from both lobes I and II, and to the sidechains of K69 and S207. Atoms in the foreground and ordered water molecules without direct contact to ATP-Mg<sup>2+</sup> are omitted for clarity.

(C) Comparison of the nucleotide binding pockets of Sse1p-ATP and of bovine Hsc70N-ADP (PDB entry code 2QWL (Jiang *et al.*, 2007)). The view is the same as in (B). The Sse1p-ATP structure is shown in dark blue, Hsc70N-ADP in orange. The Hsp70N backbone (right upper corner) is colored in red. Magnesium, potassium, and magnesium-coordinating water molecules are shown as small crosses. Metal-ligand bonds in Sse1p are indicated by dashed lines. For the shown representation, the atoms of the AMP moieties of complexed ATP and ADP molecules were superposed. The reorientation of the two lobes in the NBD of Sse1p in comparison to Hsc70N gets apparent. Especially, residues from lobe I on the left, such as K69 (K71 in Hsc70), are clearly shifted to the right and backwards.

bound nucleotide and some of which were implicated in linking ATP hydrolysis to peptide binding (Sousa and McKay, 1998), are not stringently conserved in Hsp110s, suggesting that

such allosteric coupling is not critical for Hsp110 function. For example, the following substitutions are observed in Sse1p: Thr13Asn, Thr14Asn, Tyr15Asn, Gly202His, Gly203Ser, and Thr204Ser (numbering for bovine Hsc70 and substitutions as found in the Sse1p sequence, Figure 7-1 (page 151)). Intriguingly, even the catalytic key residue Lys71 (bovine Hsc70 numbering) is replaced in several ER-homologs of Sse1p (data not shown). Taken together, these observations are consistent with the proposition from Morano and colleagues that only ATP binding – but not ATP hydrolysis – is required for Hsp110/Grp170 function (Shaner *et al.*, 2004; Raviol *et al.*, 2006a).

#### 4.4.2.2 The Sse1p inter-domain linker

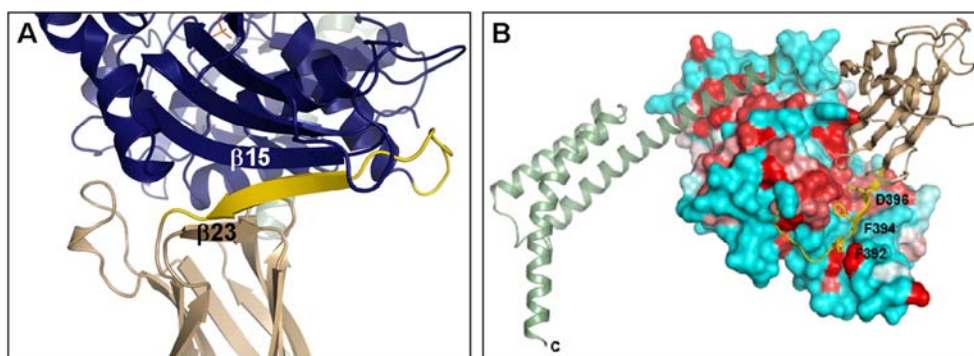


**Figure 4-9: The Sse1p linker.**

(A) A magnification of the linker region of Sse1p is shown. Sse1p domains are colored as in Figure 4-7. Whereas Sse1p is shown in ribbon representation, ATP is depicted in stick representation. The linker segment forms a rigid link between the NBD and the  $\beta$ -sandwich domain, by aligning to  $\beta$ -strands  $\beta$ 15 and  $\beta$ 23.  $\beta$ 23 bridges the two layers of the  $\beta$ -sandwich structure.

(B) The interactions of the linker with the cleft at the base of the NBD are illustrated in detail. The NBD of Sse1p is shown in surface representation, the other domains are depicted as ribbons and colored as in Figure 4-7. For the NBD, a color gradient from red over white to blue indicates decreasing conservation among Hsp70 and Hsp110 sequences: Residues identical among Hsp70/Hsp110 homologs are colored red, residue positions with 50 % identical residues are shown in white. Regions in cyan are variable. The conserved linker sidechains F392, F394 and D396 are shown in stick representation.

In the structure of Sse1p as observed in complex with Hsp70, the so-called linker segment (residues 385-399) rigidly connects the NBD with the  $\beta$ -sandwich domain. The linker is composed of a loop followed by a  $\beta$ -strand, which extends the  $\beta$ -sheet in subdomain IIa of Sse1p by aligning in a parallel fashion to  $\beta$ -strand  $\beta$ 15 and which pairs with  $\beta$ -strand  $\beta$ 23 of the  $\beta$ -sandwich domain (Figure 4-9A). Specifically, the sidechains of Phe392 and Phe394 bind into hydrophobic pockets at the cleft located at the base of the NBD, and the highly conserved residue Asp396 forms hydrogen bonds with the sidechains of Thr176 and Asn173, which both belong to NBD subdomain Ia (Figure 4-9B).

In the sequences of canonical Hsp70s, this linker region is highly conserved with the invariable aspartate residue (Sse1p numbering: Asp396) being preceded by a succession of

four hydrophobic residues (Figure 2-5C), while in Hsp110 sequences hydrophobic and polar positions alternate (Figure 7-1). Whereas the Hsp70 linker was shown to be flexible and exposed in the nucleotide-free as well as in the ADP state of the NBD, it is protected from solvent in the ATP state (Rist *et al.*, 2006; Swain *et al.*, 2007; Chang *et al.*, 2008). Since the NBD amino acid residues interacting with the linker are conserved among Hsp70 and Hsp110 sequences (Figure 4-9B), it seems plausible that the linker in Hsp70·ATP assumes a similar conformation as in Hsp70N-complexed Sse1p·ATP.

#### 4.4.2.3 The Sse1p $\beta$ -sandwich domain

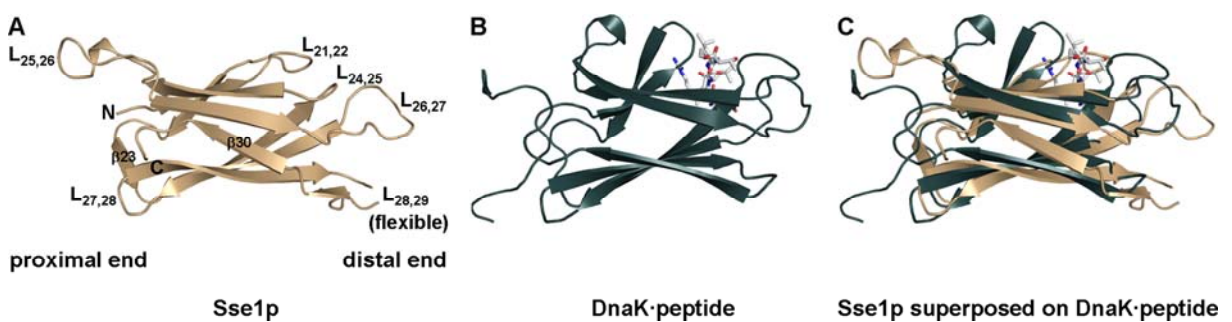


**Figure 4-10: The Sse1p  $\beta$ -sandwich domain.**

(A) A ribbon representation of the  $\beta$ -sandwich domain of Sse1p is shown. The ends proximal and distal to the NBD are indicated. Furthermore, selected  $\beta$ -strands and loop connections as well as the N- and C-termini are labeled.

(B) A ribbon representation of the  $\beta$ -sandwich domain of DnaK in complex with the substrate peptide NRLLLTG is shown (PDB entry code 1DKZ (Zhu *et al.*, 1996)). The peptide is depicted in stick representation. The molecule orientation corresponds to the one in (A).

(C) For comparison, the  $\beta$ -sandwich domains of Sse1p (brown) and DnaK (green) are shown superposed onto each other. Intriguingly, the peptide binding cleft is closed in the Sse1p structure as the loops L<sub>21,22</sub> and L<sub>24,25</sub> pack against one another.

Despite low sequence homology, the  $\beta$ -sandwich domain of Sse1p shares the general secondary structure topology (two stacked  $\beta$ -sheets) with canonical Hsp70s (Figure 4-10). However, the final  $\beta$ -strand segment  $\beta$ 30 forms hydrogen bond contacts with both  $\beta$ -sheets of the Sse1p  $\beta$ -sandwich domain. As a consequence, the  $\beta$ -sandwich domain of Sse1p is more barrel-like compared to DnaK (Figure 4-10A,B). Furthermore – probably resulting from the low sequence similarity between the  $\beta$ -sandwich domains of Hsp110s and canonical Hsp70s – the loop structures at the distal end deviate significantly (Figure 4-10C). Conspicuously, Hsp110 homologs are characterized by a variable insertion, which is located between  $\beta$ 28 and  $\beta$ 29 (L<sub>28,29</sub>) in the structure of Sse1p. In the crystallized Sse1- $\Delta$ loop construct, this segment was replaced by a short peptide linker, which was found to be disordered. Moreover and most significantly, the peptide binding cleft, which is formed by two distal loops corresponding to L<sub>21,22</sub> and L<sub>24,25</sub> in the DnaK/peptide complex, is closed in the Hsp70N-complexed Sse1p. The

flanking loops (Sse1p nomenclature: L<sub>25,26</sub> and L<sub>26,27</sub>) also differ significantly in length, sequence and position from canonical Hsp70s, in which these regions are highly conserved. Based on the structural data, it is thus unclear whether Sse1p is able to interact with substrate peptides similarly to canonical Hsp70s.

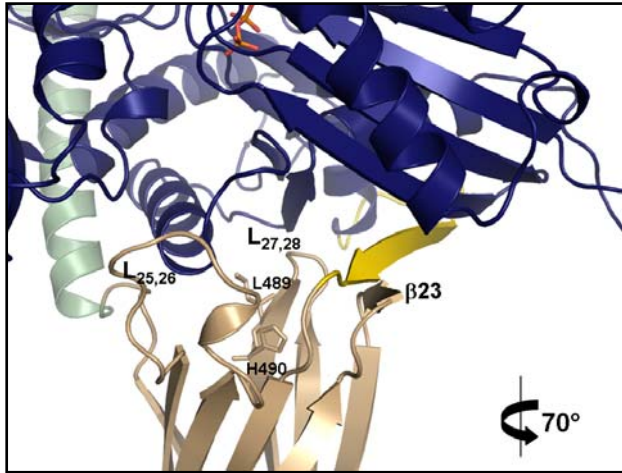


**Figure 4-11: The  $\beta$ -sandwich domain/NBD interaction in Sse1p.**

A magnification of the  $\beta$ -sandwich domain/NBD interaction region of Sse1p is shown. Sse1p domains are colored as in Figure 4-7. Whereas Sse1p is shown in ribbon representation, ATP is depicted in stick representation. The loops L<sub>25,26</sub> and L<sub>27,28</sub>, which mediate the interaction, are indicated.  $\beta$ -strand  $\beta$ 23 and the amino acid residues Leu489 and His490 are labeled. The molecule is rotated by 70° compared to the view in Figure 4-9A.

In the structure of Sse1p, the proximal end of the  $\beta$ -sandwich domain and the base of the NBD form extensive contacts. The contact between the  $\beta$ -sandwich domain and NBD lobe II is exclusively mediated *via* the linker segment (Figure 4-9 and Figure 4-11). In contrast, the contact between the  $\beta$ -sandwich domain and NBD lobe I is direct, with the most intimate contacts being formed by two loop connections, L<sub>25,26</sub> and L<sub>27,28</sub>, which are juxtaposed at the proximal end of the  $\beta$ -sandwich (Figure 4-11). L<sub>27,28</sub> also contacts  $\beta$ 23, which interacts tightly with the linker. The importance of this segment for Hsp70/Hsp110 function becomes evident from its high sequence conservation throughout the entire Hsp70 protein family (Figure 7-1). In contrast, the loop connection L<sub>25,26</sub>, which forms the interface to the 3HBD ("lid") in the DnaK/peptide complex, is poorly conserved in Hsp110 homologs. This indicates that a stable association between the  $\beta$ -sandwich domain and the 3HBD as observed in the structure of the peptide complex of DnaK (Zhu *et al.*, 1996) is dispensable for Hsp110 function.

#### 4.4.2.4 The Sse1p 3HBD

In the Sse1p/Hsp70N complex, the 3HBD of Sse1p does not form a "lid" over the peptide binding pocket as observed in the structure of the DnaK PBD/peptide complex (Figure 2-5B; Zhu *et al.*, 1996), but instead interacts with the NBD and points away from the  $\beta$ -sandwich domain (Figure 4-7A). The intimate interaction between the N-terminal segment of the 3HBD and the flank of NBD lobe I ensures the correct positioning of the 3HBD, and thus is probably critical for complex formation with Hsp70N. The core of the extensive interface is formed by

buried polar interactions of residue Arg47 with Glu554 and Asp561 (Figure 4-12A). These polar residues are flanked by large hydrophobic clusters comprising residues Phe106, Phe113, Met121, Ile163, Leu547, Leu550, Ile551, Met557, and Leu558. Interestingly, in the closed lid conformation as observed in the peptide complex of DnaK, equivalent residues of the 3HBD bind to the  $\beta$ -sandwich domain and thereby ensure tight substrate binding (Zhu *et al.*, 1996).

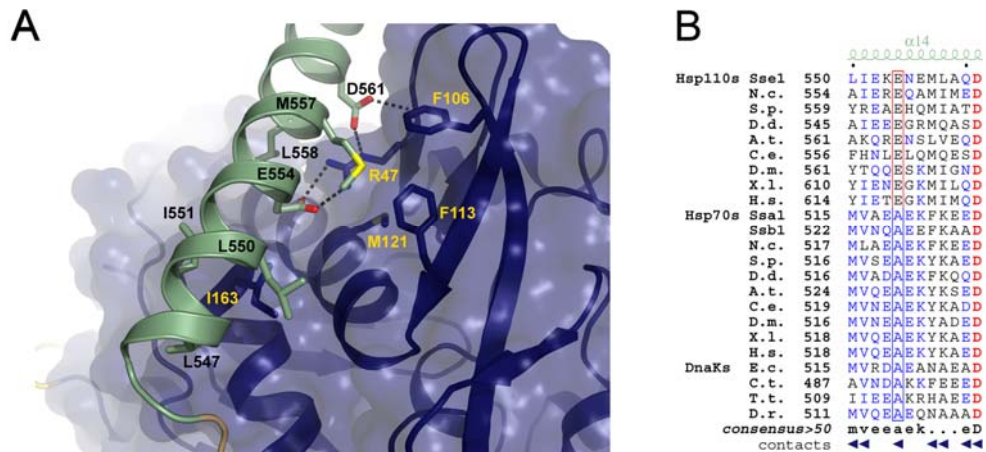


**Figure 4-12: The Sse1p 3HBD.**

(A) The tight interactions between the N-terminal part of the 3HBD and the flank of lobe I in Sse1p are shown. Sse1p domains are colored as in Figure 4-7. The buried polar interactions at the core of the interface are indicated by dashed lines. Key interacting residues are labeled.

(B) A sequence alignment of the 3HBD segment is shown, which contacts the NBD in the Sse1p and the  $\beta$ -sandwich domain in the DnaK/peptide crystal structures (Zhu *et al.*, 1996). Amino acid sequences of selected Hsp110, eukaryotic Hsp70 and bacterial DnaK homologs were aligned. Residues indicated in red are invariant, residues colored in blue are conserved in more than 50 % of the sequences. Residues that contact the NBD of Sse1p are indicated by blue arrowheads. As indicated by red and blue boxes, the consensus sequences for Hsp110s and canonical Hsp70s differ systematically at position 554 (Sse1p numbering). An unbridged version of the alignment is shown in Figure 7-1.

Since the chemical character of all the listed 3HBD and NBD lobe I residues is conserved among Hsp70/Hsp110 sequences (Figure 4-9B and Figure 7-1), such an interaction between the 3HBD and the NBD might contribute to the conformational cycle of canonical Hsp70s. One notable exception regarding the degree of conservation is Glu554, which is systematically replaced by Ala in canonical Hsp70s and by larger hydrophobic residues, such as Leu and Val, in ER-resident Hsp110s (Figure 4-12B and data not shown). On the one hand, the replacement of Glu by Ala might weaken the interaction between the 3HBD and the NBD in canonical Hsp70s, but on the other hand, the Ala residue seems to be essential for the interaction between the 3HBD and the  $\beta$ -sandwich domain in the closed conformation of the PBD. Whereas Ala is small enough to be buried at the interface between the 3HBD and the  $\beta$ -sandwich domain (Zhu *et al.*, 1996), residues with larger sidechains might prevent closure of the lid, questioning whether Sse1p can stably assume such a conformation. Taken together, the tight interaction of the lid domain with the NBD, which is likely required for efficient

catalysis of nucleotide exchange, and the formation of a stably closed conformation of the PBD might be mutually exclusive features of Hsp110 and Hsp70 chaperones, respectively.

#### 4.4.3 Intermolecular interface in the Sse1p/Hsp70 complex

The extensive protein-protein interface in the Sse1p/Hsp70N complex, which buries  $\sim 1760 \text{ \AA}^2$  of surface on each binding partner, is mostly polar in character, including a large number of ordered water molecules in hydrogen bond contact to both proteins. The high  $S_c$  value of 0.74, an overall measure of surface shape complementarity (Lawrence and Colman, 1993), is comparable to that observed in stable protein complexes such as hemoglobin ( $S_c$  0.74).

The closest interactions are found between the 3HBD of Sse1p and  $\alpha$ -helix 9 of Hsp70N (Figure 4-13A). The N-terminus of helix  $\alpha 9$  is in close contact to the sidechain of Asn572<sup>S</sup> (<sup>S</sup> indicates Sse1p residues, <sup>H</sup> Hsp70N residues). The highly conserved adjacent Hsp70 residue Ala300<sup>H</sup> mediates an intimate van-der-Waals contact to the Sse1p backbone between residues Glu575<sup>S</sup> and Glu576<sup>S</sup>, which in turn are engaged in hydrogen bond contacts to Hsp70 residues Thr298<sup>H</sup> and Lys348<sup>H</sup>, respectively (Figure 4-13A,D). Tyr579<sup>S</sup> makes additional van-der-Waals contacts to Ala300<sup>H</sup> and Glu304<sup>H</sup>. Remarkably, Glu304<sup>S</sup> replaces the corresponding Ala300<sup>H</sup> in Sse1p. This amino acid exchange might contribute to the avoidance of non-productive Hsp110 homodimer formation (see also below).

Interestingly, Hsp70 also makes close contacts to the nucleotide binding pocket of Sse1p (Figure 4-13B). Gln33<sup>H</sup> directly contacts the adenine amino group of ATP. Furthermore, Gln33<sup>H</sup> is in van-der-Waals contact to Ala280<sup>S</sup> and Ser279<sup>S</sup>, with the former intercalating between Ala54<sup>H</sup> and Gln33<sup>H</sup> and the latter forming a tight hydrogen bond to ATP. All Hsp110 homologs have a small Ala or Ser residue at position 280 of the NBD, enabling rigid backbone contacts with their binding partners (Figure 4-13E). The neighboring residue, Asn281<sup>S</sup>, is in close hydrogen bond contact to Asn57<sup>H</sup>. Two ordered water molecules mediate additional hydrogen bonds between both partners. The sidechain of Arg346<sup>S</sup> flanks the nucleobase of ATP and forms a  $\pi$ -stacking interaction with the peptide bond between Gln33<sup>H</sup> and Gly34<sup>H</sup>. These close contacts of Hsp70 to the nucleotide and the nucleotide binding residues in Sse1p can explain, at least in part, the requirement of nucleotide binding for the Sse1p/Hsp70 interaction.

A further area of close surface complementarity with Hsp70 was found at residues 364-367 in Sse1p, which contact the backbone of Hsp70 subdomain Ia at residues 133 and 134 as well as the sidechain of Tyr134<sup>H</sup> (Figure 4-13C). At this interface, intramolecular hydrogen

bonds of Thr365<sup>S</sup> and Asn367<sup>S</sup> appear to shape the surface of Sse1p into a conformation that cradles Tyr134<sup>H</sup>. The contacts between subdomain IIb of Hsp70 and the NBD of Sse1p appear to be less well defined. One notable exception is the conserved Lys262<sup>S</sup> which forms a salt bridge with Asp285<sup>H</sup>. No contacts were found to subdomain IIa of Hsp70N.

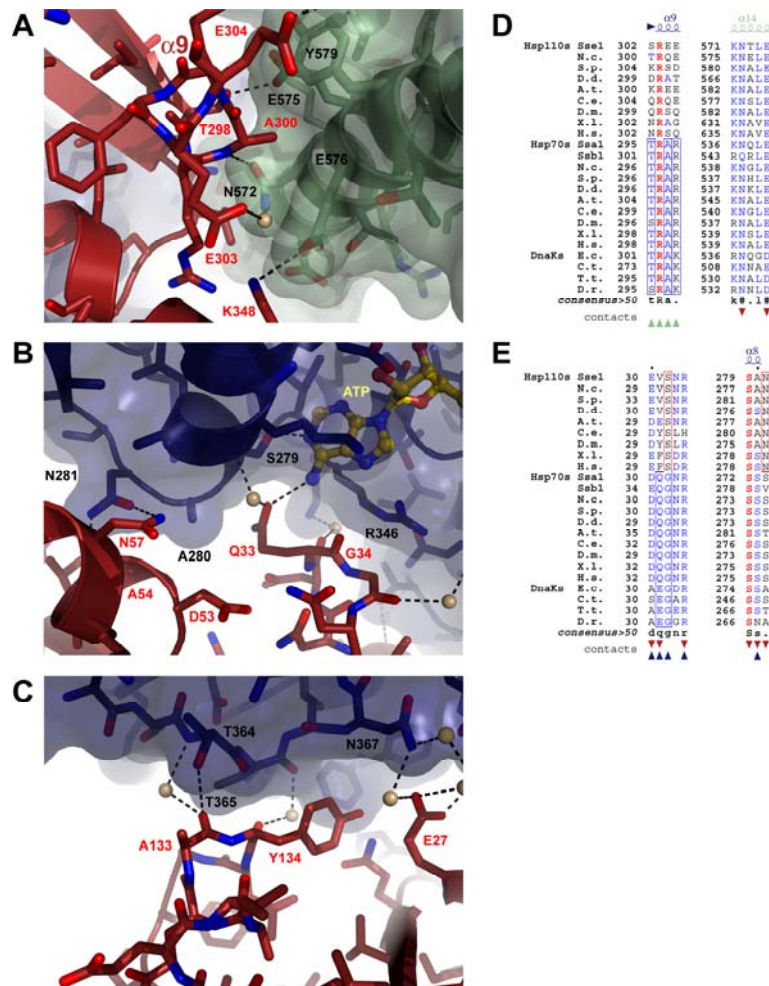


**Figure 4-13: Key interactions at the Sse1p·ATP/Hsp70N interface.**

(A) The close-up view illustrates the contacts between subdomain IIb of Hsp70N and the 3HBD of Sse1p.

(B) The contact interface in the vicinity of the Sse1p-bound ATP molecule is shown.

(C) The region of close surface complementarity between Sse1p and subdomain Ia of Hsp70N is depicted.

In panels (A)-(C), both protein backbones are shown in ribbon representation with the exception of regions involved in intermolecular contacts. These regions and the corresponding sidechains are depicted in stick representation. Sse1p is enveloped in a transparent molecular surface to highlight the close surface complementarity. The color coding for molecular surfaces, backbone and carbon atoms is identical to that in Figure 4-7. Sse1p-bound ATP is represented in a ball-and-stick model with carbon atoms colored in yellow. Nitrogen and oxygen atoms are indicated in blue and red, respectively. Ordered water molecules bridging the binding partners are shown as beige spheres. Hydrogen bonds are represented as dashed lines. Key interacting residues are indicated. In all panels, unrelated obstructing features in the foreground are omitted for clarity.

(D) Alignment of Hsp110, Hsp70 and DnaK amino acid sequences at the contact region between the 3HBD of Sse1p and subdomain IIb of Hsp70N. Contacting residues are marked by arrowheads below the sequence with the interacting domain indicated by the color scheme used in Figure 4-7. Notable differences in the consensus sequences for Hsp110s and canonical Hsp70s are boxed. For example, Ala300<sup>H</sup> is only conserved in canonical Hsp70s but not in Hsp110 homologs. The complete sequence alignment is shown in Figure 7-1.

(E) Sequence alignment of residues involved in the contact close to the nucleotide binding pocket of Sse1p. Note the high degree of conservation of Gln33<sup>H</sup> in Hsp70 homologs and of residues 279-281 (Sse1p numbering) in all aligned sequences.

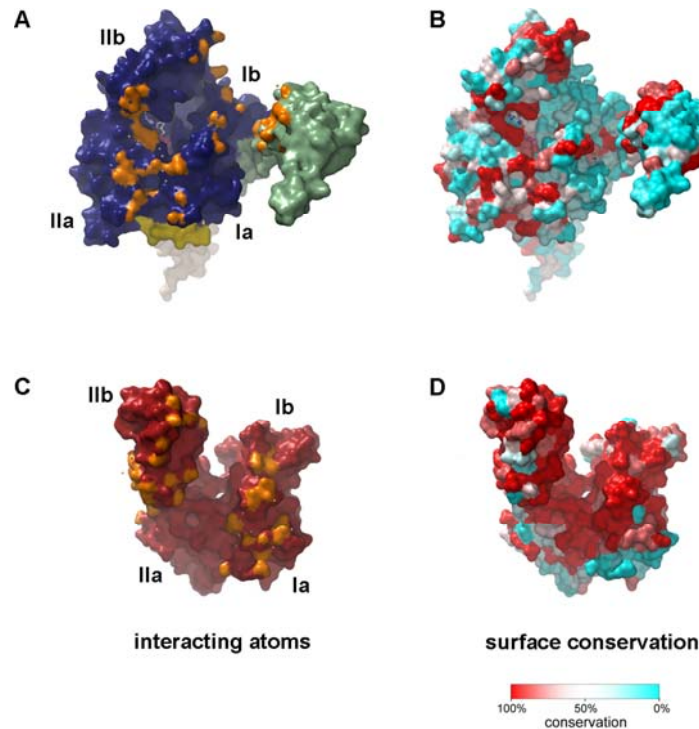


**Figure 4-14: Surface conservation of the Sse1p/Hsp70 interface.**

(A) A surface representation of Sse1p is shown. Color coding and molecule orientation correspond to that in Figure 4-7C. Hsp70N-interacting atoms are colored in orange. Water molecules are shown as beige spheres. Bound ATP is shown in ball-and-stick representation. The subdomain structure of the NBD is indicated.

(B) The surface conservation of the Sse1p interface is depicted. The degree of sequence identity in an alignment of Hsp110 homologs (group 1 in Figure 7-1) was plotted onto the surface of Sse1p. The color gradient indicates decreasing conservation. Residues identical among Hsp110 homologs are colored red, residue positions with 50 % identical residues are shown in white. Regions in cyan are variable.

(C) A surface representation of Hsp70N is shown. Sse1p-interacting atoms are colored in orange. For further details, see (A).

(D) The surface conservation of the Hsp70N interface is depicted. The degree of sequence identity in an alignment of eukaryotic Hsp70s (group 2 in Figure 7-1) was plotted onto the surface of Hsp70N. For further details, see (B).

The pattern of surface residue conservation in Hsp110 homologs generally corresponds to the residues important for complex formation with Hsp70, indicating that (i) the Sse1p/Hsp70N structure represents a useful model for all Hsp110 homologs and that (ii) complex formation and concomitant nucleotide exchange on canonical Hsp70s should be a major function of Hsp110s (Figure 4-14A,B). Likewise, the Hsp110-interacting residues in canonical eukaryotic Hsp70s are highly conserved, but the contrast against the generally high degree of sequence conservation is low (Figure 4-14C,D). Interestingly, most of these interacting residues are also conserved in bacterial homologs, indicating their general importance for Hsp70 function rather than mere co-evolution with Hsp110 homologs, which are absent in bacteria (Figure 7-1). The high conservation of Hsp110-interacting residues explains why Hsp70N can substitute for Ssa1N with respect to Sse1p binding. In contrast,

many of these Hsp70N residues are not conserved in Hsp110 homologs, thus presumably preventing the formation of non-productive Hsp110 homodimers.

## 4.5 Biochemical analysis of the cooperation of Hsp110 and Hsp70 chaperones

### 4.5.1 Overview of the Sse1p and Ssa1p mutants

In order to relate the structural data to biological function, we designed mutants of Sse1p and a cognate yeast Hsp70, Ssa1p, and analyzed them in different functional assays. Considering the large complementary interfaces between Sse1p and Hsp70N and the intimate domain-domain interactions within Sse1p, we preferentially introduced clusters of amino acid exchanges instead of single substitutions in order to effectively disrupt the observed interaction sites. Amino acid exchanges were chosen to target the three key features of the complex (Figure 4-15): The first group of mutations (red group) was meant to affect the interaction between Sse1p and Ssa1p. Mutations of the second group (blue group) were thought to destroy the interfaces between individual Sse1p domains. The third group of mutations (yellow group) was directed at the putative peptide binding site in the  $\beta$ -sandwich domain of Sse1p. At the Sse1p/Ssa1p interface, we specifically targeted (i) the contact of the Sse1p 3HBD to subdomain Iib of Ssa1p (N572Y, E575A in Sse1p and A300E in Ssa1p; Figure 4-13A), (ii) the complementary surfaces close to the nucleotide binding pocket of Sse1p (A280T, N281A in Sse1p or Q31A in Ssa1p; Figure 4-13B), and (iii) the contact of the Sse1p NBD to subdomain Ia of Ssa1p (T365V, N367S in Sse1p; Figure 4-13C). The Sse1p domain-domain interfaces were analyzed by mutating the linker region (F392A, F394A and D396A; Figure 4-9B), the conserved residues of the  $\beta$ -sandwich domain (L489A, H490A; Figure 4-11) and the N-terminal part of the 3HBD (E554A, M557S, L558S; Figure 4-12A). All three mutated regions interact with the NBD of Sse1p. The putative peptide binding cleft of Sse1p was probed with the mutation pairs L433A, N434P and F439L, M441A. L433 and N434 correspond to the *E. coli* DnaK residues F426 and S427, which are located in the peptide binding site of DnaK (Figure 7-1). The single site mutations F426S and S427P were both shown to weaken the peptide binding affinity of DnaK (Montgomery *et al.*, 1999). In addition, the ATPase deficient Sse1p variant K69M (gray) (Raviol *et al.*, 2006a), the crystallized Sse1p construct Sse1- $\Delta$ loop (black), as well as an Sse1p mutant in which the NBD was deleted (Sse1C, red) were tested. Finally, Sse1p mutants were constructed which

|                    | name                                | mutation                              | expected defect                |
|--------------------|-------------------------------------|---------------------------------------|--------------------------------|
| Sse1p              | <b>Sse1p</b>                        | none                                  |                                |
|                    | <b>Sse1-<math>\Delta</math>loop</b> | $\Delta$ (503-524)                    |                                |
|                    | <b>Sse1-1</b>                       | K69M                                  | ATP hydrolysis                 |
|                    | <b>Sse1-2</b>                       | N572Y, E575A                          | interaction with Ssa1p NBD     |
|                    | <b>Sse1-3</b>                       | A280T, N281A                          |                                |
|                    | <b>Sse1-4</b>                       | T365V, N367S                          |                                |
|                    | <b>Sse1-(2+3)</b>                   | A280T, N281A, N572Y, E575A            |                                |
|                    | <b>Sse1-(2+4)</b>                   | T365V, N367S, N572Y, E575A            |                                |
|                    | <b>Sse1C</b>                        | $\Delta$ (1-392)                      |                                |
|                    | <b>Sse1-5</b>                       | F392A, F394A                          | Sse1 domain-domain interaction |
|                    | <b>Sse1-6</b>                       | D396A                                 |                                |
|                    | <b>Sse1-7</b>                       | L489A, H490A                          |                                |
|                    | <b>Sse1-8</b>                       | E554A, M557S, L558S                   |                                |
|                    | <b>Sse1-9</b>                       | L433A, N434P                          | peptide binding                |
|                    | <b>Sse1-10</b>                      | F439L, M441A                          |                                |
| <b>Sse1-(2+9)</b>  | L433A, N434P, N572Y, E575A          | Ssa1p interaction and peptide binding |                                |
| <b>Sse1-(2+10)</b> | F439L, M441A, N572Y, E575A          |                                       |                                |
| Ssa1p              | <b>Ssa1(Q31A)</b>                   | Q31A                                  | int. with Sse1p NBD            |
|                    | <b>Ssa1(A300E)</b>                  | A300E                                 | int. with Sse1p 3HBD           |

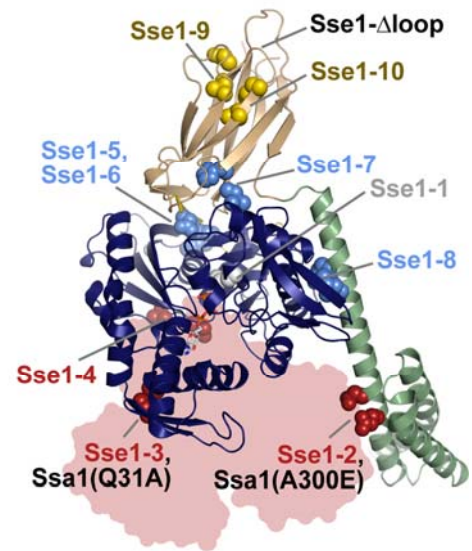


**Figure 4-15: Designed Sse1p and Ssa1p mutants.**

An overview of the constructed Sse1p and Ssa1p mutant proteins is shown. For simplicity, the mutants are denoted by a number code and are color-coded according to their expected functional defects. The location of the mutations in the Sse1p structure is indicated. Mutated residues are shown in van-der-Waals representation.

combined different mutation clusters. Mutations targeting the Sse1p/Ssa1p interaction were either combined with other mutations of the same group (A280T, N281A, N572Y, E575A and T365V, N367S, N572Y, E575A; both red group) or with mutations meant to affect putative peptide binding by Sse1p (L433A, N434P, N572Y, E575A and F439L, M441A, N572Y, E575A; both green group). For simplification, mutants are denoted by a number code in the following (Figure 4-15). Furthermore, they are color-coded according to their expected functional defects in all figures.

All mutant proteins were purified to homogeneity (data not shown). Soluble aggregates were effectively removed by size exclusion chromatography immediately before performing functional assays.

### 4.5.2 Biophysical characterization of the Sse1p variants

To ensure that the introduced mutations did not affect the secondary structure of the Sse1p variants, far-UV CD spectra were recorded for all mutants (Figure 4-16). Comparison of the CD spectra indicates that the secondary structure composition of the mutant proteins was very similar to that of the wt protein. The same was found for the Ssa1p and Ssa1N mutants (data not shown).

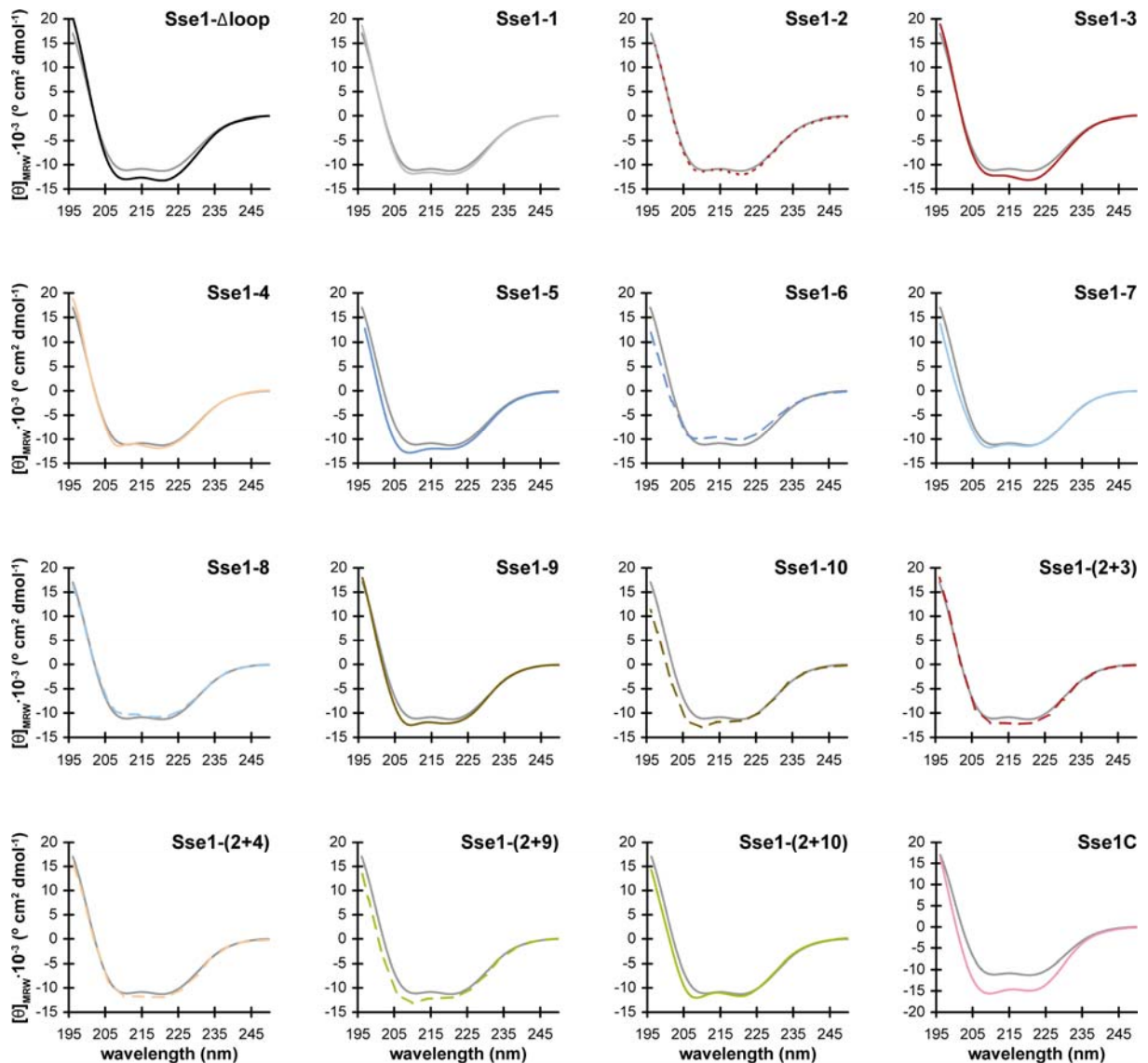


**Figure 4-16: CD spectra of the Sse1p variants.**

The CD spectra of the Sse1p mutant proteins (2.5  $\mu$ M) at 4  $^{\circ}$ C in HKM2 buffer containing 0.5 mM ATP are shown. Each panel contains the CD spectrum of wt Sse1p (gray trace) for comparison. The mutants are number- and color-coded as in Figure 4-15.

To investigate the thermal stability of Sse1p, a thermal transition was measured, following the decreasing CD signal at 222 nm upon heating. ATP-complexed Sse1p underwent a cooperative structural rearrangement with a transition midpoint at 39.0 °C, at which approximately 15 % of  $\alpha$ -helical structure was lost (Figure 4-17A). Remarkably, even at temperatures above 60 °C, a significant amount of secondary structure (~60 %) persisted (see also Raviol *et al.*, 2006a). In contrast, the secondary structure of Sse1p was almost completely lost in 6 M GdnHCl, as illustrated by the CD spectrum of Sse1p measured in presence of 6 M GdnHCl (Figure 4-17B) or by the GdnHCl transition (Figure 4-17C). Interestingly, the close homolog Sse2p revealed to be thermally more stable than Sse1p ( $T_m = 46.5$  °C, Figure 4-17A). Since Sse2p represents the stress-inducible isoform of the relatively thermo-labile Sse1p, it seems plausible that Sse2p might be adapted to take over the cellular functions of Sse1p at elevated temperatures.

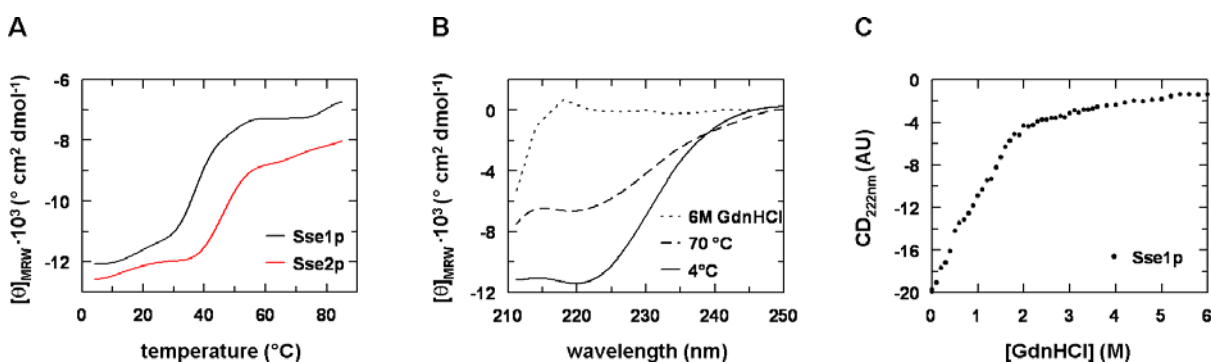


**Figure 4-17: Stability of Sse1p.**

(A) Thermal transitions of Sse1p and Sse2p (both 2.5 μM) are shown. The transition curves were recorded at a wavelength of 222 nm in HKM2 buffer containing 0.5 mM ATP. The temperatures at the midpoints of the transitions were 39.0 °C and 46.5 °C for Sse1p (black curve) and Sse2p (red curve), respectively. Note that a significant amount of secondary structure (~60 %) persisted above 60 °C in both proteins.

(B) CD spectra of different structural states of Sse1p (2.5 μM) are shown. The solid line shows the CD spectrum of Sse1p in presence of ATP at 4 °C. The spectrum of Sse1p at 70 °C is depicted as dashed line. Under these conditions, Sse1p maintained a significant amount of structure, which was absent in 6M GdnHCl (dotted line). HKM2 containing 0.5 mM ATP was used as buffer for all measurements.

(C) A GdnHCl-induced transition of Sse1p (2.5 μM) is shown. The transition was recorded at 222 nm and 20 °C in HKM2 buffer.

The Sse1p variants generally exhibited melting curves similar to unmodified Sse1p (Figure 4-18), suggesting that the mutants were not significantly compromised in terms of structural stability. The transition of the linker mutant Sse1-5 was less cooperative, but – similar to the other mutants – Sse1-5 was structured at 30 °C, the maximum temperature used in most of the *in vitro* assays (chapters 4.5.3-4.5.6). Only the test for the Sse1p holdase activity was performed at 42 °C (chapter 4.5.8).

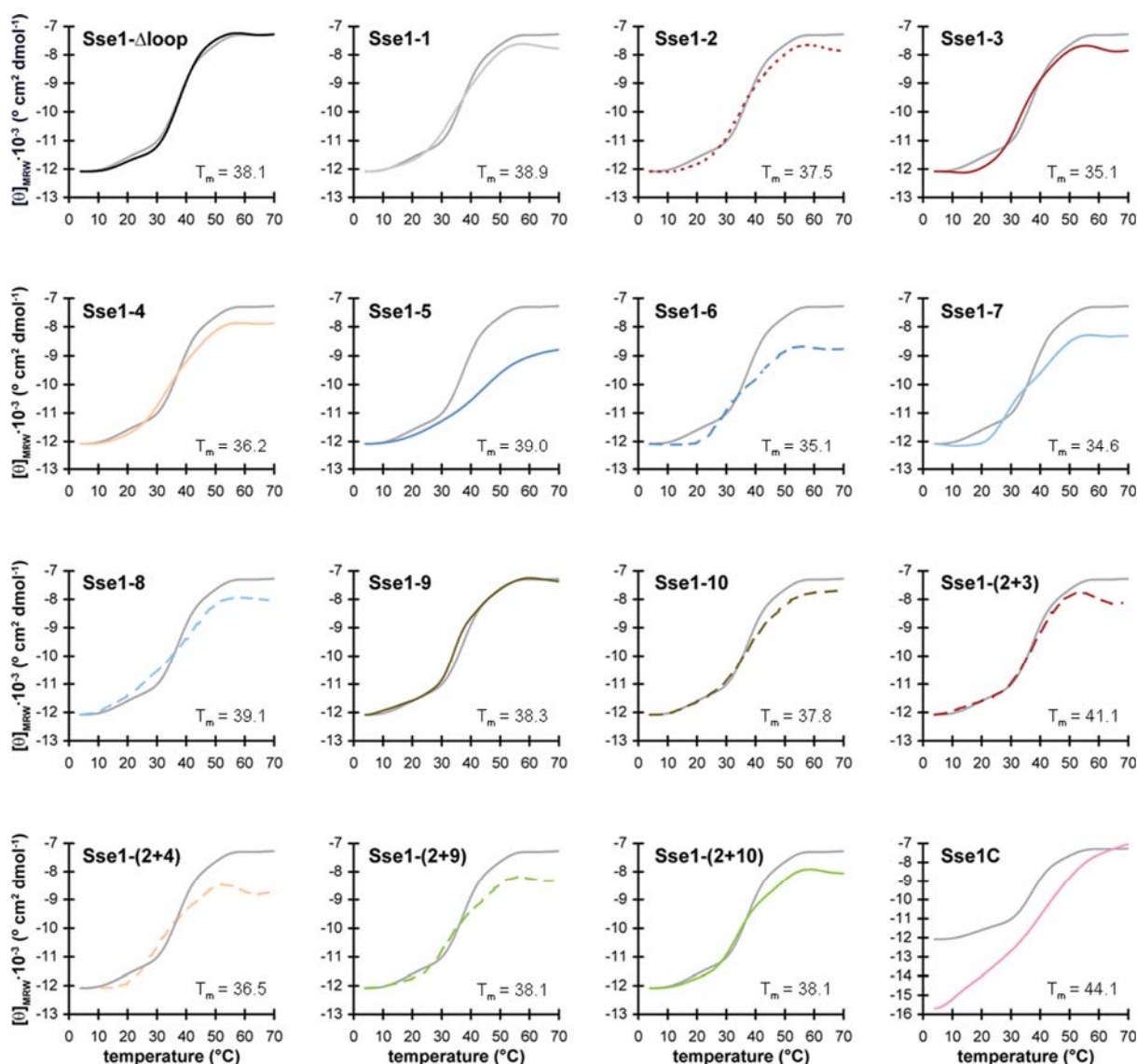


**Figure 4-18: Thermal stability of the Sse1p variants.**

The thermal transitions of the Sse1p mutant proteins (2.5  $\mu$ M, 5.7  $\mu$ M for Sse1C) recorded at a wavelength of 222 nm in HKM2 buffer containing 0.5 mM ATP are shown. The temperature at the midpoint of the transition is indicated in  $^{\circ}$ C ( $T_m$ ). For comparison, each panel contains the melting curve of wt Sse1p (gray trace). The  $T_m$  for Sse1p was 39.0  $^{\circ}$ C under the same conditions. The mutants are number- and color-coded as in Figure 4-15.

To test the reversibility of the partial unfolding observed for the Sse1p mutants at 42  $^{\circ}$ C (Figure 4-18), temperature-dependent transitions were recorded in both directions. Specifically, the protein solutions were heated to 42  $^{\circ}$ C and then cooled down to 4  $^{\circ}$ C again (temperature gradient of 1  $^{\circ}$ C  $\text{min}^{-1}$  for both un- and refolding transitions). The transition curves (Figure 4-19, left panels) as well as CD spectra recorded at 4  $^{\circ}$ C before and after heating (Figure 4-19, right panels) were in agreement with a reversible structural transition for the majority of the mutants. A partial recovery of secondary structure was observed for the Sse1p variants Sse1-9 and Sse1-10, in which the putative peptide binding cleft is mutated.

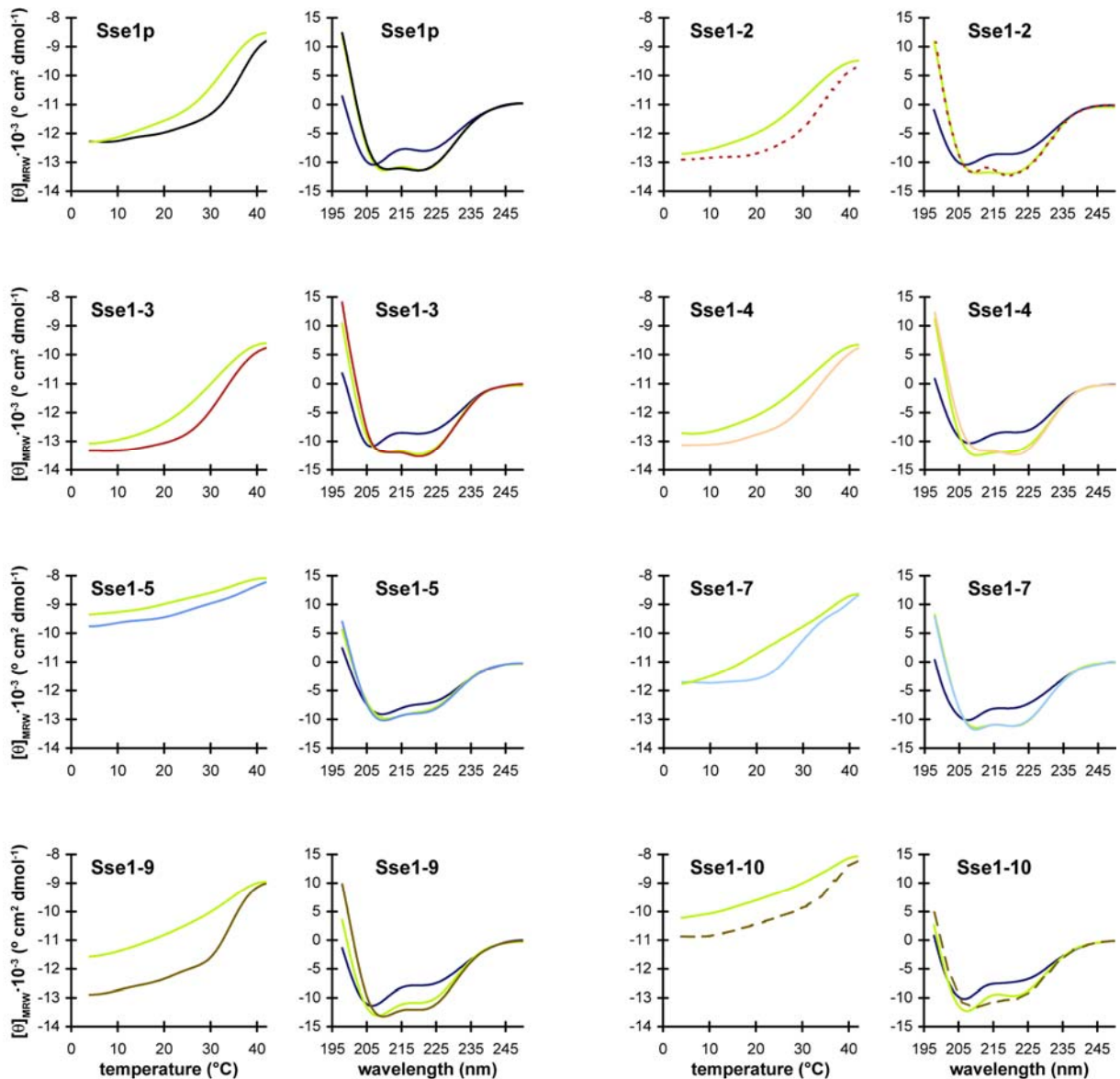


**Figure 4-19: Reversibility of the partial unfolding of selected Sse1p variants.**

For each Sse1p variant, heating and cooling curves recorded in the temperature region from 4 to 42 °C at a wavelength of 222 nm are shown (left panel). Whereas the unfolding transitions are color-coded as in Figure 4-15, the refolding transitions are colored in green. Furthermore, CD spectra at 4 °C before and after heating and at 42 °C are depicted for each variant. Spectra recorded at 4 °C before heating are color-coded according to Figure 4-15, spectra at 42 °C are shown in blue, and spectra measured at 4 °C after cooling of the sample are colored in green. The partial unfolding of mutants Sse1-9 and Sse1-10 appeared at least in part irreversible.

### 4.5.3 Complex formation of Sse1p variants and Ssa1p

In an initial biochemical assay, we tested whether the Sse1p variants were still able to form complexes with Ssa1N. Specifically, the relative binding efficiencies of the Sse1p mutants for Ssa1N were estimated by the amount of Ssa1N coeluting with the respective Sse1p variant in size exclusion chromatography experiments. The amount of Ssa1N bound to wt Sse1p was used as a reference (Figure 4-20A). Mutations targeting the Sse1p/Hsp70N interface (Sse1-2,

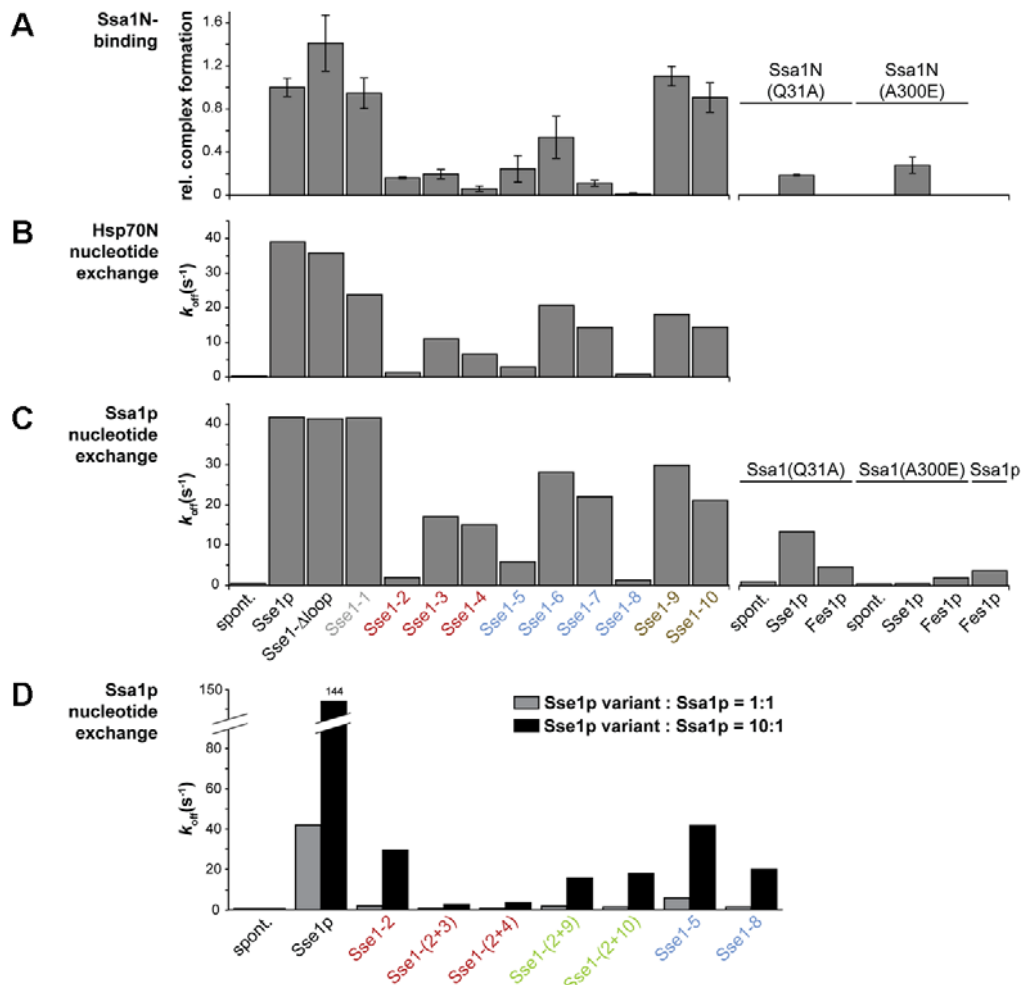


**Figure 4-20: Mutational analysis of Sse1p/Hsp70 complex formation and nucleotide exchange.**

(A) The complex formation between the Sse1p variants and Ssa1N was analyzed by size exclusion chromatography. The columns indicate the relative amount of Ssa1N coeluting with the respective Sse1p mutant (see also Figure 4-1A). The relative complex formation between Ssa1N and wt Sse1p was set to one. Binding of Ssa1N mutants was studied with wt Sse1p (right panel). The mutants are number- and color-coded as in Figure 4-15.

(B) The nucleotide exchange activities of the Sse1p variants were analyzed by determining the respective dissociation rates for MABA-ADP release from Hsp70N. The fluorescent probe MABA-ADP was bound to 2.5  $\mu$ M Hsp70N, and mixed in a stopped-flow apparatus with a solution containing 250  $\mu$ M ATP and 2.5  $\mu$ M Sse1p variant or no protein (spontaneous). The fluorescence traces of four mixing experiments were averaged, and the time-dependent decrease in fluorescence was fitted with a mono- or bi-exponential model. The bars represent the rate constants for the dominating dissociation process in a representative experiment.

(C) The dissociation rates for MABA-ADP release from Ssa1p triggered by the different ATP-bound Sse1p mutant proteins are shown (left panel). The rates of spontaneous and Sse1p-triggered MABA-ADP release for the Ssa1p mutants are shown in the right panel. For comparison, the dissociation rates for Fes1p-triggered MABA-ADP release are depicted in the right panel. Further details are as described above under (B).

(D) The nucleotide exchange activity at increased concentrations of Sse1p mutant proteins relative to Ssa1p was also analyzed. The gray and black columns represent the nucleotide release rates determined by mixing 2.5  $\mu$ M MABA-ADP complex of Ssa1p with a solution containing 2.5  $\mu$ M or 25  $\mu$ M of the indicated Sse1p mutant, respectively. Otherwise, experiments were performed as described in the legend to panel (B).

Sse1-3, Sse1-4, Ssa1N(Q31A) and Ssa1N(A300E)) reduced binding to a low basal level. This suggests that the interface of the endogenous Sse1p/Ssa1p complex is presumably very similar to that seen in the structure of the Sse1p/Hsp70N complex. Furthermore, the structural integrity of Sse1p appears to be essential for the high-affinity interaction with Hsp70

homologs, as the Sse1p mutants affecting the domain-domain interfaces, Sse1-5, Sse1-7, and Sse1-8, showed significantly diminished complex formation. In contrast, ATP hydrolysis, which is abolished in the point mutant Sse1-1 (Raviol *et al.*, 2006a), proved to be dispensable for complex formation. Consistent with the structural data, mutations in the  $\beta$ -sandwich domain of Sse1p (Sse1- $\Delta$ loop, Sse1-9 and Sse1-10) did not impair binding to Ssa1N either.

#### 4.5.4 Nucleotide exchange activities of the Sse1p variants

Nucleotide exchange activity was analyzed by determining the rate constants for the dissociation of the fluorescent nucleotide MABA-ADP from Hsp70N and Ssa1p upon addition of an equimolar concentration of the respective Sse1p variant (Figure 4-20B,C). The results for the various mutants showed the same trend irrespective of whether Hsp70N or full-length Ssa1p was used as the interaction partner, confirming that the interactions in the endogenous complex are very similar to those observed in the crystal structure.

Mutants Sse1-2 and Sse1-8 accelerated nucleotide exchange only slightly over the spontaneous rate. The same was observed upon interaction of wt Sse1p with the Ssa1p mutant A300E (Figure 4-20C). This indicates that the interaction between subdomain IIb of the canonical Hsp70 and the 3HBD of Sse1p (Figure 4-13A and Figure 4-15) is critical for nucleotide exchange activity, as predicted from the structural analysis. In contrast, Fes1p, which presumably contacts a different area of Ssa1p to perform nucleotide exchange (chapter 2.5.6, Dragovic *et al.*, 2006b), can still trigger nucleotide release from Ssa1p(A300E), suggesting that this mutant has nucleotide binding properties similar to wt Ssa1p.

Interestingly, the Sse1p mutations targeting the NBD/NBD interface (Sse1-3 and Sse1-4) lowered the rate of nucleotide exchange to a lesser extent (Figure 4-20B,C) than expected from their greatly reduced Ssa1N binding propensity (Figure 4-20A). Similarly, the mutation Q31A in subdomain Ia of Ssa1p (corresponding to Hsp70 Q33), which disrupts the direct contact to the Sse1p-bound nucleotide, had a relatively mild effect on the nucleotide exchange rate (Figure 4-13B and Figure 4-20C). In a control experiment, Fes1p was shown to exchange nucleotide on Ssa1(Q31A) as effectively as on wt Ssa1p, consistent with the prediction that Fes1p does not directly interact with Q31. In general, stable binding of Hsp70 to Hsp110 appears to be dispensable for efficient nucleotide exchange, suggesting that complex formation provides the basis for additional cooperative functions of Ssa1p and Sse1p in protein folding.

As shown in Figure 4-20D, the combination mutants Sse1-(2+3) and Sse1-(2+4) have similarly low nucleotide exchange activities as mutants Sse1-2 and Sse1-8 when applied at an equimolar ratio to Ssa1p, but could be distinguished when used at higher concentrations. While a ten-fold molar excess of Sse1-2 or Sse1-8 accelerated nucleotide exchange roughly by a factor of ten, a ten-fold excess of Sse1-(2+3) or Sse1-(2+4) did not lead to a significant acceleration in MABA-ADP release. Thus, multiple mutations at the binding interface are apparently required to efficiently disrupt the distributed interactions in the Sse1p/Ssa1p complex.

Mutation of the linker/NBD interface of Sse1p (Sse1-5, Figure 4-15) also strongly attenuated nucleotide exchange (Figure 4-9 and Figure 4-20C,D). Since the respective mutation site is remote from the Hsp70 interaction interface, this effect is likely to be indirect. The decrease in nucleotide exchange efficiency might be caused by a destabilization of the twisted, ATP-bound conformation of the Sse1p NBD. The other domain-domain interface mutants (Sse1-6 and Sse1-7) as well as Sse1p variants with mutations directed at the putative peptide binding site (Sse1-9 and Sse1-10) exhibited nucleotide exchange activities more similar to unmodified Sse1p (Figure 4-20C). Consistently, combining mutations 9 and 10 with mutation 2 (Sse1-(2+9) and Sse1-(2+10)) did not significantly aggravate the nucleotide exchange defect of Sse1-2 alone (Figure 4-20D).

#### 4.5.5 Acceleration of Ssa1p peptide release by Sse1p

Hsp70-assisted protein folding is thought to occur in nucleotide-dependent cycles of substrate binding and release (Hartl and Hayer-Hartl, 2002; Mayer and Bukau, 2005). In order to assess whether nucleotide exchange triggered by Sse1p results in increased substrate turnover by Ssa1p, we measured the release of the fluorescently labeled substrate peptide D-NR (dansyl-NRLLLTGC) from Ssa1p by stopped-flow mixing experiments. Dissociation of D-NR from Hsp70 in the presence of excess unlabeled peptide (NR) results in a fluorescence decrease (Gässler *et al.*, 2001; Dragovic *et al.*, 2006a). The spontaneous dissociation of D-NR from the ADP complex of Ssa1p was very slow (Figure 4-21A). ATP strongly increased the dissociation rate, consistent with the ATP-dependent conversion of Ssa1p into a structural state with a high off-rate for peptide. Notably, in the presence of Sse1p, dissociation of D-NR was further accelerated seven-fold, although nucleotide exchange was accelerated 90-fold under the same conditions (Figure 4-20C and Figure 4-21A). Accordingly, Sse1p mutants with a mild NEF defect were still able to stimulate peptide release like wt Sse1p, as shown

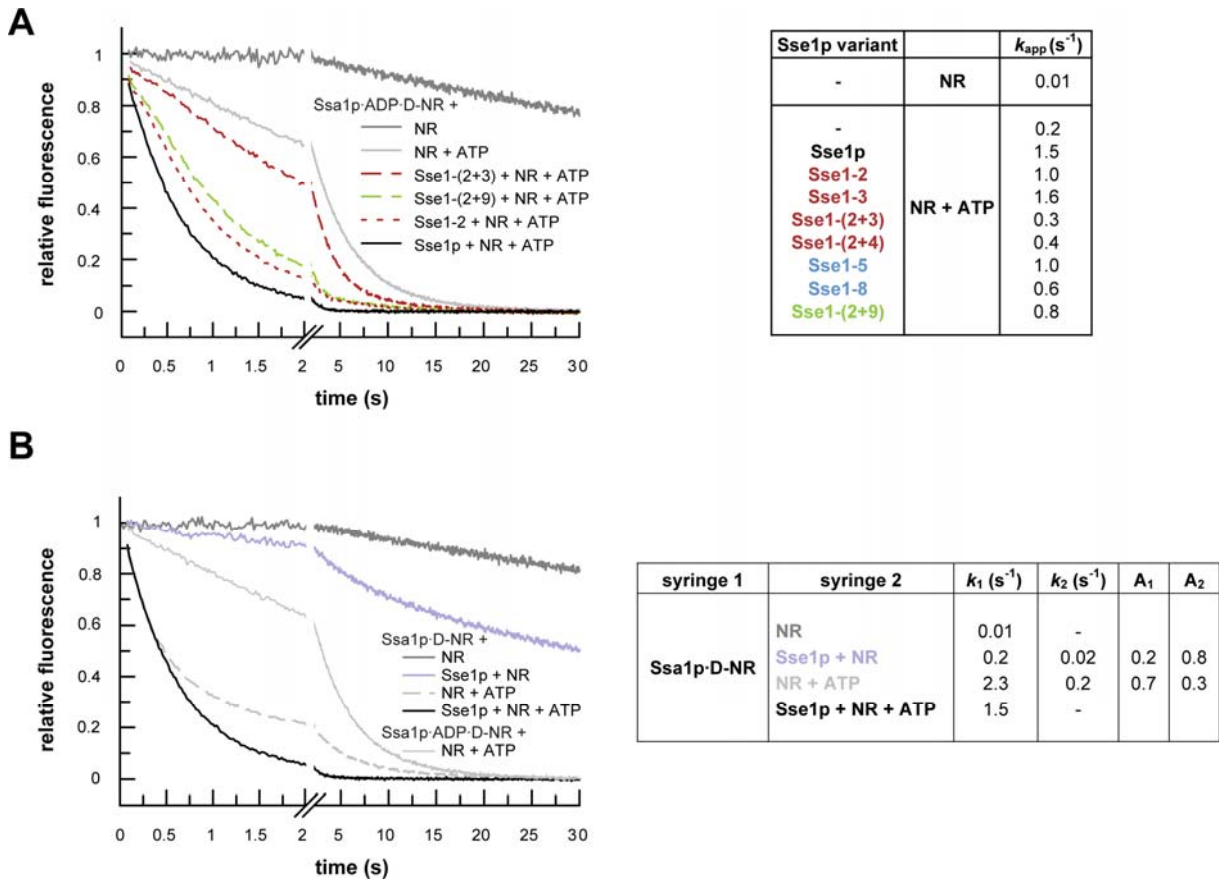


**Figure 4-21: Effects of Sse1p mutations on Hsp70 substrate release.**

(A) Sse1p accelerates substrate release from Ssa1p by catalyzing nucleotide exchange. Complexes of Ssa1p with ADP and the fluorescent peptide probe D-NR (2.5  $\mu$ M) were mixed in a stopped-flow apparatus with the indicated reagents. Whereas excesses of the unlabeled peptide probe NR and ATP were used (both 250  $\mu$ M), Sse1p variants were used at equimolar ratio. The fractional decrease of fluorescence, reflecting peptide release from Ssa1p, is shown for selected reactions. The release rates for all analyzed mutants are presented on the right. The mutants are number- and color-coded as in Figure 4-15. Rates were derived from single exponential analysis of the average of four fluorescence traces (SD  $\sim$ 2 %). Representative data are shown.

(B) Peptide release kinetics from apo-Ssa1p-D-NR are shown. An Ssa1p-ADP-D-NR complex was treated with shrimp alkaline phosphatase, resulting in partial degradation of ADP. The reaction mixture was diluted to a final concentration of 2.5  $\mu$ M Ssa1p and then mixed with reagents as indicated using a stopped-flow apparatus. Further details are as described above under (A). The fractional decrease of fluorescence is shown on the left, numerical values for the release rates as well as the respective amplitudes are indicated on the right. For comparison, the ATP-induced peptide release from Ssa1p-ADP-D-NR is shown (see also (A)).

for Sse1-3 (Figure 4-21A). However, in mutants with severely impaired NEF activity, nucleotide exchange became rate-limiting for peptide release, despite the substantial intrinsic off-rate of ADP from eukaryotic Hsp70s. For these mutants, the rates of MABA-ADP release from Ssa1p correlated with the rate of peptide dissociation: for example, Sse1-2 stimulated both the MABA-ADP and peptide release about five-fold (Figure 4-20D and Figure 4-21A).

In order to study the peptide dissociation mechanism without the complication by the ADP release step, Ssa1p-ADP-D-NR complex was treated with alkaline phosphatase to prepare D-NR-bound apo-Ssa1p (Figure 4-21B). The spontaneous release of D-NR occurred at the same rate as from the Ssa1p-ADP-D-NR complex, suggesting that apo-Ssa1p has

conformational and substrate binding properties close to ADP-bound Ssa1p (Figure 4-21A,B). Addition of Sse1p to the apo-Ssa1p·D-NR complex only moderately accelerated substrate release compared to the spontaneous dissociation<sup>2</sup>, indicating that Sse1p binding is not the principal trigger for substrate dissociation (Figure 4-21B). In contrast, ATP addition resulted in a strong acceleration of D-NR release<sup>3</sup>, consistent with an ATP-driven structural rearrangement of Ssa1p towards a conformation with low substrate binding affinity. Interestingly, mixing of apo-Ssa1p·D-NR with both Sse1p and ATP resulted in less accelerated substrate release. Thus, the presence of Sse1p might hamper the conformational transition of Ssa1p necessary for accelerated substrate dissociation in a plausible, transiently occurring quaternary complex of Sse1p, Ssa1p, ATP, and D-NR.

In summary, the datasets acquired with the Ssa1p·ADP·D-NR and the apo-Ssa1p·D-NR complexes indicate that the main purpose of Sse1p is triggering of ADP dissociation from Ssa1p·ADP·D-NR, preparing Ssa1p for ATP binding. In contrast, Sse1p binding appears to have only minor influence on substrate release from the Ssa1p·ATP·D-NR complex.

#### 4.5.6 Mutational analysis of Sse1p function in protein folding

In order to investigate how Sse1p contributes to Hsp70-assisted protein folding, the thermo-labile protein firefly luciferase was employed as a model substrate (Dragovic *et al.*, 2006a). The folding of firefly luciferase is believed to be a model reaction for the biogenesis of multi-domain proteins. Luciferase was denatured at 42 °C in the presence of Ssa1p, and refolding was initiated by addition of ATP and Ydj1p at 30 °C. Within 40 min of incubation, luciferase refolded to ~23 % of the value prior to denaturation (Figure 4-22A,B). When sub-stoichiometric amounts of Sse1p were added together with ATP and Ydj1p, refolding was accelerated and the folding yield increased to ~33 % (Figure 4-22A,B). A maximum three-fold acceleration of folding was reached at a ratio of Sse1p:Ssa1p of 1:6, whereas equimolar concentrations of Sse1p inhibited refolding, suggesting that Hsp70 cycling was no longer productive (Figure 4-22A).

The Sse1p mutants were tested under conditions where the wt protein was most efficient in luciferase folding (see Figure 4-23 for a comprehensive presentation of the refolding data). The most severely nucleotide exchange defective mutants Sse1-(2+3), Sse1-(2+4), and Sse1C

---

<sup>2</sup> The peptide release kinetic was bi-exponential with a major slow and a minor ten-fold faster process. The latter could be caused by small quantities of ATP lacking from Sse1p·ATP complexes.

<sup>3</sup> The ATP-induced release of D-NR had a bi-exponential kinetic. The rate of the minor process was in good agreement with the rate of ATP-triggered D-NR release from the Ssa1p·ADP·D-NR complex, suggesting that residual traces of Ssa1p·ADP·D-NR complex remained after the phosphatase treatment.

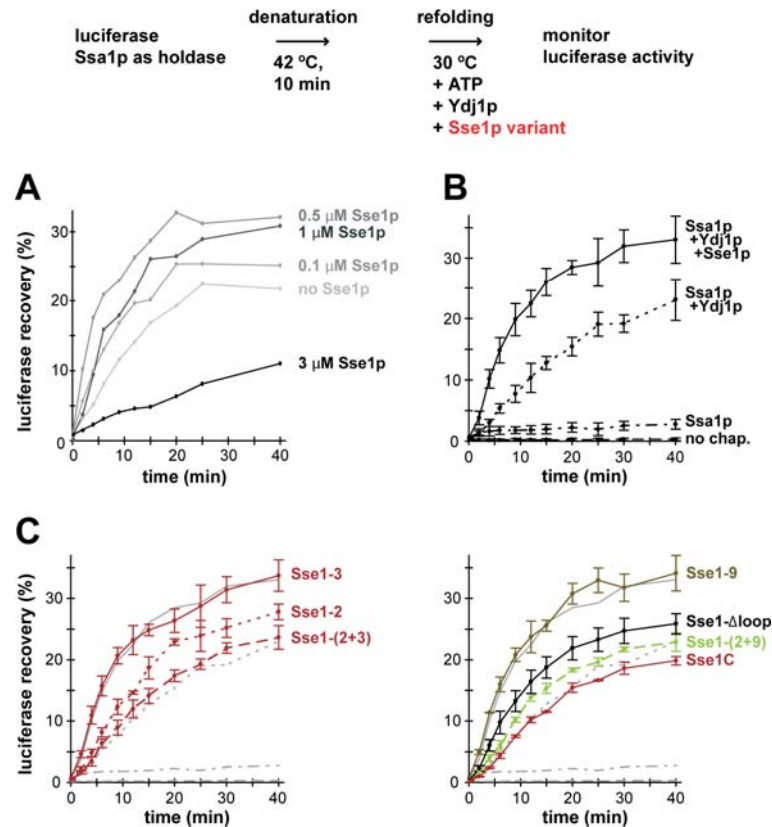


**Figure 4-22: Effects of Sse1p mutations on luciferase refolding.**

(A) The ratio of Sse1p:Ssa1p was optimized for efficient luciferase refolding. Firefly luciferase at 100 nM was denatured for 10 min at 42 °C in presence of 3 μM Ssa1p. Subsequently, protein refolding was initiated by addition of Sse1p (concentrations as indicated), 3 μM Ydj1p, and 3 mM ATP at 30 °C. Luciferase activity was determined at the indicated time points. An equimolar amount of Sse1p relative to Ssa1p was inhibitory compared to refolding in absence of Sse1p. At a ratio of Sse1p:Ssa1p of 1:6, luciferase refolding was most efficient.

(B) The presence of Sse1p enhanced the luciferase refolding rate and recovery. Firefly luciferase was thermally denatured in presence or absence (bottom curve) of Ssa1p. Refolding was initiated at 30 °C by addition of the indicated chaperones. 0.5 μM of Sse1p were used, further details are as described in (A). Each curve represents the average of at least three independent measurements, SDs are shown.

(C) Refolding of thermally denatured luciferase in the presence of representative Sse1p variants. Firefly luciferase was thermally denatured and refolded as described in (A). 0.5 μM of the respective Sse1p variant was used. Each curve represents the average of at least three independent measurements, SDs are shown. Sse1p mutants are number- and color-coded as in Figure 4-15. The gray traces correspond to the control measurements in (B). A complete representation of the luciferase refolding curves is depicted in Figure 4-23. The Sse1p mutants with the most severe nucleotide exchange defects did not improve luciferase refolding compared to Ssa1p and Ydj1p alone.

(the C-terminal fragment of Sse1p corresponding to the PBD of canonical Hsp70s (Dragovic *et al.*, 2006a)) did not improve luciferase refolding compared to Ssa1p and Ydj1p alone (Figure 4-20D, Figure 4-22C and Figure 4-23). This suggests that catalysis of nucleotide exchange and the resulting acceleration of substrate release from Hsp70 is the most important function of Sse1p in luciferase refolding. In support of this conclusion, mutants retaining weak NEF activity, including Sse1-2, Sse1-8, and Sse1-5 (Figure 4-20D), were still able to partially increase the rate and yield of refolding (Figure 4-22C and Figure 4-23), consistent with their ability to substantially accelerate peptide release from Ssa1p (Figure 4-21A). Thus,

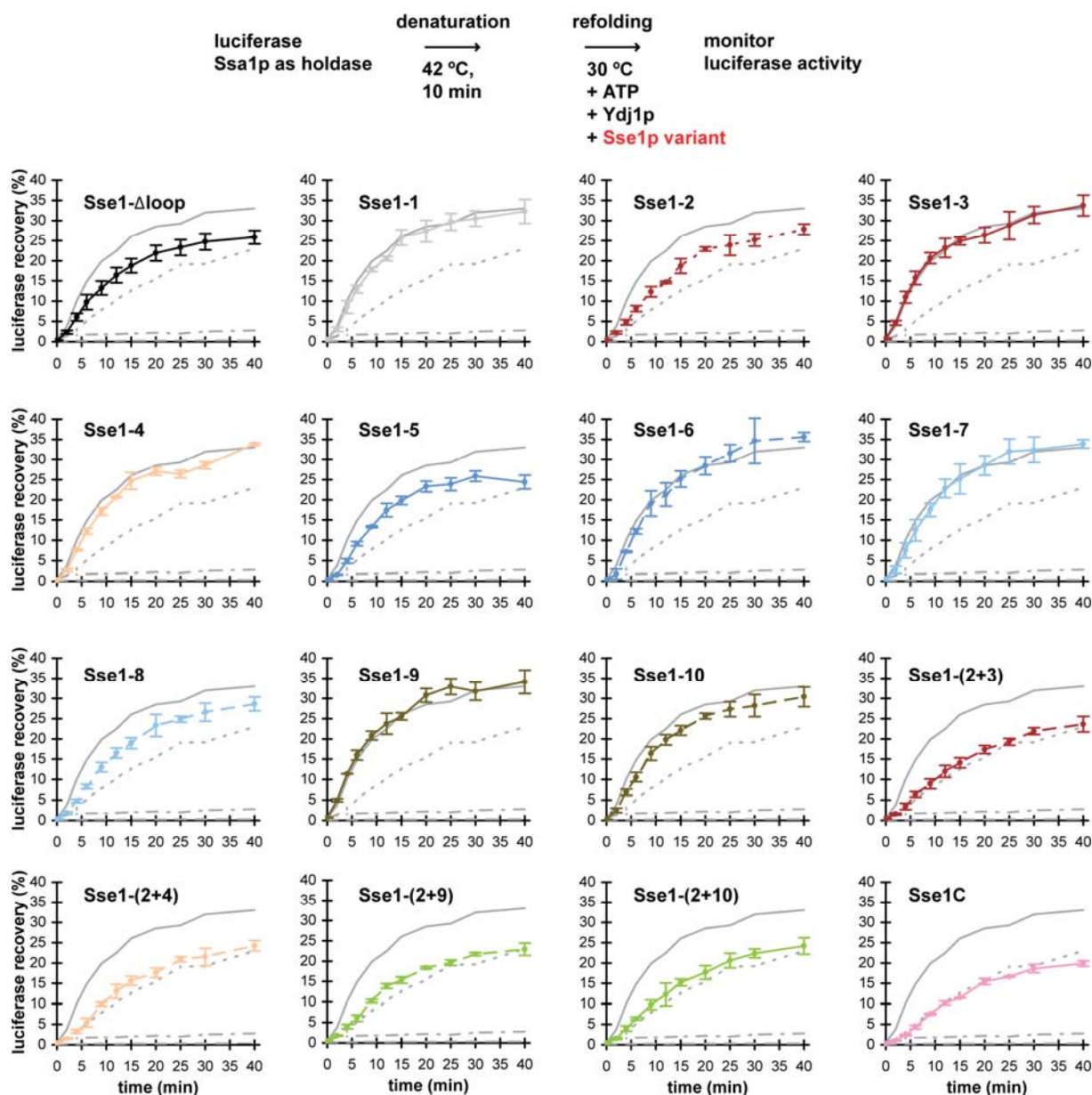


**Figure 4-23: A complete representation of the effects of Sse1p mutations on luciferase refolding.**

The refolding of firefly luciferase (100 nM) following thermal denaturation at 42 °C in the presence of 3  $\mu$ M Ssa1p is shown. Refolding was initiated by addition of 0.5  $\mu$ M Sse1p variant, 3  $\mu$ M Ydj1p, and 3 mM ATP at 30 °C. Luciferase activity was determined at the indicated time points. Each curve represents the average of at least three independent measurements, SDs are shown. Sse1p mutants are number- and color-coded as in Figure 4-15. The gray traces correspond to the control measurements in Figure 4-22B.

a small increase in nucleotide exchange over the spontaneous rate may be sufficient to cause a noticeable acceleration of protein folding. On the other hand, the combination mutants Sse1-(2+9) and Sse1-(2+10) were almost inactive in refolding (Figure 4-22C and Figure 4-23), although their exchange activity was comparable to that of the partially folding-active mutants Sse1-2 and Sse1-8 (Figure 4-20D). Mutations 9 and 10 are located in the  $\beta$ -sandwich domain and may affect the ability of Sse1p to interact with non-native luciferase. Substrate interactions mediated by the  $\beta$ -sandwich domain of Sse1p may contribute to efficient folding in addition to the nucleotide exchange function of Sse1p. In further support of this possibility,

the fully nucleotide exchange-active mutant Sse1- $\Delta$ loop (Figure 4-20C), which also affects the  $\beta$ -sandwich domain, displayed only partial refolding activity (Figure 4-22C and Figure 4-23).

All other mutants with normal or mildly reduced NEF activity – namely (i) the ATPase deficient mutant Sse1-1, (ii) the Sse1p/Ssa1p interface mutants Sse1-3, Sse1-4, and Ssa1(Q31A) (data not shown), (iii) the Sse1p domain-domain interface mutants Sse1-6 and Sse1-7, and (iv) the putative peptide binding cleft mutants Sse1-9 and Sse1-10 – supported luciferase refolding with similar efficiency as wt Sse1p, indicating that stimulated nucleotide exchange was faster than the limiting step in protein folding (Figure 4-20C, Figure 4-22C, and Figure 4-23). Since Sse1-1 is unable to hydrolyze ATP (Raviol *et al.*, 2006a), nucleotide cycling by Sse1p is apparently not required for Sse1p function in cooperative protein folding.

#### 4.5.7 Sse1p/peptide interaction

The peptide binding specificity of Sse1p was assessed in a so-called peptide scan, in which an array of peptides is covalently linked to a cellulose-PEG membrane. Specifically, the scan was performed with peptides covering the entire sequence of firefly luciferase (180 peptides in total). The peptides were each 13 amino acids long, and the sequences of neighboring peptides overlapped by ten residues. Each heptapeptide motif occurs thus in three consecutive spots. After incubation of the membrane with Sse1p, chaperone binding was detected using an Sse1p antiserum. Wt Sse1p preferentially interacted with three peptide series sharing the sequence motifs 52-TYAEYFE, 262-VVLMYRF, and 292-FSFFAKS (Figure 4-24). These findings suggest that Sse1p, similar to canonical Hsp70s, is able to recognize short

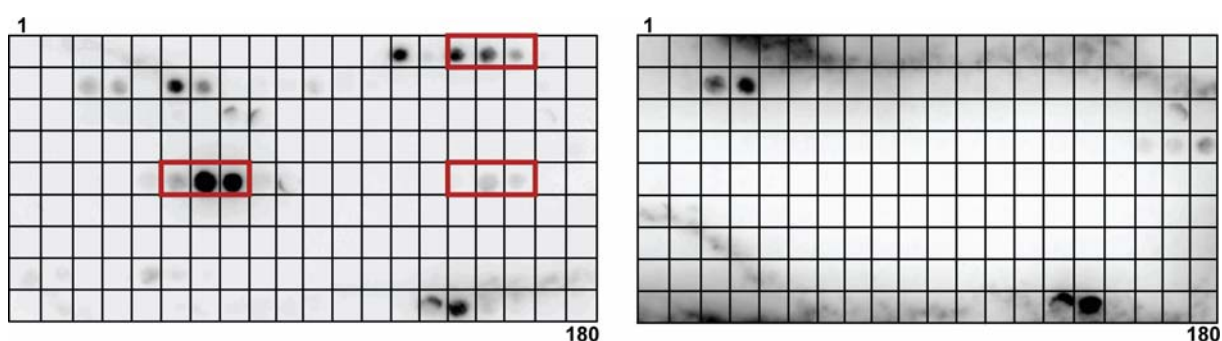


**Figure 4-24: The Sse1p/peptide interaction.**

Sse1p binds to specific luciferase sequence segments (red boxes in the left panel). Partially overlapping 13 amino acid peptides covering the sequence of firefly luciferase were synthesized on a cellulose membrane. The membrane was probed with Sse1p (10  $\mu$ g/ml), and peptide-bound Sse1p was visualized by immunodetection with Sse1p antiserum. The peptide sequences in the upper box share the amino acids TYAEYFE, those in the lower left box the amino acids VVLMYRF, and those in the lower right box the amino acids FSFFAKS. The peptide scan was performed in triplicate, a representative result is shown. The right panel shows the result of a control experiment, in which unspecific binding of the Sse1p antiserum to the membrane was tested by probing the membrane directly with the Sse1p antiserum and the HRP-conjugated secondary antibody. Apart from that, the membrane was exactly treated as in the left panel.

hydrophobic segments in substrate proteins (Rüdiger *et al.*, 1997).

Anisotropy measurements with the fluorescently labeled peptide LICGFRVVLMYRF (LIC-peptide), a generous gift from Dr. J.L. Brodsky, confirmed binding of Sse1p to this luciferase sequence segment ( $K_D \approx 10$  nM, data not shown, see also Goeckeler *et al.*, 2008). However, neither co-crystallization nor soaking of the Sse1- $\Delta$ loop/Hsp70N complex with unlabeled LIC-peptide, the closely related peptide SGFRVVLMYRFEE or the peptide TLFSFFAKST have been successful up to now.

#### 4.5.8 Sse1p prevents protein aggregation at elevated temperatures

Similar to other members of the Hsp110 protein family, Sse1p was reported to efficiently prevent the aggregation of heat-denatured luciferase *in vitro* (Oh *et al.*, 1997; Goeckeler *et al.*, 2002). We were able to reproduce these findings: As judged by the intensity of scattered light, luciferase alone started to form large aggregates after 7 min of incubation at 42 °C (Figure 4-25A). Presence of a five-fold excess of wt Sse1p reduced the increase in light scattering by approximately 43 %.

Additionally, we could demonstrate that Sse1p maintains the denatured protein in a refolding competent state. When luciferase was thermally denatured at 42 °C in the presence of Sse1p/ATP, followed by the addition of Ssa1p and Ydj1p at 30 °C, ~27 % of the initial luciferase activity was restored (Figure 4-25B, left panel). Using BSA (with ATP) as a nonspecific control protein, only a small fraction of luciferase (5 %) regained activity upon addition of Ssa1p and Ydj1p (Figure 4-25B, right panel). As reported in chapter 4.5.2, Sse1p·ATP undergoes a reversible structural rearrangement upon heating with a midpoint at ~39 °C, at which ~15 % of  $\alpha$ -helical structure is lost (Figure 4-17, Figure 4-19 and (Raviol *et al.*, 2006a)). Provided that this transition also occurs in the presence of substrate protein and Ssa1p, this conformational change may expose additional regions in Sse1p for substrate binding. Consistent with this notion, a less cooperative thermal transition in the mutant Sse1-5 (Figure 4-18 and Figure 4-19) was accompanied by a loss of function in stabilizing luciferase against heat denaturation: Sse1-5 was neither able to reduce the formation of large aggregates upon heating at 42 °C (Sse1-5/luciferase light scattering data not shown and Figure 4-25A) nor to increase the luciferase refolding yield above the background measured with BSA as holdase (Figure 4-25C). All other point mutants studied preserved the cooperative thermal transition and were clearly more effective than BSA in stabilizing luciferase in a folding-competent state (Figure 4-18 and Figure 4-25C). Differences in the luciferase refolding yields

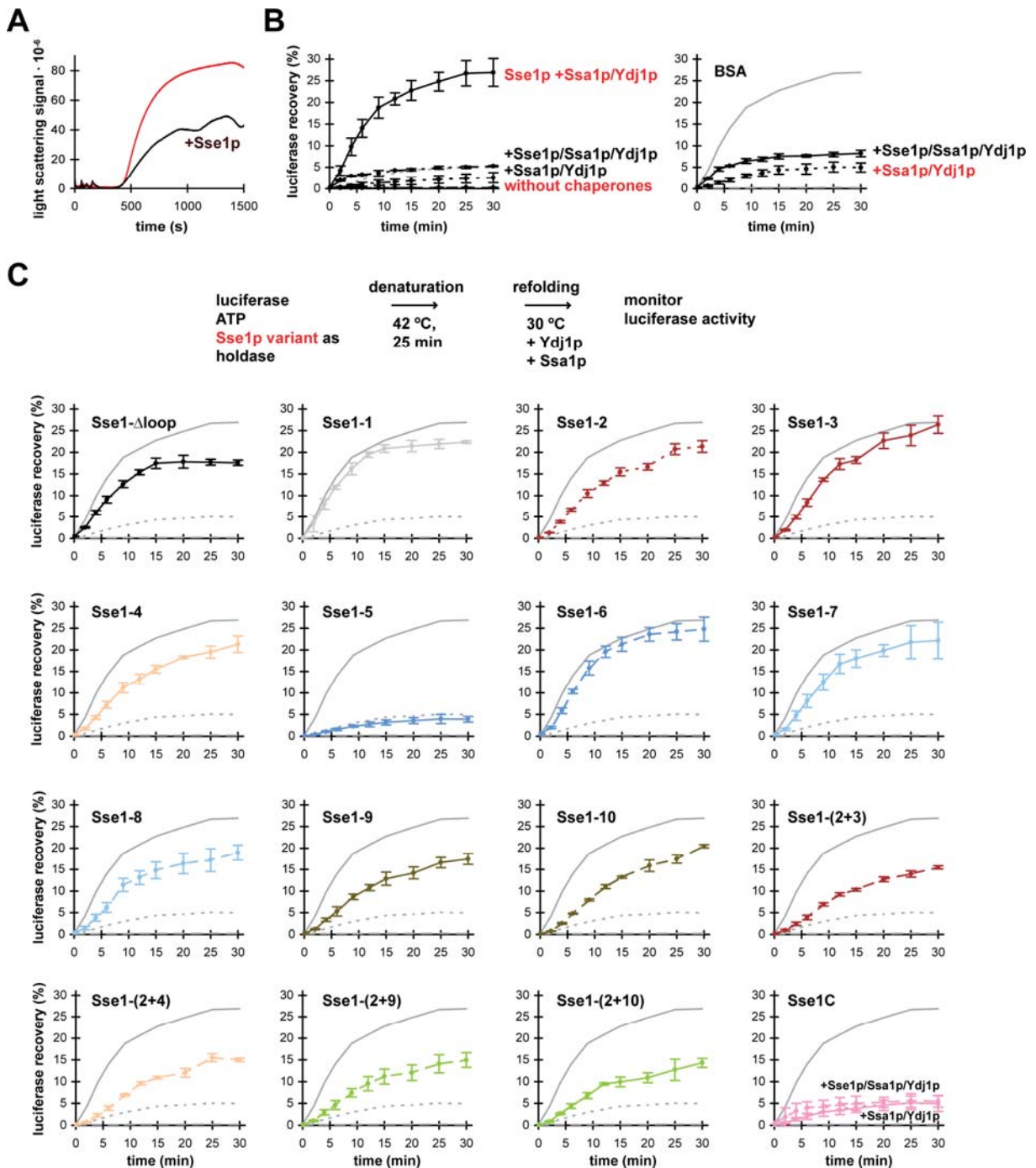


**Figure 4-25: Analysis of the holdase activity of Sse1p variants.**

(A) Sse1p can reduce the aggregation of heat-denatured luciferase. 100 nM luciferase were incubated in presence of 3 mM ATP and in absence (black curve) or presence of a five-fold excess of Sse1p (red curve) at 42 °C. The light scattering signal was followed at a wavelength of 350 nm over time.

(B) In the left panel, protein refolding after thermal denaturation of luciferase in the presence of Sse1p is shown. 100 nM luciferase were thermally denatured for 25 min at 42 °C in a buffer containing 3 mM ATP in the presence or absence of 0.5  $\mu$ M Sse1p, followed by addition of the indicated protein components (3  $\mu$ M Ssa1p, 3  $\mu$ M Ydj1p, 0.5  $\mu$ M Sse1p) and incubation at 30 °C. At the presented time points luciferase activity was analyzed. Each curve represents the average of at least three independent measurements, SDs are indicated. Presence of Sse1p in the heated sample significantly increased the luciferase refolding yield. In the right panel, protein refolding after thermal denaturation of luciferase in the presence of bovine serum albumin (BSA) is shown. In these experiments, luciferase was denatured in the presence of 0.5  $\mu$ M BSA using otherwise identical conditions as described for the left panel. Refolding was initiated by addition of the indicated components at 30 °C. For comparison, the folding reactions after denaturation in the presence of wt Sse1p (top) and spontaneous recovery (bottom) are shown in gray.

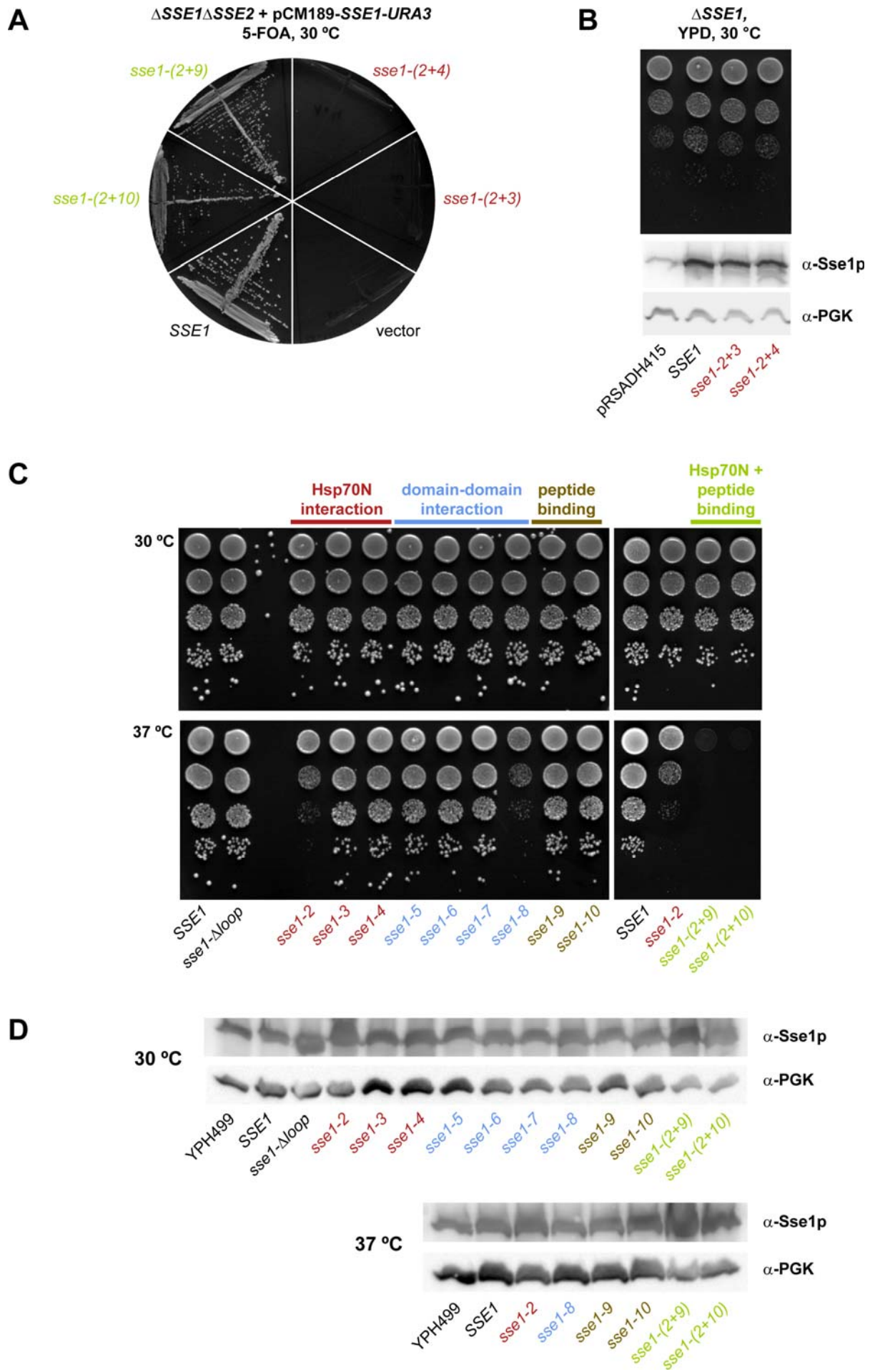
**Figure 4-25 continued: Analysis of the holdase activity of Sse1p variants.**

(C) Luciferase refolding after denaturation in the presence of Sse1p mutants is shown. 100 nM luciferase were thermally denatured for 25 min at 42 °C in the presence of 0.5 μM Sse1p mutant protein and 3 mM ATP, followed by addition of 3 μM Ssa1p and 3 μM Ydj1p (and 0.5 μM wt Sse1p when indicated) and incubation at 30 °C. Each curve represents the average of at least three independent measurements, SDs are shown. Sse1p mutants are number- and color-coded as in Figure 4-15. The gray traces correspond to the control measurements marked in red in (B).

in in experiments with different Sse1p variants can be attributed to low nucleotide exchange activity (Sse1-2, Sse1-8, Sse1-2+3, Sse1-2+4, Sse1-2+9, Sse1-2+10). The poor refolding yields observed for the nucleotide exchange active mutants Sse1-9 and Sse1-10 might be rather caused by their inability to revert quantitatively into the NEF-active state after cooling (Figure 4-19) than by a limited holdase activity. Interestingly, Sse1C, corresponding to the PBD in canonical Hsp70s, failed to reduce the light scattering signal of heat-denatured luciferase (data not shown) and could not increase the refolding yield above the background level. Importantly, addition of wt Sse1p before refolding did not correct this functional defect, indicating that it was not simply caused by the absence of NEF activity in Sse1C (Figure 4-25C). Thus, while possibly contributing to substrate binding in the context of Hsp70-mediated protein folding (see chapter 4.5.6), this segment of Sse1p does not appear to be sufficient for substrate stabilization under heat shock conditions.

#### 4.5.9 *In vivo* analysis of the Sse1p mutants

To assess the functionality of the Sse1p mutants *in vivo*, we tested the ability of the mutant proteins to complement the lethal phenotype of the combined deletion of *SSE1* and *SSE2* in yeast cells. The Sse1p variants were expressed in a  $\Delta SSE1\Delta SSE2$  yeast strain containing a rescue plasmid coding for wt *SSE1* and the *URA3* marker. To select for loss of wt *SSE1* expression, cells were grown on medium containing 5-FOA. The non-toxic 5-FOA is converted to toxic 5-fluorouracil in yeast strains expressing the functional *URA3* gene. Consequently, only yeast cells that lost the rescue plasmid and expressed a functional *sse1* mutant could multiply. The experiments showed that only mutants *sse1*-(2+3) and *sse1*-(2+4) were unable to complement the  $\Delta SSE1\Delta SSE2$  double deletion under normal growth conditions (Figure 4-26A). In these mutants, two contact sites with Hsp70 are disrupted, resulting in severely reduced complex formation with Hsp70, consistent with the finding that Sse1-(2+3) and Sse1-(2+4) have the lowest NEF activities among all mutants tested *in vitro* (Figure 4-20D). Thus, the NEF activity of Sse1p is likely to be critical for cell survival. To exclude that the lethality of *sse1*-(2+3) and *sse1*-(2+4) strains resulted from failure to express



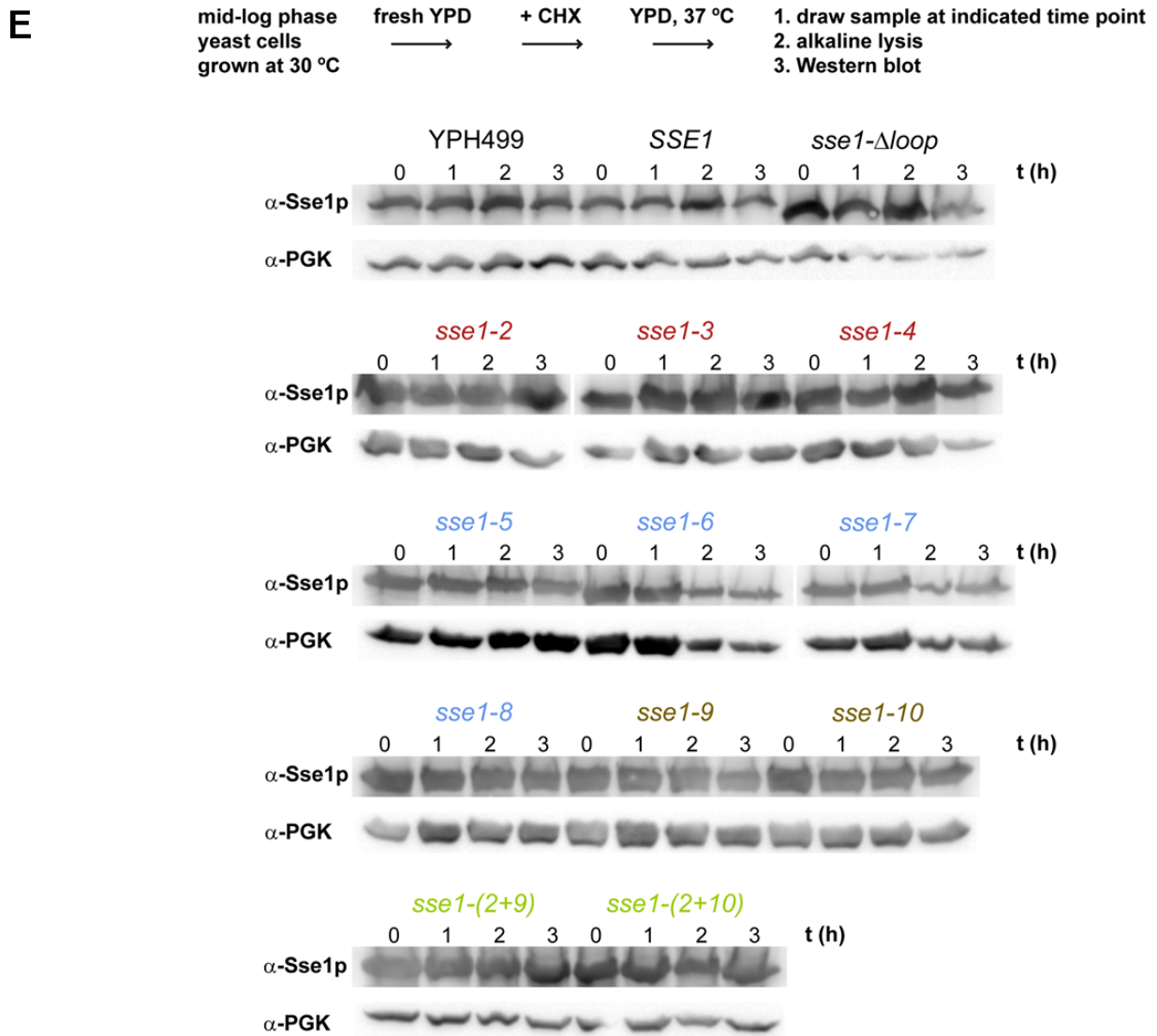


**Figure 4-26: Functionality of Sse1p variants *in vivo*.**

In all panels, the Sse1p mutants are number- and color-coded as in Figure 4-15.

(A) The *in vivo* functionality of Sse1p mutants was assessed in a yeast  $\Delta SSE1\Delta SSE2$  complementation assay. *sse1* mutant strains were generated by transforming the respective expression plasmids into an *SSE1/SSE2* deletion strain harboring the wt *SSE1* encoding rescue plasmid pCM189-*SSE1-URA3*. 5-FOA selection against the rescue plasmid showed that expression of *sse1*-(2+3) and *sse1*-(2+4) did not support growth of the deletion strain. All other *sse1* mutants analyzed resulted in viable strains.

(B) The expression levels of Sse1p mutants Sse1-(2+3) and Sse1-(2+4) in an *SSE1* deletion strain of *S. cerevisiae* were tested. Yeast cultures were grown to mid-log phase at 30 °C in YPD medium. Serial dilutions of the cultures were spotted on YPD agar plates and incubated at 30 °C for 24 h. Mutants *sse1*-(2+3) and *sse1*-(2+4) grew slightly slower than a strain expressing wt *SSE1*. Furthermore, equal cell amounts of the mid-log phase cultures were harvested and subjected to alkaline lysis. Cell extracts were separated on 10 % SDS-PAGE and probed by Western blotting against Sse1p using a polyclonal antiserum. A strain transformed with an empty plasmid served as the endogenous Sse2p level, as the Sse1p antiserum crossreacts with Sse2p. A strain transformed with a plasmid coding for wt *SSE1* was used as a positive control for the expression of non-mutated Sse1p. Endogenous phosphoglycerate kinase (PGK) served as a gel loading control. Sse1-(2+3) and Sse1-(2+4) were expressed at similar levels as plasmid-borne wt Sse1p.

(C) The growth of *sse1* mutant strains was tested under conditions of heat stress. *sse1* mutants were ectopically expressed in a *SSE1/SSE2* deletion background. Serial dilutions of mid-log phase cultures were spotted on YPD agar plates and incubated at 30 (upper panels) or 37 °C (lower panels) for 48 h. Significant growth differences could only be detected at 37 °C.

**Figure 4-26 continued: Functionality of Sse1p variants *in vivo*.**

(D) The expression levels of the Sse1p variant proteins in the mutant strains were determined. Yeast cultures were grown to mid-log phase at 30 °C in YPD medium. Equal amounts of cells were harvested and subjected to alkaline lysis. Alternatively, the cells were further incubated for 4 h at 37 °C, followed by lysis as described above. Cell extracts were separated on 10 % SDS-PAGE and probed by Western blotting against Sse1p using a polyclonal antiserum. The wt strain YPH499 served as a control for the endogenous Sse1p expression level; endogenous PGK was used as a gel loading control. All mutants were expressed at levels similar to endogenous Sse1p.

(E) The *in vivo* stability of the Sse1p variants was tested in a cycloheximide chase experiment. Yeast cells were grown to mid-log phase at 30 °C in YPD medium. Cells were harvested and resuspended at an OD<sub>600</sub> of 5 in fresh medium. Translation was terminated by addition of cycloheximide to a final concentration of 0.48 mg/ml. Subsequently, the cultures were incubated at 37 °C. Aliquots were retrieved at the indicated time points, subjected to alkaline lysis and analyzed by Western blotting against Sse1p and PGK. All Sse1p variants appeared stable against degradation under the tested conditions.

Sse1 mutant protein, respective expression plasmids were transformed in a  $\Delta SSE1$  strain (Figure 4-26B). The resulting strains grew similarly slow as a control strain, which was only transformed with an empty plasmid. In contrast, a strain expressing plasmid-borne wt *SSE1* grew slightly faster. Western blot analysis of the Sse expression levels with an antiserum recognizing both Sse1p and Sse2p showed that ectopical expression of wt and mutant Sse1 resulted in similar protein amounts (Figure 4-26B). In the control  $\Delta SSE1$  strain, the level of stress-induced endogenous Sse2p was significantly lower.

All other Sse1p mutants analyzed supported yeast growth at a level comparable to wt Sse1p at 30 °C and could only be further differentiated at an elevated growth temperature of 37 °C (Figure 4-26C). As confirmed by Western blot analysis of whole cell lysates, the mutant proteins were present at a level similar to endogenous Sse1p in wt cells under these conditions (Figure 4-26D). Furthermore, cycloheximide chase experiments showed that neither wt Sse1p nor Sse1p mutants are subjected to rapid protein turnover (Figure 4-26E). At 37 °C, cells expressing Sse1-2 or Sse1-8 exhibited a pronounced growth defect (Figure 4-26C). Both mutations are expected to interfere with the crucial interactions between the 3HBD of Sse1p and subdomain IIb of Ssa1p (Figure 4-12, Figure 4-13A, and Figure 4-15), strongly impairing nucleotide exchange. An even more severe growth defect was observed in the strains expressing Sse1-(2+9) or Sse1-(2+10), which combine mutation 2 with mutations 9 and 10 in the putative peptide binding domain (Figure 4-26C). As cells expressing mutants Sse1-9 and Sse1-10 showed no growth defects, impairment of substrate binding by Sse1p may affect cell growth only when combined with a strong defect in the nucleotide exchange function.

Finally, we tested whether the absence of functional Sse1p induces general cellular stress and thereby activates the heat shock response. In a first approach, we analyzed the protein levels of the stress-inducible chaperones Hsp12p, Hsp42p, Hsp104p, Ssa1p, and Ydj1p in the cell lysates of the different mutant strains by Western blotting. For none of these heat shock proteins apparent expression differences between *sse1* mutant and wt cells could

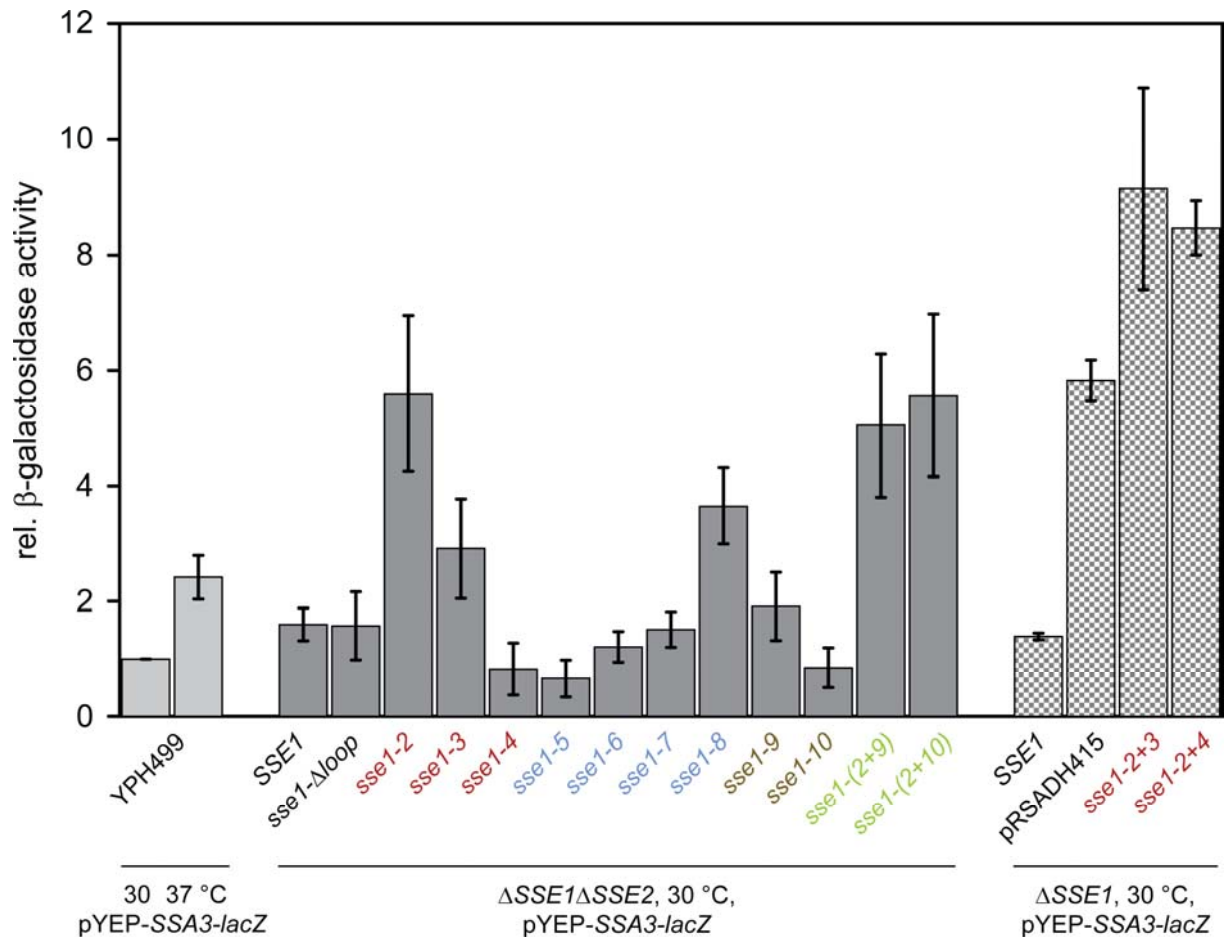


**Figure 4-27: Stress induction in *sse1* mutant strains.**

Activation of the heat shock response in *sse1* mutant yeast strains was tested using a  $\beta$ -galactosidase reporter assay. Wt YPH499 cells (light gray bars) as well as  $\Delta SSE1 \Delta SSE2$  (dark gray bars) and  $\Delta SSE1$  (checked bars) strains ectopically expressing the indicated mutants (number- and color-coded as introduced in Figure 4-15) were transformed with a plasmid coding for  $\beta$ -galactosidase under control of the stress-inducible *SSA3* promoter (pYEP-*SSA3-lacZ*). Cells were grown at 30 °C to mid-log phase, and the  $\beta$ -galactosidase activity was determined using the artificial substrate ONPG. The  $\beta$ -galactosidase activity of YPH499 cells at 37 °C was measured after additional incubation of the cultures at 37 °C for 3.5 h. The bars indicate the relative induction of  $\beta$ -galactosidase activity compared to the activity determined for wt YPH499 cells at 30 °C. Each measurement was independently repeated for at least three times, SDs are indicated as black bars. According to the  $\beta$ -galactosidase activities, yeast strains expressing nucleotide exchange defective *Sse1p* variants experience severe cellular stress.

be detected under the investigated conditions (30, 34 and 37 °C, data not shown). However, the level of the stress-inducible yeast Hsp70 homolog *Ssa3p* was significantly higher in nucleotide exchange and growth defective mutant strains (*sse1-2*, *sse1-8*, *sse1-2+9*, *sse1-2+10*, *sse1-2+3*, and *sse1-2+4*) than in strains expressing wt *Sse1p* (data not shown). Interestingly, the mutant-specific induction of *Ssa3p* expression was already observable at 30 °C. Thus, the heat shock response was already activated at seemingly normal cell growth in nucleotide exchange impaired mutants (Figure 4-26C).

In a second approach,  $\beta$ -galactosidase expression under control of the *SSA3* promoter was used as a sensitive reporter for cellular stress. The results of this assay proved to be highly consistent with the observations from the Western blot analysis of *Ssa3p* expression.

The highest  $\beta$ -galactosidase activities were found for  $\Delta SSE1\Delta SSE2$  strains expressing the nucleotide exchange impaired mutants *sse1-2*, *sse1-8*, *sse1-2+9*, and *sse1-2+10* (Figure 4-27). Strikingly, the  $\beta$ -galactosidase expression determined for *sse1-2* at 30 °C was approximately two-fold higher than in a wt yeast strain at 37 °C, illustrating that the stress induction caused by nucleotide exchange defects of Sse1p was quite severe. The strong activation of the heat shock response might be necessary to ensure normal cell growth at 30 °C. The  $\beta$ -galactosidase activities determined for  $\Delta SSE1$  strains expressing *sse1-2+3* and *sse1-2+4* were approximately five-fold higher than for a  $\Delta SSE1$  strain expressing extrachromosomal wt *SSE1*. Surprisingly, the stress response was reproducibly stronger in *sse1-2+3* and *sse1-2+4* cells than in a control strain transformed with an empty plasmid. Possibly, the stress-inducible Sse1p isoform Sse2p might compensate for Sse1p loss more effectively in absence of any Sse1p than in presence of large amounts of defective Sse1p. The Sse1p mutants might inactivate Sse2p by unproductive heterodimer formation.

In summary, the results from the *in vivo* analysis suggest that the nucleotide exchange function of Sse1p is critical for yeast growth. It is likely that nucleotide exchange defects of Sse1p lead to a decreased protein flux through the Hsp70 chaperone machinery and consequently induce general stress in the cell. Since elevated growth temperatures may require an increased protein flux through the Hsp70 chaperone system, the loss of NEF function might have more severe consequences under heat stress conditions.

## 5 DISCUSSION

Correct protein folding is crucial for cell survival. Especially the folding of larger proteins depends on the assistance of molecular chaperones. In the cell, a large number of different chaperones form a sophisticated folding network, the general principles of which are conserved from prokaryotes to eukaryotes. In this network, the molecular chaperones of the Hsp70 protein family are of particular significance. They not only participate in co- and post-translational folding of newly synthesized proteins and in protein assembly, but are also involved in refolding of stress-denatured proteins, in protein degradation, in protein transport across membranes, and in regulation of signal transduction proteins. However, canonical Hsp70s do not perform these diverse cellular functions autonomously, but depend on J-proteins and NEFs, which regulate their ATP cycle and thereby their substrate binding affinity, which is low in the ATP and high in the ADP state. In eukaryotes, four different classes of NEFs have been found, among which Hsp110 homologs are most abundant. Hsp110s apparently originated from canonical Hsp70s – as judged by their conserved domain composition – and evolved into NEFs preserving the ability to stabilize misfolded proteins in solution.

In the present study, we performed a structural and biochemical analysis of the complex between the yeast Hsp110, Sse1p, and human Hsp70. Our results lead to a model describing the functional cooperation between Hsp110 and Hsp70 homologs in the cytosol and ER of eukaryotic cells (Figure 5-3B): Central to Hsp110 function is its nucleotide exchange activity on Hsp70. Mutations that abolish Hsp110 NEF activity in the yeast cytosol are lethal. Concomitant with nucleotide exchange, Sse1p accelerates Hsp70-assisted protein folding and perhaps other Hsp70-dependent processes. Furthermore, our data suggest that direct interactions of non-native substrate proteins with Sse1p may support Hsp70-assisted protein folding in a cooperative process. Interestingly, Sse1p function does not require the nucleotide-dependent allostery and peptide binding mode of canonical Hsp70s.

### 5.1 The structure of Sse1p·ATP – a model for the ATP state of Hsp70

The structure of Sse1p·ATP as found in complex with Hsp70N confirmed the proposition that – despite low overall sequence similarity – Hsp110s share the general domain organization of canonical Hsp70 proteins, consisting of an N-terminal NBD, a  $\beta$ -sandwich domain and a C-terminal 3HBD (Figure 5-1A and Oh *et al.*, 1999). The tight interactions between these

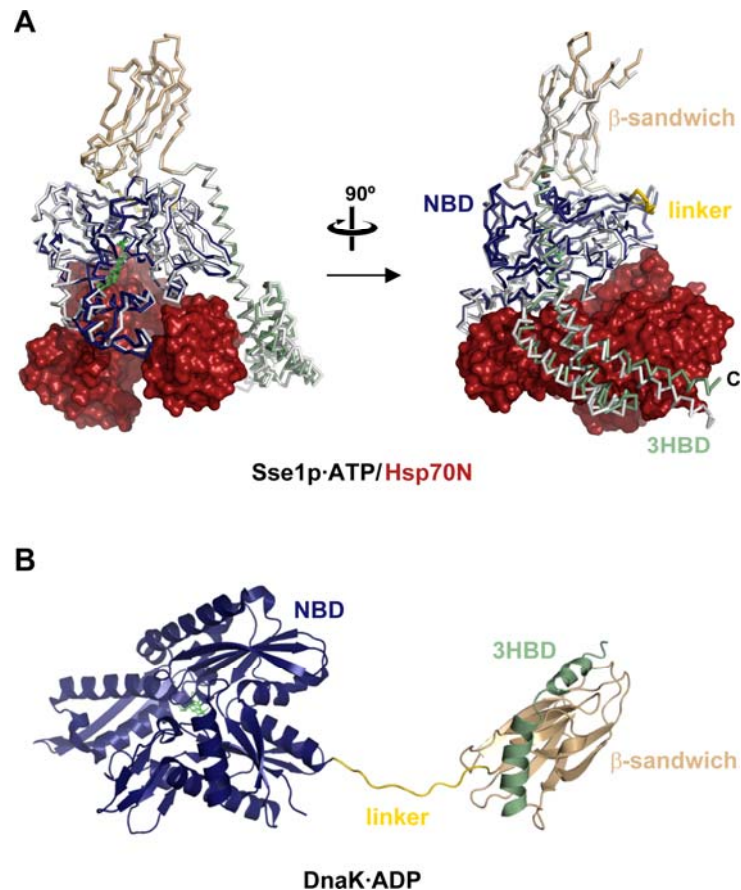


**Figure 5-1: Sse1p-ATP as model for Hsp70-ATP.**

(A) The Sse1p-ATP/Hsp70N complex is compared with the structure of Sse1p-ATP. A frontal and a side view of the superposed structures are shown in the left and right panel, respectively. Hsp70N-complexed Sse1p is shown as a C $_{\alpha}$  trace using the same color scheme as in Figure 4-7; the individual domains and the C-terminus are labeled. ATP is represented as green sticks. The Sse1p-ATP structure (PDB entry code 2QXL (Liu and Hendrickson, 2007)) is superposed as a C $_{\alpha}$  trace in white. Hsp70N is shown in surface representation. Small differences of the Sse1p conformations are apparent at the Hsp70N interface and at the C-terminus.

(B) The structure of C-terminally truncated *Geobacillus kaustophilus* HTA426 DnaK bound to ADP-P $_i$  is shown in ribbon representation (PDB entry code 2V7Y (Chang *et al.*, 2008)). ADP-P $_i$  is depicted as green sticks. The DnaK subdomains are labeled and colored as the corresponding Sse1p domains in Figure 4-7. Other than in the Sse1p-ATP structure, the linker connecting the NBD and the  $\beta$ -sandwich domain adopts an extended and solvent accessible conformation.

domains were however unanticipated. In the peculiar conformation of Sse1p-ATP, the NBD and  $\beta$ -sandwich domain associate intimately with the linker forming an inter-domain  $\beta$ -sheet. It appears plausible that NBD binding sites for both the linker and the  $\beta$ -sandwich domain become exposed as a consequence of ATP binding to Sse1p, which apparently results in a  $\sim 25^\circ$  twisting of the two NBD lobes against each other compared to the Hsp70 NBD-ADP structure (Figure 4-8A and Liu and Hendrickson, 2007). Strikingly, the 3HBD does not form a "lid" over the  $\beta$ -sandwich domain as observed in the structure of the DnaK PBD in complex with a substrate peptide (Zhu *et al.*, 1996), but instead interacts with the flank of lobe I of the NBD and points away from the  $\beta$ -sandwich domain (Figure 5-1A). The same three-dimensional domain arrangement was found in the crystal structure of Sse1p-ATP alone,

which was solved by Hendrickson and coworkers while the work presented herein was in progress (Liu and Hendrickson, 2007). For the two structures, an r.m.s.d. of 0.91 Å was determined (for 604 C<sub>α</sub> positions), indicating that Hsp70N binding causes only minor rearrangements in Sse1p (Figure 5-1A).

Notably, the NBD/linker, NBD/β-sandwich domain, and NBD/3HBD interfaces as found in Sse1p·ATP are highly conserved within canonical Hsp70s, despite limited overall sequence similarity between canonical Hsp70s and Hsp110s. Thus, it appears plausible that the conformation of Sse1p·ATP might serve as a working model for the ATP state of canonical Hsp70s, which is characterized by low-affinity peptide binding. This hypothesis is supported by extensive mutational analyses of these interfaces in Sse1p, Ssa1p, and DnaK (Liu and Hendrickson, 2007). Moreover, it is in line with the results of hydrogen deuterium (HD)-exchange and NMR experiments, which suggest that – as in the Sse1p·ATP structure – the inter-domain linker is firmly bound and protected from solvent in the ATP state of Hsp70 (Rist *et al.*, 2006; Swain *et al.*, 2007). In contrast, the ADP state of Hsp70 appears to be characterized by a solvent-exposed and protease-accessible linker and a much looser attachment of the individual domains (Buchberger *et al.*, 1995; Rist *et al.*, 2006; Swain *et al.*, 2007). A recent crystal structure of C-terminally truncated ADP-bound DnaK confirmed the notion that Hsp70 NBD and PBD are separated in the ADP state (Figure 5-1B; Chang *et al.*, 2008). The hydrophobic inter-domain linker was found bound in a substrate-like manner by an adjoining DnaK molecule with the 3HBD forming a "lid" over the β-sandwich domain. In the structure of the corresponding fragment from rat Hsc70, the PBD was disordered, which is in line with the proposed flexibility of the linker segment and loose contact between the domains (Chang *et al.*, 2008).

## 5.2 Structure and function of the Hsp110/Hsp70 chaperone system

In the Sse1p/Hsp70N complex structure, the NBD of Hsp70, which is sufficient for Sse1p binding and nucleotide exchange, is embraced by the NBD and the 3HBD of Sse1p. Through these contacts, Sse1p stabilizes the nucleotide binding cleft of Hsp70 in an open conformation with low affinity for ADP, defining the structural framework for the NEF activity of Sse1p. The involvement of both the N-terminal NBD and the C-terminal 3HBD of Sse1p in Hsp70 NBD binding explains the previous finding that essentially full-length Sse1p is needed for nucleotide exchange activity (Shaner *et al.*, 2004; Dragovic *et al.*, 2006a). The importance of the interaction between the NBD of Hsp70 and the 3HBD of Sse1p is highlighted by the

severe growth defects of yeast cells caused by mutations at this interface and by mutations that may disturb the positioning of the lid domain (this study and Liu and Hendrickson, 2007). A further prerequisite for efficient complex formation and nucleotide exchange is the presence of ATP in the nucleotide binding pocket of Sse1p, which contributes to stabilizing a conformation of the NBD in which the two lobes are twisted with respect to each other. Only this conformation appears to have the proper shape and functional group pattern for stabilizing the open, nucleotide-free state of Hsp70N in the complex. Consistently, this nucleotide-exchange active conformation is already preformed in isolated Sse1p·ATP (Figure 5-1A; Liu and Hendrickson, 2007). Several biochemical studies indicated that ATP binding is critical for the compact, active conformation of Sse1p (this study; Raviol *et al.*, 2006a; Shaner *et al.*, 2006). Subsequently, Bukau and coworkers showed with HD-exchange experiments that Sse1p is likely to undergo a two-step compacting reaction upon ATP binding, leading to the active conformation (Andréasson *et al.*, 2008b). Sse1p appears to be in fast equilibrium between its nucleotide-free, flexible form (state I) and a nucleotide-bound, stabilized, but inactive form (state II). While ATP binding favors the conversion into a fully compacted, active conformation (state III), ADP-bound Sse1p predominantly populates state II. This is in line with the finding that Sse1p·ADP accelerates nucleotide exchange on Hsp70 much less efficiently than Sse1p·ATP (this study and Andréasson *et al.*, 2008b).

In principle, Hsp110 proteins could contribute to Hsp70-assisted protein folding through different mechanisms, dependent on the nature of their interaction with Hsp70: A transient interaction that merely triggers nucleotide exchange would enable the rapid conformational cycling of Hsp70 and thus support efficient substrate binding and release for folding. Alternatively, the two chaperones could provide a platform for the conformational remodeling of substrates. While a model of cooperative folding remains plausible, at least for certain substrates, our mutational analysis stresses the significance of the NEF activity of Sse1p. The Sse1p mutants with severely reduced NEF activity failed to complement the synthetic lethality of the  $\Delta SSE1\Delta SSE2$  deletion, and did not accelerate luciferase refolding. Mutations with a milder NEF impairment still supported normal growth of yeast at 30 °C but not 37 °C and were only partially functional in refolding *in vitro*. Importantly, the reduced NEF activity of these mutants resulted in induction of the cellular stress response in the respective yeast strains already at 30 °C, suggesting a limited substrate flux through the Hsp70 system. This finding is in line with an earlier observation that deletion of *SSE1* causes a stress response at 30 °C, which was confirmed in this study (Liu *et al.*, 1999). Interestingly, the heat shock response became manifest only in the increased expression of Ssa3p. In contrast, the

expression levels of other stress-inducible chaperones (Hsp12p, Hsp42p, Hsp104p, Ssa1p, and Ydj1p) were not upregulated. Similarly, the deletion of *SSE1* was reported to have no significant effects on the expression of Ssa1/2p, Ssb1/2p, Hsp104p, Sis1p, Sti1p, and Hsp90 (Fan *et al.*, 2007). A further finding pointing towards nucleotide exchange as the major function of Sse1p is that overexpression of Fes1p can rescue a  $\Delta SSE1\Delta SSE2$  strain at least partially (Raviol *et al.*, 2006b; Sadlish *et al.*, 2008). Equivalent results were obtained, when the BAG domain of the membrane-anchored yeast BDP Snl1p was overexpressed, whereas upregulation of Ssa1p or Ssb1p was insufficient to restore viability, indicating that a potential chaperone-like function of Sse1p is secondary to its nucleotide exchange activity (Sadlish *et al.*, 2008). Finally, the finding that optimal luciferase refolding occurs only at substoichiometric concentrations of Sse1p relative to Ssa1p underlines the dynamic character of the interaction between Hsp110 and Hsp70 and thus the significance of the NEF activity of Sse1p. Consistently, the *in vivo* concentrations of Sse1p are also much lower than those of Ssa1p (Ssa1/2p : Sse1/2p : Ydj1p = 16 : 2 : 3) (Ghaemmaghami *et al.*, 2003). In contrast, high concentrations of Sse1p that favor a constitutive complex with Ssa1p inhibit refolding *in vitro*, in agreement with a slow growth phenotype caused by overexpression of Sse1p (Shaner *et al.*, 2004).

The inhibitory effect of high concentrations of Sse1p might be a consequence of preventing efficient Hsp70 cycling. Possibly, high Sse1p levels lead to an increased erroneous binding of the NEF to canonical Hsp70s in the ATP state. Assuming that the Hsp70·ATP state is not strictly defined but rather represents a rapid equilibrium of distinct conformations, the recognized Hsp70·ATP conformation could be more Hsp70·ADP- than Sse1p·ATP-like. Increased Sse1p binding to substrate-free Hsp70·ATP might hold the chaperone off binding unfolded proteins, whereas increased binding to substrate-loaded Hsp70·ATP may delay substrate release after completed nucleotide exchange. The notion that Sse1p could recognize ATP-bound Hsp70 at least with low affinity is supported by our finding that presence of Sse1p slows the release of substrate from the Ssa1p·ATP·D-NR complex.

### 5.3 Sse1p interaction with unfolded proteins

Sse1p efficiently stabilized thermally denatured luciferase in a folding-competent state, demonstrating the ability of Hsp110 to productively interact with unfolded proteins as a chaperone. It seems possible that elevated temperature activates this holdase function of Sse1p by exposing additional substrate interaction surfaces, as ATP-bound Sse1p undergoes a

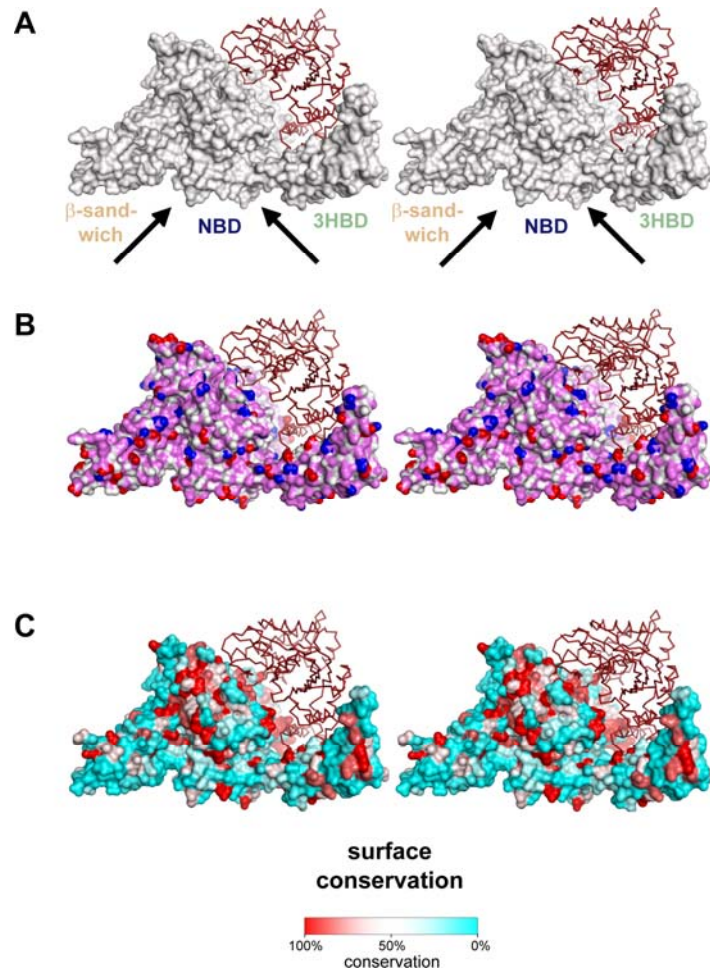


**Figure 5-2: Hypothetical substrate interaction sites on the surface of Sse1p.**

(A) A stereo representation of the surface of Sse1p in complex with Hsp70N is shown. A large surface channel running along the structure is indicated by arrows. The domain structure is indicated. Disordered side chains were modeled.

(B) The surface hydrophobicity of the Sse1p surface is shown. Carbon atoms are colored in magenta, polar groups in white, negatively and positively charged atoms in red and blue, respectively.

(C) The surface conservation of Sse1p is shown. The sequence identity from the alignment of Hsp110 sequences represented in Figure 7-1 was plotted onto the surface of Sse1p. Note the poor conservation of the  $\beta$ -sandwich domain.

cooperative conformational transition with a midpoint at  $\sim 39^\circ\text{C}$  *in vitro*. Interestingly, in contrast to Sse1p, the secondary structure of the mammalian homolog Apg-2 appears unaltered under these conditions (Raviol *et al.*, 2006a). It is tempting to speculate that yeast – an immotile organism, which is prone to be confronted with elevated temperature – possibly adapted to cope with extreme living conditions. While the physiological significance of the Sse1p conformational change remains to be experimentally investigated, our analysis of Sse1p mutants indicated that parts of Sse1p outside the  $\beta$ -sandwich domain contribute to substrate binding under these conditions: Thus, the mutants Sse1-9 (L433A/N434P) and Sse1-10 (F439L/M441A) designed to block the binding of hydrophobic peptide sequences to the putative peptide binding cleft in the  $\beta$ -sandwich domain showed holdase activities comparable to wt Sse1p, suggesting that thermally denatured luciferase is bound by a different mechanism

to Sse1p. Moreover, the C-terminal fragment of Sse1p, which comprises the PBD of canonical Hsp70s, failed to keep thermally denatured luciferase in a folding-competent state. It should be noted that Sse1C and Hsp110C were previously reported to work as holdases (Oh *et al.*, 1999; Goeckeler *et al.*, 2002). The reason for this discrepancy is unclear. However, in contrast to earlier work, we showed that our preparation of Sse1C was structured. The low degree of conservation found for the  $\beta$ -sandwich domain of Hsp110 proteins – in comparison to the highly conserved PBD of canonical Hsp70s – would be surprising in light of the  $\beta$ -sandwich domain being the exclusive substrate binding site of Hsp110s (Figure 5-2C). In fact, the  $\beta$ -sandwich domain of Hsp110 proteins might not contain a typical Hsp70-like peptide binding region, considering that no obvious peptide binding cleft could be identified in the crystal structures of Sse1p·ATP (this study and Liu and Hendrickson, 2007).

On the other hand, indirect evidence for a role of the  $\beta$ -sandwich domain in interacting with substrate was provided by the finding that mutations in this region aggravated the functional defect of partially NEF-deficient Sse1p mutants *in vitro* and *in vivo*. Moreover, the fully nucleotide exchange-active mutant Sse1- $\Delta$ loop, which also affects the  $\beta$ -sandwich domain, displayed only partial refolding activity. A negative effect on luciferase refolding had previously been reported for a similar construct of mammalian Hsp110 (Oh *et al.*, 1999). Thus, it is likely that the  $\beta$ -sandwich domain contributes to the binding of unfolded substrate proteins, however, by a mechanism distinct from the proposed model.

With the exception of the Hsp70 interface, surface residues are not well conserved among Hsp110 family members (Figure 5-2C), but we note that the Sse1p structure provides a groove-like indentation running between domain protrusions that could possibly accommodate exposed  $\alpha$ -helices or  $\beta$ -hairpins in partially unfolded substrates (Figure 5-2A). Preliminary binding studies suggest that Sse1p/substrate interactions are dynamic and do not result in stable complex formation (data not shown).

#### 5.4 Does Sse1p function require conformational cycling?

In the case of canonical Hsp70s, ATP binding and hydrolysis drive well-defined conformational transitions (Rist *et al.*, 2006; Swain *et al.*, 2007). Since Sse1p has been reported to have an intrinsic ATPase activity similar to canonical Hsp70 proteins, which can be stimulated by the essential Hsp40 cochaperone Sis1p (Raviol *et al.*, 2006a), Sse1p might undergo Hsp70-like, nucleotide-dependent conformational rearrangements. Moreover, the ATPase activities of the Hsp110 homologs Lhs1p and mouse Hsp105 $\alpha$  were reported to be

stimulated in complex with their cognate Hsp70 partners, Kar2p and Hsc70, respectively (Steel *et al.*, 2004; Yamagishi *et al.*, 2004), opening interesting possibilities for the functional cooperation of the two proteins. However, in strong contrast, the nucleotide binding pocket of Sse1p in complex with Hsp70N has been found occupied with intact ATP, indicating that at least under the employed crystallization conditions and in absence of the Hsp70 PBD Sse1p-bound ATP is not hydrolyzed. The crystallized ATP state of Sse1p might reflect the conformation of the ATP-complexed Hsp70 NBD at a precatalytic stage. Moreover, we and others could show that mutations predicted to abolish ATPase activity and conformational cycling did not impair Sse1p function *in vitro* and *in vivo* (this study; Shaner *et al.*, 2004; Raviol *et al.*, 2006b; Shaner *et al.*, 2008). Specifically, we analyzed an Sse1p linker point mutant D396A (Sse1-6) corresponding to DnaK mutant D393A, which is known to have severe defects in domain-domain communication (Vogel *et al.*, 2006b). However, Sse1-6 behaved wt-like in all functional assays. Similarly, the ATPase inactive Sse1p mutant K69M was fully active in luciferase refolding and supported yeast growth like the wt protein (this study; Raviol *et al.*, 2006a; Raviol *et al.*, 2006b). The occurrence of Leu or Gln residues at the corresponding position in several ER homologs of Hsp110 suggests that these proteins are naturally ATPase-deficient. ATP hydrolysis and associated allosteric rearrangements thus seem dispensable for Sse1p function. This implicates that – in contrast to what was suggested by Morano and colleagues (Shaner *et al.*, 2006) – Hsp110 dissociation from Hsp70 does not depend on ATP hydrolysis by Sse1p either (see also Andréasson *et al.*, 2008b). Nevertheless, the conformational state of Sse1p is strongly dependent on its nucleotide state (this study; Raviol *et al.*, 2006a; Shaner *et al.*, 2006; Andréasson *et al.*, 2008b).

### **5.5 Model for cooperative protein folding by Hsp110 and Hsp70 chaperones**

In the accepted model of the Hsp70 reaction cycle, unfolded proteins are recognized and recruited to Hsp70 with the help of J-proteins (Hsp40s). As anchor point, J-proteins appear to employ a binding site on Hsp70 distinct from that of Hsp110s (Figure 5-3A). Both, substrate and J-domain binding are known to trigger ATP hydrolysis on Hsp70 (Mayer and Bukau, 2005). As a consequence, Hsp70 undergoes a dramatic structural rearrangement leading to a conformation in which the PBD adopts a closed state that binds substrate tightly (Figure 5-3B, step 1). Subsequent association of Hsp110 with Hsp70 induces ADP release from Hsp70 (step 2). Upon binding to Hsp70, Hsp110 might interact with the unfolded substrate protein directly, provided it is of sufficient size and exposes structural elements that are recognized by

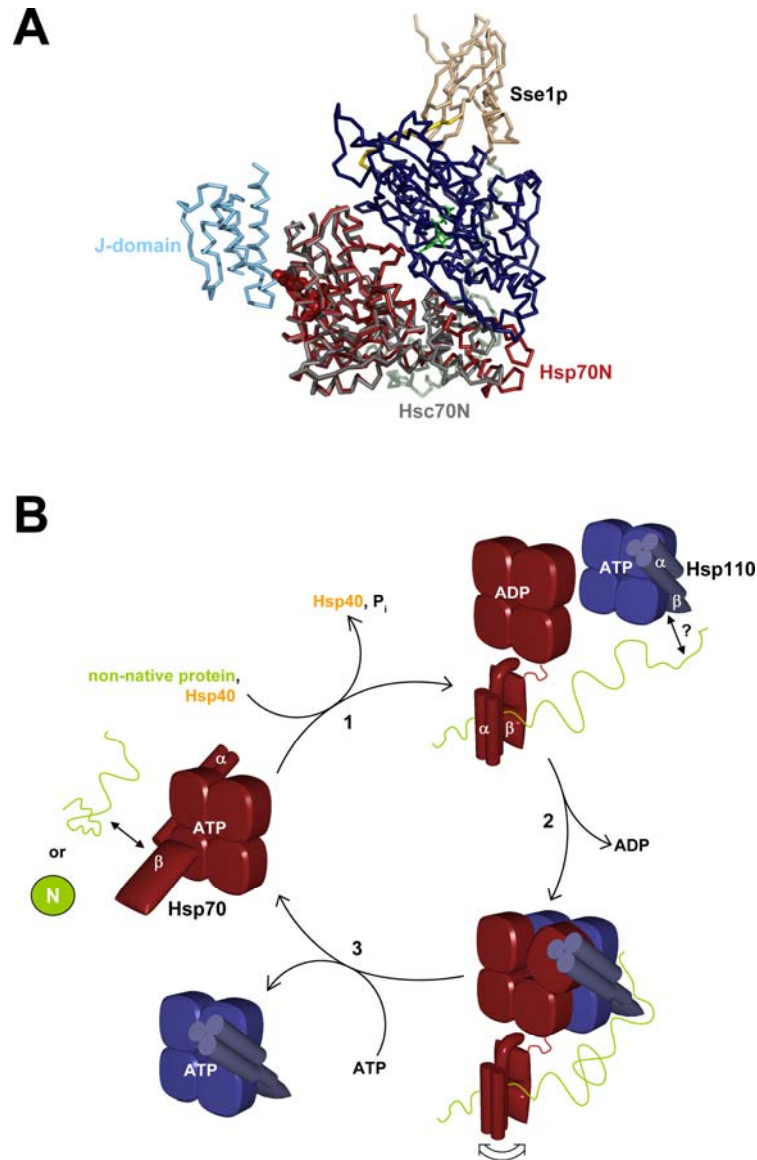


**Figure 5-3: Model for cooperative protein folding by Hsp110 and Hsp70 chaperones.**

(A) A superposition of the Sse1p/Hsp70N complex and the crystal structure of the auxilin J-domain cross-linked to the NBD/linker construct of Hsc70-ADP-P<sub>i</sub> is shown (PDB code 2QWO (Jiang *et al.*, 2007)). For aligning the structures, only the NBD of Hsp70 was considered. The orientation of the molecules corresponds to the side view of the Sse1p/Hsp70N complex shown in Figure 4-7. Both structures are represented as C<sub>α</sub> traces. Sse1p and Hsp70N are colored following the scheme introduced in Figure 4-7; Sse1p-bound ATP is depicted as green sticks. Hsc70N is colored gray and the J-domain light blue. Residues implicated in DnaJ binding by the bacterial Hsp70, DnaK, are shown in space-filling mode (Suh *et al.*, 1998).

(B) A schematic model for the cooperation of Hsp110 and Hsp70 chaperones in protein folding is depicted. Hsp70 and Hsp110 are indicated in red and dark blue, respectively. Recruitment of Hsp70 to unfolded substrate protein (green) as well as Hsp70 ATP hydrolysis are assisted by J-domain proteins (Hsp40, orange; step 1). Complex formation between Hsp70 and Hsp110 displaces ADP from the Hsp70 partner (step 2). Direct substrate binding to Hsp110 may provide an anchor aiding the unfolding of kinetically trapped intermediates through thermal motions of the substrate binding domain of Hsp70. Finally, upon binding of ATP to Hsp70, the Hsp70/Hsp110 complex dissociates and the substrate protein is released for folding (step 3). The green circle indicates natively folded substrate protein.

Hsp110. Simultaneous association of substrate protein with both chaperones might further promote Hsp70/Hsp110 complex formation. In the ternary complex, the folding of larger multi-domain proteins with a propensity to undergo intramolecular misfolding may be

facilitated. Large-scale thermal motions of the Hsp70 PBD, which is linked loosely to the NBD in the ADP-bound and presumably also in the nucleotide-free state (Rist *et al.*, 2006; Swain *et al.*, 2007; Chang *et al.*, 2008), might aid the remodeling of misfolded or kinetically-trapped substrates held by Hsp110. Finally, ATP would rebind to Hsp70. Sousa and colleagues suggested in an independent structural study on the Hsp110/Hsp70 complex that ATP might enter through an electropositive pore connecting the nucleotide binding sites of both Hsp70 and Hsp110 with the solvent (Schuermann *et al.*, 2008). ATP binding would promote extensive structural rearrangements within Hsp70, including the closure of the NBD around the nucleotide. The closed conformation of the NBD appears incompatible with Hsp110 binding, since Hsp70 and Hsp110 subdomains Iib would clash (this study; Andréasson *et al.*, 2008b; Schuermann *et al.*, 2008). Thus, the Hsp70·ATP/substrate complex would dissociate from Hsp110 and the substrate would be released from Hsp70 for folding (Figure 5-3B, step 3). The substrate protein would either reach its native structure or – if still only partially folded – rebind to Hsp70 for a new folding cycle (step 1).

## 5.6 Evolution of Hsp70 NEFs

Whereas prokaryotes and eukaryotes possess Hsp70 and Hsp40 proteins, which have clearly common ancestry, their NEF families are evolutionary unrelated. Thus, GrpE homologs have only been identified in bacteria and organelles of bacterial origin. Conversely, Hsp110 homologs, BDPs, and HspBP1 homologs have exclusively been found in eukaryotes. This observation could be explained with the absence of Hsp70 NEFs in the last common ancestor of bacteria and eukaryotes. Alternatively, bacteria might have evolved the DnaK system only after divergence of the bacterial and the archaeal/eukaryotic branches. Archaea and eukaryotes would have acquired Hsp70 and Hsp40 later through horizontal gene transfer from bacteria. The latter hypothesis is consistent with the absence of Hsp70-homologous genes in most archaeal genomes, which is difficult to reconcile with the Hsp70/Hsp40 system being already present in the last common ancestor of all three kingdoms of life. Furthermore, the genes for DnaK and DnaJ are frequently encoded as one operon in prokaryotic genomes and are thus likely to be transferred simultaneously.

Sequence homology of Hsp110 and Hsp70 homologs suggests that Hsp110 proteins presumably derive from canonical Hsp70s. In this context, it is tempting to speculate that primordial Hsp70 proteins were mutually able to catalyze nucleotide exchange in an intermolecular reaction: ATP-bound Hsp70 proteins may have been able to accelerate ADP

dissociation from peptide-charged Hsp70 molecules, using an Hsp110-like nucleotide exchange mechanism. Homodimer formation might have enabled tight coordination between Hsp70 molecules during collaborative folding of larger, possibly multi-domain protein substrates. Specifically, a peptide-charged Hsp70 molecule might have recruited an ATP-bound Hsp70 molecule, sensing its nucleotide-dependent conformation. While nucleotide exchange would have resulted in substrate dissociation from the same Hsp70 molecule, unmasked hydrophobic peptide segments could have efficiently been rebound by the adjacent accessible peptide binding cleft of the second Hsp70 molecule. Thus, two Hsp70 molecules would have been coupled in the hypothetical homodimeric Hsp70 complex similar to a two-stroke engine. Intriguingly, most key residues mediating the interactions between Sse1p and Hsp70 are conserved among sequences of canonical Hsp70s. However, using our MABA-ADP dissociation assay, we were not able to find evidence for an NEF function of canonical Hsp70s (data not shown). Possibly, present canonical Hsp70s have lost this function after the emergence of specialized NEFs and the concomitant relief of evolutionary restraints. Hsp110/Grp170 family proteins appear to have specialized for their nucleotide exchange function: The systematic substitution of the 3HBD residue 554 from Ala in canonical Hsp70s to Glu in Hsp110s appears to reinforce the interaction between the 3HBD and the NBD, which is crucial for nucleotide exchange. Glu554 forms a salt bridge to Arg47 of the NBD. Furthermore, residues implicated in ATP hydrolysis and conformational cycling in canonical Hsp70s – both features which are dispensable for Hsp110 function – are less conserved in Hsp110 sequences. Moreover, residues which might promote unproductive homodimeric association (e.g. Ala300, human Hsp70 numbering) differ from canonical Hsp70 sequences.

Both the BAG domain of BDPs and HspBP1/Fes1p homologs have generic folds, namely a three helix bundle and a succession of Armadillo repeats. These structural scaffolds are employed in many different functional contexts in eukaryotes, indicating their great adaptability for distinct protein-protein interactions.

## 5.7 Diversity of NEFs in eukaryotes

In Figure 5-4, the crystal structures and Hsp70 nucleotide exchange mechanisms of representatives of the distinct NEF families are compared. Despite different binding modes, most NEF families (GrpE, BDPs and Hsp110 homologs) appear to use similar nucleotide release mechanisms. Specifically, they stabilize the Hsp70 NBD in an open conformation by

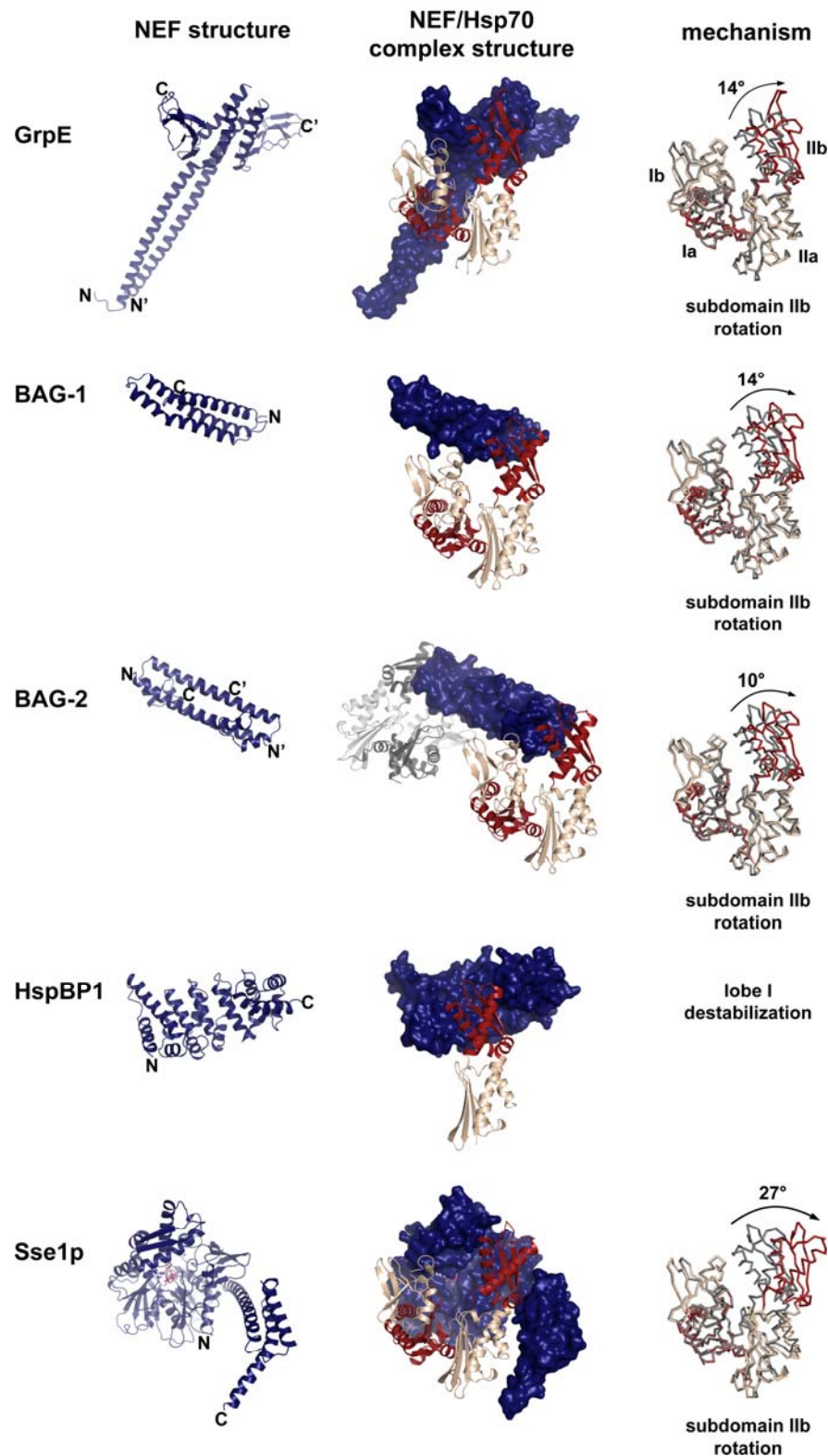


**Figure 5-4: Comparison of the NEFs of Hsp70.**

For better comparison, the Hsp70 NBDs of the different NEF/Hsp70 complexes (this study; Harrison *et al.*, 1997; Shomura *et al.*, 2005; Sondermann *et al.*, 2001; Xu *et al.*, 2008) were superposed on the NBD of bovine Hsc70 in the ADP state (Flaherty *et al.*, 1994). In the ribbon representations of the NEFs on the left, the N- and C-termini are labeled. In the complex structures, the NEFs are shown in surface representation. The Hsp70 molecules are colored as in Figure 2-5; the second Hsp70 molecule in the BAG-2/Hsc70N complex is colored in gray tones. Please note that the left end of BAG-1 points towards the reader, while it is oriented to the back in BAG-2. In the right column, the structural transitions of the Hsp70 NBD upon complex formation with the respective NEF in comparison to the ADP-bound conformation of the Hsc70 NBD are shown.

tilting subdomain IIb. HspBP1 homologs however seem to utilize a different technique to exchange nucleotide on Hsp70: They might stabilize an outward rotation of subdomain IIb as well, but mainly seem to induce local unfolding in Hsp70 lobe I (Shomura *et al.*, 2005; Andréasson *et al.*, 2008a).

The recently published crystal structure of the BAG-2/Hsc70 complex revealed that BAG-2 applies a nucleotide exchange mechanism similar to the ones of GrpE, BAG-1, and Sse1p, although being characterized by a "new" Hsp70 binding mode (Xu *et al.*, 2008): The NEF domain of BAG-2 forms a dimer, with each monomer contacting an Hsc70 NBD by binding to subdomains Ib and IIb in an end-on fashion (Figure 5-4), resulting in an opening of subdomain IIb. In contrast, the BAG domain of BAG-1 binds along the cleft between subdomains Ib and IIb. In addition to its nucleotide exchange function, the NEF domain of BAG-2 is able to interact with unfolded substrate proteins, its binding preferences being similar to those of Hsc70. Since the substrate and Hsc70 binding sites on the catalytic domain of BAG-2 overlap, BAG-2 might coordinately transfer substrate peptides to the PBD of Hsc70 (Arndt *et al.*, 2005; Xu *et al.*, 2008). Alternatively, the substrate binding activity of BAG-2 might be used to recruit the NEF to Hsp70/client complexes.

Why do eukaryotic cells have such a plethora of Hsp70 NEFs? Does the large number of NEFs ensure the robustness of the Hsp70 system, the central cellular chaperone machine, by sheer multiplicity? Or have the different NEFs adapted to specific targets during the evolution of eukaryotic cells?

The first hypothesis is supported by the redundancy of many NEFs. Thus, overexpression of Fes1p or Snl1 $\Delta$ N can rescue a  $\Delta$ SSE1 $\Delta$ SSE2 strain (Raviol *et al.*, 2006b; Sadlish *et al.*, 2008). While Fes1p is the HspBP1 homolog, Snl1 $\Delta$ N represents the catalytic domain of the unique, membrane-anchored BDP in *S. cerevisiae*. Furthermore, overexpression of Fes1p was shown to reverse the morphology defects of  $\Delta$ SSE1 $\Delta$ SWI6 cells similarly well as overexpression of Sse1p (Shaner *et al.*, 2008). The proteins Swi6p and Swi4p form a heterodimeric transcription factor. Moreover, overexpression of the ER HspBP1 homolog Sil1p is sufficient to suppress the growth defect of a  $\Delta$ IRE1 $\Delta$ LHS1 yeast strain, with Lhs1p being the yeast ER Hsp110 homolog and Ire1p a transmembrane kinase/nuclease, which is essential for the transduction of the UPR (unfolded protein response) (Tyson and Stirling, 2000).

However, the redundancy of the different NEFs is only partial, indicating a specialization of the different NEFs, which is claimed in the second hypothesis. Especially the BDPs do not seem to be general regulators of productive protein folding by the Hsp70

machinery, but appear to assist specific Hsp70 functions (Takayama and Reed, 2001; Alberti *et al.*, 2003; Kabbage and Dickman, 2008). This notion is based on their modular domain architecture. Apart from the BAG domain, which is a common feature of all BDPs, the domain composition is unique for each BDP and allows individual family members to interact with distinct target proteins. Thus, BDPs are likely to recruit Hsp70 chaperones to specific substrates or cellular localizations. In this scenario, the local concentrations of the individual BDPs, which are thought to be expressed at low cellular levels, might suffice for efficient promotion of Hsp70-mediated substrate folding (Tzankov *et al.*, 2008). Interestingly, even the BAG domain seems to have diversified in BDPs. Thus, as mentioned above, the BAG domain of BAG-2 can directly bind misfolded proteins and prevent their aggregation in contrast to the BAG domains of other BDPs (Arndt *et al.*, 2005; Xu *et al.*, 2008). Consequently, BAG-2 and Hsp70 may cooperate in chaperoning select Hsp70 clients. Furthermore, the three helix bundle in BAG-4 is considerably shorter than in BAG-1 (Brockmann *et al.*, 2004).

In contrast to BDPs, GrpE as well as both HspBP1 and Hsp110 homologs appear to serve as general NEFs. However, the functions of HspBP1 and Hsp110 homologs still seem to be only partially overlapping: First, overexpression of Fes1p cannot support the growth of a  $\Delta SSE1\Delta SSE2$  yeast strain as effectively as expression of Sse1p. Furthermore, deletion of the ER Hsp110 homolog Grp170 is lethal in mice, indicating that its function cannot be replaced by the ER-luminal HspBP1 homolog Sil1. Conversely, mutations in *SIL1* appear not to be generally compensated by Grp170, because mutations disrupting Sil1 function result in the Marinesco-Sjögren syndrome (a rare autosomal recessive neurodegenerative disorder) in humans and an ataxia phenotype in mice, which is characterized by abnormal accumulation of ubiquitinated proteins in the ER and nucleus of cerebellar Purkinje cells (Anttonen *et al.*, 2005; Senderek *et al.*, 2005; Zhao *et al.*, 2005a). Strikingly, although *SIL1* is widely expressed in the brain, protein aggregation and subsequent degeneration was only observed for Purkinje cells in certain lobules of the brain (Zhao *et al.*, 2005a). Presumably, Grp170 compensates loss of Sil1 function in the unaffected regions.

The partial functional redundancy of HspBP1 and Hsp110 homologs might have several reasons, which will be discussed in the following three paragraphs. According to our MABA-ADP release assay, human Hsp110 and yeast Sse1p appear to be much more efficient NEFs than human HspBP1 and yeast Fes1p, at least *in vitro* (this study; Shomura *et al.*, 2005; Dragovic *et al.*, 2006a). Moreover, Hsp110 and Sse1p were shown to enhance Hsp70/Hsp40-mediated refolding of firefly luciferase *in vitro*, while HspBP1 inhibited the Hsp70 refolding function (this study and Tzankov *et al.*, 2008). Consistent with an inhibitor function of

HspBP1, overexpression of this NEF was reported to block the anti-apoptotic function of Hsp70, which is upregulated in a wide variety of tumor cells (Tanimura *et al.*, 2007). On the other hand, the yeast HspBP1 homolog Fes1p was shown to be necessary for efficient Hsp70-mediated luciferase folding *in vivo*, at least under heat stress conditions (Shomura *et al.*, 2005; Raviol *et al.*, 2006b). Fes1p and HspBP1 might thus have diverged in substrate specificity, or the *in vitro* folding reaction with HspBP1 may miss crucial components such as holdases, which keep non-native proteins in solution. Built-in holdase activity might make Hsp110s more autonomous than HspBP1 homologs and consequently much better suited for minimal folding reactions.

A further difference between HspBP1 and Hsp110 homologs might be adaptation of the Hsp70/NEF complexes to different substrate pools. For example, Hsp110s might recognize specific substrates with their  $\beta$ -sandwich domain and assist Hsp70 in remodeling of the client protein. Moreover, individual substrates might require unique Hsp70 interaction intervals for efficient folding, which might possibly be governed by different average life times of the Hsp70/NEF/substrate complexes.

Another reason for the limited redundancy of HspBP1 and Hsp110 homologs might be their specialization for interaction with specific Hsp70 chaperones and cochaperones. Thus, HspBP1 was shown to bind Hsp70 in cells with much higher affinity than the constitutively expressed Hsc70 (Tanimura *et al.*, 2007). Similarly, other Hsp70 cochaperones might be able to discern complexes of Hsp70 with HspBP1 and Hsp110 proteins, perhaps by recognizing the distinct Hsp70 NBD conformations. For example, the J-domain containing factor RAC was shown to compete with Fes1p for the binding to the ribosome-associated yeast Hsp70 homolog (Dragovic *et al.*, 2006b), while Hsp110 binding should not interfere with the binding of a J-domain (Figure 5-3A, this study and Jiang *et al.*, 2007). Furthermore, yeast Hsp90 was frequently found associated with Sse1p but not Fes1p in substrate complexes. Assuming that the Hsp90 interaction occurs indirectly *via* Hsp70, the conformation of the NBD might form the basis for this distinction (Zhao *et al.*, 2005b).

The large variety of eukaryotic NEFs illustrates impressively the complexity of the eukaryotic Hsp70 machinery. Hsp110 homologs appear to be the most important cellular NEFs and are likely to assist the general Hsp70 chaperoning function. The additional eukaryotic NEFs might confer robustness to the Hsp70 system and enable specialized functions of Hsp70.

## 6 REFERENCES

- Albanese, V., Yam, A. Y., Baughman, J., Parnot, C., and Frydman, J. (2006). Systems analyses reveal two chaperone networks with distinct functions in eukaryotic cells. *Cell* *124*, 75-88.
- Alberti, S., Bohse, K., Arndt, V., Schmitz, A., and Höhfeld, J. (2004). The cochaperone HspBP1 inhibits the CHIP ubiquitin ligase and stimulates the maturation of the cystic fibrosis transmembrane conductance regulator. *Mol Biol Cell* *15*, 4003-4010.
- Alberti, S., Demand, J., Esser, C., Emmerich, N., Schild, H., and Höhfeld, J. (2002). Ubiquitylation of BAG-1 suggests a novel regulatory mechanism during the sorting of chaperone substrates to the proteasome. *J Biol Chem* *277*, 45920-45927.
- Alberti, S., Esser, C., and Höhfeld, J. (2003). BAG-1 – a nucleotide exchange factor of Hsc70 with multiple cellular functions. *Cell Stress Chaperones* *8*, 225-231.
- Ali, M. M., Roe, S. M., Vaughan, C. K., Meyer, P., Panaretou, B., Piper, P. W., Prodromou, C., and Pearl, L. H. (2006). Crystal structure of an Hsp90-nucleotide-p23/Sba1 closed chaperone complex. *Nature* *440*, 1013-1017.
- Andréasson, C., Fiaux, J., Rampelt, H., Druffel-Augustin, S., and Bukau, B. (2008a). Insights into the structural dynamics of the Hsp110-Hsp70 interaction reveal the mechanism for nucleotide exchange activity. *Proc Natl Acad Sci U S A* *105*, 16519-16524.
- Andréasson, C., Fiaux, J., Rampelt, H., Mayer, M. P., and Bukau, B. (2008b). Hsp110 is a nucleotide-activated exchange factor for Hsp70. *J Biol Chem* *283*, 8877-8884.
- Anfinsen, C. B. (1973). Principles that govern the folding of protein chains. *Science* *181*, 223-230.
- Anfinsen, C. B., Haber, E., Sela, M., and White, F. H., Jr. (1961). The kinetics of formation of native ribonuclease during oxidation of the reduced polypeptide chain. *Proc Natl Acad Sci U S A* *47*, 1309-1314.
- Anttonen, A. K., Mahjneh, I., Hämäläinen, R. H., Lagier-Tourenne, C., Kopra, O., Waris, L., Anttonen, M., Joensuu, T., Kalimo, H., Paetau, A., *et al.* (2005). The gene disrupted in Marinesco-Sjögren syndrome encodes SIL1, an HSPA5 cochaperone. *Nat Genet* *37*, 1309-1311.
- Arndt, V., Daniel, C., Nastainczyk, W., Alberti, S., and Höhfeld, J. (2005). BAG-2 acts as an inhibitor of the chaperone-associated ubiquitin ligase CHIP. *Mol Biol Cell* *16*, 5891-5900.
- Babour, A., Kabani, M., Boisrame, A., and Beckerich, J. M. (2008). Characterization of Ire1 in the yeast *Yarrowia lipolytica* reveals an important role for the Sls1 nucleotide exchange factor in unfolded protein response regulation. *Curr Genet* *53*, 337-346.
- Baxter, B. K., James, P., Evans, T., and Craig, E. A. (1996). SSI1 encodes a novel Hsp70 of the *Saccharomyces cerevisiae* endoplasmic reticulum. *Mol Cell Biol* *16*, 6444-6456.
- Becker, T., Hartl, F. U., and Wieland, F. (2002). CD40, an extracellular receptor for binding and uptake of Hsp70-peptide complexes. *J Cell Biol* *158*, 1277-1285.
- Boisramé, A., Beckerich, J. M., and Gaillardin, C. (1996). Sls1p, an endoplasmic reticulum component, is involved in the protein translocation process in the yeast *Yarrowia lipolytica*. *J Biol Chem* *271*, 11668-11675.
- Boisramé, A., Kabani, M., Beckerich, J. M., Hartmann, E., and Gaillardin, C. (1998). Interaction of Kar2p and Sls1p is required for efficient co-translational translocation of secreted proteins in the yeast *Yarrowia lipolytica*. *J Biol Chem* *273*, 30903-30908.
- Bradford, M. M. (1976). A rapid and sensitive method for the quantitation of microgram quantities of protein utilizing the principle of protein-dye binding. *Anal Biochem* *72*, 248-254.
- Braig, K., Otwinowski, Z., Hegde, R., Boisvert, D. C., Joachimiak, A., Horwich, A. L., and Sigler, P. B. (1994). The crystal structure of the bacterial chaperonin GroEL at 2.8 angstrom. *Nature* *371*, 578-586.

- Brehmer, D., Gässler, C., Rist, W., Mayer, M. P., and Bukau, B. (2004). Influence of GrpE on DnaK-substrate interactions. *J Biol Chem* 279, 27957-27964.
- Brehmer, D., Rudiger, S., Gässler, C. S., Klostermeier, D., Packschies, L., Reinstein, J., Mayer, M. P., and Bukau, B. (2001). Tuning of chaperone activity of Hsp70 proteins by modulation of nucleotide exchange. *Nat Struct Biol* 8, 427-432.
- Brockmann, C., Leitner, D., Labudde, D., Diehl, A., Sievert, V., Büssow, K., Kühne, R., and Oschkinat, H. (2004). The solution structure of the SODD BAG domain reveals additional electrostatic interactions in the HSP70 complexes of SODD subfamily BAG domains. *FEBS Lett* 558, 101-106.
- Brodsky, J. L., Werner, E. D., Dubas, M. E., Goeckeler, J. L., Kruse, K. B., and McCracken, A. A. (1999). The requirement for molecular chaperones during endoplasmic reticulum-associated protein degradation demonstrates that protein export and import are mechanistically distinct. *J Biol Chem* 274, 3453-3460.
- Buchberger, A., Schroder, H., Buttner, M., Valencia, A., and Bukau, B. (1994). A conserved loop in the ATPase domain of the DnaK chaperone is essential for stable binding of GrpE. *Nat Struct Biol* 1, 95-101.
- Buchberger, A., Theyssen, H., Schroder, H., McCarty, J. S., Virgallita, G., Milkereit, P., Reinstein, J., and Bukau, B. (1995). Nucleotide-induced conformational changes in the ATPase and substrate binding domains of the DnaK chaperone provide evidence for interdomain communication. *J Biol Chem* 270, 16903-16910.
- Chang, Y. W., Sun, Y. J., Wang, C., and Hsiao, C. D. (2008). Crystal structures of the 70-kDa heat shock proteins in domain disjoining conformation. *J Biol Chem* 283, 15502-15511.
- Chesnokova, L. S., Slepnev, S. V., Protasevich, I., Sehorn, M. G., Brouillette, C. G., and Witt, S. N. (2003). Deletion of DnaK's lid strengthens binding to the nucleotide exchange factor, GrpE: a kinetic and thermodynamic analysis. *Biochemistry* 42, 9028-9040.
- Ciechanover, A. (2006). Intracellular protein degradation: from a vague idea thru the lysosome and the ubiquitin-proteasome system and onto human diseases and drug targeting. *Hematology Am Soc Hematol Educ Program*, 1-12, 505-506.
- Corpet, F. (1988). Multiple sequence alignment with hierarchical clustering. *Nucleic Acids Res* 16, 10881-10890.
- Craven, R. A., Egerton, M., and Stirling, C. J. (1996). A novel Hsp70 of the yeast ER lumen is required for the efficient translocation of a number of protein precursors. *Embo J* 15, 2640-2650.
- de la Fortelle, E., and Bricogne, G. (1997). Maximum-likelihood heavy atom parameter refinement for multiple isomorphous replacement and multiwavelength anomalous diffraction methods. *Methods Enzymol* 276, 472-494.
- DeLano, W. L. (2002). The PyMOL Molecular Graphics System.
- Demand, J., Alberti, S., Patterson, C., and Höhfeld, J. (2001). Cooperation of a ubiquitin domain protein and an E3 ubiquitin ligase during chaperone/proteasome coupling. *Curr Biol* 11, 1569-1577.
- DePristo, M. A., Weinreich, D. M., and Hartl, D. L. (2005). Missense meanderings in sequence space: a biophysical view of protein evolution. *Nat Rev Genet* 6, 678-687.
- Deshaies, R. J., Koch, B. D., Werner-Washburne, M., Craig, E. A., and Schekman, R. (1988). A subfamily of stress proteins facilitates translocation of secretory and mitochondrial precursor polypeptides. *Nature* 332, 800-805.
- Dill, K. A., and Chan, H. S. (1996). From Levinthal to pathways to funnels. *Nature Structural Biology* 4, 10-19.
- Dobson, C. M. (1999). Protein misfolding, evolution and disease. *Trends Biochem Sci* 24, 329-332.
- Dobson, C. M. (2003). Protein folding and misfolding. *Nature* 426, 884-890.

- Dobson, C. M. (2004). Principles of protein folding, misfolding and aggregation. *Semin Cell Dev Biol* *15*, 3-16.
- Dragovic, Z., Broadley, S. A., Shomura, Y., Bracher, A., and Hartl, F. U. (2006a). Molecular chaperones of the Hsp110 family act as nucleotide exchange factors of Hsp70s. *EMBO J.* *25*, 2519-2528.
- Dragovic, Z., Shomura, Y., Tzvetkov, N., Hartl, F. U., and Bracher, A. (2006b). Fes1p acts as a nucleotide exchange factor for the ribosome-associated molecular chaperone Ssb1p. *Biol Chem* *387*, 1593-1600.
- Easton, D. P., Kaneko, Y., and Subject, J. R. (2000). The Hsp110 and Grp170 stress proteins: newly recognized relatives of the Hsp70s. *Cell Stress Chaperones* *5*, 276-290.
- Ellis, R. J. (2001). Macromolecular crowding: an important but neglected aspect of the intracellular environment. *Curr Opin Struct Biol* *11*, 114-119.
- Ellis, R. J., and Hemmingsen, S. M. (1989). Molecular chaperones: proteins essential for the biogenesis of some macromolecular structures. *Trends Biochem Sci* *14*, 339-342.
- Ellis, R. J., and Minton, A. P. (2006). Protein aggregation in crowded environments. *Biol Chem* *387*, 485-497.
- Emsley, P., and Cowtan, K. (2004). Coot: model-building tools for molecular graphics. *Acta Crystallogr D Biol Crystallogr* *60*, 2126-2132.
- Evans, G., and Pettifer, R. F. (2001). CHOOCH: a program for deriving anomalous-scattering factors from X-ray fluorescence spectra. *J Appl Cryst* *34*, 82-86.
- Evans, P. R. (1997). Scala. *Joint CCP4 and ESF-EACBM Newsletter* *33*, 22-24.
- Fan, Q., Park, K. W., Du, Z., Morano, K. A., and Li, L. (2007). The role of Sse1 in the de novo formation and variant determination of the [PSI<sup>+</sup>] prion. *Genetics* *177*, 1583-1593.
- Fändrich, M., Fletcher, M. A., and Dobson, C. M. (2001). Amyloid fibrils from muscle myoglobin. *Nature* *410*, 165-166.
- Flaherty, K. M., Wilbanks, S. M., DeLuca-Flaherty, C., and McKay, D. B. (1994). Structural basis of the 70-kilodalton heat shock cognate protein ATP hydrolytic activity. II. Structure of the active site with ADP or ATP bound to wild type and mutant ATPase fragment. *J Biol Chem* *269*, 12899-12907.
- Froesch, B. A., Takayama, S., and Reed, J. C. (1998). BAG-1L protein enhances androgen receptor function. *J Biol Chem* *273*, 11660-11666.
- Gässler, C. S., Wiederkehr, T., Brehmer, D., Bukau, B., and Mayer, M. P. (2001). Bag-1M accelerates nucleotide release for human Hsc70 and Hsp70 and can act concentration-dependent as positive and negative cofactor. *J Biol Chem* *276*, 32538-32544.
- Gelinas, A. D., Langsetmo, K., Toth, J., Bethoney, K. A., Stafford, W. F., and Harrison, C. J. (2002). A structure-based interpretation of E.coli GrpE thermodynamic properties. *J Mol Biol* *323*, 131-142.
- Gelinas, A. D., Toth, J., Bethoney, K. A., Langsetmo, K., Stafford, W. F., and Harrison, C. J. (2003). Thermodynamic linkage in the GrpE nucleotide exchange factor, a molecular thermosensor. *Biochemistry* *42*, 9050-9059.
- Genevaux, P., Georgopoulos, C., and Kelley, W. L. (2007). The Hsp70 chaperone machines of *Escherichia coli*: a paradigm for the repartition of chaperone functions. *Mol Microbiol* *66*, 840-857.
- Genevaux, P., Schwager, F., Georgopoulos, C., and Kelley, W. L. (2002). Scanning mutagenesis identifies amino acid residues essential for the in vivo activity of the *Escherichia coli* DnaJ (Hsp40) J-domain. *Genetics* *162*, 1045-1053.
- Ghaemmaghami, S., Huh, W. K., Bower, K., Howson, R. W., Belle, A., Dephoure, N., O'Shea, E. K., and Weissman, J. S. (2003). Global analysis of protein expression in yeast. *Nature* *425*, 737-741.

- Gietz, R. D., Schiestl, R. H., Willems, A. R., and Woods, R. A. (1995). Studies on the transformation of intact yeast cells by the LiAc/SS-DNA/PEG procedure. *Yeast* *11*, 355-360.
- Glickman, M. H., and Ciechanover, A. (2002). The ubiquitin-proteasome proteolytic pathway: destruction for the sake of construction. *Physiol Rev* *82*, 373-428.
- Goeckeler, J. L., Petruso, A. P., Aguirre, J., Clement, C. C., Chiosis, G., and Brodsky, J. L. (2008). The yeast Hsp110, Sse1p, exhibits high-affinity peptide binding. *FEBS Lett* *582*, 2393-2396.
- Goeckeler, J. L., Stephens, A., Lee, P., Caplan, A. J., and Brodsky, J. L. (2002). Overexpression of yeast Hsp110 homolog Sse1p suppresses ydj1-151 thermosensitivity and restores Hsp90-dependent activity. *Mol Biol Cell* *13*, 2760-2770.
- Goldberg, M. E. (1985). The second translation of the genetic message: protein folding and assembly. *Trends in Biochemical Sciences* *10*, 388-391.
- Goloubinoff, P., and De Los Rios, P. (2007). The mechanism of Hsp70 chaperones: (entropic) pulling the models together. *Trends Biochem Sci* *32*, 372-380.
- Gouet, P., Courcelle, E., Stuart, D. I., and Metz, F. (1999). ESPript: multiple sequence alignments in PostScript. *Bioinformatics* *15*, 305-308.
- Grimshaw, J. P., Jelasarov, I., Schonfeld, H. J., and Christen, P. (2001). Reversible thermal transition in GrpE, the nucleotide exchange factor of the DnaK heat-shock system. *J Biol Chem* *276*, 6098-6104.
- Haber, E., and Anfinsen, C. B. (1961). Regeneration of enzyme activity by air oxidation of reduced subtilisin-modified ribonuclease. *J Biol Chem* *236*, 422-424.
- Haber, E., and Anfinsen, C. B. (1962). Side-chain interactions governing the pairing of half-cystine residues in ribonuclease. *J Biol Chem* *237*, 1839-1844.
- Hamilton, T. G., and Flynn, G. C. (1996). Cer1p, a novel Hsp70-related protein required for posttranslational endoplasmic reticulum translocation in yeast. *J Biol Chem* *271*, 30610-30613.
- Hanahan, D. (1983). Studies on transformation of *Escherichia coli* with plasmids. *J Mol Biol* *166*, 557-580.
- Harrison, C. (2003). GrpE, a nucleotide exchange factor for DnaK. *Cell Stress Chaperones* *8*, 218-224.
- Harrison, C. J., Hayer-Hartl, M., Di Liberto, M., Hartl, F., and Kuriyan, J. (1997). Crystal structure of the nucleotide exchange factor GrpE bound to the ATPase domain of the molecular chaperone DnaK. *Science* *276*, 431-435.
- Hartl, F. U., and Hayer-Hartl, M. (2002). Molecular chaperones in the cytosol: from nascent chain to folded protein. *Science* *295*, 1852-1858.
- Hatayama, T., Yasuda, K., and Yasuda, K. (1998). Association of HSP105 with HSC70 in high molecular mass complexes in mouse FM3A cells. *Biochem Biophys Res Commun* *248*, 395-401.
- Hayward, S., and Berendsen, H. J. (1998). Systematic analysis of domain motions in proteins from conformational change: new results on citrate synthase and T4 lysozyme. *Proteins* *30*, 144-154.
- Hiller, M. M., Finger, A., Schweiger, M., and Wolf, D. H. (1996). ER degradation of a misfolded luminal protein by the cytosolic ubiquitin-proteasome pathway. *Science* *273*, 1725-1728.
- Hinault, M. P., Ben-Zvi, A., and Goloubinoff, P. (2006). Chaperones and proteases: cellular fold-controlling factors of proteins in neurodegenerative diseases and aging. *J Mol Neurosci* *30*, 249-265.
- Höhfeld, J., Minami, Y., and Hartl, F. U. (1995). Hip, a novel cochaperone involved in the eukaryotic Hsc70/Hsp40 reaction cycle. *Cell* *83*, 589-598.
- Hubbard, S. J., and Thornton, J. M. (1993). NACCESS.

- Huyton, T., Pye, V. E., Briggs, L. C., Flynn, T. C., Beuron, F., Kondo, H., Ma, J., Zhang, X., and Freemont, P. S. (2003). The crystal structure of murine p97/VCP at 3.6Å. *J Struct Biol* 144, 337-348.
- Jackson, S. E. (1998). How do small single-domain proteins fold? *Fold Des* 3, R81-91.
- Jaenicke, R. (1996). How do proteins acquire their three-dimensional structure and stability? *Naturwissenschaften* 83, 544-554.
- Jahn, T. R., and Radford, S. E. (2008). Folding versus aggregation: polypeptide conformations on competing pathways. *Arch Biochem Biophys* 469, 100-117.
- Jiang, J., Maes, E. G., Taylor, A. B., Wang, L., Hinck, A. P., Lafer, E. M., and Sousa, R. (2007). Structural basis of J cochaperone binding and regulation of Hsp70. *Mol Cell* 28, 422-433.
- Jiang, Y., Woronicz, J. D., Liu, W., and Goeddel, D. V. (1999). Prevention of constitutive TNF receptor 1 signaling by silencer of death domains. *Science* 283, 543-546.
- Jiménez, J. L., Guijarro, J. I., Orlova, E., Zurdo, J., Dobson, C. M., Sunde, M., and Saibil, H. R. (1999). Cryo-electron microscopy structure of an SH3 amyloid fibril and model of the molecular packing. *Embo J* 18, 815-821.
- Kabani, M., Beckerich, J. M., and Brodsky, J. L. (2002a). Nucleotide exchange factor for the yeast Hsp70 molecular chaperone Ssa1p. *Mol Cell Biol* 22, 4677-4689.
- Kabani, M., Beckerich, J. M., and Gaillardin, C. (2000). Sls1p stimulates Sec63p-mediated activation of Kar2p in a conformation-dependent manner in the yeast endoplasmic reticulum. *Mol Cell Biol* 20, 6923-6934.
- Kabani, M., McLellan, C., Raynes, D. A., Guerriero, V., and Brodsky, J. L. (2002b). HspBP1, a homologue of the yeast Fes1 and Sls1 proteins, is an Hsc70 nucleotide exchange factor. *FEBS Lett* 531, 339-342.
- Kabbage, M., and Dickman, M. B. (2008). The BAG proteins: a ubiquitous family of chaperone regulators. *Cell Mol Life Sci* 65, 1390-1402.
- Kabsch, W. (1976). A solution for the best rotation to relate two sets of vectors. *Acta Crystallogr A* 32, 922-923.
- Kaneko, Y., Kimura, T., Kishishita, M., Noda, Y., and Fujita, J. (1997a). Cloning of *apg-2* encoding a novel member of heat shock protein 110 family. *Gene* 189, 19-24.
- Kaneko, Y., Nishiyama, H., Nonoguchi, K., Higashitsuji, H., Kishishita, M., and Fujita, J. (1997b). A novel hsp110-related gene, *apg-1*, that is abundantly expressed in the testis responds to a low temperature heat shock rather than the traditional elevated temperatures. *J Biol Chem* 272, 2640-2645.
- Kim, P. S., and Baldwin, R. L. (1982). Specific intermediates in the folding reactions of small proteins and the mechanism of protein folding. *Annual Review of Biochemistry* 51, 459-489.
- Kitao, Y., Ozawa, K., Miyazaki, M., Tamatani, M., Kobayashi, T., Yanagi, H., Okabe, M., Ikawa, M., Yamashima, T., Stern, D. M., *et al.* (2001). Expression of the endoplasmic reticulum molecular chaperone (ORP150) rescues hippocampal neurons from glutamate toxicity. *J Clin Invest* 108, 1439-1450.
- Kleywegt, G. T., and Jones, T. A. (1994). A super position. *CCP4/ESF-EACBM Newsletter on Protein Crystallography* 31, 9-14.
- Kryndushkin, D., and Wickner, R. B. (2007). Nucleotide exchange factors for Hsp70s are required for [URE3] prion propagation in *Saccharomyces cerevisiae*. *Mol Biol Cell* 18, 2149-2154.
- Laemmli, U. K. (1970). Cleavage of structural proteins during the assembly of the head of bacteriophage T4. *Nature* 227, 680-685.
- Laskowski, R. A., MacArthur, M. W., Moss, D. S., and Thornton, J. M. (1993). PROCHECK: a program to check the stereochemical quality of protein structures. *J App Cryst* 26, 283-291.

- Laufen, T., Mayer, M. P., Beisel, C., Klostermeier, D., Mogk, A., Reinstein, J., and Bukau, B. (1999). Mechanism of regulation of Hsp70 chaperones by DnaJ cochaperones. *Proceedings of the National Academy of Sciences of the United States of America* *96*, 5452-5457.
- Lawrence, M. C., and Colman, P. M. (1993). Shape complementarity at protein/protein interfaces. *J Mol Biol* *234*, 946-950.
- Lee-Yoon, D., Easton, D., Murawski, M., Burd, R., and Subject, J. R. (1995). Identification of a major subfamily of large hsp70-like proteins through the cloning of the mammalian 110-kDa heat shock protein. *J Biol Chem* *270*, 15725-15733.
- Lee, B., and Richards, F. M. (1971). The interpretation of protein structures: estimation of static accessibility. *J Mol Biol* *55*, 379-400.
- Leroux, M. R., and Hartl, F. U. (2000). Protein folding: Versatility of the cytosolic chaperonin TRiC/CCT. *Current Biology*, 260-264.
- Leslie, A. G. W. (1992). Recent changes to the MOSFLM package for processing film and image plate data. *Joint CCP4 and ESF-EACBM Newsletter* *26*.
- Levinthal, C. J. (1968). Are there pathways for protein folding? *J Chim Phys* *65*, 44-45.
- Li, J., Qian, X., and Sha, B. (2003). The crystal structure of the yeast Hsp40 Ydj1 complexed with its peptide substrate. *Structure* *11*, 1475-1483.
- Liberek, K., Lewandowska, A., and Zietkiewicz, S. (2008). Chaperones in control of protein disaggregation. *Embo J* *27*, 328-335.
- Liu, Q., and Hendrickson, W. A. (2007). Insights into Hsp70 chaperone activity from a crystal structure of the yeast Hsp110 Sse1. *Cell* *131*, 106-120.
- Liu, X. D., Morano, K. A., and Thiele, D. J. (1999). The yeast Hsp110 family member, Sse1, is an Hsp90 cochaperone. *J Biol Chem* *274*, 26654-26660.
- Lüders, J., Demand, J., and Höhfeld, J. (2000). The ubiquitin-related BAG-1 provides a link between the molecular chaperones Hsc70/Hsp70 and the proteasome. *J Biol Chem* *275*, 4613-4617.
- Luheshi, L. M., Crowther, D. C., and Dobson, C. M. (2008). Protein misfolding and disease: from the test tube to the organism. *Curr Opin Chem Biol* *12*, 25-31.
- Maniatis, T., Fritsch, E. F., and Sambrook, J. (1989). *Molecular Cloning*. 2nd edition, Cold Spring Harbor, N.Y.
- Matthews, B. W. (1968). Solvent content of protein crystals. *J Mol Biol* *33*, 491-497.
- Matthews, C. R. (1993). Pathways of Protein Folding. *Annual Review of Biochemistry* *62*, 653-683.
- Mayer, M. P., and Bukau, B. (2005). Hsp70 chaperones: cellular functions and molecular mechanism. *Cell Mol Life Sci* *62*, 670-684.
- Mayer, M. P., Schroder, H., Rudiger, S., Paal, K., Laufen, T., and Bukau, B. (2000). Multistep mechanism of substrate binding determines chaperone activity of Hsp70. *Nat Struct Biol* *7*, 586-593.
- Mazza, C., Ohno, M., Segref, A., Mattaj, I. W., and Cusack, S. (2001). Crystal structure of the human nuclear cap binding complex. *Mol Cell* *8*, 383-396.
- McClellan, A. J., Scott, M. D., and Frydman, J. (2005). Folding and quality control of the VHL tumor suppressor proceed through distinct chaperone pathways. *Cell* *121*, 739-748.
- Mogk, A., Haslberger, T., Tessarz, P., and Bukau, B. (2008). Common and specific mechanisms of AAA+ proteins involved in protein quality control. *Biochem Soc Trans* *36*, 120-125.
- Montgomery, D. L., Morimoto, R. I., and Gierasch, L. M. (1999). Mutations in the substrate binding domain of the Escherichia coli 70 kDa molecular chaperone, DnaK, which alter substrate affinity or interdomain coupling. *J Mol Biol* *286*, 915-932.
- Morano, K. A. (2007). New tricks for an old dog: the evolving world of Hsp70. *Ann N Y Acad Sci* *1113*, 1-14.

- Moro, F., Taneva, S. G., Velazquez-Campoy, A., and Muga, A. (2007). GrpE N-terminal domain contributes to the interaction with DnaK and modulates the dynamics of the chaperone substrate binding domain. *J Mol Biol* 374, 1054-1064.
- Mukai, H., Kuno, T., Tanaka, H., Hirata, D., Miyakawa, T., and Tanaka, C. (1993). Isolation and characterization of SSE1 and SSE2, new members of the yeast HSP70 multigene family. *Gene* 132, 57-66.
- Mumberg, D., Müller, R., and Funk, M. (1995). Yeast vectors for the controlled expression of heterologous proteins in different genetic backgrounds. *Gene* 156, 119-122.
- Murshudov, G. N., Vagin, A. A., and Dodson, E. J. (1997). Refinement of Macromolecular Structures by the Maximum-Likelihood Method. *Acta Crystallogr D Biol Crystallogr* 53, 240-255.
- O'Brien, M. C., Flaherty, K. M., and McKay, D. B. (1996). Lysine 71 of the chaperone protein Hsc70 is essential for ATP hydrolysis. *J Biol Chem* 271, 15874-15878.
- Oh, H. J., Chen, X., and Subject, J. R. (1997). Hsp110 protects heat-denatured proteins and confers cellular thermoresistance. *J Biol Chem* 272, 31636-31640.
- Oh, H. J., Easton, D., Murawski, M., Kaneko, Y., and Subject, J. R. (1999). The chaperoning activity of hsp110. Identification of functional domains by use of targeted deletions. *J Biol Chem* 274, 15712-15718.
- Pace, C. N., Vajdos, F., Fee, L., Grimsley, G., and Gray, T. (1995). How to measure and predict the molar absorption coefficient of a protein. *Protein Science* 4, 2411-2423.
- Park, S. H., Bolender, N., Eisele, F., Kostova, Z., Takeuchi, J., Coffino, P., and Wolf, D. H. (2007). The cytoplasmic Hsp70 chaperone machinery subjects misfolded and endoplasmic reticulum import-incompetent proteins to degradation via the ubiquitin-proteasome system. *Mol Biol Cell* 18, 153-165.
- Pellecchia, M., Szyperski, T., Wall, D., Georgopoulos, C., and Wüthrich, K. (1996). NMR structure of the J-domain and the Gly/Phe-rich region of the Escherichia coli DnaJ chaperone. *J Mol Biol* 260, 236-250.
- Perrakis, A., Morris, R., and Lamzin, V. S. (1999). Automated protein model building combined with iterative structure refinement. *Nat Struct Biol* 6, 458-463.
- Pickart, C. M., and Cohen, R. E. (2004). Proteasomes and their kin: proteases in the machine age. *Nat Rev Mol Cell Biol* 5, 177-187.
- Ptitsyn, O. B. (1995). How the molten globule became. *Trends Biochem Sci* 20, 376-379.
- Ptitsyn, O. B. (1998). Protein folding: nucleation and compact intermediates. *Biochemistry (Mosc)* 63, 367-373.
- Ptitsyn, O. B., Pain, R. H., Semisotnov, G. V., Zerovnik, E., and Razgulyaev, O. I. (1990). Evidence for a molten globule state as a general intermediate in protein folding. *FEBS Lett* 262, 20-24.
- Qiu, X. B., Shao, Y. M., Miao, S., and Wang, L. (2006). The diversity of the DnaJ/Hsp40 family, the crucial partners for Hsp70 chaperones. *Cell Mol Life Sci* 63, 2560-2570.
- Radaev, S., Li, S., and Sun, P. D. (2006). A survey of protein-protein complex crystallizations. *Acta Crystallogr D Biol Crystallogr* 62, 605-612.
- Radaev, S., and Sun, P. D. (2002). Crystallization of protein-protein complexes. *J Appl Cryst* 35, 674-676.
- Rajawat, Y. S., and Bossis, I. (2008). Autophagy in aging and in neurodegenerative disorders. *Hormones (Athens)* 7, 46-61.
- Ramachandran, G. N., Ramakrishnan, C., and Sasisekharan, V. (1963). Stereochemistry of polypeptide chain configurations. *J Mol Biol* 7, 95-99.
- Raviol, H., Bukau, B., and Mayer, M. P. (2006a). Human and yeast Hsp110 chaperones exhibit functional differences. *FEBS Lett* 580, 168-174.
- Raviol, H., Sadlish, H., Rodriguez, F., Mayer, M. P., and Bukau, B. (2006b). Chaperone network in the yeast cytosol: Hsp110 is revealed as an Hsp70 nucleotide exchange factor. *Embo J* 25, 2510-2518.

- Raynes, D. A., and Guerriero, V. (1998). Inhibition of Hsp70 ATPase activity and protein renaturation by a novel Hsp70-binding protein. *J Biol Chem* 273, 32883-32888.
- Rist, W., Graf, C., Bukau, B., and Mayer, M. P. (2006). Amide hydrogen exchange reveals conformational changes in hsp70 chaperones important for allosteric regulation. *J Biol Chem* 281, 16493-16501.
- Rüdiger, S., Germeroth, L., Schneider-Mergener, J., and Bukau, B. (1997). Substrate specificity of the DnaK chaperone determined by screening cellulose-bound peptide libraries. *EMBO J* 16, 1501-1507.
- Sadlish, H., Rampelt, H., Shorter, J., Wegrzyn, R. D., Andreasson, C., Lindquist, S., and Bukau, B. (2008). Hsp110 chaperones regulate prion formation and propagation in *S. cerevisiae* by two discrete activities. *PLoS ONE* 3, e1763.
- Saibil, H. R. (2008). Chaperone machines in action. *Curr Opin Struct Biol* 18, 35-42.
- Sambrook, J., Fritsch, E. F., and Maniatis, T. (1989). *Molecular Cloning - A laboratory manual*. Cold Spring Harbor Laboratory press,
- Schiestl, R. H., and Gietz, R. D. (1989). High efficiency transformation of intact yeast cells using single stranded nucleic acids as a carrier. *Curr Genet* 16, 339-346.
- Schuermann, J. P., Jiang, J., Cuellar, J., Llorca, O., Wang, L., Gimenez, L. E., Jin, S., Taylor, A. B., Demeler, B., Morano, K. A., *et al.* (2008). Structure of the Hsp110:Hsc70 nucleotide exchange machine. *Mol Cell* 31, 232-243.
- Schultz, C. P. (2000). Illuminating folding intermediates. *Nat Struct Biol* 7, 7-10.
- Senderek, J., Krieger, M., Stendel, C., Bergmann, C., Moser, M., Breitbach-Faller, N., Rudnik-Schöneborn, S., Blaschek, A., Wolf, N. I., Harting, I., *et al.* (2005). Mutations in SIL1 cause Marinesco-Sjögren syndrome, a cerebellar ataxia with cataract and myopathy. *Nat Genet* 37, 1312-1314.
- Shamovsky, I., and Nudler, E. (2008). New insights into the mechanism of heat shock response activation. *Cell Mol Life Sci* 65, 855-861.
- Shaner, L., Gibney, P. A., and Morano, K. A. (2008). The Hsp110 protein chaperone Sse1 is required for yeast cell wall integrity and morphogenesis. *Curr Genet* 54, 1-11.
- Shaner, L., and Morano, K. A. (2007). All in the family: atypical Hsp70 chaperones are conserved modulators of Hsp70 activity. *Cell Stress & Chaperones* 12, 1-8.
- Shaner, L., Sousa, R., and Morano, K. A. (2006). Characterization of Hsp70 binding and nucleotide exchange by the yeast Hsp110 chaperone Sse1. *Biochemistry* 45, 15075-15084.
- Shaner, L., Trott, A., Goeckeler, J. L., Brodsky, J. L., and Morano, K. A. (2004). The function of the yeast molecular chaperone Sse1 is mechanistically distinct from the closely related hsp70 family. *J Biol Chem* 279, 21992-22001.
- Shaner, L., Wegele, H., Buchner, J., and Morano, K. A. (2005). The yeast Hsp110 Sse1 functionally interacts with the Hsp70 chaperones Ssa and Ssb. *J Biol Chem* 280, 41262-41269.
- Shiau, A. K., Harris, S. F., Southworth, D. R., and Agard, D. A. (2006). Structural Analysis of *E. coli* hsp90 reveals dramatic nucleotide-dependent conformational rearrangements. *Cell* 127, 329-340.
- Shomura, Y., Dragovic, Z., Chang, H. C., Tzvetkov, N., Young, J. C., Brodsky, J. L., Guerriero, V., Hartl, F. U., and Bracher, A. (2005). Regulation of Hsp70 function by HspBP1: structural analysis reveals an alternate mechanism for Hsp70 nucleotide exchange. *Mol Cell* 17, 367-379.
- Siegenthaler, R. K., and Christen, P. (2005). The importance of having thermosensor control in the DnaK chaperone system. *J Biol Chem* 280, 14395-14401.
- Siegenthaler, R. K., and Christen, P. (2006). Tuning of DnaK chaperone action by nonnative protein sensor DnaJ and thermosensor GrpE. *J Biol Chem* 281, 34448-34456.

- Sikorski, R. S., and Hieter, P. (1989). A system of shuttle vectors and yeast host strains designed for efficient manipulation of DNA in *Saccharomyces cerevisiae*. *Genetics* 122, 19-27.
- Skarzynski, T. (1988). Contact.
- Sondermann, H., Scheufler, C., Schneider, C., Höhfeld, J., Hartl, F. U., and Moarefi, I. (2001). Structure of a Bag/Hsc70 complex: convergent functional evolution of Hsp70 nucleotide exchange factors. *Science* 291, 1553-1557.
- Song, J., Takeda, M., and Morimoto, R. I. (2001). Bag1-Hsp70 mediates a physiological stress signalling pathway that regulates Raf-1/ERK and cell growth. *Nat Cell Biol* 3, 276-282.
- Soto, C. (2003). Unfolding the role of protein misfolding in neurodegenerative diseases. *Nat Rev Neurosci* 4, 49-60.
- Sousa, M. C., and McKay, D. B. (1998). The hydroxyl of threonine 13 of the bovine 70-kDa heat shock cognate protein is essential for transducing the ATP-induced conformational change. *Biochemistry* 37, 15392-15399.
- Sousa, R., and Lafer, E. M. (2006). Keep the traffic moving: mechanism of the Hsp70 motor. *Traffic* 7, 1596-1603.
- Spieß, C., Meyer, A. S., Reissmann, S., and Frydman, J. (2004). Mechanism of the eukaryotic chaperonin: protein folding in the chamber of secrets. *TRENDS in Cell Biology* 14, 598-604.
- Steel, G. J., Fullerton, D. M., Tyson, J. R., and Stirling, C. J. (2004). Coordinated activation of Hsp70 chaperones. *Science* 303, 98-101.
- Subjectek, J. R., Sciandra, J. J., and Johnson, R. J. (1982). Heat shock proteins and thermotolerance; a comparison of induction kinetics. *Br J Radiol* 55, 579-584.
- Suh, W. C., Burkholder, W. F., Lu, C. Z., Zhao, X., Gottesman, M. E., and Gross, C. A. (1998). Interaction of the Hsp70 molecular chaperone, DnaK, with its cochaperone DnaJ. *Proc Natl Acad Sci U S A* 95, 15223-15228.
- Suh, W. C., Lu, C. Z., and Gross, C. A. (1999). Structural features required for the interaction of the Hsp70 molecular chaperone DnaK with its cochaperone DnaJ. *J Biol Chem* 274, 30534-30539.
- Swain, J. F., Dinler, G., Sivendran, R., Montgomery, D. L., Stotz, M., and Gierasch, L. M. (2007). Hsp70 chaperone ligands control domain association via an allosteric mechanism mediated by the interdomain linker. *Mol Cell* 26, 27-39.
- Takayama, S., and Reed, J. C. (2001). Molecular chaperone targeting and regulation by BAG family proteins. *Nat Cell Biol* 3, E237-241.
- Tanimura, S., Hirano, A. I., Hashizume, J., Yasunaga, M., Kawabata, T., Ozaki, K., and Kohno, M. (2007). Anticancer drugs up-regulate HspBP1 and thereby antagonize the prosurvival function of Hsp70 in tumor cells. *J Biol Chem* 282, 35430-35439.
- Terwilliger, T. C. (2000). Maximum-likelihood density modification. *Acta Crystallogr D Biol Crystallogr* 56 (Pt 8), 965-972.
- Theysen, H., Schuster, H. P., Packschies, L., Bukau, B., and Reinstein, J. (1996). The second step of ATP binding to DnaK induces peptide release. *J Mol Biol* 263, 657-670.
- Towbin, H., Staehelin, T., and Gordon, J. (1979). Electrophoretic transfer of proteins from polyacrylamide gels to nitrocellulose sheets: procedure and some applications. *Proc Natl Acad Sci U S A* 76, 4350-4354.
- Tyson, J. R., and Stirling, C. J. (2000). LHS1 and SIL1 provide a luminal function that is essential for protein translocation into the endoplasmic reticulum. *Embo J* 19, 6440-6452.
- Tzankov, S., Wong, M. J., Shi, K., Nassif, C., and Young, J. C. (2008). Functional Divergence between Co-chaperones of Hsc70. *J Biol Chem* 283, 27100-27109.
- Uson, I., and Sheldrick, G. M. (1999). Advances in direct methods for protein crystallography. *Curr Opin Struct Biol* 9, 643-648.

- Van Duyne, G. D., Standaert, R. F., Karplus, P. A., Schreiber, S. L., and Clardy, J. (1993). Atomic Structures of the Human Immunophilin FKBP-12 Complexes with FK506 and Rapamycin. *Journal of Molecular Biology* 229, 105-124.
- Vogel, M., Bukau, B., and Mayer, M. P. (2006a). Allosteric regulation of Hsp70 chaperones by a proline switch. *Mol Cell* 21, 359-367.
- Vogel, M., Mayer, M. P., and Bukau, B. (2006b). Allosteric regulation of Hsp70 chaperones involves a conserved interdomain linker. *J Biol Chem* 281, 38705-38711.
- Walsh, P., Bursac, D., Law, Y. C., Cyr, D., and Lithgow, T. (2004). The J-protein family: modulating protein assembly, disassembly and translocation. *EMBO Rep* 5, 567-571.
- Wandinger, S. K., Richter, K., and Buchner, J. (2008). The Hsp90 chaperone machinery. *J Biol Chem* 283, 18473-18477.
- Wang, X. Y., Chen, X., Oh, H. J., Repasky, E., Kazim, L., and Subject, J. (2000). Characterization of native interaction of hsp110 with hsp25 and hsc70. *FEBS Lett* 465, 98-102.
- Weiner, M. P., Costa, G. L., Schoettlin, W., Cline, J., Mathur, E., and Bauer, J. C. (1994). Site-directed mutagenesis of double-stranded DNA by the polymerase chain reaction. *Gene* 151, 119-123.
- Wilbanks, S. M., and McKay, D. B. (1995). How potassium affects the activity of the molecular chaperone Hsc70. II. Potassium binds specifically in the ATPase active site. *J Biol Chem* 270, 2251-2257.
- Wu, Y., Li, J., Jin, Z., Fu, Z., and Sha, B. (2005). The crystal structure of the C-terminal fragment of yeast Hsp40 Ydj1 reveals novel dimerization motif for Hsp40. *J Mol Biol* 346, 1005-1011.
- Xu, Z., Page, R. C., Gomes, M. M., Kohli, E., Nix, J. C., Herr, A. B., Patterson, C., and Misra, S. (2008). Structural basis of nucleotide exchange and client binding by the Hsp70 cochaperone Bag2. *Nat Struct Mol Biol* 15, 1309-1317.
- Yam, A. Y., Albanese, V., Lin, H. T., and Frydman, J. (2005). Hsp110 cooperates with different cytosolic HSP70 systems in a pathway for de novo folding. *J Biol Chem* 280, 41252-41261.
- Yamagishi, N., Ishihara, K., and Hatayama, T. (2004). Hsp105alpha suppresses Hsc70 chaperone activity by inhibiting Hsc70 ATPase activity. *J Biol Chem* 279, 41727-41733.
- Yamagishi, N., Nishihori, H., Ishihara, K., Ohtsuka, K., and Hatayama, T. (2000). Modulation of the chaperone activities of Hsc70/Hsp40 by Hsp105alpha and Hsp105beta. *Biochem Biophys Res Commun* 272, 850-855.
- Yasuda, K., Nakai, A., Hatayama, T., and Nagata, K. (1995). Cloning and expression of murine high molecular mass heat shock proteins, HSP105. *J Biol Chem* 270, 29718-29723.
- Young, J. C., Agashe, V. R., Siegers, K., and Hartl, F. U. (2004). Pathways of chaperone-mediated protein folding in the cytosol. *Nat Rev Mol Cell Biol* 5, 781-791.
- Zhang, Y., and Zuderweg, E. R. (2004). The 70-kDa heat shock protein chaperone nucleotide-binding domain in solution unveiled as a molecular machine that can reorient its functional subdomains. *Proc Natl Acad Sci U S A* 101, 10272-10277.
- Zhao, L., Longo-Guess, C., Harris, B. S., Lee, J. W., and Ackerman, S. L. (2005a). Protein accumulation and neurodegeneration in the woozy mutant mouse is caused by disruption of SIL1, a cochaperone of BiP. *Nat Genet* 37, 974-979.
- Zhao, R., Davey, M., Hsu, Y. C., Kaplanek, P., Tong, A., Parsons, A. B., Krogan, N., Cagney, G., Mai, D., Greenblatt, J., *et al.* (2005b). Navigating the chaperone network: an integrative map of physical and genetic interactions mediated by the hsp90 chaperone. *Cell* 120, 715-727.

- 
- Zhou, H. X., Rivas, G., and Minton, A. P. (2008). Macromolecular crowding and confinement: biochemical, biophysical, and potential physiological consequences. *Annu Rev Biophys* 37, 375-397.
- Zhu, X., Zhao, X., Burkholder, W. F., Gragerov, A., Ogata, C. M., Gottesman, M. E., and Hendrickson, W. A. (1996). Structural analysis of substrate binding by the molecular chaperone DnaK. *Science* 272, 1606-1614.

## 7 APPENDICES

### 7.1 List of primers

**Table 7-1: Primers utilized for sequencing.**

The constructs sequenced with the help of the shown primers are listed in the last column.

| Primer         | Sequence (5'→3')                             | Sequenced constructs   |
|----------------|--|------------------------|
| pProEx for     | GAGCGGATAACAATTCACACAGG                      | pProEx constructs      |
| pProEx rev     | CTGTTTTATCAGACCGCTTCTGCG                     | pProEx constructs      |
| Sse1_100 rev   | CCAAAACCAACAACAGATGGGGTGGAAACG               | <i>sse1</i> constructs |
| Sse1-750       | GAACATTCGCCGATGAGTTC                         | <i>sse1</i> constructs |
| Sse1-1500      | AAGAACCTATTCCATTACCAG                        | <i>sse1</i> constructs |
| SP1001         | CCTGTAAGGATTGTCAACGATGTGACTGCAGC             | <i>SSE2</i> construct  |
| Sse2_Dloop2rev | CGCGGATCCGGCCGTTGTGTAAGCGTTCTCGATAATATGCAAGC | <i>SSE2</i> construct  |

**Table 7-2: Primers utilized for cloning of the *sse1-Δloop* construct.**

While the N-terminal part of the *Sse1-Δloop* construct was amplified with the help of primers *Ehe1\_SSE1ORF* and *Sse1\_BamHIrev*, the C-terminal part was amplified with the help of primers *Sse1\_BamHIfor* and *SSE1ORF\_Xho1*. The introduced *Bam*HI restriction site was used for the ligation of the two fragments. In *Sse1-Δloop*, aminoacid residues 503-524 are replaced by the peptide linker AGSD. Nucleotides that code for the tetrapeptide are highlighted in red. The endonuclease restriction sites are underlined, and the respective endonucleases are listed in the last column. 5'-phosphorylation of the *Ehe1\_SSE1ORF* primer is indicated by @.

| Primer               | Sequence (5'→3')                                 | Endo-nuclease |
|----------------------|--|---------------|
| <i>Ehe1_SSE1ORF</i>  | @-GCCATGAGTACTCCATTTGGTTTAGATTTAGGTAAACAATAACTCT | <i>Ehe1</i>   |
| <i>SSE1ORF_Xho1</i>  | GCATCTCGAGTTAGTCCATGTCAACATCACCTTCAGTGCCTTC      | <i>Xho1</i>   |
| <i>Sse1_BamHIfor</i> | CGCGGATCCGGACACTAAAAGTGTAAAGAAGGATGACTTAACCATCG  | <i>Bam</i> HI |
| <i>Sse1_BamHIrev</i> | CGCGGATCCGGCTTCAATATCTTCAATAGTGTAAAGCCTTCAATTGTG | <i>Bam</i> HI |

**Table 7-3: Primers utilized for site-directed mutagenesis on *SSE1*.**

Point mutants of *SSE1* were produced *via* a PCR-based mutagenesis strategy, which relies on the amplification of the full-length plasmid using blunt end primers that contain the required nucleotide alterations (Weiner *et al.*, 1994). Nucleotides that diverge from the wt *SSE1* DNA sequence were always introduced in the forward (fw) primer and are shown in red. The corresponding amino acid exchanges are indicated in the primer names and highlighted in red. The respective SseI<sub>p</sub> variant names are listed in the last column. 5'-phosphorylation of reverse (rev) primers is indicated by Ⓢ.

| Primer                | Sequence (5'→3')   | SseI <sub>p</sub> variant |
|-----------------------|--|---------------------------|
| E_K69Mfw              | ACTGTCGCCAACTTGATGAGAATTATTGGTTTGGATTACC                 | SseI-1                    |
| E_K69MrevP            | Ⓢ-GTTCTTGATGTTGGAAGTCTGCTTGTCTTACC                       |                           |
| E_N572YE575Afw        | ACAGAAGACCGTAAGTACACTCTTGCAGAGTACATCTACACATTGCG          | SseI-2                    |
| E_N572YE575ArevP      | Ⓢ-TCAGCAACTAGCTTATCTTGAGCAAGCATTTTCATTTTC                |                           |
| E_A280TN281Afw        | AAGAAAGTTTTGTCTACTGCTACTAATGCCCATTTCTCTGTTG              | SseI-3                    |
| E_A280TN281ArevP      | Ⓢ-CAACTTTTCAGCAGCAGTTAGAATTCTGTTGTAAGC                   |                           |
| E_T365VN367Sfw        | CCATTGTCCACCGTTTTGAGCCAAGATGAAGCCATCG                    | SseI-4                    |
| E_T365VN367SrevP      | Ⓢ-CTTGCCGAAGGCTTCAGAAATGGATTGTTTCAATG                    |                           |
| E_F392AF394Afw        | CTAAGAGTTAGACCAGCCAAGGCTGAGGATATCCATCCTTAC               | SseI-5                    |
| E_F392AF394ArevP      | Ⓢ-AGTTGGAGAGTGAATGGCGCAAATAAAGGCG                        |                           |
| E_D396Afw             | CCATTCAAGTTTGAGGCTATCCATCCTTACTCTGTC                     | SseI-6                    |
| E_D396ArevP           | Ⓢ-TCTAACTCTTAGAGTTGGAGAGTGAATGGCGC                       |                           |
| E_L489AH490Afw        | TGCGACCCCTCTGGTGCAGCCACAATTGAAGAGGC                      | SseI-7                    |
| E_L489AH490ArevP      | Ⓢ-TCTCAACTTAACTTAACAGGAACAGAGTCTTGACC                    |                           |
| E_E554AM557SL558Sfw   | GAAAAAGCAAATGAAAGCAGTGCTCAAGATAAGCTAGTTGCTGAGACAGAAGACCG | SseI-8                    |
| E_E554AM557SL558SrevP | Ⓢ-ATTAATTCATTCAACTTTTTAGCGTCTAGGCCAAAGGTGTGTGC           |                           |
| E_L433AN434Pfw        | CTACTAAATTGATCACTGCGCCCGTACGGGTGACTTTTC                  | SseI-9                    |
| E_L433AN434PprevP     | Ⓢ-ATGGGAAGGATGAACCAGCTGGGAAAACCTTC                       |                           |
| E_F439LM441Afw        | GTACGGGTGACTTGTCA GCGGCTGCTAGCTACTG                      | SseI-10                   |
| E_F439LM441ArevP      | Ⓢ-TTCAAAGTGATCAATTTAGTAGATGGGAAGGATGAACC                 |                           |

**Table 7-4: Primers utilized for cloning of the *ssa1N* construct (amino acid residues 1-378).**

The endonuclease restriction sites are underlined, and the respective endonucleases are listed in the last column. The introduced stop codon is highlighted in blue.

| Primer         | Sequence (5'→3')                           | Endo-nuclease |
|----------------|--|---------------|
| Ssa1N_BamHIfor | CGCGGATCCAAAGCTGTCGGTATTGATTTAGGTACAACATAC | <i>Bam</i> HI |
| AB11r          | CCGCTCGAGTCAAGTCAAAATAGCAGCTTGAACAGCAGC    | <i>Xho</i> I  |

**Table 7-5: Primers utilized for site-directed mutagenesis on *SSA1* and *ssa1N*.**

Nucleotides that diverge from the wt *SSA1* DNA sequence are shown in red. The corresponding amino acid exchanges are indicated in the primer names and highlighted in red. The respective Ssa1p variant names are listed in the last column. 5'-phosphorylation of reverse (rev) primers is indicated by Ⓟ.

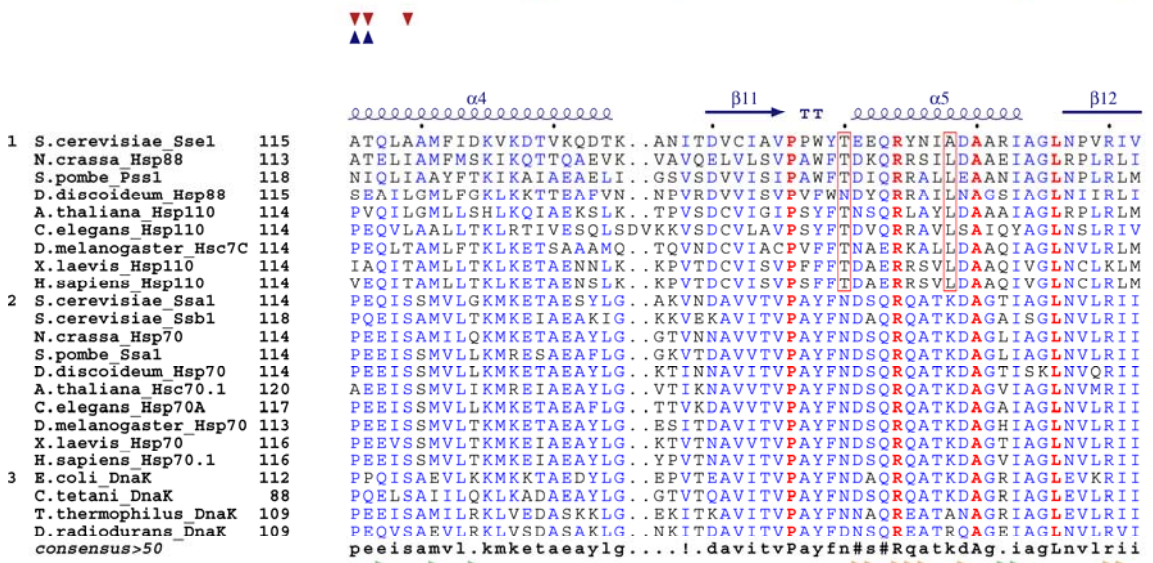
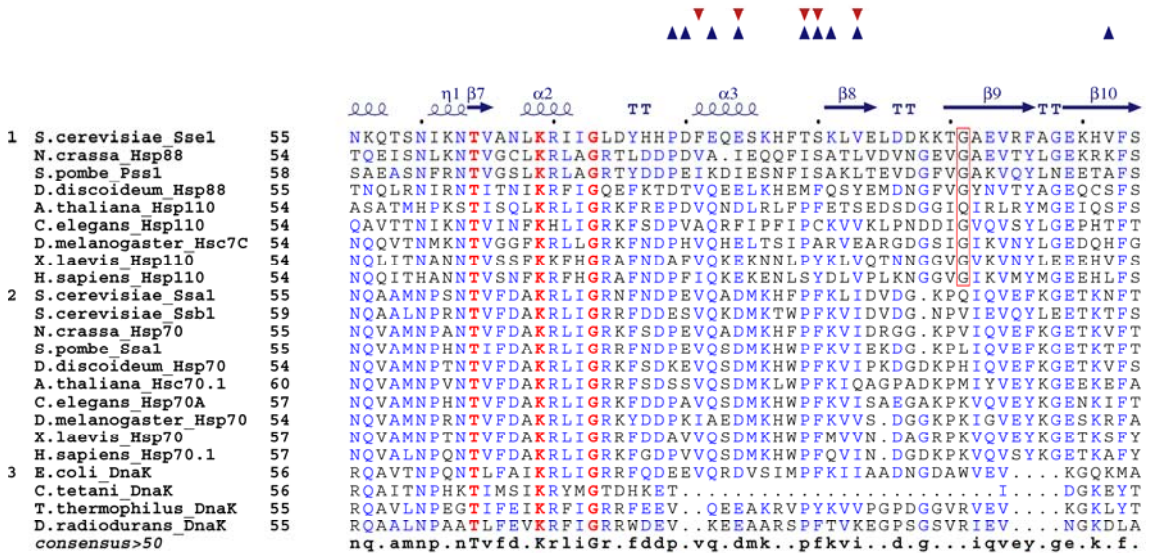
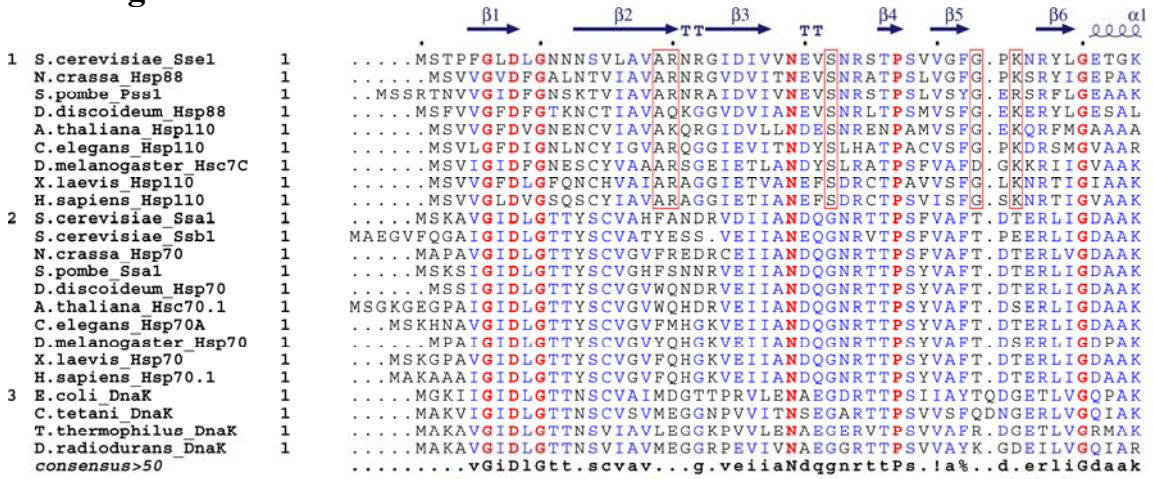
| Primer      | Sequence (5'→3')                        | Ssa1p variant                |
|-------------|---|------------------------------|
| A_Q31Afw    | ATTATTGCCAACGATGCAGGTAACAGAACCACTCC     | Ssa1(Q31A) and Ssa1N(Q31A)   |
| A_Q31ArevP  | Ⓟ-GTCCACACGATCATTAGCAAAGTGAGCAAC        | Ssa1(Q31A) and Ssa1N(Q31A)   |
| A_A300Efw   | ACTTCCATCACCAGAGAAAGATTCTGAAGAATTGTGTGC | Ssa1(A300E) and Ssa1N(A300E) |
| A_A300ErevP | Ⓟ-GTAGAAATCGATACCTTCGAACAAAGAGTCAATTC   | Ssa1(A300E) and Ssa1N(A300E) |

**Table 7-6: Primers utilized for cloning of the *SSE2* construct.**

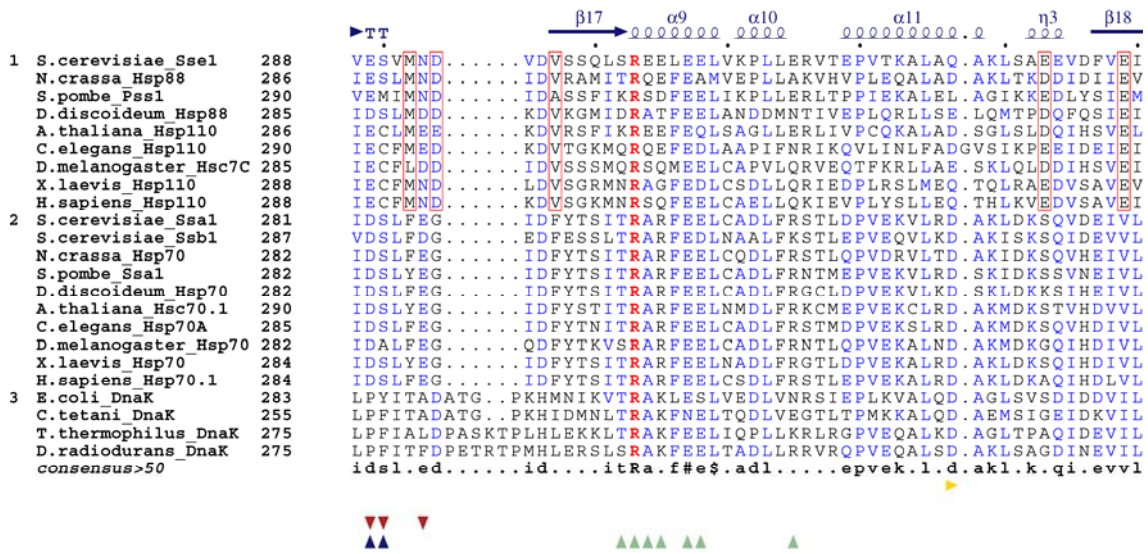
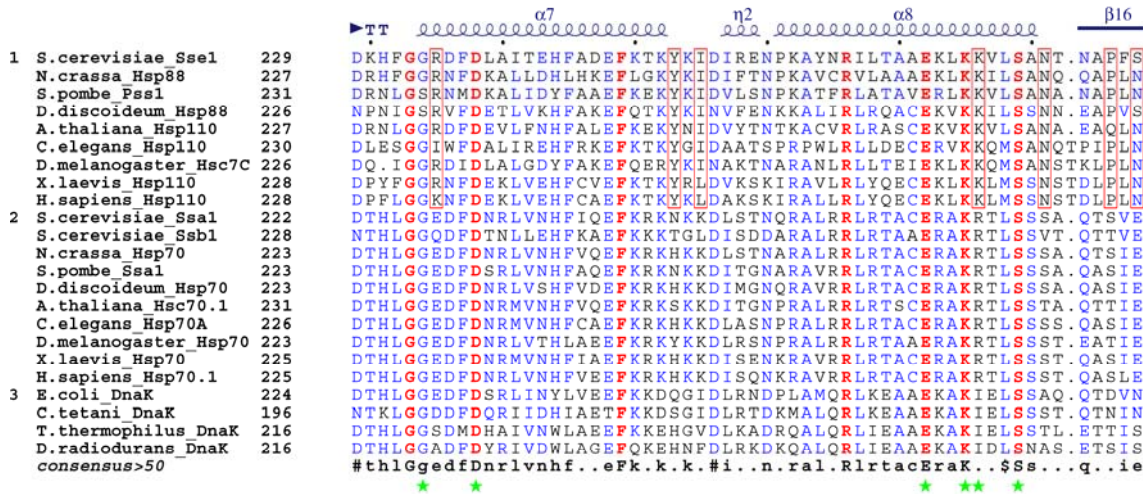
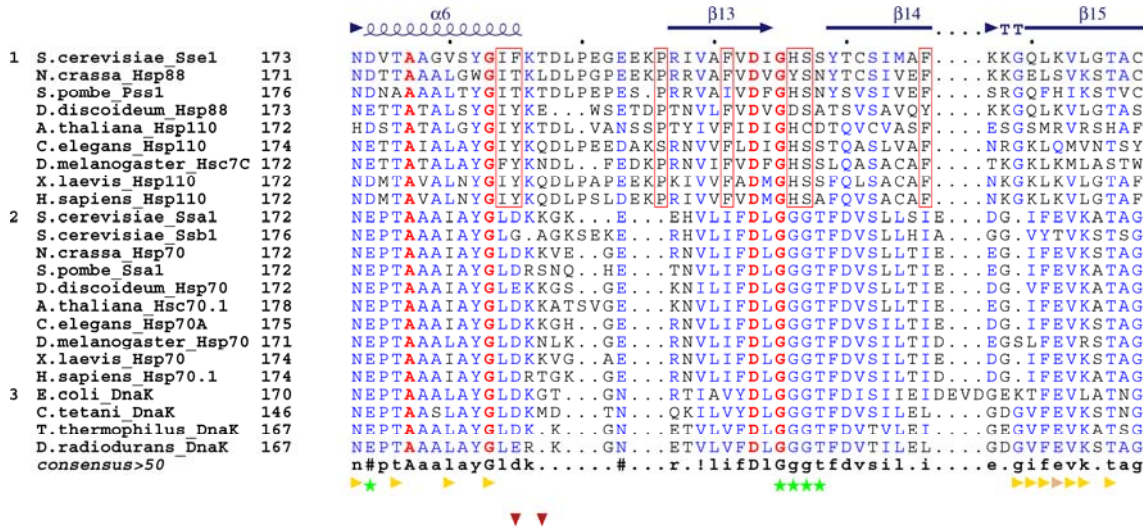
The endonuclease restriction sites are underlined, and the respective endonucleases are listed in the last column. 5'-phosphorylation of the EhelSse2ORF primer is indicated by Ⓟ.

| Primer      | Sequence (5'→3')                                | Endo-nuclease |
|-------------|---|---------------|
| EhelSse2ORF | Ⓟ-GCCATGAGCACTCCATTTGGCTTAGATTTAGGTAACAATAACTCA | <i>Ehe</i> I  |
| Sse2ORFXhoI | GCATCTCGAGTTAATCAAGGTCCATGTTTTTCATCATTGTTGTCA   | <i>Xho</i> I  |

## 7.2 Amino acid sequence alignment of selected Hsp110 and Hsp70 homologs



★ ATP-binding  
 ▲ Sse1 domain contacts  
 ▼ contacts to Hsp70N  
 ▲ contacts to Sse1



\* ATP-binding  
 ▶ Sse1p domain contacts  
 ▼ contacts to Hsp70N  
 ▲ contacts to Sse1p



|   |                             |     |  |
|---|-----------------------------|-----|--|
| 1 | <i>S.cerevisiae</i> Ssel    | 507 | IPL.....   |
|   | <i>N.crassa</i> Hsp88       | 509 | VKD.....   |
|   | <i>S.pombe</i> Pss1         | 512 | VET.....   |
|   | <i>D.discoideum</i> Hsp88   | 497 | AAPA.....  |
|   | <i>A.thaliana</i> Hsp110    | 505 | SEEM..... I SEENH  |
|   | <i>C.elegans</i> Hsp110     | 509 | PAAE.....  |
|   | <i>D.melanogaster</i> Hsc7C | 502 | AAAAE..... QAASEEK   |
|   | <i>X.laevis</i> Hsp110      | 507 | EEQT.GEMVGDNQSATETLETDKGVQDSSDAGTQPQVQTDGQHC... PPSPETSSGDHK |
|   | <i>H.sapiens</i> Hsp110     | 507 | EMSSEADMDECLNRFPENPDTDKNVQDQNSAGTQPQVQTDAAQQTSSQSPPELTSSEENK |
| 2 | <i>S.cerevisiae</i> Ssal    |     | .....  |
|   | <i>S.cerevisiae</i> Ssbl    |     | .....  |
|   | <i>N.crassa</i> Hsp70       |     | .....  |
|   | <i>S.pombe</i> Ssal         |     | .....  |
|   | <i>D.discoideum</i> Hsp70   |     | .....  |
|   | <i>A.thaliana</i> Hsc70.1   |     | .....  |
|   | <i>C.elegans</i> Hsp70A     |     | .....  |
|   | <i>D.melanogaster</i> Hsp70 |     | .....  |
|   | <i>X.laevis</i> Hsp70       |     | .....  |
|   | <i>H.sapiens</i> Hsp70.1    |     | .....  |
| 3 | <i>E.coli</i> DnaK          |     | .....  |
|   | <i>C.tetani</i> DnaK        |     | .....  |
|   | <i>T.thermophilus</i> DnaK  |     | .....  |
|   | <i>D.radiodurans</i> DnaK   |     | .....  |
|   | <i>consensus</i> >50        |     | .....  |

|   |                             |     |  |     |       |
|---|-----------------------------|-----|--|-----|-------|
|   |                             |     | β29  | β30 | ..... |
| 1 | <i>S.cerevisiae</i> Ssel    | 510 | ..P..EDAPEDAEQ..EFKVKTKTVKDDDTIVAHTFG.LDAKKLNELIEKENEMLAQDK  |     |       |
|   | <i>N.crassa</i> Hsp88       | 512 | ..E.NGDVVMGDKP.KTRKVKQVRKGLPVVSATPS.LDPAAKNAAIEREQAMIEDDK    |     |       |
|   | <i>S.pombe</i> Pss1         | 515 | ..SPEEEAEKKTDEPVMKVKVKKLVKVLVSVQEDR.LPTVELEKYREAEHQMIATDK    |     |       |
|   | <i>D.discoideum</i> Hsp88   | 501 | ..ETPAETPANGEAAKPAEBEKVKVKETSIVFTTSRKG.LTNELKAAIEEGRMQASDL   |     |       |
|   | <i>A.thaliana</i> Hsp110    | 515 | QSSAMKDGSLDPPSSGSIGNEPK.AIKRMEIPVVANVSGALTKDELSEAKQENSLVEQDL |     |       |
|   | <i>C.elegans</i> Hsp110     | 513 | ..MEVDGDAKTEAPAELEPVKTKLVPLVLEVIESIPVSYDVQK.FHNLLELQMQESDA   |     |       |
|   | <i>D.melanogaster</i> Hsc7C | 515 | GDQTNNTGEPADGQEGADKKKASKATELPLECTTHGFSPVDSL.N.YTQGESKMIQNDQ  |     |       |
|   | <i>X.laevis</i> Hsp110      | 563 | MTETDKGNEKKTDPPEAKPKIKVKNIELPIETNLWQLSKDLLNMYIENEGKMLIQDK    |     |       |
|   | <i>H.sapiens</i> Hsp110     | 567 | IPDADKANEKKVDQPPEAKPKIKVNVNELPIEANLVWQLGKDLLNMYIETEGKMLIQDK  |     |       |
| 2 | <i>S.cerevisiae</i> Ssal    | 488 | .....VKGTKGSKNKITIT.NDKGRLSKEDIEMVABAEKFKBEDDE               |     |       |
|   | <i>S.cerevisiae</i> Ssbl    | 495 | .....VEKSTGKSSNITIS.NAVGRLSSEEIEKMNQAEFPKADE                 |     |       |
|   | <i>N.crassa</i> Hsp70       | 490 | .....LEKGTGKTNQITIT.NDKGRLSKEEIERMLAEAEKFKBEDDE              |     |       |
|   | <i>S.pombe</i> Ssal         | 489 | .....LEKGTGKTQKITIT.NDKGRLSKEEIERMVAEAEKFKBEDDE              |     |       |
|   | <i>D.discoideum</i> Hsp70   | 489 | .....EDKSTGNKQKITIT.NDKGRLSKEEIEKMVADAEPKQODE                |     |       |
|   | <i>A.thaliana</i> Hsc70.1   | 497 | .....EDKTTGQKNKITIT.NDKGRLSKEDIEMVQAEAEKFKSDE                |     |       |
|   | <i>C.elegans</i> Hsp70A     | 492 | .....TDKSTGKQNKITIT.NDKGRLSKDDIERMVNAEAEKFKADDE              |     |       |
|   | <i>D.melanogaster</i> Hsp70 | 489 | .....KEMSTGKAKNITIK.NDKGRLSQAEIDRMVNAEAEKFKADDE              |     |       |
|   | <i>X.laevis</i> Hsp70       | 491 | .....VDKSTGKENKITIT.NDKGRLSKEDIEMVQAEAEKFKADDE               |     |       |
|   | <i>H.sapiens</i> Hsp70.1    | 491 | .....TDKSTGKANKITIT.NDKGRLSKEEIERMVQAEAEKFKADDE              |     |       |
| 3 | <i>E.coli</i> DnaK          | 489 | .....DKKNSGKEQKITIK.ASSG.LNEDEIQKMYRDAEAMAEADR               |     |       |
|   | <i>C.tetani</i> DnaK        | 461 | .....KDKGTGKEANITIT.ASTN.LSDEDEKAVNDAAKPFEEEDK               |     |       |
|   | <i>T.thermophilus</i> DnaK  | 483 | .....KERSTGREASITIQ.NTTT.LSBEIIRIEBAKRAHEADR                 |     |       |
|   | <i>D.radiodurans</i> DnaK   | 485 | .....KKTSGKESSITIE.NTTT.LDKTDVERMVQAEQNAAADK                 |     |       |
|   | <i>consensus</i> >50        |     | .....ek.tgk...iti...n..g.lskeie.mveeaek...ed.                |     |       |

|   |                             |     |   |    |     |    |  |
|---|-----------------------------|-----|---|----|-----|----|--|
|   |                             |     | α14   | η6 | α15 | η7 |  |
| 1 | <i>S.cerevisiae</i> Ssel    | 563 | LVAETE <sup>DR</sup> KNTLE <sup>EY</sup> IYTLR <sup>GK</sup> LEE.BYAPFASDAEKT <sup>KL</sup> QGM <sup>DK</sup> NKA <sup>EW</sup> LY <sup>DE</sup> GF <sup>DS</sup> I   |    |     |    |  |
|   | <i>N.crassa</i> Hsp88       | 567 | LVADTE <sup>EK</sup> KNELE <sup>TY</sup> IYDLR <sup>NK</sup> LDD.QYADLAS <sup>EEEE</sup> KIRAK <sup>LM</sup> EV <sup>ED</sup> WLY <sup>DE</sup> GG <sup>DD</sup> AT   |    |     |    |  |
|   | <i>S.pombe</i> Pss1         | 572 | LVAETV <sup>DR</sup> KNALE <sup>EY</sup> IYTRAK <sup>LD</sup> DD.IYAPFTNE <sup>EESS</sup> KFKEM <sup>LTK</sup> AE <sup>BD</sup> WLY <sup>EG</sup> ED <sup>DT</sup>  |    |     |    |  |
|   | <i>D.discoideum</i> Hsp88   | 558 | LAIETA <sup>EK</sup> KNALES <sup>EY</sup> IYDMR <sup>SK</sup> LQS.SLKEVYVTPADAE <sup>TF</sup> MTQL <sup>NK</sup> QMDW <sup>LE</sup> SE <sup>EG</sup> ED <sup>QT</sup>   |    |     |    |  |
|   | <i>A.thaliana</i> Hsp110    | 574 | KMESTK <sup>EK</sup> KNALES <sup>FV</sup> YEMRD <sup>KML</sup> N.TYRNTATESERE <sup>CI</sup> ARN <sup>LQ</sup> ET <sup>EW</sup> LY <sup>EG</sup> DD <sup>ES</sup>  |    |     |    |  |
|   | <i>C.elegans</i> Hsp110     | 569 | REKAKA <sup>DA</sup> KNSLE <sup>EY</sup> VYEMRD <sup>KV</sup> SD.QYAEFIPAAADE <sup>FR</sup> SV <sup>LT</sup> ST <sup>ED</sup> WLY <sup>DE</sup> GE <sup>DA</sup> E  |    |     |    |  |
|   | <i>D.melanogaster</i> Hsc7C | 574 | KETERI <sup>DA</sup> KNALE <sup>FV</sup> YDMRN <sup>KL</sup> GGPFERYVVEAERE <sup>KIV</sup> SQ <sup>LN</sup> DL <sup>EN</sup> WLY <sup>EG</sup> ED <sup>CE</sup>   |    |     |    |  |
|   | <i>X.laevis</i> Hsp110      | 623 | LEKERN <sup>DA</sup> KNAVE <sup>EY</sup> VYPRD <sup>KL</sup> SG.PYEKPVSDK <sup>DQ</sup> SR <sup>FL</sup> EL <sup>LT</sup> ET <sup>EN</sup> WLY <sup>EG</sup> ED <sup>DQ</sup> R   |    |     |    |  |
|   | <i>H.sapiens</i> Hsp110     | 627 | LEKERN <sup>DA</sup> KNAVE <sup>EY</sup> VYPRD <sup>KL</sup> CG.PYEKFCIQ <sup>DH</sup> QNF <sup>LR</sup> IL <sup>LT</sup> ET <sup>ED</sup> WLY <sup>EG</sup> ED <sup>QA</sup>   |    |     |    |  |
| 2 | <i>S.cerevisiae</i> Ssal    | 528 | KESQRIAS <sup>KN</sup> QLES <sup>IAY</sup> SLKNTIS <sup>EAG</sup> ..DKLEQADK <sup>DT</sup> VTKKAB <sup>ET</sup> ISW <sup>L</sup> ..DS <sup>NT</sup> TA <sup>S</sup>   |    |     |    |  |
|   | <i>S.cerevisiae</i> Ssbl    | 535 | AFAKKHEAR <sup>QR</sup> LESYVASIE <sup>QT</sup> VT <sup>DP</sup> VLS <sup>SK</sup> LKRG <sup>SK</sup> IEAAL <sup>SD</sup> ALAAL <sup>..</sup> QI <sup>ED</sup> PSA  |    |     |    |  |
|   | <i>N.crassa</i> Hsp70       | 530 | AEAKRVA <sup>AK</sup> NGLES <sup>YAS</sup> LRN <sup>TL</sup> SD <sup>SK</sup> VDE <sup>KL</sup> DAAD <sup>EK</sup> KLKSEI <sup>DK</sup> I <sup>V</sup> AWL <sup>..</sup> DEN <sup>Q</sup> AT  |    |     |    |  |
|   | <i>S.pombe</i> Ssal         | 529 | AETSRIQ <sup>AK</sup> NHLES <sup>YAS</sup> LRN <sup>SL</sup> DD <sup>PN</sup> LK <sup>DK</sup> VDA <sup>SK</sup> EAI <sup>DK</sup> AV <sup>KE</sup> TI <sup>EW</sup> ..DH <sup>NT</sup> TA <sup>A</sup>                             |    |     |    |  |
|   | <i>D.discoideum</i> Hsp70   | 529 | QKDRVES <sup>KN</sup> KLENYA <sup>FT</sup> VKN <sup>SI</sup> KDEKVA <sup>AK</sup> IS <sup>DS</sup> DK <sup>ST</sup> IES <sup>ET</sup> SVL <sup>KW</sup> ..ES <sup>NQ</sup> TA <sup>E</sup>  |    |     |    |  |
|   | <i>A.thaliana</i> Hsc70.1   | 537 | EHK <sup>KK</sup> VEAKNALE <sup>NY</sup> AYNMR <sup>NT</sup> IQ <sup>EK</sup> IG <sup>EK</sup> LPAA <sup>DK</sup> KK <sup>IE</sup> DS <sup>I</sup> EQAI <sup>QW</sup> ..EG <sup>NQ</sup> LA <sup>E</sup>                            |    |     |    |  |
|   | <i>C.elegans</i> Hsp70A     | 532 | AQKDRIG <sup>AK</sup> NGLES <sup>YAF</sup> NL <sup>QTI</sup> E <sup>DE</sup> KL <sup>DK</sup> IS <sup>PE</sup> DK <sup>KK</sup> IED <sup>CK</sup> IE <sup>IL</sup> KW <sup>L</sup> ..DS <sup>NQ</sup> TA <sup>E</sup>               |    |     |    |  |
|   | <i>D.melanogaster</i> Hsp70 | 529 | KHRQRI <sup>TS</sup> RNALES <sup>YVF</sup> NV <sup>QAV</sup> EQAP.AG <sup>KL</sup> DEAD <sup>KN</sup> SV <sup>LD</sup> KC <sup>ND</sup> TIR <sup>WL</sup> ..DS <sup>NT</sup> TA <sup>E</sup>  |    |     |    |  |
|   | <i>X.laevis</i> Hsp70       | 531 | KQRDKV <sup>SS</sup> KNSLES <sup>YAF</sup> NKAT <sup>VE</sup> DE <sup>KL</sup> QK <sup>IN</sup> DE <sup>DQ</sup> K <sup>IL</sup> DK <sup>CE</sup> NI <sup>SW</sup> L <sup>..</sup> DK <sup>NQ</sup> TA <sup>E</sup>                 |    |     |    |  |
|   | <i>H.sapiens</i> Hsp70.1    | 531 | VQRE <sup>RV</sup> SAKNALES <sup>YAF</sup> NK <sup>SA</sup> VE <sup>DE</sup> GL <sup>GK</sup> IS <sup>EA</sup> DK <sup>KK</sup> V <sup>LD</sup> K <sup>CO</sup> E <sup>VI</sup> SW <sup>L</sup> ..DAN <sup>TL</sup> EA <sup>E</sup> |    |     |    |  |
| 3 | <i>E.coli</i> DnaK          | 528 | KFELVQ <sup>TR</sup> NQGD <sup>HLL</sup> STR <sup>KQ</sup> VE <sup>EAG</sup> ..DKLPAD <sup>DK</sup> TA <sup>IE</sup> SAL <sup>TA</sup> LETAL <sup>..</sup> KG <sup>ED</sup> KA <sup>A</sup>   |    |     |    |  |
|   | <i>C.tetani</i> DnaK        | 500 | KR <sup>KE</sup> SE <sup>VK</sup> NNAE <sup>QI</sup> FY <sup>Q</sup> TE <sup>KL</sup> NEL <sup>EG</sup> ..DKVSAED <sup>KAT</sup> IE <sup>EK</sup> L <sup>N</sup> AL <sup>KG</sup> VK <sup>..</sup> DG <sup>ED</sup> IEA             |    |     |    |  |
|   | <i>T.thermophilus</i> DnaK  | 522 | RR <sup>RE</sup> HA <sup>EL</sup> KNAL <sup>DS</sup> ARV <sup>Q</sup> AER <sup>V</sup> LQER...QGAP <sup>E</sup> .ARAR <sup>LE</sup> AA <sup>I</sup> GK <sup>AE</sup> L <sup>V</sup> ...BR <sup>DA</sup> P                           |    |     |    |  |
|   | <i>D.radiodurans</i> DnaK   | 524 | QR <sup>KE</sup> V <sup>KR</sup> NN <sup>LD</sup> S <sup>LR</sup> V <sup>Q</sup> AV <sup>QL</sup> EEQ...EGAA <sup>QDA</sup> K <sup>DR</sup> L <sup>KA</sup> AA <sup>DE</sup> AE <sup>AV</sup> ..RS <sup>ED</sup> DS <sup>K</sup>    |    |     |    |  |
|   | <i>consensus</i> >50        |     | ...e.ve.k#.l#sy.ynmrn.led...dk...e.dke.i...lne...ewl..d.ndda.   |    |     |    |  |

- ★ ATP-binding
- ▶ Ssel domain contacts
- ▼ contacts to Hsp70N
- ▲ contacts to Ssel



**Figure 7-1: Amino acid sequence alignment of selected Hsp110 and Hsp70 homologs.**

Amino acid sequences of selected Hsp110, eukaryotic Hsp70 and bacterial DnaK homologs (groups 1, 2 and 3, respectively) were aligned using the MultAlin server. Residues indicated in red are invariable, and residues indicated in blue are conserved in more than 50 % of the sequences. Residues which are conserved in Hsp110 homologs but dissimilar in canonical Hsp70s are boxed in red. A consensus sequence using the standard symbols of the MultAlin analysis program (Corpet, 1988) is given in the bottom row of the alignment. The secondary structure elements and the residue numbering for Sse1p are indicated above the sequences. The colors of the secondary structure elements reflect the domain structure; the same colors as in Figure 4-7 of the main text are used. Contact residues are indicated below the consensus sequence. Residues in contact with ATP are labeled by green asterisks. Horizontal arrowheads indicate residues involved in domain-domain interactions in Sse1p. Vertical arrowheads indicate contact residues in the Sse1p/Hsp70N complex (downward pointing arrowheads indicate residues in Sse1p, upward pointing arrowheads residues in Hsp70N). The arrowhead color indicates the domain in contact. SwissProt accession numbers of the sequences shown are as follows: *Saccharomyces cerevisiae* Sse1p (P32589), *Neurospora crassa* Hsp88 (O74225), *Schizosaccharomyces pombe* Pss1 (O59838), *Dictyostelium discoideum* Hsp88 (Q6TMK3), *Arabidopsis thaliana* Hsp110 (Q9SAB1), *Caenorhabditis elegans* Hsp110 (Q05036), *Drosophila melanogaster* Hsp110 (Q9XZT5), *Xenopus laevis* Hsp110 (Q1PAH4), *Homo sapiens* Hsp110 (Q92598), *Saccharomyces cerevisiae* Ssa1p (P10591), *Saccharomyces cerevisiae* Ssb1p (P11484), *Neurospora crassa* Hsp70 (Q01233), *Schizosaccharomyces pombe* Ssa1 (Q10265), *Dictyostelium discoideum* Hsp70 (Q55C64), *Arabidopsis thaliana* Hsc70.1 (P22953), *Caenorhabditis elegans* Hsp70A (P09446), *Drosophila melanogaster* Hsp70 (P82910), *Xenopus laevis* Hsp70 (A1L3K5), *Homo sapiens* Hsp70.1 (P08107), *Escherichia coli* DnaK (P0A6Z0), *Clostridium tetani* DnaK (Q892R0), *Thermus thermophilus* DnaK (Q72IK5), and *Deinococcus radiodurans* DnaK (Q9RY23).

**7.3 List of abbreviations**

Units are expressed according to the international system of units (SI). For the amino acids, one and three letter codes were used.

|         |  |
|---------|--|
| A       | amplitude  |
| AA      | acrylamide   |
| AAA     | ATPases associated with various cellular activities                    |
| ADA     | N-(carbamoylmethyl)iminodiacetic acid                                  |
| ADP     | adenosine 5'-diphosphate   |
| Amp     | ampicillin   |
| AMP     | adenosine 5'-monophosphate   |
| AMP-PNP | adenylyl imidodiphosphate  |
| Apg     | A: ATP binding domain, p: peptide binding domain, g: germ cell derived |
| apoB    | apolipoprotein B   |
| APS     | ammonium peroxodisulfate   |
| ATP     | adenosine 5'-triphosphate  |
| BAG     | Bcl2-associated athanogene   |
| BAP     | BiP-associated protein   |
| BDP     | BAG domain protein   |

---

|                |  |
|----------------|--|
| BiP            | binding immunoglobulin protein   |
| bp             | base pairs   |
| BSA            | bovine serum albumin   |
| c              | concentration  |
| CCD            | charge coupled device  |
| CD             | circular dichroism   |
| CD             | C-terminal domain  |
| CFTR           | cystic fibrosis transmembrane conductance regulator                    |
| CHIP           | C-terminus of heat shock cognate 70 stress protein-interacting protein |
| CHO            | chinese hamster ovary  |
| CLIP           | chaperones linked in protein synthesis                                 |
| Clp            | caseinolytic protease  |
| Cm             | chloramphenicol  |
| CTD            | carboxy terminal domain  |
| CV             | column volume  |
| DEAE           | diethylaminoethyl  |
| Δ (delta)      | deletion   |
| DMF            | dimethylformamide  |
| DNA            | deoxyribonucleic acid  |
| DnaJ           | bacterial Hsp40 chaperone  |
| DnaK           | bacterial Hsp70 chaperone  |
| D-NR           | dansyl-NRLLLTGC  |
| dNTPs          | deoxyribonucleotides   |
| DTT            | dithiothreitol   |
| ECL            | enhanced chemiluminescence   |
| <i>E. coli</i> | <i>Escherichia coli</i>  |
| EDTA           | ethylenediaminetetraacetic acid  |
| ER             | endoplasmic reticulum  |
| ESRF           | European Synchrotron Radiation Facility                                |
| Fes1p          | factor exchange for Ssa1p  |
| FFF-MALS       | field flow fractionation - multiangle light scattering                 |
| FFT            | fast fourier transformation  |
| 5-FOA          | 5-fluoroorotic acid  |
| GdnHCl         | guanidinium hydrochloride  |

---

|                  |   |
|------------------|---|
| GroEL            | large <i>growthE</i> gene product                                     |
| GroES            | small <i>growthE</i> gene product                                     |
| Grp              | glucose-regulated protein   |
| GrpE             | Growth P-like gene E  |
| 3HBD             | three helix bundle domain   |
| HD               | hydrogen deuterium  |
| Hdj              | human DnaJ-like protein   |
| HEPES            | N-(2-hydroxyethyl)piperazin-N'-2-ethanesulfonic acid                  |
| HIP              | Hsp70 interacting protein   |
| His <sub>6</sub> | histidine tag   |
| HOP              | Hsp organizing protein  |
| HRP              | horseradish peroxidase  |
| Hsc              | heat shock cognate protein  |
| HSF              | heat shock factor   |
| Hsp              | heat shock protein  |
| HspBP1           | Hsp70 binding protein 1   |
| IPTG             | isopropyl- $\beta$ -D-1-thiogalactopyranoside                         |
| Ire1p            | high inositol-requiring protein 1                                     |
| <i>k</i>         | rate  |
| KAc              | potassium acetate   |
| Kar2p            | karyogamy 2 protein   |
| K <sub>D</sub>   | dissociation constant   |
| kDa              | kilodalton  |
| LB               | Luria Bertani   |
| LDL              | low density lipoprotein   |
| Lhs1p            | luminal hsp seventy protein 1   |
| LiAc             | lithiumacetate  |
| MABA-ADP         | N8-(4N'-methylanthraniloylaminobutyl)-8 aminoadenosine 5'-diphosphate |
| MAD              | multiple wavelength anomalous diffraction                             |
| MD               | middle domain   |
| MES              | 2-morpholinoethanesulfonic acid                                       |
| MOPS             | 3-(N-morpholino)propanesulfonic acid                                  |
| MPP11            | M-phase phosphoprotein 11   |
| MS               | mass spectrometry   |

---

|                      |  |
|----------------------|--|
| MW                   | molecular weight                               |
| MWCO                 | molecular weight cut off                       |
| n                    | refractive index                               |
| NAC                  | nascent chain-associated complex               |
| NBD                  | nucleotide binding domain                      |
| ND                   | N-terminal domain                              |
| NEF                  | nucleotide exchange factor                     |
| NLS                  | nuclear localization signal                    |
| NMR                  | nuclear magnetic resonance                     |
| OAc                  | acetate  |
| OD                   | optical density                                |
| ONPG                 | o-nitrophenyl- $\beta$ -D-galactopyranoside    |
| Orp                  | oxygen-regulated protein                       |
| PAGE                 | polyacrylamide gel electrophoresis             |
| PBD                  | peptide binding domain                         |
| PCR                  | polymerase chain reaction                      |
| PDB                  | protein data bank                              |
| PEG                  | polyethylene glycol                            |
| PFD                  | prefoldin                                      |
| <i>Pfu</i>           | <i>Pyrococcus furiosus</i>                     |
| PGK                  | phosphoglycerate kinase                        |
| PMSF                 | phenyl-methyl-sulfonyl fluoride                |
| RAC                  | ribosome-associated complex                    |
| Raf-1                | rapidly growing fibrosarcoma kinase 1          |
| r.m.s.d.             | root mean square deviation                     |
| RNA                  | ribonucleic acid                               |
| ROI                  | region of interest                             |
| rpm                  | revolutions per minute                         |
| RT                   | room temperature                               |
| Sba1                 | sensitive to benzoquinoid ansamycins protein 1 |
| SC                   | synthetic complete                             |
| <i>S. cerevisiae</i> | <i>Saccharomyces cerevisiae</i>                |
| SD                   | standard deviation                             |
| SDS                  | sodium dodecylsulfate                          |

---

|             |   |
|-------------|---|
| SeMet       | selenomethionine  |
| sHsp        | small heat shock protein  |
| Sil1p       | suppressor of the $\Delta IRE1\Delta LHS1$ double mutant number 1 |
| Sis1p       | <i>sit4</i> suppressor number 1                                   |
| SLS         | Swiss Synchrotron Light Source                                    |
| Sls1p       | synthetic lethal mutation with the 7S RNA mutation protein 1      |
| Snl1p       | suppressor of nucleoporin 116-C lethal number 1                   |
| SODD        | silencer of death domains   |
| Ss          | Stress seventy  |
| Sti1p       | stress inducible protein 1  |
| Swi         | switching   |
| <i>Taq</i>  | <i>Thermus aquaticus</i>  |
| TCA         | trichloroacetic acid  |
| TEMED       | <i>N,N,N',N'</i> -tetramethylethylenediamine                      |
| TEV         | tobacco etch virus  |
| TF          | trigger factor  |
| <i>Tgo</i>  | <i>Thermococcus gorgonarius</i>                                   |
| TLS         | translation libration screw                                       |
| TNFR1       | tumor necrosis factor receptor 1                                  |
| TOM         | translocase of the outer mitochondrial membrane                   |
| TPR         | tetratricopeptide repeat  |
| TRiC        | tailless complex peptide 1 (TCP1) ring complex                    |
| Tris        | trishydroxymethylaminomethan                                      |
| UPR         | unfolded protein response   |
| <i>URA3</i> | orotidine-5'-monophosphate decarboxylase                          |
| UV          | ultraviolet   |
| v/v         | volume per volume   |
| wt          | wildtype  |
| w/v         | weight per volume   |
| Ydj1p       | yeast DnaJ-like protein 1   |
| YPD         | yeast extract peptone dextrose                                    |

## 7.4 Publication

Polier, S., Dragovic, Z., Hartl, F.U., Bracher, A. (2008). Structural Basis for the Cooperation of Hsp70 and Hsp110 Chaperones in Protein Folding. *Cell* 133, 1068-1079.

## 7.5 Lebenslauf

### Persönliche Daten

Name: Sigrun Polier  
Geburtsdatum: 15. Oktober 1982  
Geburtsort: Höxter  
Nationalität: deutsch  
Familienstand: ledig

### Wissenschaftlicher Werdegang

#### Hochschulreife

Juni 2001 Allgemeine Hochschulreife am Gymnasium Bad Aibling

#### Hochschulstudium

Oktober 2001 – Juni 2006 Studium der Biochemie an der Universität Bayreuth  
Diplomprüfung in den Fächern Biochemie, Bioorganische Chemie, Biophysikalische Chemie, Genetik und Naturstoffchemie

Diplomarbeit am Lehrstuhl für Biochemie bei Prof. Dr. F. X. Schmid

*“Analyse der Stabilität und Faltung zweier Esterasen”*

Oktober 2004 – September 2008 Elitestudienprogramm Macromolecular Science an der Universität Bayreuth

#### Dissertation

September 2006 – heute Experimentelle Doktorarbeit in der Abteilung Zelluläre Biochemie von Prof. Dr. F. U. Hartl am Max-Planck-Institut für Biochemie in Martinsried  
*“Structural Basis for the Cooperation of Hsp110 and Hsp70 Molecular Chaperones in Protein Folding”*

München, den